RADAR REMOTE SENSING FOR RETRIEVAL OF SOIL PARAMETERS

A THESIS

Submitted in partial fulfilment of the requirements for the award of the degree of

DOCTOR OF PHILOSOPHY

in

ELECTRONICS AND COMPUTER ENGINEERING

by

RISHI PRAKASH

M.G. CENTRAL LIBRARY
ACC No. G21591
Date 4/10/12
I.I.T. ROORKEE

DEPARTMENT OF ELECTRONICS AND COMPUTER ENGINEERING
INDIAN INSTITUTE OF TECHNOLOGY ROORKEE
ROORKEE-247 667 (INDIA)

JULY, 2011

©INDIAN INSTITUTE OF TECHNOLOGY ROORKEE, ROORKEE-2011
ALL RIGHTS RESERVED

INDIAN INSTITUTE OF TECHNOLOGY ROORKEE
ROORKEE

CANDIDATE'S DECLARATION

I hereby certify that the work which is being presented in the thesis entitled **RADAR REMOTE SENSING FOR RETRIEVAL OF SOIL PARAMETERS** in partial fulfilment of the requirements for the award of the Degree of Doctor of Philosophy and submitted in the Department of Electronics and Computer Engineering of the Indian Institute of Technology Roorkee, Roorkee is an authentic record of my own work carried out during a period from July 2006 to July 2011 under the supervision of Dr. Dharmendra Singh, Associate Professor and Dr. Nagendra Prasad Pathak, Assistant Professor, Department of Electronics and Computer Engineering, Indian Institute of Technology Roorkee, Roorkee.

The matter presented in this thesis has not been submitted by me for the award of any other degree of this or any other Institute.

Rishi Prakash

(RISHI PRAKASH)

This is to certify that the above statement made by the candidate is correct to the best of our knowledge.

NPpathak

(Nagendra Prasad Pathak)
Supervisor

(Dharmendra Singh)
Supervisor

Date: 14/7/2011

The Ph.D. Viva-Voce Examination of **Mr. Rishi Prakash**, Research Scholar, has been held on ..... 9/11/11 .....

Signature of Supervisors

NPpathak
9/11/2011

Signature of External Examiners

9 NOV 2011

Abstract

Soil moisture, surface roughness and soil texture are important soil parameters in various applications, such as, agriculture, weather forecasting, soil erosion, hydrological studies and flood and draught prediction. Studies in the field of active microwave remote sensing have shown the feasibility to monitor these soil parameters with ground based, airborne and spaceborne sensors. Therefore, this thesis has two main objectives. First main aim is to analyze soil parameters, specifically soil texture which is less reported in bistatic domain because it is well known that bistatic domain provides several flexibilities over monostatic domain and very lesser experimental studies have been carried out to characterize the soil parameters in this domain. Second aim is to retrieve the soil moisture in vegetated area with SAR and optical satellite data for minimizing the use of *apriori* information.

Thesis has been composed of seven chapters. First chapter deals with the introduction, experiment performed, data used and study area. The second chapter presents the brief literature review, discussing the studies carried out in the field of microwave remote sensing for the soil parameters retrieval and its limitations along with the need of research in the present scenario.

Chapter 3 analyzes the effect of soil texture on specular scattering coefficient at 10 GHz (X–band) in both like polarizations, i.e., HH– and VV–polarization for various incidence angles (i.e., 30° to 70° in step of 10°). If (θ, φ) (where, θ *and* φ are the incidence angle and azimuthal angle respectively) define the incident direction of the transmitted power $P_p(\theta, \varphi)$ at polarization p, and (θ_s, φ_s) is the direction of the received power $P_q(\theta_s, \varphi_s)$ at polarization q then specular scattering is defined as: $\theta = \theta_s$, $\varphi = 0$ and $\varphi_s = 0$. To study the soil texture effect on the specular scattering coefficient, four different soil texture fields were prepared on the basis of variation in

soil constituent, i.e., the percentage of sand (i.e., 78.14% to 28.72%), silt (i.e., 33.16% to 9.12%) and clay (i.e., 18.75% to 4.32%) was changed for different fields. The major changes were observed for sand constituent. It is observed from the study of dry and smooth soil that by changing soil texture there is a considerable amount of change in specular scattering coefficient for both like polarizations. The effect was more prominent at higher incidence angles (i.e., $\geq 50°$), i.e., better differentiation in specular scattering coefficient for different soil texture field was observed at higher incidence angles. The dynamic range of specular scattering coefficient with incidence angle changes with the change is sand constituent in soil. The dynamic range of 8.7 dB and 10.5 dB was observed for higher sand content (i.e., 78.14%) and lower sand content (i.e., 28.72%), respectively for dry and smooth soil in HH–polarization whereas in case of VV–polarization dynamic range was 18.2 dB and 19.4 dB respectively. Further, the effect of soil texture on specular scattering coefficient was examined in the presence of four different soil moisture contents (i.e., dry to 0.21 cm^3 cm^{-3}) and three different periodic surface roughness conditions (i.e., smooth to 1.4 cm). Thus in order to check the soil texture effect, 48 different field conditions were considered for the observations of specular scattering coefficient in both like polarizations at various incidence angles. The effect of soil texture on specular scattering has been clearly observed at different soil moisture condition. A better differentiation in specular scattering coefficient was observed for change in soil texture with the increase in moisture content though the effect is more prominent at higher incidence angles. Further, the effect of soil texture on specular scattering coefficient has been observed in the presence of different periodic surface roughness conditions. The observation has shown the difficulty in analyzing the effect of soil texture on specular scattering at higher roughness values (i.e., 0.9 cm and 1.4 cm).

Chapter 4 analyzes the effect of soil texture on microwave specular scattering at 6 GHz (C–band) in both like polarizations, i.e., HH– and VV–polarization. A more regress analysis was carried out because it is observed that soil constituents with roughness and moisture are giving more effect on specular scattering coefficient at 6 GHz than 10 GHz. So, ten different soil texture fields were prepared and to check the angular behavior, the incidence angle was changed from 25° to 70° degree in step of 5°. The percentage of sand (i.e., 85.3% to 2.3%), silt (i.e., 70.6% to 7.5%) and clay (i.e., 81.6% to 2.5%) was changed for different soil texture fields. Six soil moisture

and five periodic roughness conditions were studied to get an understanding of the soil texture effect on specular scattering in presence of various moisture contents and periodic surface roughness conditions. Therefore, total 300 different field conditions were analyzed. The study at 6 GHz is important as the longer wavelength is relatively less sensitive to the roughness variation in comparison to the shorter wavelength. Although the study of this chapter is concentrated for the bare soil only, it may be tested for the vegetated area as a future work. The analysis part is subdivide, firstly analyzing the effect of soil texture on specular scattering coefficient in the presence of various soil moisture contents (i.e., 0.027 cm^3 cm^{-3} to 0.425 cm^3 cm^{-3}) by keeping the periodic surface roughness condition constant. Secondly, the effect of soil texture on specular scattering coefficient while varying the periodic surface roughness (i.e., 0.43 cm to 2.46 cm) was studied. Furthermore, the combined effect of soil moisture and periodic surface roughness on specular scattering coefficient for change in soil texture has been considered. The observation in HH–polarization with dry and smooth field has shown that the dynamic range of specular scattering coefficient with high sand content (i.e., 85.3% sand) was 9.8 dB whereas in case of high clay content (i.e., 81.6% clay) the dynamic range was 13.6 dB. The differentiation among different soil texture field based on specular scattering coefficient can be made when the volumetric soil moisture content is less 0.368 cm^3 cm^{-3} whereas, it is difficult to observe the soil texture effect for higher soil moisture contents (i.e., $\geq$ 0.368 cm^3 cm^{-3}) in both like polarizations. Further, the surface roughness does not exhibit such kind of effect and even at higher periodic roughness value (i.e., $\leq$ 2.46 cm) the change in specular scattering coefficient can be observed with the change in soil texture at 6 GHz. The experimental observations carried out at 6 GHz points out that higher incidence angles (i.e., $\geq 45°$) are more appropriate than the lower incidence angles for the study of soil texture in presence of soil moisture and periodic surface roughness in both like polarizations.

Chapter 5 deals with the retrieval of soil parameters at 6 GHz in association to the observation made in specular direction. Specular scattering data at 6 GHz has been considered for soil parameters retrieval studies instead of specular scattering data at 10 GHz due to its response for different soil texture field in the presence of periodic surface roughness whereas, in case of 10 GHz it has been very difficult to distinguish among different soil texture fields based on specular scattering coefficient in the

presence of periodic surface roughness. Soil parameters retrieval in domain of microwave remote sensing is a challenging task owing to the dependence of many soil parameters on one scattering coefficient value only. By the virtue of this, more sensor parameters were utilized to minimize the effect of one or more soil parameters on specular scattering coefficient, in consequence of which the desired soil parameters can be retrieved easily and more accurately. In the first approach, copolarization ratio has been utilized for minimizing the soil texture effect in order to retrieve the volumetric soil moisture content. The periodic surface roughness condition during the observation was kept constant whereas, the changes in soil texture and soil moisture were considered. There was negligible changes in copolarization ratio with the change in soil texture whereas, copolarization ratio changes with the change in soil moisture. In accordance to the observations obtained with the copolarization ratio an empirical relation between the copolarization ratio and volumetric soil moisture was developed. The volumetric soil moisture content was retrieved with developed empirical relationship along with the Kirchhoff scalar approximation (SA) to draw the comparison. The RMSE for soil moisture retrieval was 0.021, 0.079 and 0.095 for developed empirical relationship, SA in HH–polarization and VV–polarization, respectively. The obtained results clearly signify that the developed empirical relationship performed better than SA for retrieving the bare soil moisture. In next approach, multi–incidence data have been used to retrieve the soil surface roughness. These surface roughness values were subsequently used to retrieve the soil moisture and soil texture. Ratio of specular scattering coefficient at two different incidence angles provides the normalized specular scattering coefficient which depends on surface roughness and shows negligible dependency on soil moisture and soil texture. This property led to the development of a relationship between normalized specular scattering coefficient and roughness parameters, rms surface height, s and correlation length, l. The developed empirical relationship in conjunction with SA and empirical relationship developed by Hallikainen *et al.* (1985) has been utilized for the retrieval of roughness parameters, soil moisture and soil texture. The retrieved results were in good agreement with the ground truth data. Root mean square error (RMSE) for the retrieval of rms surface height, correlation length, volumetric soil moisture, percentage of sand, and percentage of clay were 0.027, 0.051, 0.036, 5.94, and 8.15, respectively. The developed approach reduces the need of *apriori* information which

is required in form of surface roughness characterization when the objective is to retrieve the soil moisture and soil texture.

Till now we have concentrated our work for analyzing soil parameters in bistatic domain but still satellite data for bistatic domain is awaited as TanDEM–X is in progress. The satellite data which is available are for the case of backscattering. So, we have considered the satellite data such as PALSAR and MODIS for retrieval of soil moisture in vegetated area. The retrieval of vegetation covered soil moisture is a challenging task with the existing SAR sensors. Though, the backscattering coefficient contains the information of vegetation as well as underlying soil moisture, the complex scattering behavior of microwave form vegetated area give rise to the development of complex relationship among backscattering coefficient, vegetation parameter (e.g., leaf area index, biomass, plant height) and soil parameters (i.e., soil moisture, surface roughness). The optical data which can characterize the vegetation may be efficiently utilized in vegetation covered soil moisture retrieval algorithm with SAR data.

The aim of the chapter 6 is to retrieve the soil moisture in vegetated area with minimum *apriori* information by using satellite data like the ALOS–PALSAR (Advanced Land Observation Satellite– Phased Array type L–band Synthetic Aperture Radar), a SAR data and MODIS (Moderate-resolution Imaging Spectroradiometer), an optical data. The PALSAR image is full polarimetric, L–band (1.27 GHz) image and was acquired on April 06, 2009. The MODIS data used is of band 1 (620–670 nm) and band 2 (841–847 nm) and the date of image acquisition was April 03, 2009. The area of study was Roorkee city (Uttarakhand, India) and its surroundings. The first set of images (one PALASR and one MODIS) that lie between longitudes 77.803° E and 77.980° E and latitudes 30.000° N and 29.823° N were used for the algorithm development and subsequently testing the developed algorithm for soil moisture retrieval. The second set of images that were used for validating the algorithm lie between longitudes 77.847° E and 78.024° E and latitudes 29.859° N and 29.682° N. The date of acquisition of PALSAR and MODIS images were April 6, 2009 and April 3, 2009, respectively. The land cover is fairly flat and mostly consists of the urban, water and agriculture classes. It is always the possibility to find the mixed land cover classes therefore, as a first step PALSAR data was used to classify the land cover in urban, water, vegetated land and bare soil by utilizing knowledge

based approach involving the various polarizations (linear, circular, linear 45°, co– and cross–polarized ratios for both linear and circular polarization) and subsequently the urban and water region can be masked. The objective of this chapter is to analyze the feasibility of the relating the information available from SAR data and optical data to envisage such an approach that mostly rely on the information content of satellite image and require minimum *apriori* information. The concept of such an approach arises as the vegetation can be modeled through the SAR data as well as the optical data. In case of SAR data the backscattering is affected by the vegetation cover and contains the information regarding vegetation whereas, the normalized index vegetation index (NDVI) provides a good estimate of the crop cover. The utilization of the information content from the optical data reduces the requirement of *apriori* information which is required in the vegetation parameters characterization. Therefore, two different normalizing approaches have been used for scattering coefficient of PALSAR data and then the empirical relationships have been developed with NDVI to incorporate the vegetation effect in soil moisture retrieval. In first approach, scattering coefficient of image is normalized with the scattering coefficient of bare soil (calculated with in situ observation of moisture and roughness) making the normalized data a function of vegetation cover which is represented by the NDVI. A quadric relationship was observed between the normalized scattering coefficient data and NDVI with coefficient of determination (R^2) 0.83. This quadric relationship sets the basis for the retrieval of soil moisture with the help of NDVI and normalized scattering coefficient from the PALSAR image. The root mean square error (RMSE) is 0.036 and 0.041 for retrieval of soil moisture when the algorithm is applied on test image and validating image, respectively. In the second approach, scattering coefficient of PALSAR data was normalized with the scattering coefficient of the dry soil providing the normalized data as a function of the soil moisture and vegetation cover defined by the NDVI. The relationship between normalized scattering coefficient and NDVI was explored which provide a set of lines defining the different range of soil moistures. The coefficient of determination (R^2) for all regressed lines was greater than 0.81. Hence, the soil moisture is retrieved with the developed empirical relationship between the normalized scattering coefficient of PALSAR data and NDVI. The root mean square error (RMSE) is 0.039 and 0.052 for retrieval of soil

moisture when the algorithm is applied on test image and validating image, respectively.

Finally chapter 7 draws the conclusion and contribution made in the thesis as well as presents the future work of the study carried out in this thesis.

Acknowledgements

This thesis could not have been in its present form without the assistance and support of many people who deserve special mention. First, I would like to express my sincere gratitude to my supervisor, Dr. Dharmendra Singh, for his unique guidance and supervision at every stage of the thesis work. He spent his precious time and effort directing this thesis work. His constant encouragement and stimulating discussions with him were helpful in taking this research to its fruitful ending.

I would also like to thank my supervisor Dr. N. P. Pathak for his generous support and encouragement from time to time. I would like to thank the members of my research committee Dr. M. K. Arora, Dr. M. V. Kartikeyan and Dr. M. J. Nigam for their helpful comments and suggestions during all my presentations related to research work. I would like to show my gratitude towards Head of the department for providing all the necessary facilities. It's my pleasure to thank University Grant Commission for financial support throughout the research work.

I am thankful to Mr. Giri, Mr. Raja Ram and Mr. B.S. Panwar, lab technicians of Basic and advanced microwave lab, for their help during the experimental work.

My heartfelt thanks and gratitude goes to Dr. Dharmendra Singh for providing me a space in his research lab with an ideal environment. I would like to thank all the former and present research scholars as well as the Junior Research Fellow, Mr. Vivek, Mr. Dharmveer and Mr. Tasneem, of Remote Sensing Lab for their support and help.

I would like to thank my seniors, Dr. Basudeb, Dr. Ravi and Dr. Rohit for their support, encouragement and suggestions during the initial days of my research. These were very fortunate years working with Triloki and Gaikwad Sir with whom I had

several discussions. Their patience and kind attention towards the problems faced by me during my research and their generous and ever ready attitude to help me find the solution is appreciated. I would like to thank Pooja and Vivek for their helping hand during image analysis studies. I am thankful to IDD and M. Tech. students, Pramod, Col. Prashant, Shivram, Maulik, Upendra, working with whom was an entirely different experience. I would like to thank Shashi Kant, Prashant, Ajaey and Vishal for the round of discussions we had altogether sometimes regarding research, some time social and philosophical. It was a very good experience to share my ideas and acknowledge theirs.

I would like to thank Shiv Sir, Manoj and Uma Shnkar for their constant support during the stay at campus. Special thanks to Mrs. Deepali and Mrs. Ragini for delicious food I had and homely environment I felt during my stay in the campus.

I would like to thank my younger brother and sister for their loving attitude and persistent support. At the end, I am and always will be the short of words to acknowledge the support of my parents. It was their patience, encouragement and faith in me that I could complete this work.

Rishi Prakash

Table of Contents

List of Figures

List of Tables

Acronyms

ADSSC	Angular Dynamic Range in Specular Scattering Coefficient
AIEM	Advanced Integral Equation Model
ALOS	Advanced Land Observing Satellite
ASCAT	Advanced Scatterometer
DLR	German Aerospace Centre
ENVISAT	Environmental Satellite
ERS	European Remote Sensing Satellite
ERSDAC	Earth Remote Sensing Data Analysis Center
HH–Polarization	Horizontal Horizontal Polarization
HV–Polarization	Horizontal Vertical Polarization
IEM	Integral Equation Model
LL–Polarization	Left Left Polarization
LR–Polarization	Left Right Polarization
MetOp	Meteorological Satellites operated by the European Organisation
MODIS	Moderate Resolution Imaging Spectroradiometer
MSAVI	Modified Soil Adjusted Vegetation Index
NDVI	Normalized Difference Vegetation Index
PALSAR	Phased Array Type L-band Synthetic Aperture Radar
QuikSCAT	Quick Scatterometer
RADARSAT	Radar Satellite
RISAT	Radar Image Satellite
RL–Polarization	Right Left Polarization
RR–Polarization	Right Right Polarization
SA	Scalar Approximation

SAR	Synthetic Aperture Radar
SPA	Stationary Phase Approximation
SPM	Small Perturbation Method
TanDEM–X	TerraSAR-X add-on for Digital Elevation Measurement
TerraSAR–X	Terrestrial SAR–X
VH–Polarization	Vertical Horizontal Polarization
VV–Polarization	Vertical Vertical Polarization
VWC	Vegetation Water Content

Chapter 1

Introduction

RADAR is an acronym for 'RAdio Detection And Ranging'. Radar is used for several purposes in which it is used as active sensing system which generates and uses its own energy to illuminate the target and record the scattered energy which carries the information content. Hertz in 1886 demonstrated the transmission of microwave and its reflection for various objects. The first fundamental radar was developed for ship detection. The detection of distant objects were made with ground based pulsed radar in 1920s and 1930s. The major developments on radar technology were during World War II and first imaging radar that was developed for detection and positioning of aircrafts and ships was during this time. After World War II, there was a pause in the development of new radar technology. The surplus military radars were put into the service for civilian use, primarily as weather and air traffic control radar. Further in 1960s, the radar were specifically developed and used for earth mapping purposes. Since this time, the development of air borne and space borne radar for environmental and earth mapping purposes has flourished [27].

The terms radar remote sensing and active microwave remote sensing are used interchangeably when the observations of earth are made in microwave spectrum with

radar technology. The active remote sensing systems that operate in the microwave region of electromagnetic spectrum include radiation with frequency spectrum ranges from 0.3 GHz to 300 GHz. This spectrum is subdivided in various bands, which are designated by letters. For earth observation studies, the most important bands are: L–band (frequency f = 1 to 2 GHz, wavelength λ = 30 to 15 cm), C–band (f = 4 to 8 GHz, λ = 7.5 to 3.8 cm) and X–band (f = 8 to 12 GHz, λ = 3.8 to 2.5 cm) [211]. The active microwave sensors on the basis of imaging techniques can generally be kept in two broad categories, i.e., imaging and non–imaging. The imaging active microwave sensors include the Real Aperture Radar (RAR) and Synthetic Aperture Radar (SAR), whereas the non–imaging active microwave sensors are Altimeter and Scatterometer. Microwave active sensors have many advantages like ability to obtain measurements anytime, regardless of the time of day or season as these systems do not rely on the solar illumination, and have capability to penetrate through the cloud, moderate rain and smoke. In addition to this the penetration ability of microwave at low frequency is such that it can penetrate through the vegetation by which soil characteristic covered by vegetation can be retrieved through proper inclusion of scattering behaviour of vegetation. The most commonly used applications of the microwave remote sensing are soil parameter monitoring, hydrological modeling, watershed mapping, land cover classification, fractional vegetation cover mapping, drought and flood predictions, urban modeling, sea surface temperature estimation, weather forecasting, environmental monitoring, agriculture and several other [33, 47, 52, 61, 63, 65, 79, 89, 99, 102, 109, 111, 112, 147–149, 163, 197, 198, 206, 208, 210, 224].

The active microwave sensors can be subdivided into two configurations which are based on the receiving mechanism of scattered energy. First configuration is when the transmitter and receiver are collocated or the transmitting antenna itself works as the receiving antenna and measures the radiation that is scattered back to its direction. Such kind of configuration is termed as monostatic active microwave sensor and second configuration is based on bistatic concept which utilizes the setup in which the receiver and the transmitter are located on different platforms and receiver operates passively to collect the scattered signal by the earth surface, originating from the microwave transmitter [155]. In the last two decades, most of the satellite missions carrying active microwave sensors are of monostatic configuration. Recently launched monostatic active microwave sensors are RADARSAT–2 (Radar Satellite,

Launch Year: 2007), PALSAR (Phased Array Type L–band Synthetic Aperture Radar, Launch Year: 2007), TerraSAR–X (Terrestrial SAR–X, Launch Year: 2007). The newly launched satellite mission that operates in bistatic domain is TanDem–X (TerraSAR–X add–on for Digital Elevation Measurement, Launch Year: 2010) which has been developed by the German Aerospace Centre (DLR) in association with the Astrium GmbH [195]. India has planned to launch RISAT–1 (Radar Image Satellite) at C–band in year 2011.

1.1. Motivation

The prominent soil parameters are soil texture, soil moisture and surface roughness which can be retrieved with active microwave remote sensing data. The knowledge of spatial distribution of these soil parameters is desirable in many applications. Prediction of erosion, irrigation scheduling, improving crop yield, climatology, meteorology, land use and management are some of the important applications related to soil texture, soil moisture and surface roughness [22, 83].

Characterization of soil parameters with active microwave remote sensing has been well documented in the literature when one is interested in monostatic domain [5, 10, 20, 41, 47, 50, 68, 80, 109, 169, 181, 190, 213, 216]. However, till date, the research in monostatic domain have been confined to develop an efficient and accurate tool and algorithm to retrieve soil parameters so that some simplified model can be developed to circumvent the complexity and need of *apriori* information. These requirements emphasize to explore the other domain of active microwave remote sensing. Scattering behavior in the bistatic configuration may be explored to investigate the characteristic of the soil parameters. The prime concern in bistatic was the complexity inherited for having transmitter and receiver on different platform. But, there has been a renewed interest of the researchers in the field of bistatic due to the extra degree of freedom gained in remote sensing observations of natural and manmade targets as well as the low cost of operation by sharing the expensive transmitter part of the system among several receivers [96, 140]. Along with this advantage, the bistatic configuration explores the possibility of mapping the earth with the existing monostatic satellite sensors, e.g., TanDEM–X. The TanDEM–X is

synchronized SAR satellite working in association with TerraSAR–X which is proposed to provide data in bistatic domain [97].

Soil moisture, surface roughness and soil texture are important soil parameters and these parameters show potential to be measured with active microwave remote sensing methods. Soil moisture and surface roughness has gained much attention of the research community involved in soil parameter characterization. At times the prime concern has been soil moisture retrieval and researchers have applied the methodology such as copolarization ratio to minimize the soil roughness and predict the soil moisture content [115]. Though, in case of soil roughness retrieval, multi–incidence angle approach has been utilized [159, 232], several other techniques such as change detection are prevalent in soil moisture and surface roughness retrieval. But in all these scenarios, more or less, the effect of soil texture has been neglected. Some of the researchers however incorporated the effect of soil texture in soil moisture retrieval but less attention has been given to soil texture [191, 212]. In addition to this, it has been shown that soil dielectric constant is dependent on soil texture. Further, it has proven that change in dielectric constant with moisture shows its dependency on soil texture [78, 127, 215]. Therefore, active microwave remote sensing, which is highly dependent on dielectric constant, may be explored to study the soil texture.

Another important factor in soil parameters analysis in active microwave remote sensing is soil parameters retrieval. Scattering coefficient, that is the only measured parameter in active microwave remote sensing, is a function of sensor parameters and target parameters. Sensor parameters include operating frequency, incidence angle and polarization whereas, target parameters include mainly dielectric constant and roughness that means when interest lies in soil parameters characterization then it will be soil moisture, surface roughness and soil texture. Many empirical and theoretical relationships exist that determines the dependence of scattering coefficient on various soil parameters [48, 59, 142, 144, 182, 202]. But, the inversion of these relations is difficult task due the involvement of many parameters on single scattering coefficient. To solve the problem of inversion, researchers have applied multi–incidence, multi–frequency and multi–polarization analysis [21, 100, 115, 122, 159, 180, 232]. Even though the empirical relations have the limitation of site and data dependency, theoretical models require specifying the surface characteristic with one or more surface roughness parameter(s); the problem of

defining optimal parameter for describing surface roughness has been investigated in many studies [25, 26, 41, 42, 86, 129, 143, 150, 160]. Unfortunately, these models have failed to accurately account for the complex geometry of natural soil surfaces. In these models, they have neglected the scattering from vegetation layer [211]. Therefore, there is a need to focus on soil parameters retrieval studies with remote sensing data.

In natural case, there is very less availability of bare soil fields. Generally, fields are covered with vegetation/crop/trees or pasture fields. So, the modeling of scattering and absorption effect in vegetation is another concern for soil moisture retrieval studies in vegetated areas with active microwave sensors. Scattering from the vegetated area incorporates the volume scattering from the vegetation cover and surface scattering from the underlying soil. In addition to this, vegetation provides the two way attenuation for the signal scattering from the underlying soil. Further, most of the models for soil moisture retrieval have been developed, tested and validated for the bare soil surfaces [5, 48, 80, 144, 193, 202]. However, bare fields are only a special case and agriculture fields are over large periods of their yearly cycle covered by different types of vegetation [76]. Most of the studies have used the water–cloud model proposed by Attema and Ulaby [8] to circumvent the problem of vegetation [2, 17, 220]. The other prevalent technique for soil moisture retrieval in vegetated areas are change detection techniques [131, 137, 145]. These techniques consider the scattering from the vegetation area to be time invariant. As the scattering contribution from the vegetation cover is a time variant process therefore, it restricts the applicability of the change detection techniques [88]. Some of the researchers have explored the possibility of employing the optical data in conjunction to microwave data to retrieve the soil moisture [141, 214]. Assumptions made during the development of these algorithms require quite *apriori* information. The existing models whatever methodology they employ, posses the limitation on the operational applicability. Therefore, more attention should be given to correct the vegetation effect in soil moisture retrieval studies with satellite data.

With the discussion made in the preceding paragraphs in nutshell following can be pointed:

- Active microwave remote sensing in monostatic domain has been widely and prominently used for soil parameters characterization. Whereas, the characterization in bistatic domain more or less remains elusive.
- The analysis of soil moisture and surface roughness has got more attention in comparison to soil texture.
- Several theoretical and empirical relationships have been developed to demonstrate the scattering behavior form different soil conditions but, retrieval of soil parameters with these developed relations still poses several limitations.
- To quantitatively analyze the soil moisture in vegetated area the researchers have utilized the water–cloud model, change detection techniques and the information fusion with optical data. Some of these models either require *apriori* information or are more complex for their operational applicability. The applicability of some models in larger domain has to be tested.

1.2. Problem Statement

This thesis deals mostly with the analysis soil parameters in bistatic domain. Along with the bistatic domain, the attention has also been given to retrieve soil moisture in vegetated areas with satellite image in monostatic domain. Following issues are addressed in the thesis.

- Characterization of soil parameters, i.e., soil texture, soil moisture and periodic surface roughness, in specular direction has been studied which is a special case of bistatic domain. It has been observed by various researchers that the strongest signal returns are in specular direction when the measurements are carried out in bistatic domain for soil parameter characterization.
- The response of specular scattering coefficient has been analyzed at 10 GHz (X–band) and 6 GHz (C–band) for the change is soil texture by varying the soil moisture and periodic surface roughness. Most of the reported work as well as the satellite missions that may be available in near future are proposed in X– and C–band, e.g., TanDEM–X. Therefore in this thesis the observations

of different soil fields in specular direction have been made at 10 GHz (X–band) and 6 GHz (C–band).

- Effect of soil texture on microwave scattering is still a less attended problem. Hence, attention has to be given to know the soil texture effect on microwave scattering with various field conditions in bistatic domain.
- Most of the soil parameter retrieval algorithms, both theoretical and empirical, have been developed and tested for the monostatic domain therefore; their applicability in bistatic domain has to be examined. However, the developed or available algorithm needs a quite good number of *apriori* information or guess value, like field data (e.g., roughness characterization for moisture retrieval), for retrieving soil parameters with monostatic or bistatic data. Still, there is a need to develop the retrieval algorithm specifically for bistatic domain.
- The effect of sensor parameters, i.e., polarization, frequency and incidence angle in bistatic domain for characterization of soil parameters has to be analyzed along with their utilization in retrieval of soil parameters.
- Soil moisture retrieval in vegetated area inherits several complexities because of the difficulties in describing the scattering phenomenon form the vegetation cover. Therefore there is a need to circumvent the problem of vegetation in soil moisture retrieval.

Based on these issues the thesis work has divided in four major tasks which are as following:

(a) To study the soil texture effect on specular scattering (i.e., in bistatic domain) at various incidence angles in both like polarizations (i.e., HH– and VV–polarization) at 10 GHz (X–band) by changing the soil moisture and periodic surface roughness.

(b) To study the specular scattering response of soil texture with varying soil moisture and periodic surface roughness at various incidence angles in both like polarizations at 6 GHz (C–band).

(c) To develop the soil parameters retrieval algorithm for bistatic configuration to minimize the need of *apriori* information.

(d) Development of a synergic approach for available satellite data like PALSAR (Phased Array type L–band Synthetic Aperture Radar) and MODIS (Moderate

Resolution Imaging Spectroradiometer) to minimize the vegetation effect for the retrieval of crop/vegetation covered soil moisture.

1.3. Details of Experiment Performed

This thesis concentrates on two major objectives. Firstly, it aims to study the effect of soil texture on specular scattering coefficient with change in soil moisture and periodic surface roughness which is performed by the ingeniously developed ground based scatterometer. The second main objective is to tackles the problem of soil moisture retrieval in vegetated area using satellite data especially SAR data which is performed by using PALSAR and MODIS data.

For achieving first objective, a ground based scatterometer is ingeniously developed whose brief description is as following:

1.3.1. Bistatic Scatterometer

Bistatic scatterometer was ingeniously developed in laboratory to operate at 6 GHz (C–band) and 10 GHz (X–band) in both like polarizations, i.e., HH– and VV–polarization. The designed bistatic scatterometer is capable of performing observations by changing the incidence angles form 25° to 70°. The schematic diagram of the bistatic scatterometer used for experimental analysis is shown in Figure 1.1. The system parameters such as antenna gain, beam width, frequency of operation, antenna type and cross–polarization isolation are given in Table 1.1. Figure 1.2 represents the coordinate system for scattering geometry. (θ, φ) define the incident direction of the transmitted power $P_p(\theta, \varphi)$ at polarization p, and (θ_s, φ_s) is the direction of the received power $P_q(\theta_s, \varphi_s)$ at polarization q. In case of specular scattering $\theta = \theta_s$, $\varphi = 0$ and $\varphi_s = 0$.

Table 1.1. System parameters

	6 GHz	10 GHz
Antenna type	Dual polarized paramedical horn	Dual polarized paramedical horn
Central frequency	6 GHz	10 GHz
Beam width in *H*–plane	16.7°	21.6°
Beam width in *E*–plane	15.2°	16.8°
Antenna gain	21 dB	20 dB
Cross-polarization isolation	40 dB	35 dB

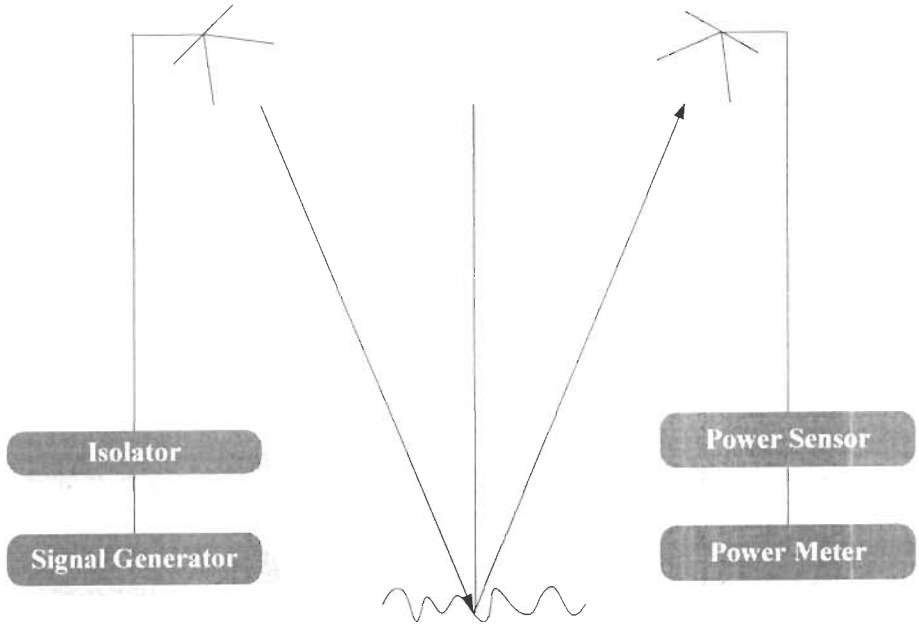

Figure 1.1. Schematic diagram of the bistatic scatterometer used for the specular scattering measurement.

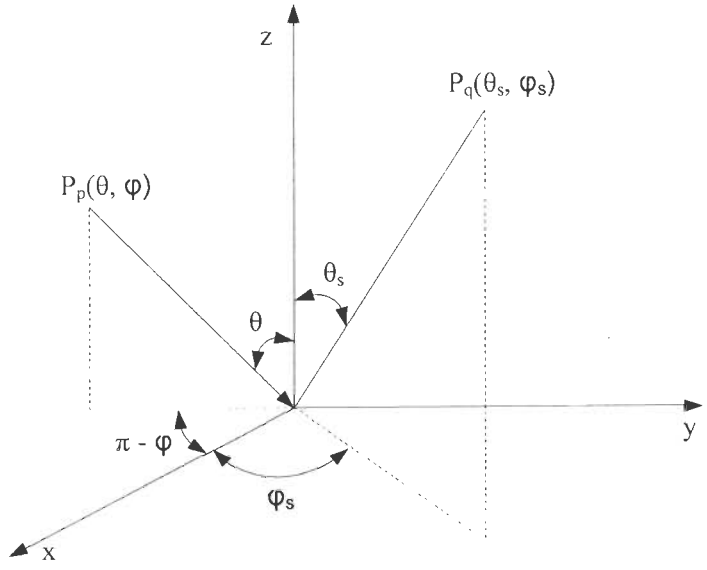

Figure 1.2. Coordinate system of scattering geometry.

To perform the experiment some scatterometer parameters have to be computed which are given as following:

(a) Illumination Area and its Need

The most important problem in radar measurement system is to maintain the main lobe of the radiation pattern in the area of interest. The main lobe of the radiation pattern is generally referred as the illumination area and is approximated by elliptical shape. The area of interest in case of characterization of soil parameters in controlled laboratory environment is the artificially generated soil bed. Figure 1.3 shows the geometry of the setup for illumination area [199]. To maintain the illumination area in the area of interest with the change in incidence angle, the position of antenna has to be varied in the x–y plane. In accordance to the Figure 1.3, the x and y position of the antenna are given by Equations 1.1 and 1.2, respectively [38].

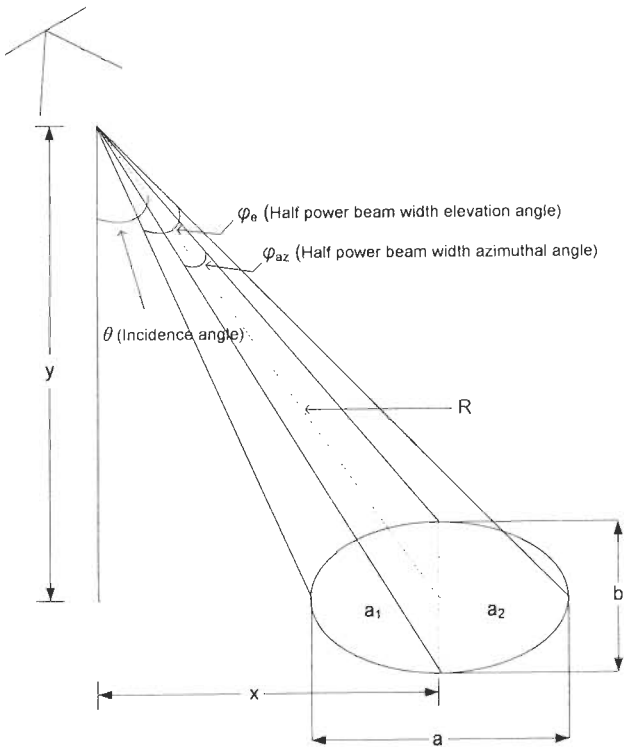

Figure 1.3. Illumination geometry to calculate the antenna position in the x–y plane.

$$x = R\sin\theta \tag{1.1}$$

and

$$y = R\cos\theta \tag{1.2}$$

where R is the distance from the antenna to the center point of the ellipse and θ is the incidence angle.

The major axis of the ellipse (a) is calculated by using Equation 1.3.

$$a = a_1 + a_2 \tag{1.3}$$

where

$$a_1 = R\sin\left(\frac{\varphi_e}{2}\right)\sec(\theta + \frac{\varphi_e}{2}) \tag{1.4}$$

$$a_2 = R\sin\left(\frac{\varphi_e}{2}\right)\sec(\theta - \frac{\varphi_e}{2}) \tag{1.5}$$

where φ_e is the elevation angle.

The minor axis (b) is calculated by Equation 1.6.

$$b = 2R\tan(\frac{\varphi_{az}}{2}) \tag{1.6}$$

where, φ_{az} is the azimuthal angle.

The area of Illumination (I) is equal to the area of ellipse and calculated by Equation 1.7.

$$I = \pi\left(\frac{a}{2}\right)\left(\frac{b}{2}\right) \tag{1.7}$$

Therefore,

$$I = \frac{\pi R^2}{2}\tan\left(\frac{\varphi_{az}}{2}\right)\sin\left(\frac{\varphi_e}{2}\right)\left[\sec\left(\theta + \frac{\varphi_e}{2}\right) + \sec\left(\theta - \frac{\varphi_e}{2}\right)\right] \tag{1.8}$$

It is evident from Equation 1.8 that I depends on R. In our experiment, we have kept I constant at approximately 1 m^2 and computed R by substituting antenna parameters, i.e., φ_e, φ_{az} and θ and according to that antenna position in x–y plain has been fixed.

(b) Computation of Specular Scattering Coefficient for Bistatic Scatterometer

Specular scattering coefficient was calculated at various incidence angles for different soil texture fields. Moisture and periodic surface roughness conditions were also considered. Following steps were involved in retrieval of specular scattering coefficient:

1) *Calibration*: Calibration is required to provide accurate quantitative results from the data collected. For the purpose, amplitude calibration was performed using absolute calibration technique [38]. Reference target used for calibration was aluminum sheet. Radar Cross Section (RCS) of flat aluminum sheet is given by Equation 1.9 [38]:

$$\sigma_{pp_{Al}}(\theta) = \frac{4\pi A^2}{\lambda^2}\left[\frac{\sin(kb\sin\theta)}{kb\sin\theta}\right]^2 \cos^2\theta \tag{1.9}$$

where $\sigma_{pp_{Al}}$ is radar cross section of aluminum sheet, A is area of aluminum sheet, λ is wavelength used, θ is the incidence angle, b is the dimension of square aluminum sheet, pp employs for HH– or VV–polarization and $k = 2\pi/\lambda$.
In decibel (dB), RCS of aluminum sheet can be written as Equation 1.10.

$$\sigma_{pp_{Al}}(\theta)(dB) = 10\log_{10}\sigma_{pp_{Al}}(\theta) \tag{1.10}$$

2) Radar cross section for soil can now be computed as given by Equation 1.11.

$$\sigma_{pp_{soil}}(\theta) = \left(\frac{P_{pp_{soil}}(\theta)}{P_{pp_{Al}}(\theta)}\right)\sigma_{pp_{Al}}(\theta) \tag{1.11}$$

where, $\sigma_{pp_{soil}}(\theta)$ is radar cross section for soil, $P_{pp_{soil}}(\theta)$ is power received for soil at various incidence angles and $P_{pp_{Al}}(\theta)$ is the corresponding power received for aluminum sheet at various incidence angles.

Scattering coefficient is defined as the radar cross section per unit area. In present case the illumination cell size was kept 1 m^2. Therefore, the division of radar cross section for soil by illumination area provides scattering coefficient [38]. Scattering coefficient for soil is represented by $\sigma^{\circ}_{pp_{soil}}(\theta)$. Scattering coefficient of soil in decibel (dB) can be written as Equation 1.12.

$$\sigma^{\circ}_{pp_{soil}}(\theta)(dB) = 10\log_{10}\sigma^{\circ}_{pp_{soil}}(\theta) \tag{1.12}$$

(c) Response of Sensor Parameters

Wavelength or Frequency, incidence angle and polarization are important sensor parameters that affect the scattering coefficient.

(i) Wavelength or Frequency: Wavelength is an important sensor parameter that decides the roughness and smoothness of the surface. A surface may be considered as smooth for one particular wavelength whereas the surface may be considered as rough for other particular wavelength. Two criterions are generally used to define the roughness or smoothness of the surface that is Rayleigh criterion and Fraunhofer criterion. Rayleigh criterion for characterizing the surface as smooth or rough is used in case of optical region, while for modeling the scattering behavior of natural surfaces in microwave region we use Fraunhofer criterion for characterizing the surface roughness [202]. Rayleigh criterion lays down the following criterion for characterizing a surface as smooth that is based on rms surface height (s).

$$s < (\lambda/8\cos\theta) \tag{1.13}$$

and the Fraunhofer criterion is given by Equation 1.14.

$$s < (\lambda/32\cos\theta) \tag{1.14}$$

where, λ and θ is the operating wavelength and incidence angle, respectively. Further, penetration of wave into the medium is also a wavelength dependent parameter. The penetration depth is the depth below the surface at which the wave's power has been reduced to 37% of its value at the point just below the boundary [86]. The penetration depth represents a measure of penetrability of a radar wave into the soil medium and the depth over which one would expect radar reflection [202]. A shorter wavelength penetrate less in to the medium whereas, a longer wavelength penetrates more.

(ii) Incidence angle: Incidence angle is another important sensor parameter that determines the scattering coefficient. Incidence angle describe the angular relationship between the radar beam and the target. The incidence angle causes variation in radar backscattering. The higher incidence angle returns less backscattering than the lower incidence angle from the same observed area. The incidence angle, usually considered different in the case of an inclined surface, is the angle between the incident radar beam and a line that is normal to inclined surface.

(iii) Polarization: The polarization of a uniform plane wave refers to the time varying behavior of the electric field strength vector at some fixed point in space. The horizontal and vertical polarizations are defined based on the direction of electric vector to the plane of incidence. The plane of incidence is the plane containing the incidence ray and normal to the surface. Therefore, when the electric vector is perpendicular to the plane of incidence, it is defined as the horizontal polarization (H–polarization) and when the electric vector is parallel to the plane of incidence, it is defined as the vertical polarization (V–polarization) [86]. Figures 1.4(a) and (b) show the wave having horizontal and vertical polarization respectively. The active microwave systems are capable of measuring the scattering response from target using different polarization configurations such as copolarized (HH and VV) and crosspolarized (HV and VH). The first term corresponds to the transmitted radiation from antenna whereas the second term corresponds to the received radiation by the antenna. The polarization configurations are used to retrieve more accurate information from the soil target. The need of multi–polarization is required for accurate retrieval of soil moisture [17, 144].

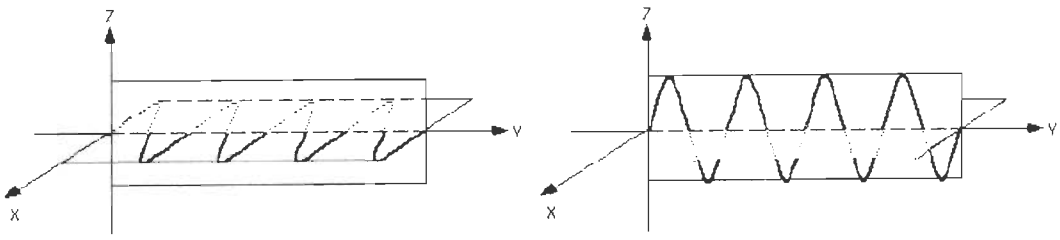

(a) (b)

Figure 1.4. (a) Horizontal polarization and (b) vertical polarization.

1.3.2. Soil Texture Measurement

Soil texture is a term commonly used to designate the proportionate distribution of the different sizes of particles in a soil. According to United States Department of Agriculture (USDA) system of nomenclature these soil particles are categorized as sand, silt and clay. The characterization of soil particles in differed categories is based on their diameter limits. The details on soil particle distribution are given in Table 1.2 [24, 55]. Different soil texture fields were artificially prepared by changing the percentage of soil constituent, i.e., sand, silt and clay. Sieve analysis and hydrometric tests were conducted to find out the percentage of sand, silt, and clay in soil. Sieve analysis using various sieves of different mesh opening (4.75 mm to 0.075 mm) were used to calculate the percentage of sand. The percentage of soil retained on each sieve is calculated on the basis of the total mass of the soil sample. In addition, soil fraction finer than 0.075 mm were separated out for further hydrometric test. Hydrometric test was carried out for particle size lesser than 0.075 mm to determine the percentage of silt and clay in soil [6].

Table 1.2. Nomenclature of soil constituent

Name of soil constituent	Diameter limits (mm)
Sand	2–0.05
Silt	0.05–0.002
Clay	Less than 0.002

1.3.3. Soil Moisture Measurement

Soil moisture is represented as the volumetric water content and defined as the fraction of the total volume of soil that is occupied by water contained in soil. Ten soil samples of up to 5 cm depth were chosen randomly to measure the soil moisture and average value of soil moisture were reported. Firstly these moist samples were weighted, afterwards kept for 24 hours at 110° C in oven and subsequently these dry samples were weighed. Volumetric soil moisture (m_v cm^3 cm^{-3}) was measured with the help of Equation 1.15 [42].

$$m_v = \frac{w_{moist} - w_{dry}}{w_{dry}} \times \rho_b \tag{1.15}$$

where w_{moist} and w_{dry} are weight of moist and dry soil sample, respectively and ρ_b is the dry soil bulk density.

1.3.4. Surface Roughness Measurement

(a) Characterization of Surface Roughness

Figure 1.5(a) shows the photograph of the periodic surface roughness generated with a wooden harrow. The aim of this thesis is to give more attention to characterize the soil texture by varying the moisture and roughness condition for bistatic domain. It is very difficult to generate the same isotropic surface for different soil texture fields in a controlled condition. Similar periodic surface roughness may be generated for different texture fields. Therefore, periodic roughness is considered for observing the effect of soil texture on specular scattering coefficient. The surface roughness can be explained based on horizontal roughness (i.e., x roughness) and vertical roughness (i.e., y roughness). The estimate of horizontal roughness is made with the correlation length, whereas the estimate of vertical roughness is made with rms surface height. The changes in surface roughness conditions, i.e., x and y roughness were made in controlled way with the ingeniously designed wooden spiked harrow [100, 129, 183]. The characterization of the soil surface roughness, i.e., the measurement of the rms surface height (s) and correlation length (l) were made with the help of pin profilometer. Figures 1.5(b) and 1.5(c) represent the example of

surface height profile and corresponding autocorrelation function respectively [202]. The rms surface height, s is defined by the mean height of the surface along with its second moment and given by Equation 1.16.

$$s = \left(\overline{z^2} - \bar{z}^2\right)^{1/2} \tag{1.16}$$

The autocorrelation function measures the similarity between the height z at a point x and at a point x' distant from x. The normalized autocorrelation function in discreet case is given by Equation 1.17.

$$\rho(x') = \frac{\sum_{i=1}^{N+1-j} z_i z_{j+i-1}}{\sum_{i=1}^{N} z_i^2} \tag{1.17}$$

where $x' = (j - 1)\Delta x$ and j is an integer ≥ 1. The surface correlation length l is defined as the displacement x' for which $\rho(x')$ is equal to $1/e$. The autocorrelation length of a surface explains the statistical independence of two points on the surface; if the two points are separated by a horizontal distance greater than l, then their heights may be considered to be approximately statistically independent of one another [202]. The autocorrelation function of each surface roughness condition was measured and exponential autocorrelation function was observed for each surface roughness profile. The exponential autocorrelation has been observed by several researchers for their measurements of roughness profile [26, 41, 177, 209]. Davidson *et al.* [41] have observed that the experimental correlation function and the exponential model are in very good agreement, whereas the match in the case of a Gaussian autocorrelation function is not as good.

(a)

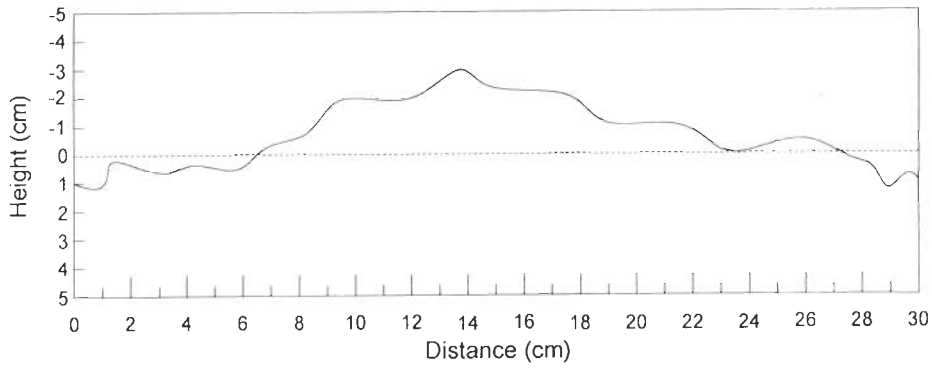

(b)

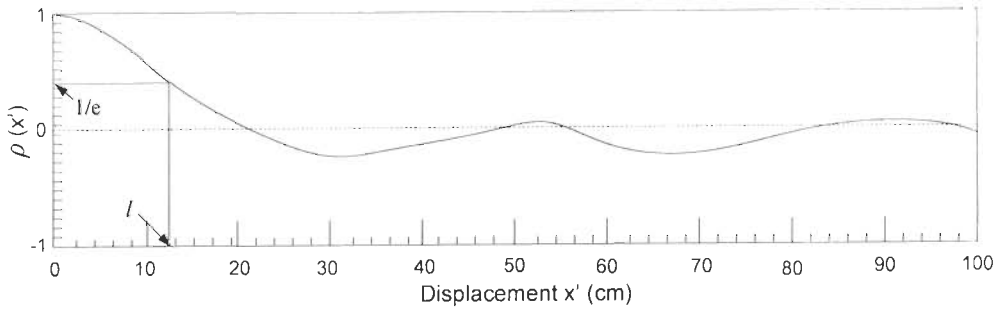

(c)

Figure 1.5. (a) Photograph of periodic surface roughness (b) example of surface height profile (c) corresponding autocorrelation function [202].

(b) Wooden Harrow for Creating the Periodic Surface Roughness

The periodic surface roughness of the soil fields was made with the help of the wooden harrow. Figure 1.6(a) depicts the photo of wooden harrow used during experimental investigation and Figure 1.6(b) shows a sample field roughness created by the wooden harrow. The design of wooden harrow provides the flexibility to increase or decrease the length of the spikes. This property of the wooden harrow is utilized to change the vertical roughness of soil field. Similar types of wooden harrows were designed so as to have different spacing between the consecutive spikes. Such measure provides the opportunity to vary the horizontal roughness of the field.

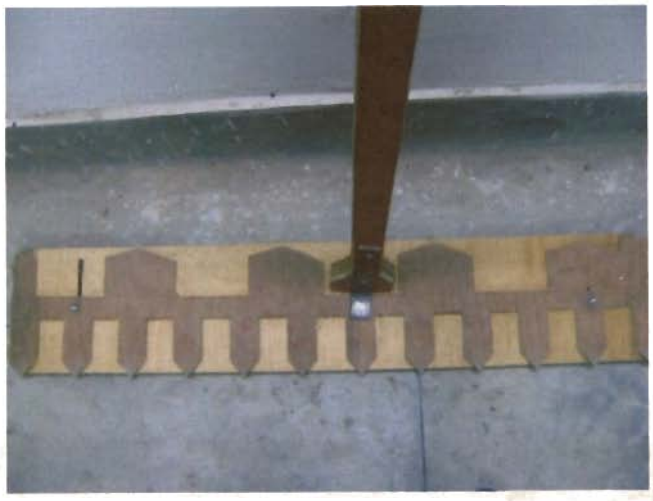

(a)

(b)

Figure 1.6. (a) Wooden harrow (b) Surface roughness created by the wooden harrow.

(c) Pin Profilometer for Measurement of Roughness

The measurement of the surface roughness parameters, s and l, was made with the help of pin profilometer of 1 m profile length [160]. Figure 1.7 shows the photograph of pin profilometer. The pin profilometer consist of equally spaced pin with separation of 1 cm in successive pins. The surface height variations were traced by the pin profilometer on a long graph paper. These values were subsequently used to retrieve the value of rms height and correlation length. The autocorrelation function of the each surface roughness condition was measured and exponential autocorrelation function was observed for each surface roughness profile.

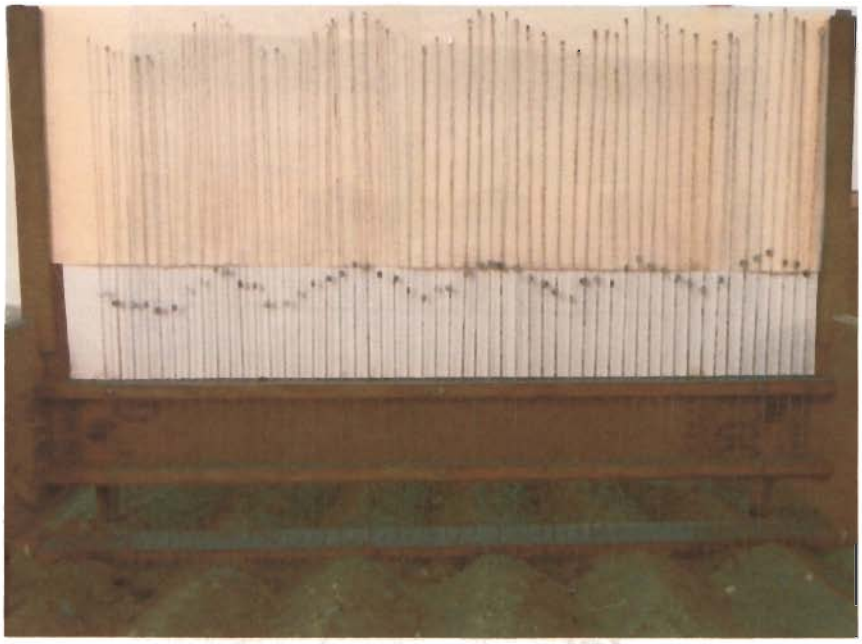

Figure 1.7. Pin profilometer for measurement of roughness.

1.4. Experimental Data Set

The objective of soil parameter characterization in bistatic domain has been achieved by analyzing the response of specular scattering coefficient whereas, the study of soil moisture retrieval in vegetated area has been performed by acquiring the satellite data.

1.4.1. Data in Bistatic Domain

The analysis for characterization of soil parameters in bistatic domain have been studied at 10 GHz (X–band) as well as at 6 GHz (C–band). Specular scattering coefficients at 10 GHz have been computed for four different soil texture fields (the sand, silt and clay constituents were varied from 78.4% to 38.7%, 33.1% to 9.1% and 18.7% to 4.3%, respectively) by changing the moisture contents from dry soil to 0.21 cm^3 cm^{-3} and periodic surface roughness from smooth surface to rms surface height 1.4 cm in both like polarizations (i.e., HH– and VV–polarization). The angular variation of these fields was analyzed by changing the incidence angle form 30° to 70° in 10° steps. A detailed discussion regarding the specular scattering data at 10

GHz and their analysis have been presented in Chapter 3. The response of specular scattering coefficient at 6 GHz has been checked in both like polarizations by changing the incidence angle from 25° to 70° in 5° steps for ten different soil texture fields (the sand, silt and clay constituent were varied from 85.3% to 2.3%, 70.6% to 7.5% and 81.6% to 2.5%, respectively) by varying the soil moisture content from dry soil to 0.425 cm^3 $cm^{-3}$and periodic surface roughness from smooth surface to rms surface height 2.45 cm. A detailed description of data and their analysis at 6 GHz has been given in Chapter 4.

The response of soil texture for specular scattering coefficient at 10 GHz was first analyzed. The observations revealed that it is difficult to observe change in specular scattering coefficient with change in soil texture for rough surfaces at 10 GHz. Therefore, less number of fields (i.e., 48 different fields conditions) as well as less number of incident angles (i.e., 30° to 70° in 10° steps) were observed to check the response of specular scattering coefficient (details are given in Chapter 3). Further, observations were made at 6 GHz with same number of fields and incidence angles and it was noticed that the differentiation among different soil texture fields can be made based on specular scattering coefficient at different periodic surface roughness conditions. Therefore more rigorous analysis was made at 6 GHz by observing 360 different field conditions and the incidence angle was changed from 25° to 70° in 5° steps which was earlier 30° to 70° in 10° steps at 10 GHz. Detailed field conditions of observations carried out at 10 GHz and 6 GHz have been given in Chapter 3 (Tables 3.1 and 3.2) and Chapter 4 (Tables 4.1, 4.2 and 4.3) respectively.

1.4.2. Satellite Data

Synthetic aperture radar (SAR) and optical data were used to effectively retrieve soil moisture in agriculture area. PALSAR (Phased array L–type synthetic aperture radar) is a polarimetric SAR sensor (i.e., contains HH–, HV–, VH– and VV– polarization) onboard Japan's Advanced Land Observing Satellite (ALOS). PALSAR sensor operates at 1.27 GHz frequency. Raw data was acquired on April 6, 2009 at an incidence angle 23.766°. Japan Aerospace Exploration agency (JAXA) and Earth remote sensing data analysis center (ERSDAC) are the two PALSAR data provider agencies. April 6, 2009 data was procured through the ERSDAC and is of VEXCEL 1.1 data format.

MODIS (Moderate Resolution Imaging Spectroradiometer) on board Terra (formerly EOS AM) and Aqua (formerly known as EOS PM) satellites provides data in optical, near infrared, shortwave infrared and thermal band. The instrument captures data in 36 bands and the data availability is at various resolution, i.e., 2 bands at 250 m, 5 bands at 500 m and 29 bands at 1 km. Band–1(620–670 nm) and band–2 (842–876 nm) data of spatial resolution 250 m acquired by the Terra satellite were utilized in conjunction with the PALSAR data of 25 m spatial resolution. The temporal resolution of PALSAR data is 46 days whereas MODIS data is available every day.

(a) Study Area for Satellite Data

Roorkee city of Uttarakhand state of India and its surrounding areas were chosen for the study of soil moisture with satellite data. Figures 1.8(a)–(d) show the map of India, map of Uttarakhand, topographic map of study area and Google earth image of study area, respectively. Two different areas were chosen for the study. The first study area lies between longitudes 77.803° E and 77.980° E and latitudes 30.000° N and 29.823° N. The second study area lies between longitudes 77.847° E and 78.024° E and latitudes 29.859° N and 29.682° N. The land cover of both the study areas is fairly flat and mainly consists of urban, water and agriculture classes. The major water bodies are Solani River and Upper Ganga Canal. Sugarcane, wheat and mustard were prominent vegetation cover in agriculture land along with barren land at the time of image acquisition (first week of April 2009). The key urban area in the study site is Roorkee city besides small villages scattered throughout the study site.

1.5. Framework of Research

The proposed research work has been carried out in two major domains. Firstly, the applicability of bistatic domain for soil parameters characterization have been analyzed and secondly, the problem of soil moisture retrieval in vegetated area has been investigated in monostatic domain for which satellite based SAR images with MODIS images have been used. Following steps were involved to accomplish the said task.

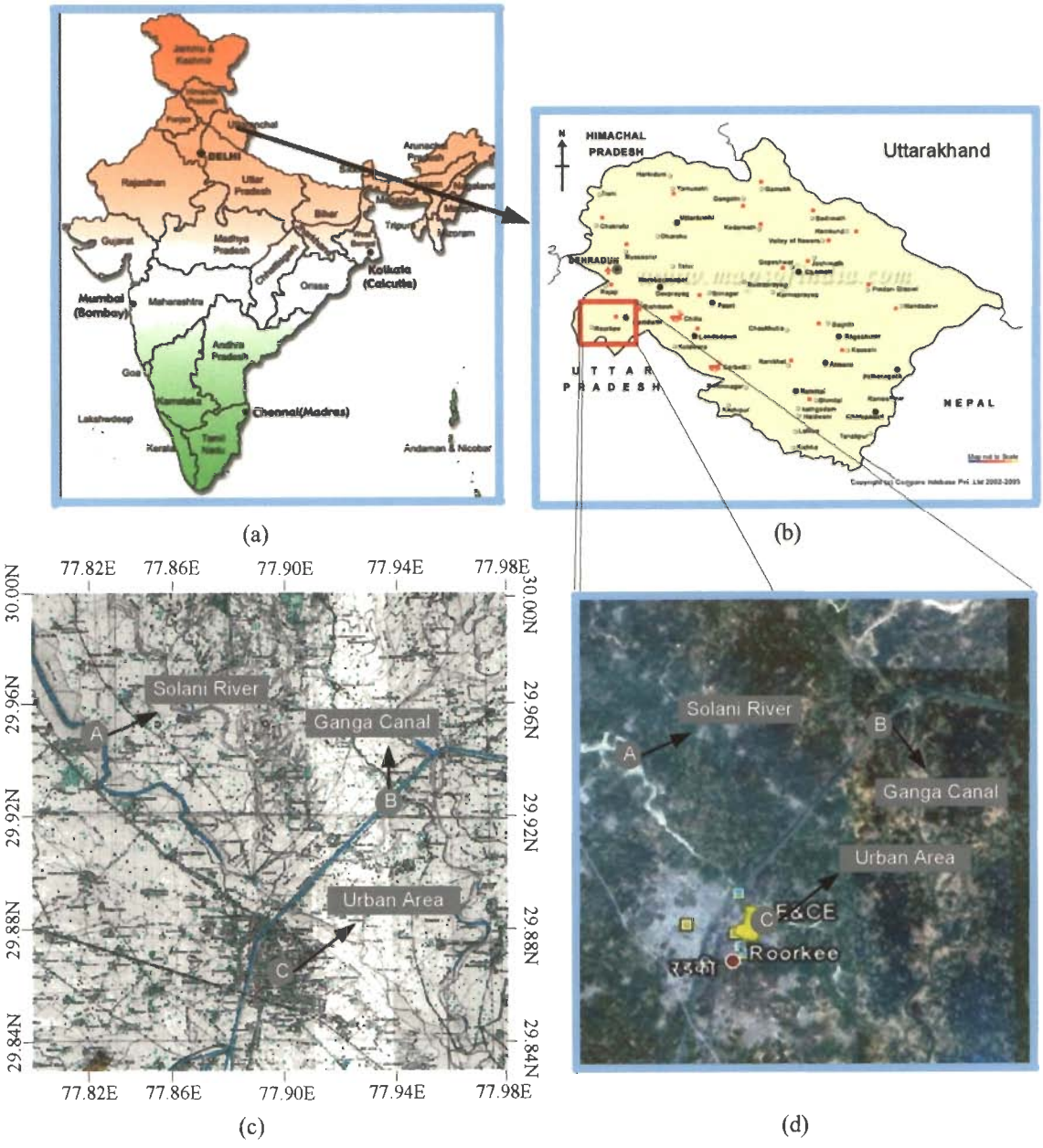

Figure 1.8. Study area (a) India (b) Uttarakhand (c) Toposheet of the study area (d) Google earth image of study area.

(a) Task Performed in Bistatic Domain

1. Bistatic scatterometer was developed for 6 GHz and 10 GHz that is capable of taking observations at various incidence angles in both like polarizations.
2. The experiment was carried out at 10 GHz for four different soil texture fields by observing four different moisture condition and three different periodic

surface roughness conditions. Therefore, total 48 field conditions were prepared for the observations.

3. The analysis of data observed as specular scattering coefficient was firstly studied for different soil texture fields. Secondly, the changes in soil moisture and periodic surface roughness were made to study the effect of specular scattering coefficient for different soil texture fields.
4. The response of specular scattering coefficient for different soil parameters was analyzed at 6 GHz by observing ten different soil texture fields and varying their moisture (6 moisture condition) and periodic roughness conditions (one smooth and 5 periodic roughness conditions). Therefore, total 360 field conditions were prepared for the observations.
5. The copolarization ratio was studied to check its response for various soil parameters. The study emphasizes the minimization of soil texture effect with copolarization ratio. This strategy was applied for retrieval of soil moisture whereas the periodic surface roughness of different soil fields was kept constant.
6. The effect of periodic surface roughness has major effect on scattering in microwave domain. The multi–incidence angle approach was studied which shows that the ratio of specular scattering coefficient at two incidence angle varies only with the surface roughness values whereas, its value is approximately same for change in soil moisture and soil texture. This strategy was followed for the retrieval of soil moisture, periodic surface roughness and soil texture.

(b) Satellite Data for Soil Moisture Retrieval in Vegetated Area

1. PALSAR data of level 1.1 VEXCEL format was preprocessed to calibrate and geocode.
2. MODIS optical data of band–1 and band–2 were utilized to generate the NDVI image.
3. Study was carried out to check the feasibility of retrieving the soil moisture in vegetated area with the information available through SAR and optical data in order to minimize the requirement of *apriori* information (like plant parameters i.e., leaf area index, crop height, biomass etc).

4. Different schemes were devised to normalize the scattering coefficient of the image and then relations between the normalized scattering coefficient and the NDVI (Normalized Difference Vegetation Index) obtained from MODIS data were developed to facilitate the retrieval of soil moisture crop/vegetation covered.

1.6. Organization of Thesis

Figure 1.9 show the flow chart of work carried out in this thesis. The organization of the thesis is as following:

A brief literature review consisting of research conducted in monostatic and bistatic domain for soil parameter characterization has been presented in Chapter 2. In continuation, this chapter discusses problems in soil parameters characterization, scheme for retrieval of soil parameters and their limitations. Chapter 3 discusses the experiments carried out to study the effect of soil texture on specular scattering coefficient with different soil moisture and periodic surface roughness conditions at 10 GHz in both like polarizations. The observations were made at different incidence angles to analyze the angular behavior of specular scattering coefficient for different fields (four different soil texture fields, four moisture conditions and three periodic roughness conditions and therefore a total of 48 different field conditions were analyzed). The problem encountered at 10 GHz was the study with periodic surface roughness. It was difficult to observe the change in specular scattering coefficient with change in soil texture for rough surfaces in both like polarizations at all incidence angles. Therefore, the experiments were carried out at 6 GHz (C–band) to circumvent the problem of surface roughness on specular scattering coefficient while observing the soil texture. A detailed analysis of change in specular scattering coefficient for change is soil texture with different moisture and periodic roughness conditions (ten different soil texture fields, six moisture conditions and six periodic roughness conditions and therefore a total of 360 different field conditions were analyzed) in both like polarizations for various incidence angles is made at 6 GHz and discussed in Chapter 4. The problem of soil parameter retrieval is taken in Chapter 5. Two methodologies based on copolarization ratio and multi–incidence angle have been utilized to retrieve soil parameters. Further, Chapter 6 presents a synergistic

approach based on satellite data (PALSAR and MODIS images) to retrieve soil moisture in vegetated area. This chapter discusses the importance of the SAR data in concurrence with optical data to retrieve the soil moisture incorporating vegetation effect with the requirement of minimum *apriori* information. Finally, Chapter 7 includes the contribution along with the future prospect of the work carried out in the thesis.

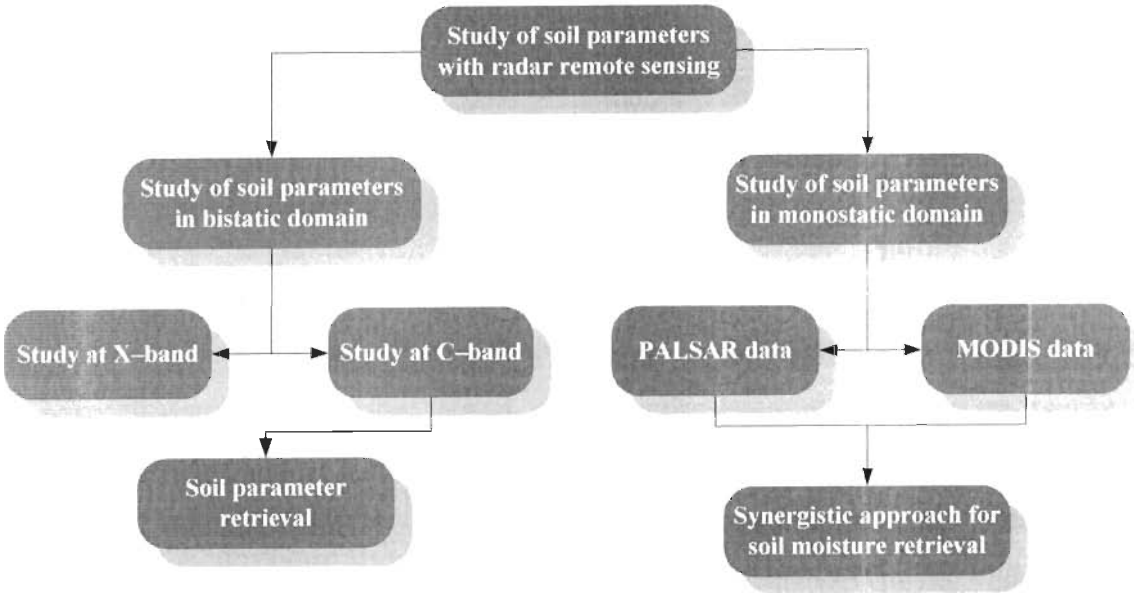

Figure 1.9. Flow chart of the organization of thesis.

Chapter 2

Brief Literature Review

This thesis aims to characterize the soil parameters in the bistatic domain as well as soil moisture retrieval in vegetated area with the fusion of information from synthetic aperture radar and optical data. Therefore, this chapter will present a brief review on the studies carried out for soil parameter characterization and its retrieval with active microwave remote sensing. For last forty years (approximately), researchers have been working in this field, but, still lots of challenges exist. Researchers have used various sensors like ground based, airborne and spaceborne sensors to study various parameters for earth, atmosphere and ocean. For analyzing the data, various theoretical, empirical and semi–empirical models have been developed and work is still going on. It is already mentioned that this thesis is focused to characterize soil parameters with active microwave remote sensing data. Therefore, the brief review on theoretical models, empirical and semi–empirical models for soil parameters characterization is presented first. Further, the matters related to the soil moisture retrieval in vegetated area with satellite data has been reviewed along with the various methodologies used to circumvent the problem in vegetation characterization for soil moisture retrieval.

2.1. Theoretical Models

The measurement in active remote sensing is in the form of scattering coefficient. The scattering coefficient is the fraction that describes the amount of average scattered energy in the direction of receiver compared to the energy of the incident field. Sensor parameters (i.e., frequency, incidence angle and polarization) and soil parameters (i.e., soil texture, soil moisture and surface roughness) are the deciding factors for the intensity of scattering coefficient [124, 165, 201, 202]. The knowledge of soil parameter, i.e., surface parameters and dielectric constant, was exploited to develop the models based on the scattering laws [170, 175]. The surface parameters are generally defined by the rms surface height, s, and correlation length, l. A detailed discussion regarding the surface parameters has been given in Chapter 1. The most popular theoretical models based on scattering laws are Kirchhoff Approximation (KA), Small Perturbation Model (SPM) and Integral Equation Model (IEM) with its amendment to Advanced Integral Equation Model (AIEM) [15, 35, 51, 168, 202, 209]. Kirchhoff Approximation considers the horizontal dimension of the surface to be larger than the wavelength whereas, no such restriction is required on the surface standerd deviation. KA is further divided in two parts viz., Kirchhoff Stationary Phase Approximation (SPA) that is also known as Geometrical Optics model (GO) and Kirchhoff Scalar Approximation (SA) that is also known as Physical Optics model (PO), based on the surface standard deviation [15, 202]. SPA works for the large surface standard deviation and considers purely noncoherent scattering whereas, SA can be applied where the surfaces generate both coherent and noncoherent scattering. The validity range for SPA is $ks > 2$ and SA is $ks < 1$ and $rms_{slope} < 0.25$, where k, s and rms_{slope} are the wave number, surface standard deviation and rms surface slope, respectively [202]. The consideration of SPM is made when both the surface standard deviation and correlation length are smaller than the wavelength [51, 168, 202]. The validity range for the SPM is $ks < 0.3$ and $rms_{slope} < 0.3$ [202]. The IEM encompasses the validity range of both the KA and SPM therefore; it is capable of characterizing the scattering coefficient for a wide range of surface roughness values [57, 59, 218]. The IEM model considers surface scattering term only whereas, second order scattering is not considered. However, Fung *et al.* [58] improved the model to take into account multiple scattering terms but due to the

complexity inherited the original version is rarely used and often replaced by the approximate solutions [15].

These theoretical models have been employed by several researchers for retrieval of soil parameters with active microwave remote sensing data [2, 3, 18, 25, 35, 37, 39, 86, 107, 141, 156, 157, 160, 177, 189, 202]. Franceschetti *et al.* [56] has explored the SA and SPM to retrieve the soil dielectric constant and surface geometry while defining the surface geometry with fractal parameters, i.e., fractal dimension, Hurst coefficient and topothesy. They have used the fractal parameter instead of the conventional surface roughness parameters, i.e., correlation length and surface standard deviation, as these parameters better represent the natural surfaces [66, 67, 164, 200, 222]. The copolarization ratio approach has been used to minimize the roughness effect and to retrieve of dielectric constant the copolarization ratio at two incidence angel was used to optimize. This retrieved dielectric constant was used with theoretical model to give the estimate of the surface roughness values [56]. Collaro *et al.* [35] have retrieved the mean radius of curvature for Gaussian rough surfaces with the utilization of Kirchhoff Approximation. The retrieval of soil parameters with IEM generally includes the fitting of IEM numerical simulation for a verity of soil moisture and roughness conditions, including look up tables [25, 196], neural networks [141, 174], Bayesian approaches [141] and minimization techniques [11, 146].

Some of the researchers had pointed out the difficulty in simulating the radar scattering coefficient from the theoretical model as two fold. Firstly, the mathematical modeling of the natural surfaces is still insufficient and secondly, the physical approximations introduced in the model are not *a posteriori* verified [209, 230]. These theoretical models have been generally validated in the laboratory environment therefore, providing quite satisfactory results [82, 113, 116]. However, in case of natural surfaces some contradictory results have also been reported [1, 13, 161]. This may arise due to the large intra field variability in surface roughness and moisture content of the agriculture fields which is not encountered in the laboratory conditions [209]. The inversion of theoretical models is another area of concern due to their complexity as well the need of *apriori* information.

These theoretical models have been basically developed with consideration of the soil surface roughness and soil moisture, whereas very less attention has been provided to include the soil texture effect in these developed models. Nevertheless, the studies have shown the dependency of scattering behavior on soil constituents. It

has been shown that the scattering coefficient changes with the change in soil constituents [202]. Singh and Kathpalia [181] have retrieved the soil texture map based on backscattering coefficient data that was acquired with ERS–2. Aubert *et al.* [9] has studied the effect of soil texture on TerraSAR–X data and have analyzed the change in backscattering coefficient with change in soil composition. Prakash *et al.* [156, 157] have conducted the experiment with bistatic scatterometer and shown the dependency of specular scattering coefficient on soil constituents. Some other researchers have also shown the feasibility of studying the soil texture with active microwave data [32, 78, 84, 119, 127, 162, 179, 191, 212, 215, 228, 229]. Although, these theoretical models have been solved based on scattering laws, they have been developed, tested and validated in monostatic domain [2, 3, 25, 35, 37, 56, 88, 107, 141, 158, 177, 189] and their applicability have lesser been checked in bistatic domain [30, 43, 90, 140, 155, 156, 157].

2.2. Empirical Models

The inherent complexity of the theoretical models as well as other difficulties encountered in the retrieval of soil parameters led to the development of the empirical and semi–empirical models. Several researchers have developed empirical relationships between soil parameters and scattering coefficient [26, 31, 34, 80, 101, 114, 123, 135, 136, 141, 145, 150, 157, 167, 171, 182, 193, 202, 207, 231]. In case of bare soil, a linear relationship was observed between the scattering coefficient and soil moisture with the assumption of the constant surface roughness over the different span of observation of the same field [132]. Some other forms of the relationships have also been devised. But, the inconsistency has been generally observed in the empirical coefficients, as well as, these coefficients vary for the different fields. Therefore, the applicability of these models can not be confirmed for the study area other than the area where they have been developed. However, to employ the empirical relation to the environmental condition where they have not been developed, the empirical relationships have to be again calibrated or the empirical coefficients have to be again established with data set of that particular study region. This kind of approach will always need a substantial amount of data. Further, the empirical relationships are solely developed based on the available data and in situ measurements therefore; their robustness cannot be ascertained.

2.3. Semi–Empirical Models

Semi–empirical models represent a compromise between the complexity of the theoretical models and simplicity of empirical models. The semi–empirical models are developed initially with the theoretical foundation and then the simulated or the experimental data sets are used to simplify the theoretical model [15, 19, 138, 209]. These models are more robust than empirical model. The most widely used semi–empirical models for soil parameters retrieval studies are Oh *et al.* [144] and Dubois *et al.* [48]. Some other semi–empirical models are Shi *et al.* [177], Loew and Mauser [108], Song *et al.* [189]. Oh *et al.* [144], Tabatabaeenejad and Moghaddam [194] and Kseneman *et al.* [98] carried out the experiment with truck mounted scatterometer in L–, C– and X–band. The experiment was carried out in polarimetric mode, calculating the scattering coefficient in HH–polarization (σ°_{HH}), HV–polarization (σ°_{HV}) and VV–polarization (σ°_{VV}). This model relates the dielectric constant of soil and rms surface height to the copolarization ratio p ($=\sigma^{\circ}_{HH}/\sigma^{\circ}_{VV}$) and crosspolarization ratio q ($=\sigma^{\circ}_{HV}/\sigma^{\circ}_{VV}$). The validity range of the model is $0.09 \leq m_v \leq 0.31$ and $0.1 \leq ks \leq 6$. Where m_v is volumetric soil moisture, k is wave number and s is rms surface height. Dubois *et al.* [48] developed a model that relates the scattering coefficient in HH– and VV–polarization to the dielectric constant of soil and rms surface height. The model development was based on the data acquired through the scatterometer in the frequency range 1.5 GHz and 11 GHz. The model is best applicable to the bare soil whereas significant amount of vegetation cause the under estimation of soil moisture and overestimation of rms surface height. Dubois *et al.* restricted the validity of the model to $ks \leq 2.5$ and $m_v \leq 0.35$. Shi *et al.* [177] developed a semi–empirical model based on the Integral Equation Model (IEM). Firstly, backscattering coefficients were simulated by IEM and then a regression analysis was applied to provide more simplified model in order to make the implementation of the IEM more practical as well as inversion more cohesive. The model development was based on the data observed in L–band and the model is valid for copolarized terms. Song *et al.* [189] has simplified the complicated the IEM model so that the radar backscattering coefficient becomes an explicit function of soil dielectric constant or the soil dielectric constant is an explicit function of radar

backscattering coefficient. This model had been named empirical adopted IEM (EA–IEM). The average difference of the backscattering coefficient between EA–IEM and original IEM was 0.14 dB in HH–polarization and 0.12 dB in VV–polarization. They have used this model to retrieve the soil moisture directly from radar backscattering coefficient. Tabatabaeenejad and Moghaddam [194] have studied the retrieval of soil moisture by developing the algorithm based on small perturbation model. They modeled soil as a layered structure with a rough boundary on top and a stratified medium below to represent moisture profile and retrieval has been carried out by simulated annealing. Kseneman *et al.* [98] have modified the Shi *et al.* [177] model to retrieve the soil moisture. They have utilized the high–resolution and dual polarized Spotlight TerraSAR-X images for soil moisture parameter retrieval.

The semi–empirical models mentioned above, like theoretical and empirical model, have been developed to retrieve the soil parameters in monostatic domain. The basic concept of the semi–empirical model is based on the simplification of complex theoretical models to make the retrieval of soil parameters more practical and cohesive. Therefore, to simplify the theoretical model the experimental data set is used in a way to develop some new algorithm whose foundation lies on theoretical model. Because of the experimental data evolved in the processes of algorithm development and if the experimental data belong to monostatic domain, the developed algorithm cannot be directly applied for the data in bistatic domain. In this regard, semi–empirical model, that should be applicable in bistatic domain, have to be developed based on the data set obtained in bistatic domain. Further, as discussed in Section 2.1 that soil texture is an important soil parameter and more or less has been neglected in development of theoretical models. Similar is the case of semi–empirical model where the effect of soil texture in the model development has been overlooked.

2.4. Research in Bistatic Domain

The characterization of soil parameters has been prominently established for monostatic system [42, 48, 50, 146, 174, 181, 182] and lesser studies have been performed for bistatic system [30, 129, 140, 180]. Chapter 1 has discussed in detail the need and advantage of bistatic domain for characterization of soil parameters. The research in bistatic domain for characterization of soil parameters has mostly been performed with theoretical model and simulation study. The prevalent theoretical

models, i.e., SPM, SPA, KA, IEM and AIEM, have been solved to provide the scattering coefficient in bistatic domain. Wu *et al.* [219] studied the bistatic scattering using AIEM. The bistatic scattering coefficient was obtained by keeping all the surface current term in the Kirchhoff surface field. Additionally, they compared the SPM, SPA and SA models at their respective validity region. The scattering coefficients were computed by keeping the transmitted angle and received angle constant whereas, changes in received azimuthal angles were made [219]. They have concluded that the AIEM predictions for bistatic scattering are in good agreement with the known models at respective valid regions in term of angular, frequency and polarization. Pierdicca *et al.* [155] has analyzed the contribution of bistatic radar measurement for bare soil moisture retrieval. They performed a simulation study based on AIEM model and discussed the feasibility of soil moisture analysis in specular direction. Ceraldi *et al.* [30] provided a copolarization ratio based scheme for the retrieval of soil dielectric constant in bistatic case minimizing the effect of surface roughness. The proposed scheme is based on the use of the ratio of power densities scattered at HH– and VV–polarization along the specular direction and it has been shown that in the specular case SPM, SA and SPA all leads to the same expression of the copolarization ratio; therefore, the proposed method is expected to hold a wide range of surface roughness. Further, they have used the method of moment simulation to support their theoretical analysis. Khenchaf [93] has analyzed scattering in bistatic domain from randomly rough surface using Kirchhoff approximation (stationary approximation and scalar approximation) and small perturbation model. They have also established the validity of the Kirchhoff and small–perturbation rough surface scattering models in bistatic domain. A comparison between the numerical calculations and the models has been made for various surface heights and correlation lengths. Xu and Tsang [221] have studied the bistatic scattering and emissivities of surfaces with exponential correlation function by numerical simulation. They have utilized the Maxwell model with 2–D simulation. Brogioni *et al.* [23] have investigated the bistatic scattering coefficient to soil moisture and surface roughness. The simulation has been carried out with advanced integral equation model and small perturbation model. These models where then validated with the numerical simulation carried out with FDTD (Finite Difference Time Domain). The study was carried out for L– and C–band. Some other researchers have carried out the theoretical as well as simulation study to describe the scattering in bistatic domain [29, 36, 44, 46, 49, 53,

60, 94, 95, 104, 117, 120, 121, 130, 180, 225] as well as the system conceptualization such as antenna design, resolution [62, 64, 70–74, 151]. The experimental analysis in bistatic domain for characterization of soil parameter has been less reported. Very few researchers have made the experimental measurements in controlled environment to verify the simulated and theoretical results. Such kind of experiments are very much necessary when the observations are made in natural conditions for soil parameters, i.e., soil moisture, surface roughness and soil texture, because these parameters are highly variable in space and time. In addition to this, all the simulation and theoretical studies rely on the parameterization of surface roughness and utilizes rms surface height and correlation length as surface parameter but, studies have shown that correlation length is a highly variable parameter. Nashashibi and Ulaby [139, 140] explored the nature of bistatic scattering from soil surface by performing the measurement at 35 GHz. The acquired data was analyzed to determine the angular sensitivities of several attributes of the scattered field, including amplitude and phase different of the polarized scattering coefficient and their copolarized and crosspolarized ratios. They have observed the strongest bistatic returns along the specular direction. In addition to this, it has also been shown that the calculation based on Kirchhoff Scalar Approximation provides good agreement between the theory and observations. Khadhra *et al.* [90] has carried out the well controlled experiment in bistatic domain at X–band for different roughness and moisture values. They have utilized the copolarization ratio approach develop by Ceraldi *et al.* [30] to retrieve the soil moisture and subsequently the IEM to retrieve the surface roughness. De Roo and Ulaby [43] conducted the experiment to determine the nature of the bistatic scattering from rough dielectric surface at 10 GHz. The observation was obtained for specular scattering with incidence angle varying from 20° to 60° in both HH– and VV–polarization for different moisture and roughness conditions. They have shown that the Kirchhoff Scalar Approximation provide good agreement with the experimental data. Therefore, it may be said that studies in bistatic domain for characterization of soil parameters should be made in specular direction due to the strongest bistatic return in this direction [30, 139, 140].

2.5. Retrieval of Soil Parameters

Empirical, semiempirical or theoretical model generally describe the behavior of scattering coefficient at different polarization, frequency and incidence angle as a function of soil parameters, i.e., soil texture, soil moisture and surface roughness. But, the main objective is to retrieve soil parameters from radar observations, i.e., scattering coefficient at different polarizations, incidence angles and frequencies. The major research work, till date, is in the direction of monostatic domain and there exist several ground based, airborne and spaceborne data in monostatic domain. Therefore, substantial amount of studies have followed this path by developing the direct model, i.e., scattering coefficient as function of soil parameters, and their inverse analysis. The retrieval of soil parameters with inversion of direct relationship is generally referred as the ill–posed problem because the direct relationship explain the dependency of single scattering coefficient on several soil parameters, i.e., soil texture, soil moisture and surface roughness. Therefore, researchers have utilized the data available at different polarization, incidence angel and different frequency to solve the problem of soil parameters retrieval [77, 118, 152]. In addition to this, several researches have applied the change detection techniques [5, 153, 211, 231].

Srivastava *et al.* [192] have proposed an approach based on scattering coefficient data at two incidence angels to incorporate the effect of surface roughness in the estimation of soil moisture. The scattering coefficient data of RADARSAT–1 at low incidence angle (= 25°) was normalized with high incidence angle (= 50°) to incorporate the effect of soil roughness in retrieve the soil moisture. Zribi *et al.* [232, 233] has demonstrated the use of multiincidence angle data to retrieve the rms surface height. They have shown that the normalization of data at one incidence angle to other incidence angle provides the normalized scattering data that varies only with rms surface height and independent to the changes in soil moisture content. They have utilized this methodology to retrieve the soil moisture with ERS (Scatterometer and SAR) and ENVISAT–ASAR data. Rahman *et al.* [159] have shown with IEM simulation that normalized scattering coefficient data with two incidence angles is function of surface roughness only. Further, they utilized this concept in retrieval of surface roughness and subsequently used IEM model to retrieve soil moisture.

Several researchers have proposed the use of multi–polarization data to minimize the roughness effect in order to retrieve the soil moisture without

characterizing surface roughness [30, 56, 115, 156]. Franceschetti *et al.* [56] has shown the potential of theoretical models, SPM and KA, to retrieve the dielectric constant with minimizing the roughness effect by copolarization ratio approach. Whereas, Ceraldi *et al.* [30], Prakash *et al.* [156] and Singh and Dubey [180] have shown the strength of copolarization ratio for minimization of roughness effect in bistatic domain with theoretical models, e.g., SPM, SPA and SA. Magagi and Kerr [115] investigated the semi–empirical model developed by Oh *et al.* [144] to minimize the soil roughness effect in soil moisture retrieval by copolarization ratio approach. Therefore, the use of SAR data with both like polarization, i.e., HH– and VV–polarization, (e.g., PALSAR) will provide an upper hand in soil moisture retrieval in comparison to single polarization SAR data, e.g., ERS data.

Scattering coefficient data at different frequencies have also been utilized to retrieve soil parameters [21, 31, 54, 100, 116, 122, 146]. Paloscia *et al.* [146] has utilized the microwave emission data at L–band to retrieve the soil moisture whereas the data at X–band has been utilized to correct the effect of vegetation. Ferrazzoli *et al.* [54] has investigated the use of SAR data at different frequency in discriminating among various vegetations and its sensitivity to agriculture. It has been shown that a combined use of P– and L–band data allow to discriminate between agriculture field and other targets while a combined use of L– and C–band data allows discriminating within agriculture area. L–band data is useful for crop with low plant density, while crop with high plant density, both L– and C–band are useful. Mattia *et al.* [122] have analyzed effect of the multi–frequency, polarimetric SAR data over the Matera (Italy) test site. They have studied the possibility of extracting relevant information about surface roughness using multi–frequency and polarimetry.

Most of the theoretical or empirical models have been developed and tested for monostatic case and consider back scattering. Empirical relationship developed for monostatic case cannot be applied for bistatic case as they are highly data dependent and scattering for both the cases follow different set of rules. Whereas, theoretical models based on scattering laws can be solved for bistatic case. But the problem with the theoretical model is that they describe the surface in terms of rms surface height and correlation length and studies have shown that the precision of correlation length measurement is very poor and highly variable [12, 41]. In addition, the complexity inherited with the theoretical models make the inversion a tedious job. Neural Network, a machine learning approach and Bayesian, a statistical based approach

finds it's application in many fields such as predication of ground vibration in mines, multi–target tracking [91, 92, 184, 185, 227]. These approaches have also been utilized for retrieval of soil parameters [15, 146, 209].

The algorithms for retrieval of soil parameters has been mostly dealt in monostatic domain because maximum researchers used various experimental studies (i.e., ground based, air borne) in monostatic domain due to easy implement in the hardware. Therefore, the general trend of research is directed in the analysis of soil parameters in monostatic domain. But, due to several advantages of bistatic domain such as low cost of operation, integration with existing satellite constellation have made the interest of researchers in bistatic domain. Theoretical models deal with the fundamental of scattering laws and have been solved for monostatic case whereas for the interest on bistatic these models can be solved to provide the scattering coefficient in bistatic domain. Further, the soil parameters retrieval scheme carried out in monostatic domain with multi–incidence, multi–polarization and multi–frequency can also be checked for their applicability in bistatic domain with theoretical models. The empirical and semi–empirical approach developed in monostatic domain is fundamentally based on the data in monostatic domain; hence they cannot be directly applicable in bistatic domain. However, the basic principle involved in the development of algorithm in the monostatic approach can be carried out for bistatic data and their applicability can be tested and validated.

2.6. Soil Moisture Retrieval in Vegetated Areas with Satellite Data

Most of the techniques for soil moisture retrieval through active microwave remote sensing have been developed for bare soil [5, 16, 48, 80, 144, 193, 205]. These techniques cannot be directly applied in the vegetated areas as the vegetation provides the multiple scattering effects. Due to this multiple scattering effect the observed backscatter is highly nonlinear [141, 173]. Now the problem arises in the separation of the scattering contribution of the vegetation and scattering contribution of the soil moisture from the observed backscattering coefficient. Some advances have been made to characterize the vegetation. Most of the technique to retrieve the soil moisture in presence of vegetation utilizes semi–empirical water cloud model [2, 17, 178, 220]. Water cloud model represents the canopy as a cloud of water droplet and

higher order scattering contribution are neglected. Bindlish and Barros [17] incorporated water cloud model to retrieve the soil moisture in vegetated area. They have introduced the concept of the vegetation correlation length to model the vegetation spacing within the water cloud model. To implement the proposed model several vegetation parameter have to be estimated or one should have *apriori* information of these vegetation parameters. Xu *et al.* [220] has utilized the water cloud mode to remove the vegetation effect from the observed backscattering coefficient, while having the knowledge of vegetation parameters, i.e., vegetation height, vegetation water content etc. Several other researchers [2, 18, 40, 105, 204] have also attempted to retrieve the soil moisture while utilizing the water cloud model to characterize scattering from vegetation but, the measurement of the vegetation parameter is of main concern in the applicability of these approaches. The vegetation parameters show temporal behavior and to characterize these parameter field visit have to made each time, as well as, these parameters differ from one crop to other crop. The other techniques used frequently for soil moisture retrieval in vegetated area are the change detection technique. These techniques consider the scattering from the vegetation area to be time invariant. Whereas the scattering contribution from the vegetation cover is very much dependent on the vegetation parameters and these parameters are time variant therefore the scattering contribution from the vegetation cover will be a time variant process and it will be restrict the applicability of the change detection techniques [88]. Several researchers have utilized the passive microwave data to retrieve the vegetation covered soil moisture [28].

The problem of vegetation parameterization in soil moisture retrieval has been primarily dealt with the microwave data by characterizing the scattering form vegetated area. However, some other form of the remote sensing has also been exploited to parameterize the vegetation and subsequently this information may be fused with the microwave data to retrieve the soil moisture. Optical data has been utilized to parameterize the vegetation [7]. The red, near–infrared (NIR) and shortwave–infrared (SWIR), are commonly employed to the retrieve the vegetation water content, canopy height, leaf area index etc. [4, 33, 226]. Optical data with fusion of SAR data is used to yield the crop information [125, 126]. These studies led us to conclude that the information available with optical data may be efficiently employed with SAR data to provide the soil moisture information in vegetated area. Some studies have been performed to use SAR and optical data in soil moisture

retrieval [141, 214]. Wang *et al.* [214] made use of ERS–2 (European remote sensing satellite–2) and TM (Thematic Mapper) imagery for retrieval of soil moisture. They have used multi–temporal ERS data, i.e., one image of dry season and the other of wet season. The dry season image was used to normalize the wet season image and the several empirical relationships with NDVI were developed based on isomoisture lines. The developed empirical relationship does not provide the absolute value of soil moisture rather it gives a range within which the moisture value may lie. Further, the assumption has been made that the surface roughness in the wet season and the dry season does not change remarkably, which limits it applicability. Notarnicola *et al.* [141] calculated the probability density function (pdf) for the various corps to parameterize the vegetation and then investigated its correlation with the normalized difference water index (NDWI). This information has been used in the inversion model to retrieve the soil moisture. The developed model employs pdf and its value differs from crop to crop, as well as, in development phase *apriori* information is needed.

The classification of the SAR data is an important task to accurately demarcate the land cover and choose the area of interest while masking the other. Vegetated and bare soil is the area of interest in soil moisture retrieval studies. Several image processing techniques such as supervised classification, unsupervised classification, and knowledge based approach have been utilized to classify the SAR data [110, 128, 166, 172, 176, 186, 187]. In addition to this, polarimetric techniques have also been utilized to classify the SAR images [45, 102, 118, 175, 223].

Following conclusion may be drawn after exhaustive literature review in monostatic and bistatic domain for soil parameters studies and retrieval.

- Existing studies for soil parameters retrieval have been mainly devoted to the monostatic domain whereas, less attention has been given to characterize the soil parameters in bistatic domain.
- Characterization of soil parameters in bistatic domain has been limited to the simulation studies, whereas lesser experimental work has been reported.
- The utilization of various sensor parameters, i.e., multi–incidence, multi–polarization and multi–frequency has been established for retrieval of soil parameters in monostatic domain. The applicability of these schemes has to be tested for bistatic domain.

- The developed theoretical, empirical, semi–empirical models in monostatic or bistatic domain consider the soil moisture and surface roughness as soil parameters and the role of soil texture has been mostly neglected. Even though, the studies have shown the significant effect of soil texture on microwave scattering.
- The developed available models are quite complex like IEM or needs a lot of *apriori* information to solve for retrieval of soil parameters.
- Retrieval of soil moisture in vegetated area with active microwave data has been generally carried out with water–cloud model and change detection techniques. However, water cloud model requires a lot of *apriori* information and change detection technique suffers with the temporal behaviour of vegetation parameters. Some of the researchers have tried to incorporate the information available through optical data with SAR data to retrieve the vegetation covered soil moisture. So, the fusion of optical data and SAR data for soil moisture retrieval has to be given more attention.

Chapter 3

Study of Specular Scattering Response for Soil Texture at 10 GHz

Several applications regarding the estimation of soil parameters, i.e., soil texture, soil moisture and surface roughness have been discussed in Chapter 1 and Chapter 2. Radar remote sensing is capable of providing a good estimate of these soil parameters due to the sensitivity of microwave radiation towards soil texture, soil moisture and surface roughness. These active sensors do not measure the soil parameters directly, a relationship has to be developed between soil parameters and measured signal intensity that is scattering coefficient in case of radar remote sensing. Usually, such kind of relationship is termed as forward relationship and describes the change in scattering coefficient for corresponding change in soil parameters. These developed models may be theoretical, empirical or semiempirical. Whatsoever be the case, experiments are always necessary to validate the theoretical models and develop empirical or semiempirical models. Study of soil parameters with active microwave remote sensing has been mostly dealt in monostatic domain and a fairer literature has been discussed in Chapter 2 with its advantages and limitations. In this regard the

experiments carried out to describe and validate the models available in monostatic domain. Whereas, with the advancement of the technology, researchers have renewed interest in bistatic domain and some of the researchers have performed the simulation studies to check the response of soil parameters in bistatic domain. But, still less experimental studies have been reported. Therefore, there is a need to perform experiments to analyze the effects of soil parameters on microwave scattering in bistatic domain. This chapter discusses the experimental analysis carried out at 10 GHz (X–band) in special case of bistatic domain (i.e., specular direction) to analyze the effect of soil texture on specular scattering coefficient with change in soil moisture and periodic surface roughness.

Soil texture is an important soil parameter and is defined based on their particle size. Particles are characterized based on their diameter limits and divided in sand, silt and clay constituents. Table 1.2 gives the detail description of these soil constituents. Most of the work for soil parameter characterization considers soil moisture and surface roughness whereas the role of soil texture has been neglected. However, studies have shown that the dielectric constant is a function of soil texture and the change in dielectric constant with soil moisture is very much dependent on soil texture [78, 127, 215]. In addition to this, some of the researchers have tried to incorporate the effect of soil texture in soil moisture and surface roughness retrieval [191, 212].

3.1. Introduction

Different studies on radar remote sensing have been realized in the resent years in order to retrieve and monitor the soil parameters from satellite measurement. It has been discussed in Chapter 2 that studies to parameterize the soil parameters have been extensively planned in monostatic domain. Therefore, most of the existing models, theoretical, empirical or semiempirical, discuss the behavior of scattering coefficient for different soil parameters in monostatic domain. In addition to this, the retrieval of soil parameters with several techniques have been discussed, developed, tested and validated owing to the parameters of the monostatic domain. Although considerable research had been reported in the literature in monostatic domain and most of the satellite missions carrying active microwave sensors operate in monostatic

domain, still uncertainty exists. Alternative to the monostatic domain, bistatic domain may serve the purpose efficiently. The major advantage with the bistatic domain includes the low cost operation, because in bistatic domain the expensive transmitter can be shared by several receivers. Also, the existing monostatic constellation can also be explored to provide the data in bistatic domain as with the case of TanDEM–X that operates in association with TerraSAR–X. In this regard, the bistatic domain will provide a good alternative to the monostatic domain as well as strengthen the existing technology in active microwave remote sensing. Recent trends in bistatic domain have extended from examining the fundamentals of bistatic radar to the signal design and processing of different types of radars, including bistatic synthetic aperture radar, to the application of bistatic radar to specific problems, such as air target detection, short–range anticollision warning and detection of buried objects [140]. Still, less attention has been provided to study the behavior of soil parameter in bistatic domain. The existing studies for characterization of soil parameters are mostly dealt with simulation studies and Chapter 2 has discussed in the detail about these phenomenology. Even less experimental observation has been carried in bistatic domain. Therefore, there is a need to carry out experimental observations to gain the knowledge of the scattering behavior on bistatic domain. Experimental observations are necessary as they play significant role in developing the new remote sensing methods and these observations are important to validate various scattering models. Experiments carried out in the controlled laboratory environment sets the basis for their application on the data obtained through airborne or spaceborne sensors. The controlled experimental analysis are more important when the concerned parameters are nature parameter as in the case of soil parameters, i.e., soil texture, soil moisture and surface roughness. These soil parameters, being the nature parameter, show significant spatial and temporal variations and these variations cannot be controlled in nature. In this regard, controlled experiments are more necessary where the variation in one parameter can be made while keeping the other parameters constant to check their effect on the measurable quantity which in radar remote sensing is scattering coefficient. This chapter presents the experiments carried out in controlled environment at 10 GHz in both like polarization at various incidence angles for soil parameters studies in bistatic domain. Changes in soil texture, soil moisture, and periodic surface roughness were made artificially to analyze the effect of soil texture

on specular scattering coefficient with change in moisture and periodic roughness conditions of the field.

The chapter is organized as following:

Section 3.2 discusses about various field conditions chosen for observations and Section 3.3 presents the methodology used to carry out the experiments. The results and discussions part have been analyzed in Section 3.4 and finally, Section 3.5 gives the conclusion of the study.

3.2. Test Fields and Observations Carried out

Four different soil texture fields were considered for study of scattering behavior in specular direction. Field size of different soil fields was 2 m × 2 m (It is chosen such that swath area is more than 1 m^2 so that for every incidence angle the swath is inside the soil bed). These different soil texture fields were artificially prepared in the laboratory by varying the soil constituents, i.e., the percentage of sand silt and clay were changed to prepare different fields. Soil texture information of these fields is given in Table 3.1. Changes in soil moisture condition of these different soil texture fields were made to analyze the moisture effect on the specular scattering coefficient when the objective is to study different soil texture field. Therefore, for each field, one dry and three moisture values were taken into account. Five independent measurements were taken to estimate the volumetric soil moisture content of each moisture contents. The mean values of soil moisture were taken into account which ranges from 0.10 $cm^3\ cm^{-3}$ to 0.21 $cm^3\ cm^{-3}$ with standard deviation of 0.016. Table 3.2 gives the details of soil moisture contents. Surface roughness is another important soil parameter that significantly affects the scattering phenomenon in microwave spectrum. In this regard, for each soil texture field with one dry and three moisture conditions, one smooth (s_1) and two periodic roughness values (s_2 and s_3) were considered. Periodic surface roughness was prepared with the help of wooden harrow and measurements were made with pin profilometer (as given in Section 1.3.4(c)). Table 3.2 provides the values of measured rms surface height for different fields. It means each field with four conditions of moisture and three conditions of periodic roughness were analyzed and a total of 48 different field conditions were taken for study.

Table 3.1. Soil texture information of fields used for observation

	% of Sand	% of Silt	% of Clay	% of Gravels
Field 1	78.4	9.1	4.3	8.1
Field 2	58.8	23.1	8.5	9.3
Field 3	44.3	35.8	11.7	7.5
Field 4	38.7	33.1	18.7	9.1

Table 3.2. Moisture and periodic roughness values used for the study of each field

Moisture $cm^3\ cm^{-3}$	RMS Surface Height in cm		
	s_1	s_2	s_3
m_{v1}=Dry	Smooth	0.9	1.4
m_{v2}=0.10	Smooth	0.9	1.4
m_{v3}=0.15	Smooth	0.9	1.4
m_{v4}=0.21	Smooth	0.9	1.4

Table 3.3. Different combination of fields (48) prepared for the observations

m_{v1}				m_{v2}			
Field 1	Field 2	Field 3	Field 4	Field 1	Field 2	Field 3	Field 4
s_1	s_1	s_1	s_1	s_1	s_1	s_1	s_1
s_2	s_2	s_2	s_2	s_2	s_2	s_2	s_2
s_3	s_3	s_3	s_3	s_3	s_3	s_3	s_3
m_{v3}				m_{v4}			
Field 1	Field 2	Field 3	Field 4	Field 1	Field 2	Field 3	Field 4
s_1	s_1	s_1	s_1	s_1	s_1	s_1	s_1
s_2	s_2	s_2	s_2	s_2	s_2	s_2	s_2
s_3	s_3	s_3	s_3	s_3	s_3	s_3	s_3

3.3. Methodology

The specular scattering response of different fields as discussed in Section 3.2 has been studied. Experiments with bistatic scatterometer were carried out in both like polarizations, i.e., HH– and VV–polarization at different incidence angles (as discussed in Section 1.3). Incidence angles were varied from 30° to 70° in step of 10°. Specular scattering coefficient has been computed with Equation 1.12. The details of computation of specular scattering have been given in Section 1.3.1(b).

3.4. Results and Discussions

3.4.1. Response of Specular Scattering Coefficient for Soil Texture

(a) Dry and Smooth Soil Surface in HH–Polarization

In order to analyze the response of microwave scattering for different soil texture fields, specular scattering coefficient were plotted with varying incidence angles for both like polarizations. It is clearly evident from Figure 3.1(a) that the change in specular scattering coefficient occurs with change in soil texture field. Dynamic range of specular scattering (i.e., change with incidence angle) changes in soil texture field. The dynamic range of specular scattering for Field 1 (sand = 78.4%, silt = 9.1% and clay = 4.3%), Field 2 (sand = 58.8%, silt = 23.1% and clay = 8.5%), Field 3 (sand = 44.3%, silt = 35.8% and clay = 11.7%) and Field 4 (sand = 38.7%, silt = 33.1% and clay = 18.7%) is 8.4 dB, 9.1 dB, 9.8 dB and 11.5 dB, respectively. It is difficult to distinguish different soil texture fields at lower incidence angles as vey less change have been observed in specular scattering coefficient for change in soil texture at lower incidence angles (i.e., $< 50°$). However, higher incidence angles are suitable to discriminate different soil texture fields based on specular scattering coefficient which can be observed form Figure 3.1(a) where significant changes have been observed in specular scattering coefficient at higher incidence angles (i.e., $\geq 50°$). Therefore, higher incidence angles are better suited than lower incidence angles to observe different soil texture fields based on specular scattering coefficient in HH–polarization at 10 GHz.

(b) Dry and Smooth Soil Surface in VV–Polarization

The behavior of specular scattering coefficient with incidence angle is shown in Figure 3.1(b) for four different soil texture fields in VV–polarization at 10 GHz. Less changes in specular scattering coefficient have been observed for change in soil texture in VV–polarization whereas, significant changes were observed in HH–polarization. The dynamic range of specular scattering coefficient for Field 1(sand = 78.4%, silt = 9.1% and clay = 4.3%) and Field 4 (sand = 38.7%, silt = 33.1% and clay = 18.7%) is 19.2 dB and 20.4 dB respectively. However, the dynamic range for Field 2 (sand = 58.8%, silt = 23.1% and clay = 8.5%) and Field 3 (sand = 44.3%, silt = 35.8% and clay = 11.7%) is approximately 19.7 dB. The response of specular scattering coefficient for different soil texture fields is approximately same at all incidence angles. A dip in specular scattering coefficient at 60° incidence angle in VV–polarization can be observed from Figure 3.1(b). This phenomenon may be explained by Brewster angle effect. At Brewster angle, there is no reflected wave when the incidence wave is vertically polarized. The experimental and simulation study conducted by De Roo and Ulaby [43] also show a similar behavior for dry and smooth soil in VV–polarization.

It is observed from the study of dry and smooth soil that by changing soil texture there is a change in specular scattering coefficient for both like polarizations. The effect is more prominent in HH–polarization than in VV–polarization and in case of HH–polarization at higher incidence angles (i.e., ≥ 50°) better differentiation in specular scattering coefficient is observed for different soil texture fields. It may be due to the reason that HH–polarized wave interacts with different soil texture fields more prominently than VV–polarized wave in specular direction [43, 140].

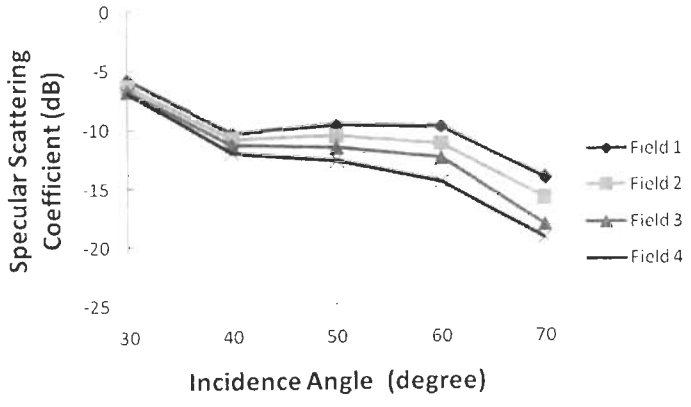

(a)

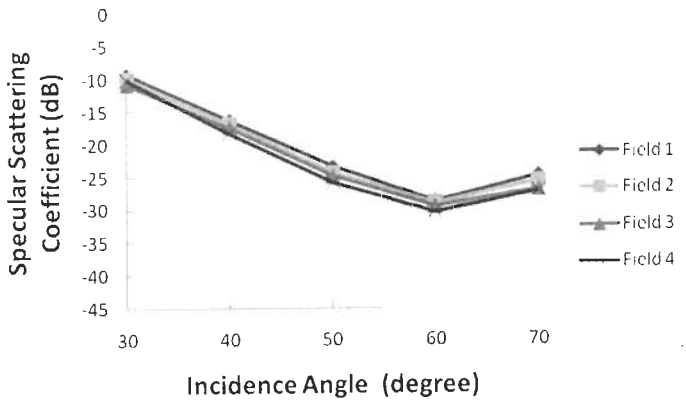

(b)

Figure 3.1. Response of specular scattering coefficient for different soil texture fields with varying incidence angle for smooth and dry soil (a) HH–polarization (b) VV–polarization.

3.4.2. Moisture Effect on Response of Specular Scattering from Different Soil Texture Fields

(a) HH–Polarization

Figure 3.2(a)–(c) show the behavior of specular scattering for four different soil texture fields with moisture 0.10 cm^3 cm^{-3}, 0.15 cm^3 cm^{-3}, and 0.21 cm^3 cm^{-3}, respectively in HH–polarization. With different soil texture fields, change in specular scattering coefficient are difficult to observe at 30° incidence angle, but as the incidence angle is increased, changes in scattering coefficient are observed. At higher incidence angles better differentiation in specular scattering coefficient are obtained, i.e., changing sand percentage from 78.14% to 58.87%, 58.87% to 44.35% and further from 44.35% to 38.72%, change in specular scattering coefficient is obtained at 50°, 60° and 70° incidence angles for moisture variation of 0.10 cm^3 cm^{-3} to 0.21 cm^3 cm^{-3}. At volumetric soil moisture contents 0.15 cm^3 cm^{-3} and 0.21 cm^3 cm^{-3}, a continuous decrease in specular scattering coefficient is observed from 30° to 50° incidence angles for all four fields, but in contrast an increase is observed at 60° incidence angle. Increase in specular scattering coefficient at 60° incidence angle was also observed by Nashashibi and Ulaby [139, 140]. Effect of soil texture on specular scattering in the presence of soil moisture is noticed from the change in specular

scattering coefficient that is valid for a range of soil moisture (0.10 cm^3 cm^{-3} to 0.21 cm^3 cm^{-3}). These observations can be clearly seen from the Figures 3.2(a)–(c).

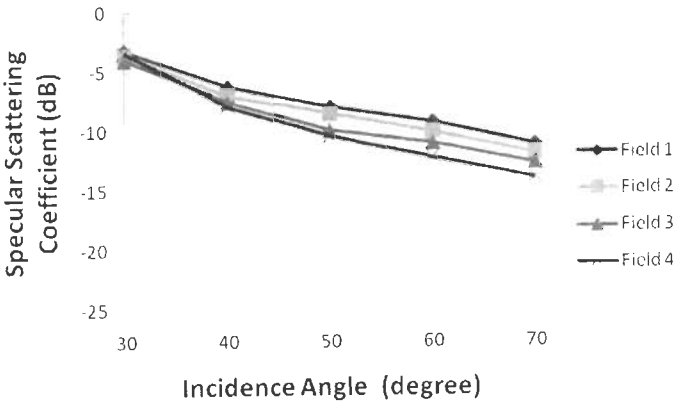

(a)

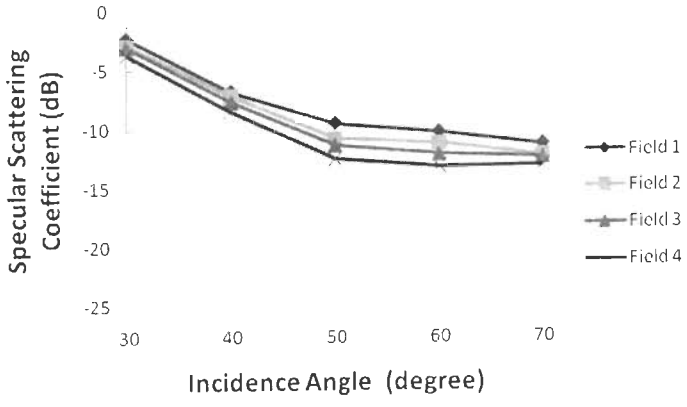

(b)

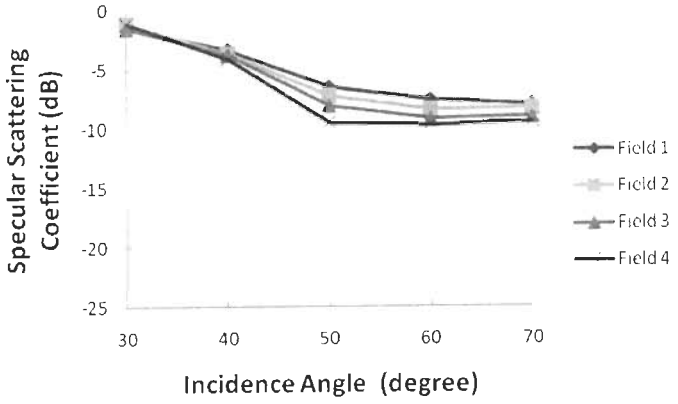

(c)

Figure 3.2. Response of specular scattering coefficient for different soil texture fields with varying incidence angle for smooth surface in HH–polarization (a) volumetric soil moisture 0.10 cm^3 cm^{-3} (b) volumetric soil moisture 0.15 cm^3 cm^{-3} (c) volumetric soil moisture 0.21 cm^3 cm^{-3}.

(b) VV–Polarization

Figure 3.3(a)–(c) show the scattering behavior of four different soil texture fields in specular direction for VV–polarization having soil moisture values 0.10 cm^3 cm^{-3}, 0.15 cm^3 cm^{-3} and 0.21 cm^3 cm^{-3}, respectively. For VV–polarization, at lower incidence angle (i.e., < 50°), less changes are observed in specular scattering coefficient with the change in soil texture field for all moisture conditions. But, better differentiation in specular scattering coefficient was observed at 50° and 60° incidence angle. With the study of moisture effect it is noticed that the change in specular scattering coefficient is better observed with moist soil than for dry soil for both like polarizations (Figure 3.2 and 3.3). Further, at higher incidence angles (i.e., ≥ 50°), differentiation in specular scattering coefficients are better than lower incidence angles for all considered moisture values. It can be observed form Figure 3.3(a) that specular scattering coefficient differentiation is more at 60° incidence angle when the percentage of sand changes from 78.3% to 38.7%. The percentage of sand decreases from 78.4% to 38.7% from Field 1 to Field 4 and with decrease in percentage of sand, a decrease in specular scattering coefficient can be observed at 60° incidence angle (Figure 3.3(a)). In a similar manner, for higher moisture content, i.e., 0.15 cm^3 cm^{-3} and 0.21 cm^3 cm^{-3}, it can be observed form Figure 3.3(b) and (c) that the specular

scattering coefficient decreases with the decrease in sand percentage at 60° incidence angle.

If we compare the angular variation results of HH–polarization and VV–polarization, similar decreasing behavior of specular scattering coefficient with incidence angle at low soil moisture values (volumetric soil moisture 0.10 cm^3 cm^{-3}) is observed for both like polarizations (Figure 3.2(a) and 3.3(a)). Whereas, due to increase in moisture content from 0.15 cm^3 cm^{-3} to 0.21 cm^3 cm^{-3}, an increment of specular scattering coefficient is observed at higher incidence angles (i.e., ≥ 50°) for HH–polarization (Fig. 3.2(b) and 3.2(c)). Very less changes were observed (Fig. 3.3(b) and (c)) for VV–polarization.

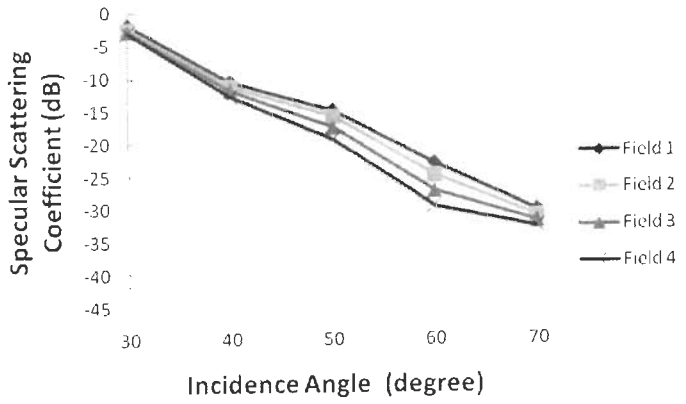

(a)

M.G. CENTRAL LIBRARY
ACC No. G21591
Date 4/10/12
I.I.T. ROORKEE

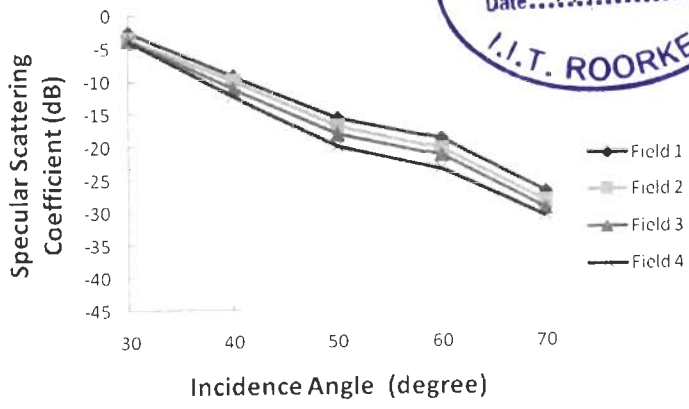

(b)

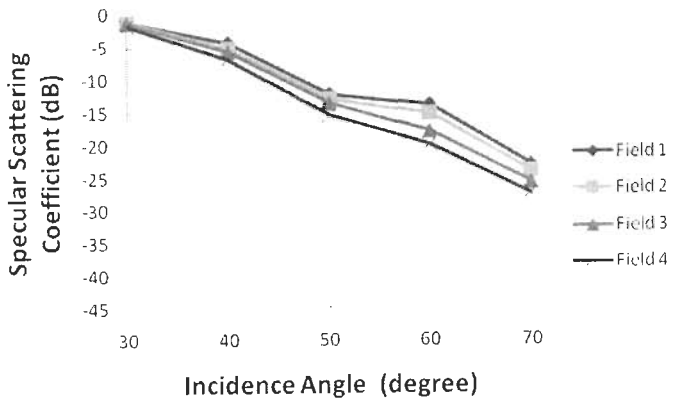

(c)

Figure 3.3. Response of specular scattering coefficient for different soil texture fields with varying incidence angle for smooth surface in VV–polarization (a) volumetric soil moisture 0.10 cm^3 cm^{-3} (b) volumetric soil moisture 0.15 cm^3 cm^{-3} (c) volumetric soil moisture 0.21 cm^3 cm^{-3}.

3.4.3. Periodic Surface Roughness Effect on Response of Specular Scattering from Different Soil Texture Fields

(a) HH–polarization

Figures 3.4 and 3.5 show the specular scattering response in HH–polarization for four different soil texture fields at various soil moisture contents when the rms surface height is 0.9 cm. It can be observed form Figure 3.4(a) that it is difficult to observe any change in specular scattering coefficient for different soil texture fields at rms surface height 0.9 cm for dry soil at all incidence angles. The change in specular scattering coefficient can be observed for different soil texture fields at all incidence angles for different soil moisture contents (0.10, 0.15 and 0.21 cm^3 cm^{-3}) at rms surface height 0.9 cm (Figure 3.4(b) to 3.4 (d)). However, it is difficult to define any trend of specular scattering coefficient, i.e., there is no any certainty in the behavior of specular scattering coefficient with change in soil texture. The specular scattering coefficient, at one particular incidence angle show a decreasing behavior (e.g., 70°) for the change in soil texture (Field 1 to Field 4) whereas, at any other incidence angle it shows an entirely different trend. Therefore, it is difficult to describe any changing trend of specular scattering coefficient with change in soil texture at rms height 0.9

cm for different soil moisture contents. Figure 3.5 explains that for specular scattering behavior at rms surface height 1.4 cm, similar conclusion can be drawn. In this regard, it may be inferred that it is difficult to make any decision regarding the change in specular scattering coefficient with change in soil texture at different periodic roughness values (i.e., 0.9 and 1.4 cm) in HH–polarization for various soil moisture contents (i.e., dry soil to volumetric soil moisture 0.21 cm^3 cm^{-3}).

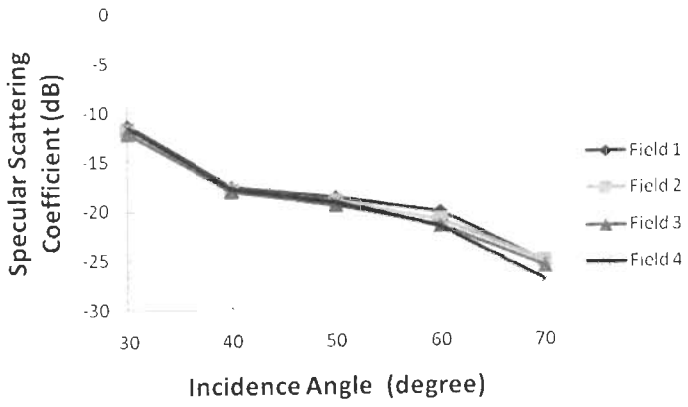

(a)

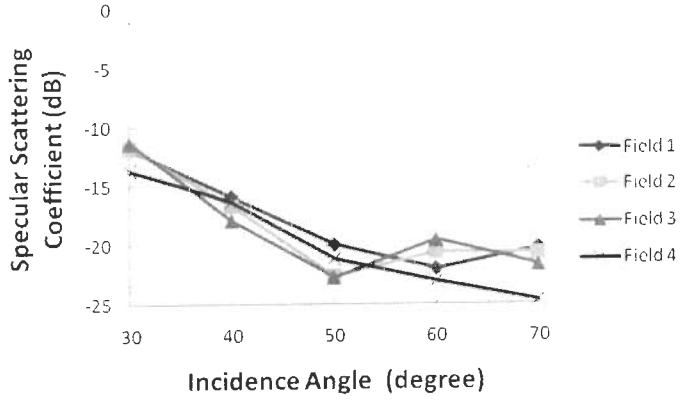

(b)

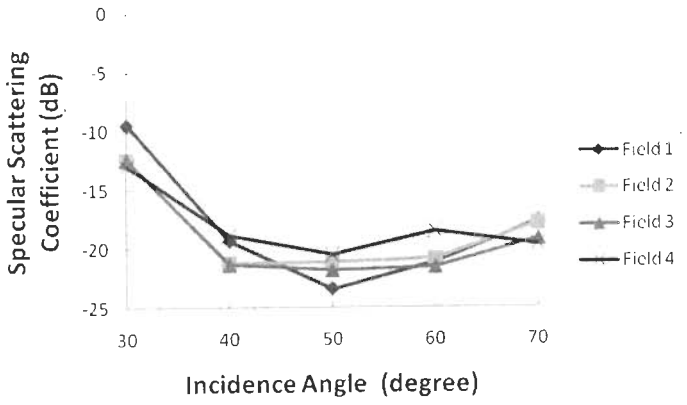

(c)

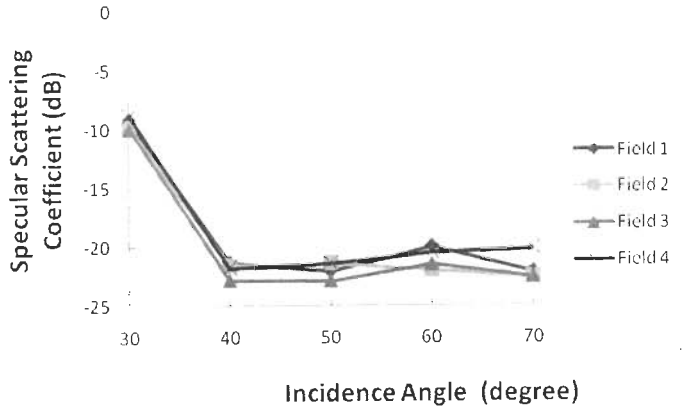

(d)

Figure 3.4. Response of specular scattering coefficient for different soil texture fields with varying incidence angle for rms surface height 0.9 cm in HH–polarization (a) Dry soil (b) volumetric soil moisture 0.10 cm^3 cm^{-3} (c) volumetric soil moisture 0.15 cm^3 cm^{-3} (d) volumetric soil moisture 0.21 cm^3 cm^{-3}.

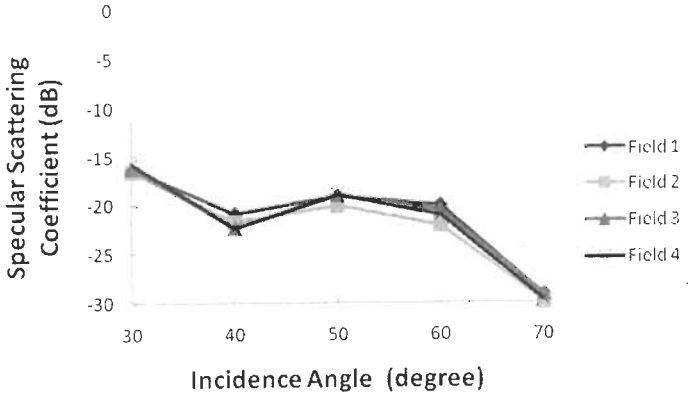

(a)

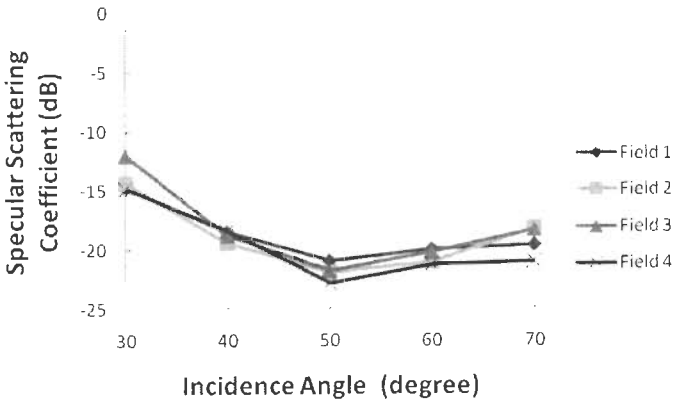

(b)

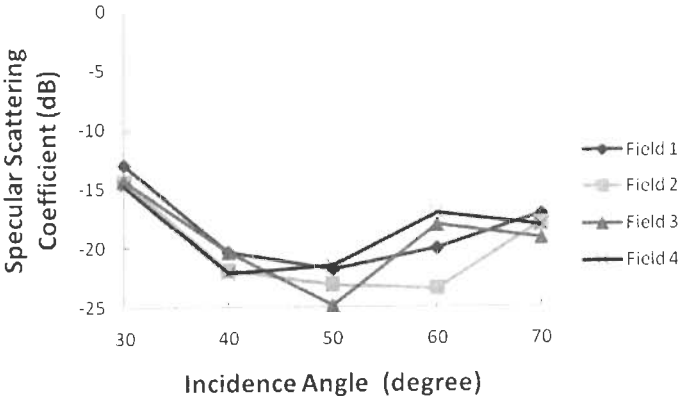

(c)

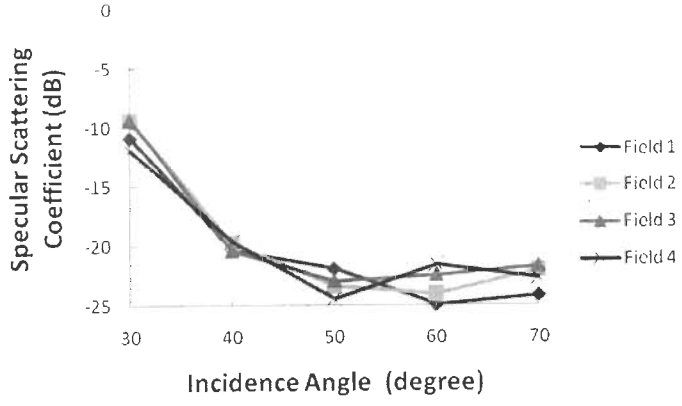

(d)

Figure 3.5. Response of specular scattering coefficient for different soil texture fields with varying incidence angle for rms surface height 1.4 cm in HH–polarization (a) Dry soil (b) volumetric soil moisture 0.10 cm^3 cm^{-3} (c) volumetric soil moisture 0.15 cm^3 cm^{-3} (d) volumetric soil moisture 0.21 cm^3 cm^{-3}.

(b) VV–Polarization

The specular scattering response in VV–polarization at rms surface height 0.9 cm and 1.4 cm has been shown in Figures 3.6 and 3.7 respectively for four different soil texture fields at different soil moisture content. It can be observed form Figure 3.6(a) and 3.7(a) that approximately same specular scattering coefficient has been observed for different soil texture fields at all incidence angles for dry soil. The rms surface height of these fields was 0.9 cm and 1.4 cm respectively. Change in moisture condition (i.e., 0.10 cm^3 cm^{-3} to 0.21 cm^3 cm^{-3}), causes change in specular scattering coefficient for different soil texture fields (Figures 3.6(b)–3.6(d) and Figures 3.7(b)–3.7(d)). However, again, as with the case of HH–polarization, in VV–polarization also, it has been difficult to observe a clear trend in specular scattering coefficient with change in soil texture for periodic surface roughness 0.9 cm and 1.4 cm.

Therefore, the observation of specular scattering coefficient at different soil periodic surface roughness conditions (i.e., 0.9 cm and 1.4 cm) when the objective is to check the effect of soil texture, it is difficult to analyze the soil texture effect on specular scattering coefficient in both like polarizations at 10 GHz. Although, the change in specular scattering coefficient can be observed at different incidence angles, a clear behavior is difficult to be inferred. It infers that it is difficult to make the distinction among different soil texture fields based on specular scattering coefficient in presence of periodic surface roughness in both like polarizations at 10 GHz. The difficulty in observing the soil texture effect in presence of surface roughness at 10 GHz may be the shorter wave length (i.e., 3 cm) that is comparable to the rms surface height (i.e., 0.9 and 1.4 cm).

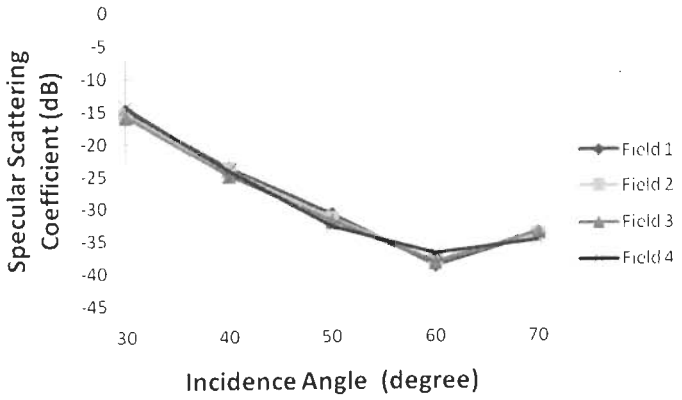

(a)

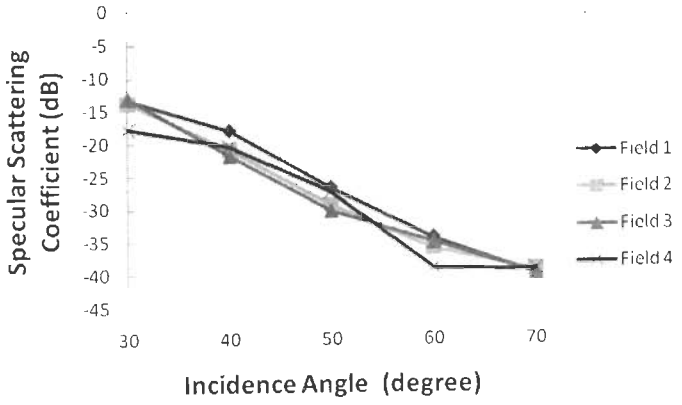

(b)

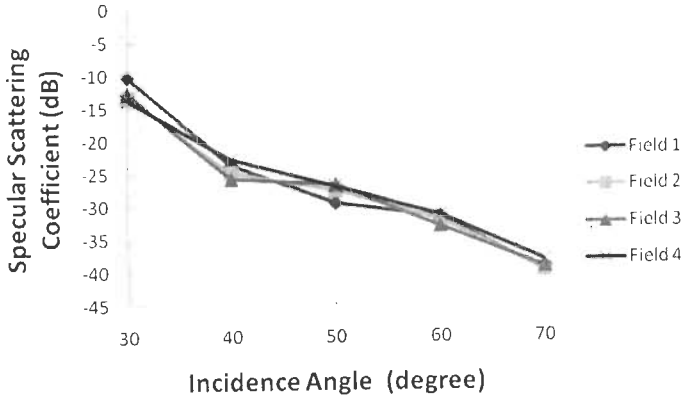

(c)

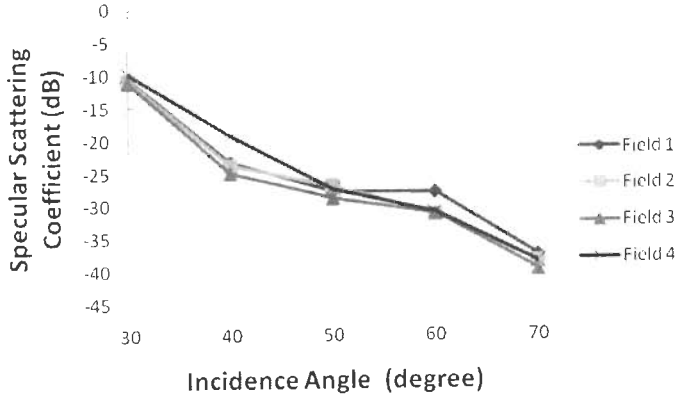

(d)

Figure 3.6. Response of specular scattering coefficient for different soil texture fields with varying incidence angle for rms surface height 0.9 cm in VV–polarization (a) Dry soil (b) volumetric soil moisture 0.10 cm^3 cm^{-3} (c) volumetric soil moisture 0.15 cm^3 cm^{-3} (d) volumetric soil moisture 0.21 cm^3 cm^{-3}.

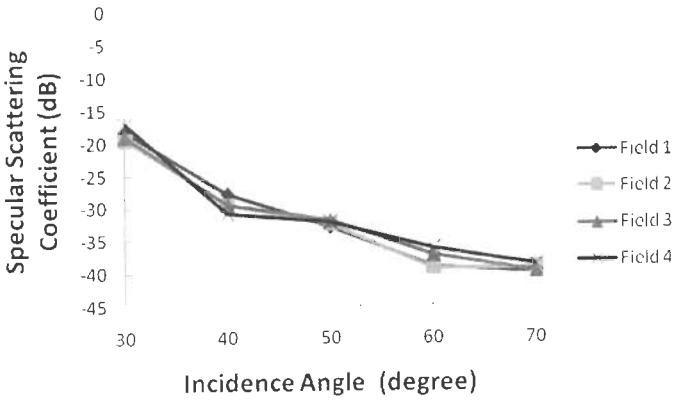
Specular Scattering Coefficient (dB)
0
-5
-10
-15
-20
-25
-30
-35
-40
-45
30
40
50
60
70
Incidence Angle (degree)
Field 1
Field 2
Field 3
Field 4

(a)

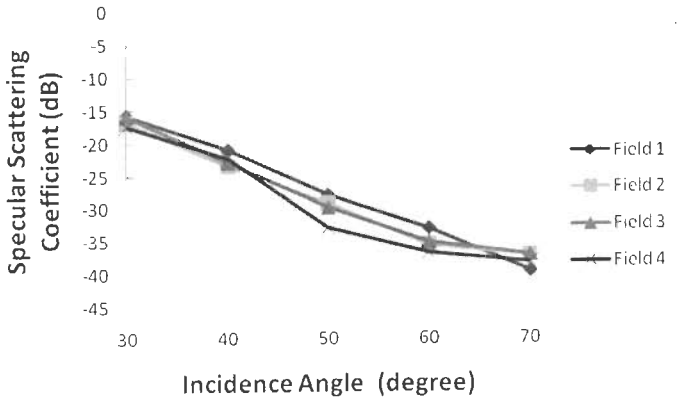
Specular Scattering Coefficient (dB)
0
-5
-10
-15
-20
-25
-30
-35
-40
-45
30
40
50
60
70
Incidence Angle (degree)
Field 1
Field 2
Field 3
Field 4

(b)

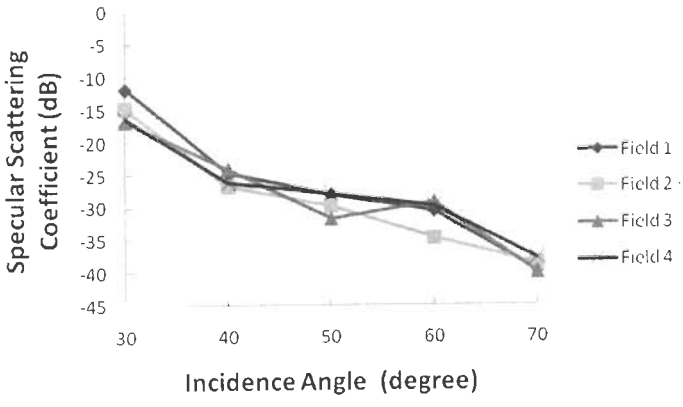
Specular Scattering Coefficient (dB)
0
-5
-10
-15
-20
-25
-30
-35
-40
-45
30
40
50
60
70
Incidence Angle (degree)
Field 1
Field 2
Field 3
Field 4

(c)

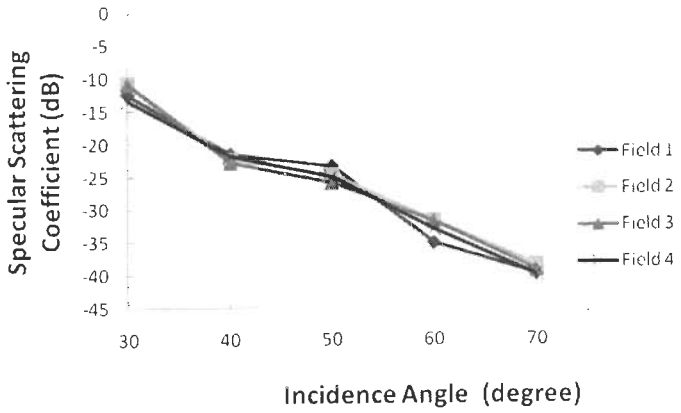

(d)

Figure 3.7. Response of specular scattering coefficient for different soil texture fields with varying incidence angle for rms surface height 1.4 cm in VV–polarization (a) Dry soil (b) volumetric soil moisture 0.10 cm^3 cm^{-3} (c) volumetric soil moisture 0.15 cm^3 cm^{-3} (d) volumetric soil moisture 0.21 cm^3 cm^{-3}.

3.5. Conclusion

This chapter analyses the angular with like polarization specular scattering response for different soil texture fields at various soil moisture and periodic surface roughness conditions at X–band. Significant changes in specular scattering coefficient were observed with change in soil texture in HH–polarization whereas, lesser changes in specular scattering coefficient were observed in VV–polarization for the dry and smooth soil. It was observed that change in soil texture, i.e., percentage of sand, silt and clay causes change in specular scattering coefficient in HH–polarization more prominently at higher incidence angles (i.e., $\geq 50°$) whereas, it was difficult to observe the changes in specular scattering coefficient at lower incidence angles (i.e., $< 50°$). Moisture conditions of different soil texture fields were changed in controlled environment to check the effect of specular scattering coefficient with change in soil texture in presence of soil moisture. The observations revealed that the change in specular scattering coefficient occurs for change in percentage of sand from 78.4 to 38.7 at various soil moisture contents (i.e., 0.10 cm^3 cm^{-3} to 0.21 cm^3 cm^{-3}) and smooth surface. Periodic surface roughness of different fields were changed to study its effect on specular scattering coefficient for different soil texture fields. Change in

periodic surface roughness has major effect on specular scattering coefficient at 10 GHz when the objective is to analyze different soil texture fields with specular scattering coefficient. It has been difficult to observe a specified trend in change of specular scattering coefficient for change in soil texture at different periodic surface roughness values (i.e., 0.9 and 1.4 cm) in both like polarizations.

Therefore, the study points out that soil texture information can be obtained with specular scattering coefficient at 10 GHz for moist and smooth surface whereas no significant change in specular scattering coefficient have been observed for periodic surface in both like polarizations. The effect of soil texture is easily observable for smooth surface at various soil moisture contents in both like polarizations at higher incidence angles whereas, it is difficult to observe a clear trend in specular scattering coefficient with change in soil texture in both like polarizations at all incidence, whatever be the soil moisture content.

Chapter 4

Study of Specular Scattering Response for Soil Texture at 6 GHz (C–band) with the Change in Soil Moisture and Surface Roughness Conditions

Wavelength contributes a major role in radar remote sensing observations along with the other sensor parameters, i.e., polarization and incidence angle. It is the wavelength that decides the roughness and smoothness of the surface. A surface that is considered as smooth for one particular wavelength may be considered as rough for other particular wavelength. Rayleigh criterion for characterizing the surface as smooth or rough is used in case of optical region, while for modeling the scattering behavior of natural surfaces in microwave region we use Fraunhofer criterion for characterizing the surface roughness [202]. A surface is considered smooth according to Rayleigh criterion if the rms surface height is less than ($\lambda/8\ \cos\theta$) whereas, according to Fraunhofer criterion surface is smooth if rms surface height < ($\lambda/32\ \cos\theta$)

[202], where, λ and θ are the operating wavelength and incidence angel, respectively as discussed in Section 1.3.1(c). Further, penetration of wave into the medium is also a wavelength dependent parameter. A shorter wavelength penetrate less into the medium whereas, a longer wavelength penetrates more as discussed in Section 1.3.1(c). Therefore, it is always of considerable interest to analyze the response of soil parameters, i.e., soil texture, soil moisture and surface roughness at different wavelength. A study of specular scattering coefficient at X–band (10 GHz frequency or 3 cm wavelength) has been carried out in Chapter 3 and it is observed that this frequency is not so suitable for observing the soil texture at high periodic roughness and moisture conditions. So, to explore bi-static aspect further, we have considered C–band (frequency = 6 GHz) for soil texture analysis. Therefore, in this chapter the change in specular scattering coefficient for different soil texture with variation in soil moisture and periodic surface roughness has been studied at 6 GHz frequency of C–band.

4.1. Introduction

The significance of experimental analysis has been discussed in Chapter 3 whereas in Chapter 2 the importance of observation in bistatic domain has been discussed. The specular scattering coefficient is a function of sensor parameters as well as soil parameters. The objective of the study is to analyze and retrieve the soil parameters which can be fulfilled by optimized selection of sensor parameters. The study in Chapter 2 at X–band was carried out at 10 GHz in both like polarizations at various incidence angles. The major objective was to check the response of soil texture on specular scattering coefficient and it was observed that for dry soil with smooth surface, the effect of soil texture was clearly observed on specular scattering coefficient at 10 GHz. The study of change in moisture while keeping the periodic surface roughness smooth led to the conclusion that at different moisture values the effect of soil texture on specular scattering is quite significant at 10 GHz. Whereas, the change in periodic surface roughness has drastic effect on the observations of soil texture effect for specular scattering coefficient, i.e., it was difficult to observe the clear behavior of change in specular scattering coefficient for change in soil texture at 10 GHz. This kind of observation led to study the behavior of soil parameters at other

wavelengths. Therefore, the study was carried out at 6 GHz in both like polarizations at various incidence angles. In the initial phase the study was carried out for some of the soil texture fields only to check the behavior of soil texture on specular scattering coefficient in the presence of periodic roughness and moisture. The obtained results were quite encouraging and it was observed that the effect of soil texture on specular scattering coefficient can be observed at different soil moisture contents as well as at different periodic surface roughness conditions which was not the case at 10 GHz. Therefore, a wider range of periodic surface roughness and moisture conditions were considered, i.e., ten different soil texture fields were studied at 6 GHz where each field has six moisture and five periodic roughness conditions.

This chapter has been organized as following:

A detailed description of different field conditions has been given in Section 4.2. The methodology of experiment performed is discussed in Section 4.3. Section 4.4 presents the results and analysis part and finally Section 4.5 draws the conclusion.

4.2. Test Fields and Observations Carried Out

Ten different soil texture fields were prepared on the basis of change in its constituent, i.e., percentage of sand silt and clay. Field size of different soil fields was 2 m × 2 m. Table 4.1 provides the quantitative values of soil constituent of ten different fields. Soil moisture and surface roughness are inherent soil parameters for natural soil therefore, it is very much important to check the effect of soil moisture and surface roughness on specular scattering coefficient for different soil texture fields. In this regard, the analysis of soil texture for specular scattering coefficient was carried out for six different soil moisture conditions with one smooth and five periodic roughness conditions. Table 4.2 and 4.3 give details of soil moisture and periodic surface roughness conditions, respectively. Table 4.4 shows the different combination of fields prepared for the observations.

4.3. Methodology

The experiment was carried out to compute specular scattering coefficient at 6 GHz with Equation 1.12 as discussed in Chapter 1. The response of specular scattering coefficient was studied in both like polarizations, i.e., HH– and VV–

polarization, by varying incidence angle form 25° to 70° in step of 5° for different fields. The description of field conditions are given in Tables 4.1, 4.2 and 4.3 and total 360 fields conditions have been analyzed to study the response of specular scattering coefficient. A detailed description of experimental setup and computation of specular scattering coefficient has been given in Section 1.3.

Table 4.1. Soil constituent of 10 different soil texture fields used for observations

	% of Sand	% of Silt	% of Clay	% of Gravels
Field 1	85.3	7.5	2.5	4.1
Field 2	62.6	26.1	5.3	5.2
Field 3	47.2	32.7	15.4	4.5
Field 4	24.6	20.1	48.7	6.3
Field 5	25.5	41.3	21.7	11.2
Field 6	17.4	51.2	20.8	10.4
Field 7	11.2	70.6	4.8	13.1
Field 8	12.8	29.3	51.5	5.6
Field 9	7.5	23.4	64.2	4.8
Field 10	2.3	10.3	81.6	5.6

Table 4.2. Volumetric soil moisture values used for each field

	m_{v1} $cm^3\ cm^{-3}$	m_{v2} $cm^3\ cm^{-3}$	m_{v3} $cm^3\ cm^{-3}$	m_{v4} $cm^3\ cm^{-3}$	m_{v5} $cm^3\ cm^{-3}$	m_{v6} $cm^3\ cm^{-3}$
Field 1	0.028	0.083	0.201	0.265	0.346	0.420
Field 2	0.030	0.096	0.183	0.281	0.379	0.403
Field 3	0.031	0.104	0.174	0.240	0.351	0.441
Field 4	0.023	0.108	0.197	0.255	0.395	0.415
Field 5	0.028	0.114	0.181	0.270	0.380	0.411
Field 6	0.024	0.091	0.207	0.258	0.373	0.426
Field 7	0.025	0.097	0.168	0.261	0.361	0.408
Field 8	0.027	0.084	0.212	0.274	0.382	0.434
Field 9	0.023	0.081	0.176	0.252	0.386	0.441
Field 10	0.026	0.098	0.185	0.255	0.390	0.455
mean	0.027	0.096	0.188	0.261	0.374	0.425
STDEV	0.003	0.011	0.015	0.012	0.017	0.017

Table 4.3. Periodic roughness measurement for different fields

rms surface height (s) cm	Correlation length (l) cm
s_1 (smooth surface)	l_1 (smooth surface)
$s_2 = 0.43$	$l_2 = 4.68$
$s_3 = 0.94$	$l_3 = 5.66$
$s_4 = 1.51$	$l_4 = 5.39$
$s_5 = 2.11$	$l_5 = 4.47$
$s_6 = 2.46$	$l_6 = 4.55$

Table 4.4. Different combination of fields (360) prepared for the observations

m_{v1}									
F1	F2	F3	F4	F5	F6	F7	F8	F9	F10
(s_1, l_1)	(s_1, l_1)	(s_1, l_1)	(s_1, l_1)	(s_1, l_1)	(s_1, l_1)	(s_1, l_1)	(s_1, l_1)	(s_1, l_1)	(s_1, l_1)
(s_2, l_2)	(s_2, l_2)	(s_2, l_2)	(s_2, l_2)	(s_2, l_2)	(s_2, l_2)	(s_2, l_2)	(s_2, l_2)	(s_2, l_2)	(s_2, l_2)
(s_3, l_3)	(s_3, l_3)	(s_3, l_3)	(s_3, l_3)	(s_3, l_3)	(s_3, l_3)	(s_3, l_3)	(s_3, l_3)	(s_3, l_3)	(s_3, l_3)
(s_4, l_4)	(s_4, l_4)	(s_4, l_4)	(s_4, l_4)	(s_4, l_4)	(s_4, l_4)	(s_4, l_4)	(s_4, l_4)	(s_4, l_4)	(s_4, l_4)
(s_5, l_5)	(s_5, l_5)	(s_5, l_5)	(s_5, l_5)	(s_5, l_5)	(s_5, l_5)	(s_5, l_5)	(s_5, l_5)	(s_5, l_5)	(s_5, l_5)
(s_6, l_6)	(s_6, l_6)	(s_6, l_6)	(s_6, l_6)	(s_6, l_6)	(s_6, l_6)	(s_6, l_6)	(s_6, l_6)	(s_6, l_6)	(s_6, l_6)
m_{v2}									
F1	F2	F3	F4	F5	F6	F7	F8	F9	F10
(s_1, l_1)	(s_1, l_1)	(s_1, l_1)	(s_1, l_1)	(s_1, l_1)	(s_1, l_1)	(s_1, l_1)	(s_1, l_1)	(s_1, l_1)	(s_1, l_1)
(s_2, l_2)	(s_2, l_2)	(s_2, l_2)	(s_2, l_2)	(s_2, l_2)	(s_2, l_2)	(s_2, l_2)	(s_2, l_2)	(s_2, l_2)	(s_2, l_2)
(s_3, l_3)	(s_3, l_3)	(s_3, l_3)	(s_3, l_3)	(s_3, l_3)	(s_3, l_3)	(s_3, l_3)	(s_3, l_3)	(s_3, l_3)	(s_3, l_3)
(s_4, l_4)	(s_4, l_4)	(s_4, l_4)	(s_4, l_4)	(s_4, l_4)	(s_4, l_4)	(s_4, l_4)	(s_4, l_4)	(s_4, l_4)	(s_4, l_4)
(s_5, l_5)	(s_5, l_5)	(s_5, l_5)	(s_5, l_5)	(s_5, l_5)	(s_5, l_5)	(s_5, l_5)	(s_5, l_5)	(s_5, l_5)	(s_5, l_5)
(s_6, l_6)	(s_6, l_6)	(s_6, l_6)	(s_6, l_6)	(s_6, l_6)	(s_6, l_6)	(s_6, l_6)	(s_6, l_6)	(s_6, l_6)	(s_6, l_6)
m_{v3}									
F1	F2	F3	F4	F5	F6	F7	F8	F9	F10
(s_1, l_1)	(s_1, l_1)	(s_1, l_1)	(s_1, l_1)	(s_1, l_1)	(s_1, l_1)	(s_1, l_1)	(s_1, l_1)	(s_1, l_1)	(s_1, l_1)
(s_2, l_2)	(s_2, l_2)	(s_2, l_2)	(s_2, l_2)	(s_2, l_2)	(s_2, l_2)	(s_2, l_2)	(s_2, l_2)	(s_2, l_2)	(s_2, l_2)
(s_3, l_3)	(s_3, l_3)	(s_3, l_3)	(s_3, l_3)	(s_3, l_3)	(s_3, l_3)	(s_3, l_3)	(s_3, l_3)	(s_3, l_3)	(s_3, l_3)
(s_4, l_4)	(s_4, l_4)	(s_4, l_4)	(s_4, l_4)	(s_4, l_4)	(s_4, l_4)	(s_4, l_4)	(s_4, l_4)	(s_4, l_4)	(s_4, l_4)
(s_5, l_5)	(s_5, l_5)	(s_5, l_5)	(s_5, l_5)	(s_5, l_5)	(s_5, l_5)	(s_5, l_5)	(s_5, l_5)	(s_5, l_5)	(s_5, l_5)
(s_6, l_6)	(s_6, l_6)	(s_6, l_6)	(s_6, l_6)	(s_6, l_6)	(s_6, l_6)	(s_6, l_6)	(s_6, l_6)	(s_6, l_6)	(s_6, l_6)

Table 4.4. Continued...

m_{v4}									
F1	F2	F3	F4	F5	F6	F7	F8	F9	F10
(s_1, l_1)	(s_1, l_1)	(s_1, l_1)	(s_1, l_1)	(s_1, l_1)	(s_1, l_1)	(s_1, l_1)	(s_1, l_1)	(s_1, l_1)	(s_1, l_1)
(s_2, l_2)	(s_2, l_2)	(s_2, l_2)	(s_2, l_2)	(s_2, l_2)	(s_2, l_2)	(s_2, l_2)	(s_2, l_2)	(s_2, l_2)	(s_2, l_2)
(s_3, l_3)	(s_3, l_3)	(s_3, l_3)	(s_3, l_3)	(s_3, l_3)	(s_3, l_3)	(s_3, l_3)	(s_3, l_3)	(s_3, l_3)	(s_3, l_3)
(s_4, l_4)	(s_4, l_4)	(s_4, l_4)	(s_4, l_4)	(s_4, l_4)	(s_4, l_4)	(s_4, l_4)	(s_4, l_4)	(s_4, l_4)	(s_4, l_4)
(s_5, l_5)	(s_5, l_5)	(s_5, l_5)	(s_5, l_5)	(s_5, l_5)	(s_5, l_5)	(s_5, l_5)	(s_5, l_5)	(s_5, l_5)	(s_5, l_5)
(s_6, l_6)	(s_6, l_6)	(s_6, l_6)	(s_6, l_6)	(s_6, l_6)	(s_6, l_6)	(s_6, l_6)	(s_6, l_6)	(s_6, l_6)	(s_6, l_6)
m_{v5}									
F1	F2	F3	F4	F5	F6	F7	F8	F9	F10
(s_1, l_1)	(s_1, l_1)	(s_1, l_1)	(s_1, l_1)	(s_1, l_1)	(s_1, l_1)	(s_1, l_1)	(s_1, l_1)	(s_1, l_1)	(s_1, l_1)
(s_2, l_2)	(s_2, l_2)	(s_2, l_2)	(s_2, l_2)	(s_2, l_2)	(s_2, l_2)	(s_2, l_2)	(s_2, l_2)	(s_2, l_2)	(s_2, l_2)
(s_3, l_3)	(s_3, l_3)	(s_3, l_3)	(s_3, l_3)	(s_3, l_3)	(s_3, l_3)	(s_3, l_3)	(s_3, l_3)	(s_3, l_3)	(s_3, l_3)
(s_4, l_4)	(s_4, l_4)	(s_4, l_4)	(s_4, l_4)	(s_4, l_4)	(s_4, l_4)	(s_4, l_4)	(s_4, l_4)	(s_4, l_4)	(s_4, l_4)
(s_5, l_5)	(s_5, l_5)	(s_5, l_5)	(s_5, l_5)	(s_5, l_5)	(s_5, l_5)	(s_5, l_5)	(s_5, l_5)	(s_5, l_5)	(s_5, l_5)
(s_6, l_6)	(s_6, l_6)	(s_6, l_6)	(s_6, l_6)	(s_6, l_6)	(s_6, l_6)	(s_6, l_6)	(s_6, l_6)	(s_6, l_6)	(s_6, l_6)
m_{v6}									
F1	F2	F3	F4	F5	F6	F7	F8	F9	F10
(s_1, l_1)	(s_1, l_1)	(s_1, l_1)	(s_1, l_1)	(s_1, l_1)	(s_1, l_1)	(s_1, l_1)	(s_1, l_1)	(s_1, l_1)	(s_1, l_1)
(s_2, l_2)	(s_2, l_2)	(s_2, l_2)	(s_2, l_2)	(s_2, l_2)	(s_2, l_2)	(s_2, l_2)	(s_2, l_2)	(s_2, l_2)	(s_2, l_2)
(s_3, l_3)	(s_3, l_3)	(s_3, l_3)	(s_3, l_3)	(s_3, l_3)	(s_3, l_3)	(s_3, l_3)	(s_3, l_3)	(s_3, l_3)	(s_3, l_3)
(s_4, l_4)	(s_4, l_4)	(s_4, l_4)	(s_4, l_4)	(s_4, l_4)	(s_4, l_4)	(s_4, l_4)	(s_4, l_4)	(s_4, l_4)	(s_4, l_4)
(s_5, l_5)	(s_5, l_5)	(s_5, l_5)	(s_5, l_5)	(s_5, l_5)	(s_5, l_5)	(s_5, l_5)	(s_5, l_5)	(s_5, l_5)	(s_5, l_5)
(s_6, l_6)	(s_6, l_6)	(s_6, l_6)	(s_6, l_6)	(s_6, l_6)	(s_6, l_6)	(s_6, l_6)	(s_6, l_6)	(s_6, l_6)	(s_6, l_6)

F1 to F10 denotes the Field 1 to Field 10

4.4. Results and Discussions

4.4.1. Specular Scattering Analysis for Smooth Surface

Angular variation of specular scattering coefficient for different soil texture and moisture for both like polarizations are shown in Figures 4.2 and 4.3 and details about the fields are given in Tables 4.2 and 4.3.

(a) Specular Scattering Response for Different Dry Soil Texture fields in HH–Polarization

Discrimination in specular scattering coefficient can be observed in different soil texture fields at 6 GHz for dry soil, i.e., $m_v = 0.027$ cm^3 cm^{-3} (Figure 4.1(a)). Field 1 (sand = 85.3%, silt = 7.5%, and clay = 2.5%) which consists of maximum amount of sand have Angular Dynamic range in Specular Scattering Coefficient (ADSSC) of 9.8 dB while Field 10 (sand = 2.3%, silt = 10.3%, and clay = 81.6%) which contains the maximum amount of clay have ADSSC of 13.6 dB with incidence angle. The observation suggests that the discrimination between sandy soil and clay soil can be made on the basis of the specular scattering coefficient. It was observed that with the decrease of sand percentage in soil (Field 1 to Field 4) the ADSSC increases, whereas the increase in ADSSC occurs with the increase in clay percentage in soil (Field 7 to field 10). Further, major changes in silt percentage (Field 5 to Field 7) have lesser effect on specular scattering coefficient and the ADSSC remain approximately 12.2 dB. These observations are clearly evident in Figure 4.1(a). Therefore, it may be inferred that when the silt constituent in the soil is changed from the 41.3% to 70.6% it has the minimum effect on the specular scattering coefficient for 6 GHz in HH–polarization. Further, in case of higher incidence angle (i.e., $\geq 45°$) decrease in specular scattering coefficient is observed with the decrease in sand percentage, i.e., decreasing the sand percentage from 85.3% to 24.6%, whereas keeping the percentage of sand and clay lower in soil and making the changes in silt percentage in major amount does not affect the specular scattering coefficient significantly and provides a kind of saturation in specular scattering coefficient (Figure 4.1(a)). Additionally, a decrease in specular scattering coefficient is again observed with the increase in clay percentage from 51.5% to 81.6% (Figure 4.1(a)).

The observations made with different soil texture field for dry soil at 6 GHz in HH–polarization suggest that the higher incidence angle ($\geq 45°$) better discriminate between different soil texture fields and the changes made in sand constituent and clay constituent have greater effect on the specular scattering coefficient, whereas the change in silt constituent has very less effect on specular scattering coefficient [157].

(b) Specular Scattering Response for Different Moist Soil Texture Fields in HH–Polarization

To study the effect of soil moisture on different soil texture fields, fields were irrigated artificially. The details about the fields are given in Table 4.2. Figures 4.1(b)–(f) explain the angular behavior of specular scattering coefficient when the volumetric soil moisture contents were 0.096 cm^3 cm^{-3}, 0.188 cm^3 cm^{-3}, 0.261 cm^3 cm^{-3}, 0.374 cm^3 cm^{-3} and 0.425 cm^3 cm^{-3}, respectively for 10 different soil texture fields. The effect of soil texture on specular scattering can be noticed for lower soil moisture contents, i.e., with the change in soil texture field, significant changes in specular scattering coefficient can be observed (Figures 4.1(b)–(d)). The ADSSC of 11.2 dB, 12.3 dB, and 13.4 dB was observed at volumetric soil moisture contents 0.096 cm^3 cm^{-3} for Field 1, Field 2 and Field 3, respectively. The ADSSC for Field 4 to Field 8 is approximately 14 dB and in case of Field 9 and Field 10 the ADSSC is 14.5 dB and 15.7 dB respectively (Figure 4.1(b)). These observations clearly signify the soil texture effect on specular scattering coefficient in the presence of lower soil moisture (i.e., 0.096 cm^3 cm^{-3}) and infer that the Field 1 to Field 3 and Fields 9, 10 which has the higher amount of the sand and clay respectively may be the key factors for changes in specular scattering coefficient while Field 4 to Field 8 which has higher amount of the silt has almost same response for the specular scattering coefficient. Further, with the increase in soil moisture content, it was observed that the ADSSC for Field 3 to field 8 were approximately same at volumetric soil moisture content 0.188 cm^3 cm^{-3} and 0.261 cm^3 cm^{-3}, whereas Field 1 and Field 2 that possess the high amount of sand (85.3% and 62.6% respectively) have lowest ADSSC while Field 9 and Field 10 that possess the high amount of clay content (64.2% and 81.6% respectively) have maximum ADSSC (Figures 4.1(c) and (d)). The effect of soil texture on specular scattering coefficient is difficult to observe at high moisture content (m_v = 0.374 cm^3 cm^{-3} and 0.425 cm^3 cm^{-3}), i.e., with the change in soil texture very less changes occur in specular scattering coefficient (Figures 4.1(e) and (f)). The effect may arise due to high dielectric constant of water, i.e., after some particular soil moisture content saturation occurs and moisture effect dominates the soil texture effect. Further, Figure 4.1(b)–(d) suggest that for soil moisture less than or equal to 0.261 cm^3 cm^{-3}, higher incidence angle ($\geq 45°$) provide the better changes in specular

scattering coefficient for the change in sand constituent (Field 1 to Field 3) and clay constituent (Field 8 to Field 10) but lesser changes have been observed for the change in silt constituent (Field 4 to Field 7).

Observation with the moisture content in soil for different soil texture field at 6 GHz in HH–polarization infer that the sand and clay constituent of the soil has its effect on specular scattering coefficient for soil moisture content up to 0.261 cm^3 cm^{-3} whereas the silt constituent has the minimum effect at 6 GHz. The effect is more prominent at higher incidence angel (i.e., $\geq 45°$). Soil moisture content higher than 0.261 cm^3 cm^{-3} provides minimum changes in specular scattering coefficient with change in soil texture and only the angular variation was observed.

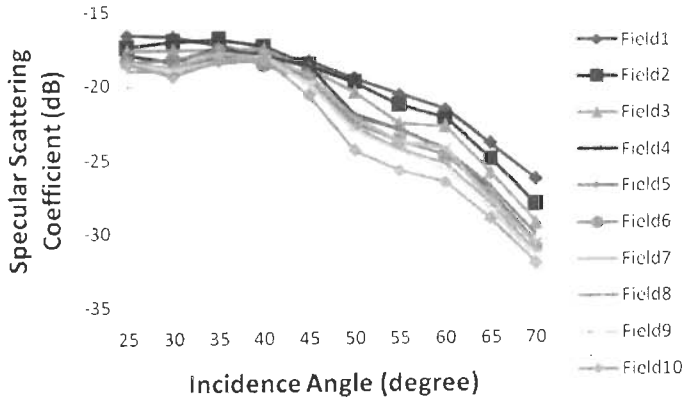

(a)

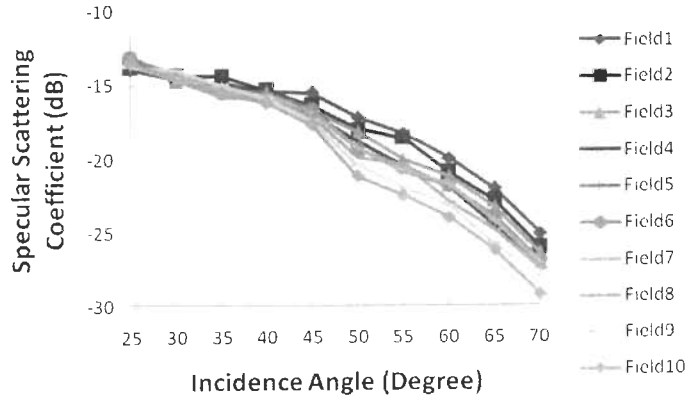

(b)

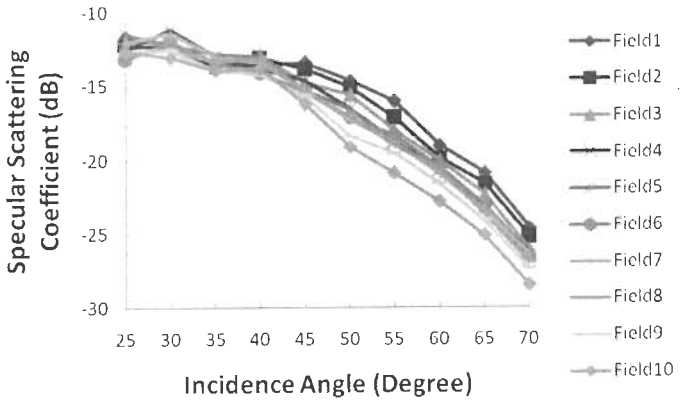
Specular Scattering Coefficient (dB)
-10
-15
-20
-25
-30
25 30 35 40 45 50 55 60 65 70
Incidence Angle (Degree)
Field1
Field2
Field3
Field4
Field5
Field6
Field7
Field8
Field9
Field10

(c)

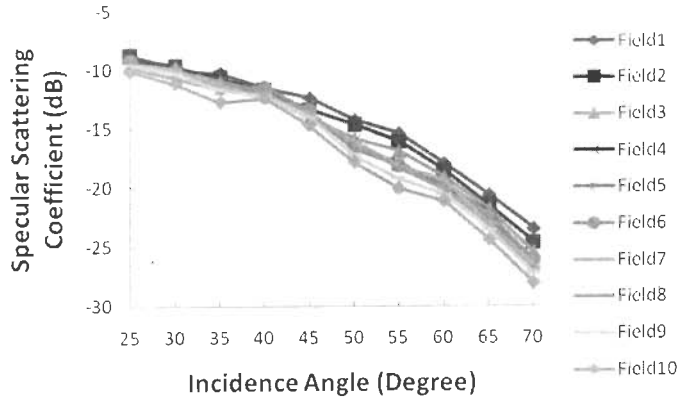
Specular Scattering Coefficient (dB)
-5
-10
-15
-20
-25
-30
25 30 35 40 45 50 55 60 65 70
Incidence Angle (Degree)
Field1
Field2
Field3
Field4
Field5
Field6
Field7
Field8
Field9
Field10

(d)

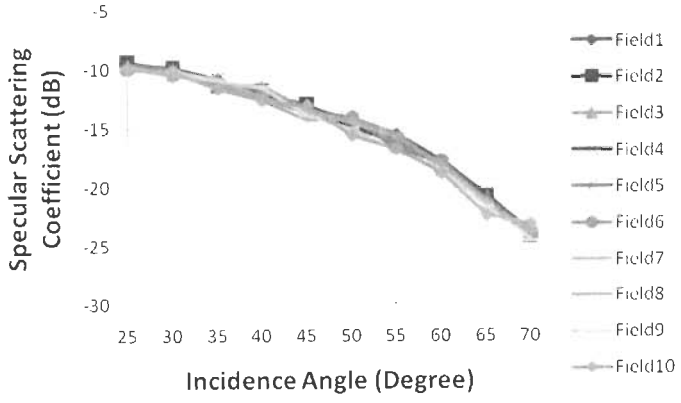
Specular Scattering Coefficient (dB)
-5
-10
-15
-20
-25
-30
25 30 35 40 45 50 55 60 65 70
Incidence Angle (Degree)
Field1
Field2
Field3
Field4
Field5
Field6
Field7
Field8
Field9
Field10

(e)

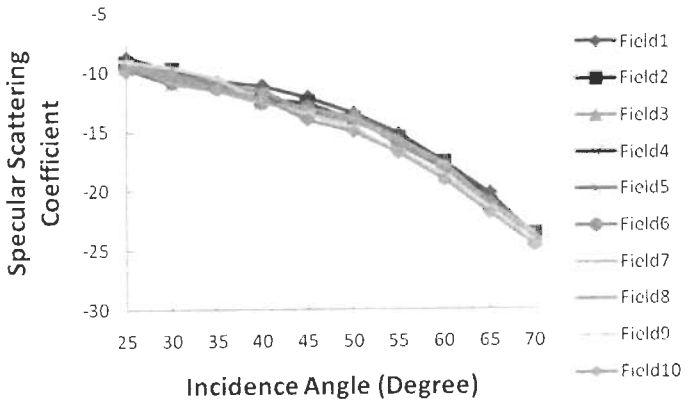

(f)

Figure 4.1. Specular scattering coefficient behavior with incidence angle for 10 different soil texture fields in HH–polarization. (a), (b), (c), (d), (e), and (f) show volumetric soil moisture content 0.027 cm^3 cm^{-3}, 0.096 cm^3 cm^{-3}, 0.188 cm^3 cm^{-3}, 0.261 cm^3 cm^{-3}, 0.374 cm^3 cm^{-3}, and 0.425 cm^3 cm^{-3} respectively.

(c) Specular Scattering Response for Different Dry Soil Texture fields in VV–Polarization

Figure 4.2(a) provides the insight for the variation in specular scattering coefficient with incidence angle in VV–polarization for 10 different soil texture fields for dry soil (i.e. volumetric soil moisture is 0.027 cm^3 cm^{-3}). The change in specular scattering coefficient was observed with the change in soil texture in VV–polarization also, as was the case with HH–polarization. Figure 4.2(a) explains the behavior of specular scattering coefficient for dry soil and the observation infers that higher incidence angle (i.e., $\geq 45°$) has better discrimination for different soil texture field than at lower incidence angle. It can be observed from Figure 4.2(a) that a sharp decrease in specular scattering coefficient occur for all 10 different soil texture fields at 60° incidence angle. This phenomenon may be due to Brewster angle effect in VV–polarization. Brewster angle is characterized as the incidence angle at which all the incident power is transmitted and theoretically there should be no reflected power. But, the undulation and inhomogeneity in the medium provide lower values of specular scattering coefficient.

The observations at 6 GHz in VV–polarization for dry soil with different soil texture fields suggest the utilization of the higher incidence angles (i.e., $\geq 45°$) for soil texture characterization.

(d) Specular Scattering Response for Different Moist Soil Texture Fields in VV–Polarization

Figure 4.2(b)–(f) explains the angular behavior of specular scattering coefficient when volumetric soil moisture contents were 0.096 cm^3 cm^{-3}, 0.188 cm^3 cm^{-3}, 0.261 cm^3 cm^{-3}, 0.374 cm^3 cm^{-3} and 0.425 cm^3 cm^{-3}, respectively for 10 different soil texture fields in VV–polarization. A shift in Brewster angle from 60° to 65° is observed with the increase in soil moisture, i.e., m_v = 0.096 cm^3 cm^{-3} (Figure 4.2(b)). This occurs due to change in dielectric constant of soil with moisture content that causes the shift in Brewster angle. Further, at volumetric soil moisture content 0.188 cm^3 cm^{-3} only the soil with higher clay content (Field 8, Field 9, and Field 10) exhibits the Brewster angle effect while the soil with higher sand or silt content (Field 1 to Field 7) does not exhibit Brewster angle (Figure 4.2(c)). This may be due to the lower dielectric constant of soil having greater amount of clay constituent and high dielectric constant of soil having high amount of sand or silt constituent. Similar results were also found by De Roo and Ulaby [43] and Nashashibi and Ulaby [140]. The Brewster angle effect is not observed at high moisture values (Figure 4.2(d)–(f)). Further, it may be noticed from Figure 4.2(e) and (f) that when the moisture content in soil is high (m_v = 0.374 cm^3 cm^{-3} and 0.425 cm^3 cm^{-3} respectively), approximately same specular scattering coefficient values have been obtained with the change in soil texture at all incidence angle. Albeit, at these high moisture contents the ADSSC for soil having high amount of sand (Field 1) and high amount of clay (Field 10) show significant changes. ADSSC for Field 1 (sand = 85.3%, silt = 7.5%, and clay = 2.5%) is 22.9 dB and ADSSC for Field 10 (sand = 2.3%, silt = 10.3%, and clay = 81.6%) is 26.6 dB.

The observation made with moist soil for different soil texture field at 6 GHz in VV–polarization suggest the use of higher incidence angle (i.e., ≥ 45°) as was the case with HH–polarization. The Brewster angle effect has not been observed for soil moisture content equal to or greater than 0.261 cm^3 cm^{-3} and the discrimination for the high amount of sand in soil (Field1) and high amount of clay in soil (Field 10) can be made at all soil moisture values. Further, the effect of silt constituent on specular scattering coefficient is minimum as was observed in HH–polarization.

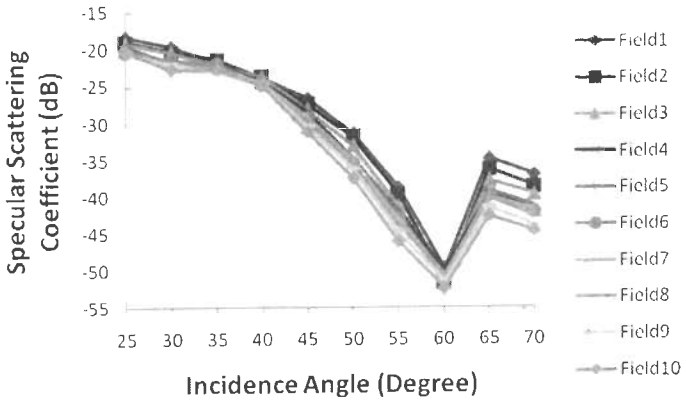
Specular Scattering Coefficient (dB)
-15
-20
-25
-30
-35
-40
-45
-50
-55
25 30 35 40 45 50 55 60 65 70
Incidence Angle (Degree)
Field1
Field2
Field3
Field4
Field5
Field6
Field7
Field8
Field9
Field10

(a)

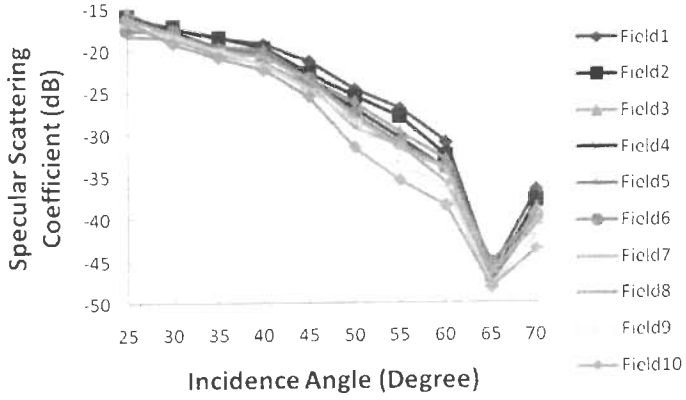
Specular Scattering Coefficient (dB)
-15
-20
-25
-30
-35
-40
-45
-50
25 30 35 40 45 50 55 60 65 70
Incidence Angle (Degree)
Field1
Field2
Field3
Field4
Field5
Field6
Field7
Field8
Field9
Field10

(b)

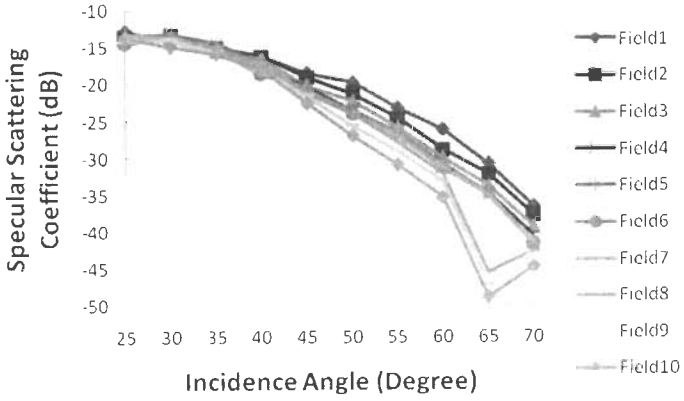
Specular Scattering Coefficient (dB)
-10
-15
-20
-25
-30
-35
-40
-45
-50
25 30 35 40 45 50 55 60 65 70
Incidence Angle (Degree)
Field1
Field2
Field3
Field4
Field5
Field6
Field7
Field8
Field9
Field10

(c)

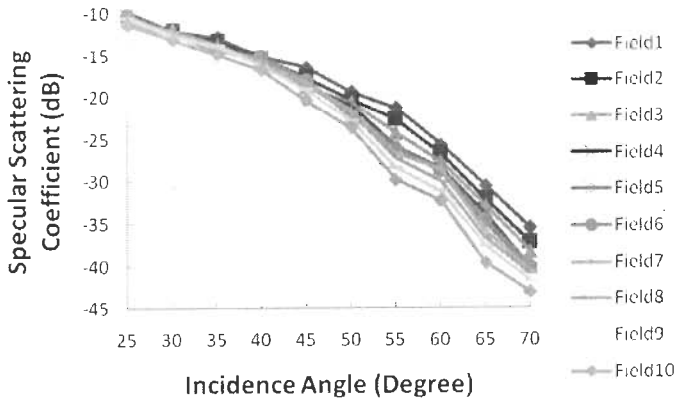

(d)

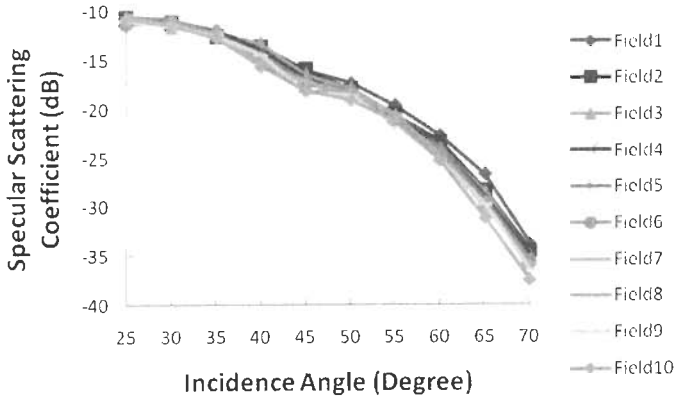

(e)

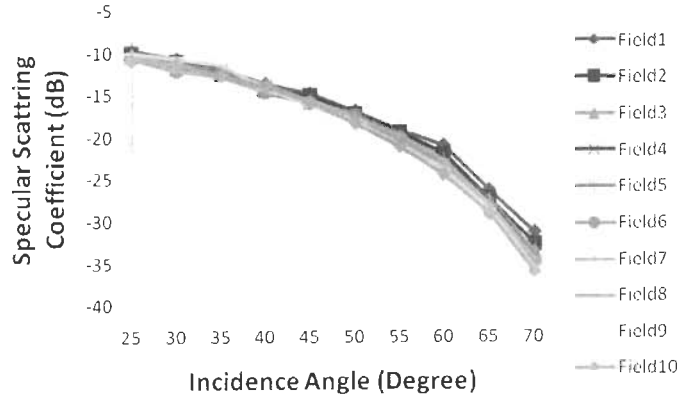

(f)

Figure 4.2. Specular scattering coefficient behavior with incidence angle for 10 different soil texture fields in VV–polarization. (a), (b), (c), (d), (e), and (f) show volumetric soil moisture content 0.027 cm^3 cm^{-3}, 0.096 cm^3 cm^{-3}, 0.188 cm^3 cm^{-3}, 0.261 cm^3 cm^{-3}, 0.374 cm^3 cm^{-3}, and 0.425 cm^3 cm^{-3} respectively.

4.4.2. Specular Scattering Analysis for Rough and Moist Soil Surfaces

Figures 4.3 to 4.12 show the angular response of specular scattering coefficient for different soil texture fields at various soil moisture and periodic surface roughness conditions for both like polarizations, i.e., HH– and VV–polarization at 6 GHz.

(a) Specular Scattering Response with Change in Soil Moisture Content in HH–Polarization for Constant Roughness

Figures 4.3(a)–(f) show the angular response of specular scattering coefficient for different soil textures and soil moisture at rms surface height 0.43 cm and correlation length 4.68 cm in HH–polarization. The ADSSC (i.e., minimum to maximum value of specular scattering coefficient for all incidence angle) for Field 1(sand = 85.3%, silt = 7.5% and clay =2.5%) which consists of the maximum amount of sand is 11.04 dB, whereas for Field 10 (sand = 2.3%, silt = 10.3%, and clay =81.6%) which consist of maximum amount of clay percentage the ADSSC is 14.26 dB at volumetric soil moisture 0.028 cm^3 cm^{-3} (Figure 4.3(a)). This observation indicates that the separation between the sandy soil and clay soil can be done based on the specular scattering coefficient. It can be observed from the Figure 4.3(a) that the ADSSC increases with the decrease in sand percentage, e.g., the ADSSC for the Field 1(sand = 85.3%, silt = 7.5%, and clay =2.5%) is 11.04 dB, for Field 2 (sand = 62.6%, silt = 26.1%, and clay =5.3%) is 11.35 dB and for Field 3 (sand = 47.2%, silt = 32.7%, and clay = 15.4%) is 11.47 dB, whereas the ADSSC again increases with the increase in clay percentage in soil, e.g., the ADSSC for the Field 9 (sand = 7.5%, silt = 23.4%, and clay =64.2%) is 13.81 dB and for Field 10 (sand = 2.3%, silt = 10.3%, and clay =81.6%) is 14.28 dB. However, the major changes in silt percentage have very less effect on specular scattering coefficient. Further, the observations (Figures 4.3(a)–(d)) at lower incidence angel (i.e., $\theta < 45°$) show almost same specular scattering coefficient for different soil texture fields, whereas the distinction among different soil texture fields can be done at higher incidence angle (i.e., $\geq 45°$). Use of higher incidence angle for soil parameters characterization has also been recommended by various researches [30, 140, 156, 180] for scattering in specular direction. Very less angular variation of specular scattering coefficient at lower incidence angle (i.e., $\theta < 45°$) was observed for all ten soil texture fields at volumetric

soil moisture 0.258 cm^3 cm^{-3} and higher (Figures 4.3(d)–(f)) whereas, significant angular variation in specular scattering coefficient was observed for higher incidence angles (i.e., $\geq 45°$) (Figures 4.3(d)–(f)). In addition, the observation from Figures 4.3(e) and (f) revealed approximately the same specular scattering coefficient for different soil texture fields at all incidence angles when soil moisture content is more than or equal to 0.368 (i.e., $m_v \geq 0.368$). The higher soil moisture values signify the higher amount of water in soil medium, therefore this high amount of water has greater effect on the specular scattering coefficient and may minimize the contribution of the soil texture on the specular scattering coefficient.

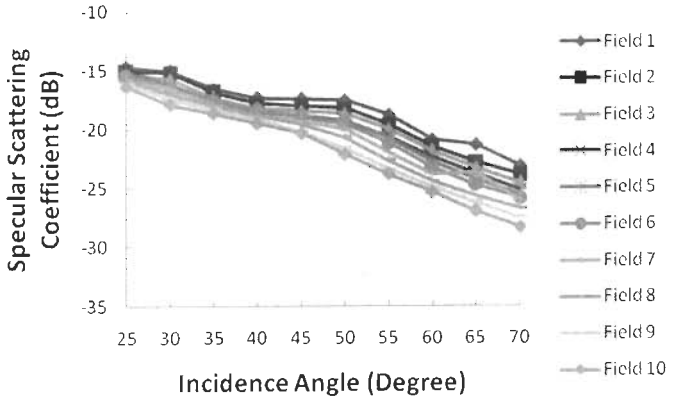

(a)

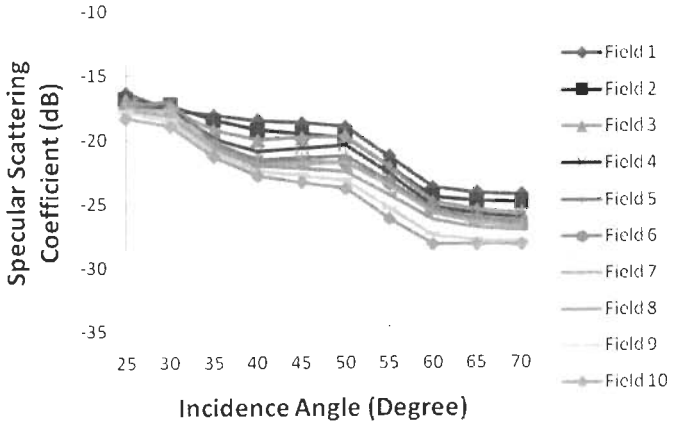

(b)

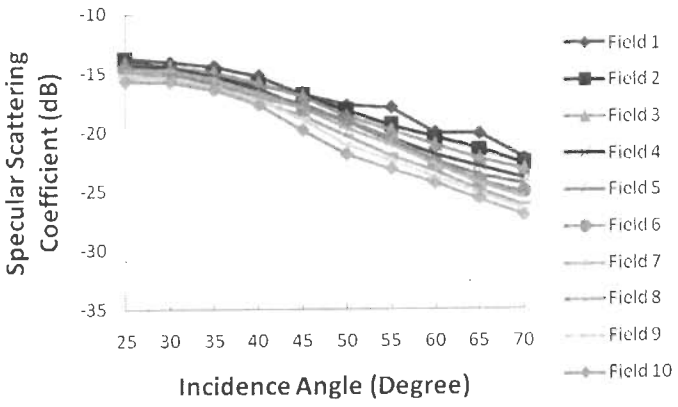
Specular Scattering Coefficient (dB)
-10
-15
-20
-25
-30
-35
25 30 35 40 45 50 55 60 65 70
Incidence Angle (Degree)
Field 1
Field 2
Field 3
Field 4
Field 5
Field 6
Field 7
Field 8
Field 9
Field 10

(c)

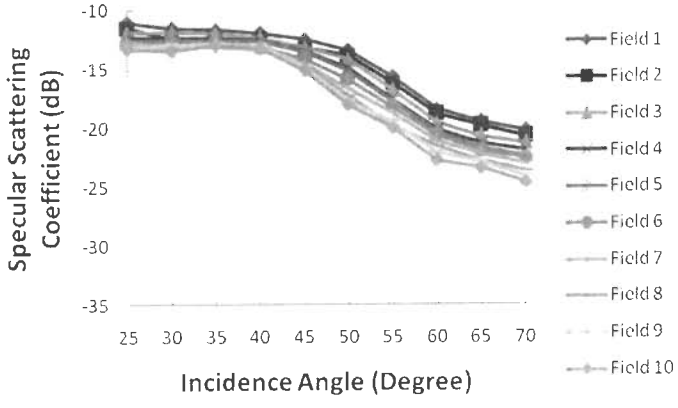
Specular Scattering Coefficient (dB)
-10
-15
-20
-25
-30
-35
25 30 35 40 45 50 55 60 65 70
Incidence Angle (Degree)
Field 1
Field 2
Field 3
Field 4
Field 5
Field 6
Field 7
Field 8
Field 9
Field 10

(d)

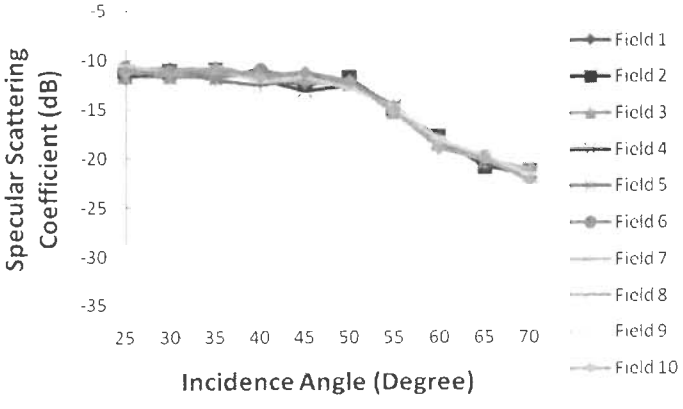
Specular Scattering Coefficient (dB)
-5
-10
-15
-20
-25
-30
-35
25 30 35 40 45 50 55 60 65 70
Incidence Angle (Degree)
Field 1
Field 2
Field 3
Field 4
Field 5
Field 6
Field 7
Field 8
Field 9
Field 10

(e)

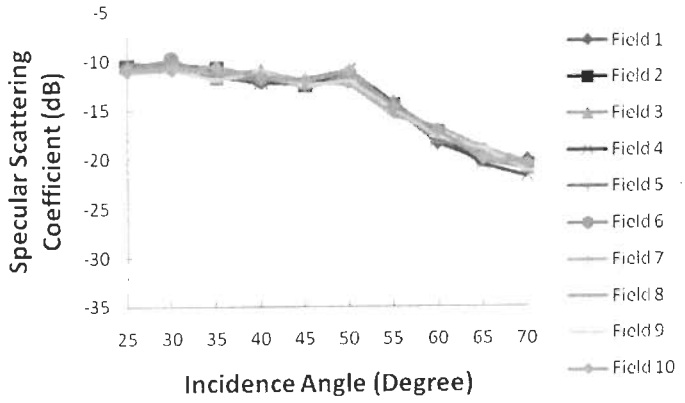

(f)

Figure 4.3. Represents the change in specular scattering coefficient with incidence angel for five different soil textue fields in HH–polarization at rms surfcace height 0.43 and correlation length 4.68 when volumetric soil moisture (cm^3 cm^{-3}) is (a) 0.027, (b) 0.092, (c) 0.195, (d) 0.258, (e) 0.368, and (f) 0.435.

(b) Specular Scattering Response in HH–Polarization for Change in Periodic Surface Roughness and Moisture Content

Figures 4.3 to 4.7 explain the angular behaviour of the specular scattering coefficient for five different soil texture fields at six soil moisture contents in HH–polarization when the rms surface heights and correlation lengths (s, l) are (0.43 cm, 4.68 cm), (0.94 cm, 5.66 cm), (1.51 cm 5.39 cm), (2.11 cm, 4.47 cm) and (2.46 cm 4.55 cm) respectively. Fields were prepared as discussed in Chapter 1. It is noticed that the ADSSC for the Field 1 (sand = 85.3%, silt = 7.5%, and clay =2.5%) and Field 10 (sand = 2.3%, silt = 10.3%, and clay =81.6%) for periodic roughness (s_2, l_2) is 11.04 dB and 14.26 dB, respectively (Figure 4.3(a)), at volumetric soil moisture 0.027 cm^3 cm^{-3}. Similarly, the ADSSC for the Field 1 and Field 10 for periodic roughness (s_3, l_3) is 10.58 dB and 13.08 dB (Figure 4.4(a)), for periodic roughness (s_4, l_4) is 10.27 dB and 12.45 dB (Figure 4.5(a)), for periodic roughness (s_5, l_5) is 7.27 dB and 10.43 dB (Figure 4.6(a)), for periodic roughness (s_6, l_6) is 2.48 dB and 5.63 dB (Figure 4.7(a)), respectively. These observations suggest that the separation between the sandy soil and the clay soil can be made on the basis of the specular scattering coefficient even at the moderately high periodic surface roughness values when the soil moisture content is 0.027 cm^3 cm^{-3}. Observations made at other volumetric soil moisture contents (0.092 cm^3 cm^{-3}, 0.195 cm^3 cm^{-3}, and 0.258 cm^3 cm^{-3}) also show the similar behavior, i.e., differentiation in the sandy soil and clay soil can easily be

made on the basis of the specular scattering coefficient for a range of periodic roughness values (s = 0.43 to 2.46 cm and l = 4.47 to 5.66 cm). Such as, at volumetric soil moisture 0.258 cm^3 cm^{-3} the ADSSC for the sandy soil (Field 1) with the incidence angle for periodic roughness (s_2, l_2), (s_3, l_3), (s_4, l_4), (s_5, l_5), and (s_6, l_6) are 11.95 dB, 11.67 dB, 11.11 dB, 10.82 dB, and 6.05 dB, respectively and for the clay soil (Field 10) the ADSSC is 14.56 dB, 13.12 dB, 13.72 dB, 7.80 dB and 3.71 dB, respectively. The observations at the higher soil moisture content, i.e., m_v = 0.368 cm^3 cm^{-3} and m_v = 0.435 cm^3 cm^{-3}, imply that there are negligible changes in the specular scattering coefficient with the change in soil texture, irrespective of the periodic surface roughness condition. The effect may arise due to the increased amount of water in the soil medium which minimizes the effect of soil texture on specular scattering.

Additionally, it is noticed that the ADSSC decreases with the increase in rms surface height, e.g., for the Field 1 at volumetric soil moisture 0.027 cm^3 cm^{-3} the ADSSC for periodic roughness (s_2, l_2), (s_3, l_3), (s_4, l_4), (s_5, l_5), and (s_6, l_6) are 11.04 dB, 10.58 dB, 10.27 dB, 7.27 dB, and 2.48 dB, respectively. Similar results were observed for the different soil texture fields and at all soil moisture conditions, i.e., the decrease in the ADSSC with increase in rms surface height and vice versa.

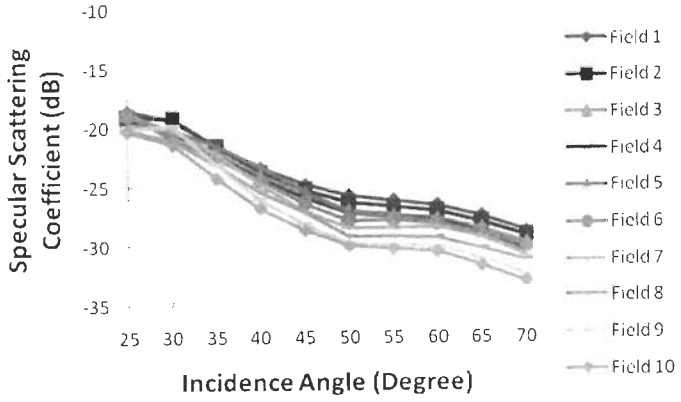

(a)

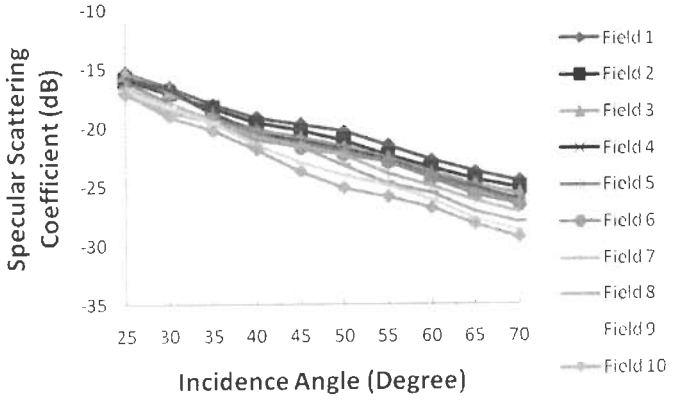
Specular Scattering Coefficient (dB)
-10
-15
-20
-25
-30
-35
25 30 35 40 45 50 55 60 65 70
Incidence Angle (Degree)
Field 1
Field 2
Field 3
Field 4
Field 5
Field 6
Field 7
Field 8
Field 9
Field 10

(b)

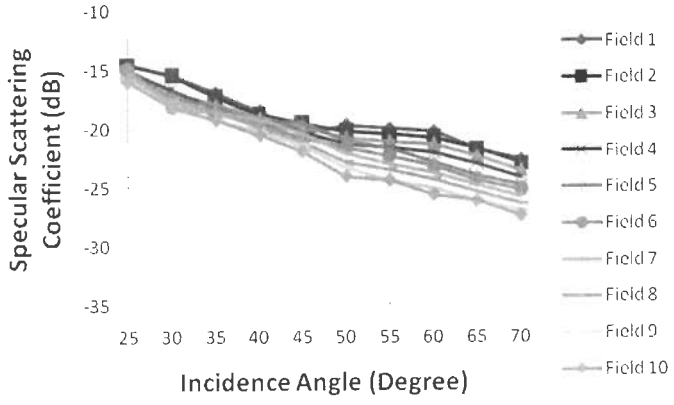
Specular Scattering Coefficient (dB)
-10
-15
-20
-25
-30
-35
25 30 35 40 45 50 55 60 65 70
Incidence Angle (Degree)
Field 1
Field 2
Field 3
Field 4
Field 5
Field 6
Field 7
Field 8
Field 9
Field 10

(c)

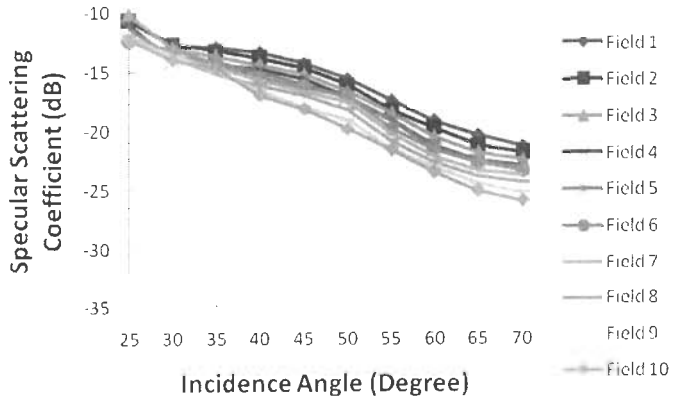
Specular Scattering Coefficient (dB)
-10
-15
-20
-25
-30
-35
25 30 35 40 45 50 55 60 65 70
Incidence Angle (Degree)
Field 1
Field 2
Field 3
Field 4
Field 5
Field 6
Field 7
Field 8
Field 9
Field 10

(d)

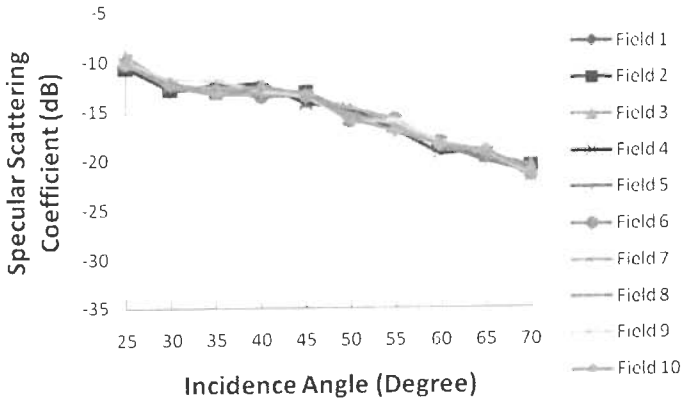

(e)

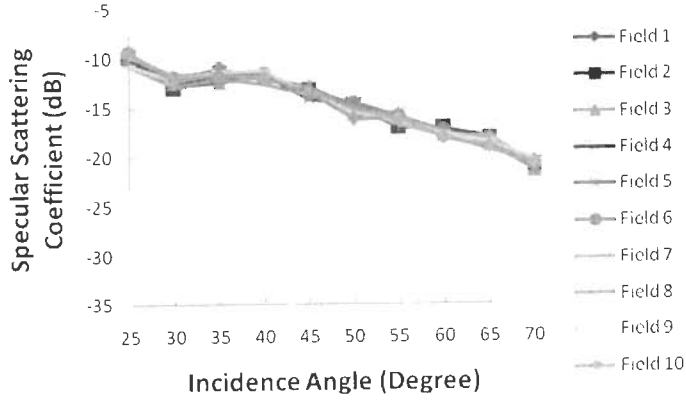

(f)

Figure 4.4. Represents the change in specular scattering coefficient with incidence angel for five different soil textue fields in HH–polarization at rms surfcace height 0.94 and correlation length 5.66 when volumetric soil moisture (cm^3 cm^{-3}) is (a) 0.027, (b) 0.092, (c) 0.195, (d) 0.258, (e) 0.368, and (f) 0.435.

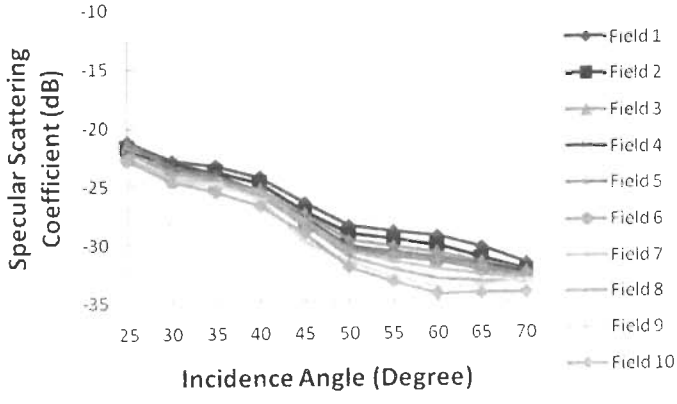

(a)

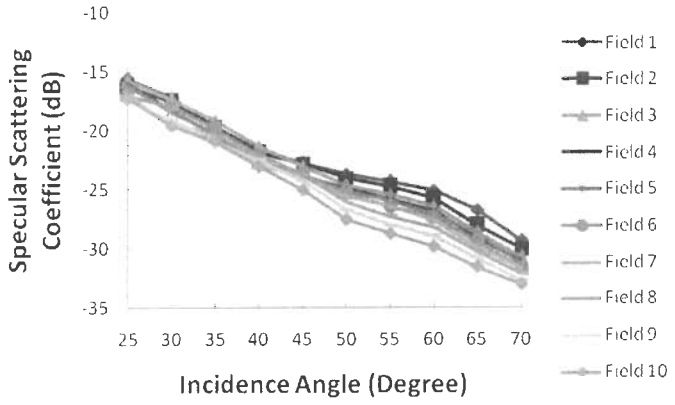
Specular Scattering Coefficient (dB)
-10
-15
-20
-25
-30
-35
25 30 35 40 45 50 55 60 65 70
Incidence Angle (Degree)
Field 1
Field 2
Field 3
Field 4
Field 5
Field 6
Field 7
Field 8
Field 9
Field 10

(b)

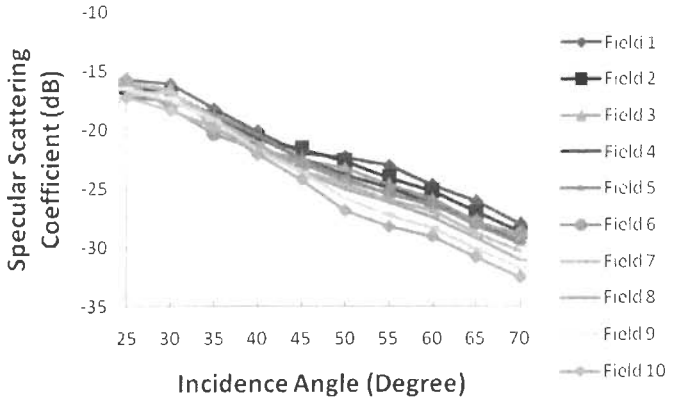
Specular Scattering Coefficient (dB)
-10
-15
-20
-25
-30
-35
25 30 35 40 45 50 55 60 65 70
Incidence Angle (Degree)
Field 1
Field 2
Field 3
Field 4
Field 5
Field 6
Field 7
Field 8
Field 9
Field 10

(c)

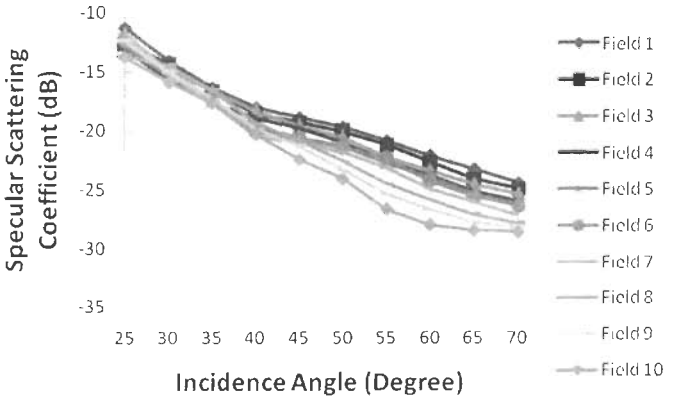
Specular Scattering Coefficient (dB)
-10
-15
-20
-25
-30
-35
25 30 35 40 45 50 55 60 65 70
Incidence Angle (Degree)
Field 1
Field 2
Field 3
Field 4
Field 5
Field 6
Field 7
Field 8
Field 9
Field 10

(d)

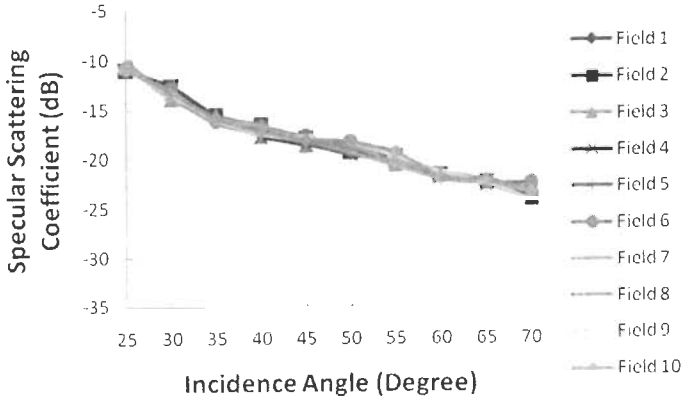

(e)

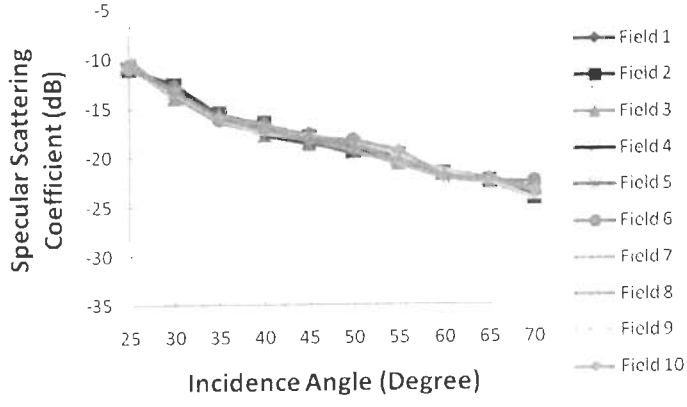

(f)

Figure 4.5. Represents the change in specular scattering coefficient with incidence angel for five different soil textue fields in HH–polarization at rms surfcace height 1.51 and correlation length 5.39 when volumetric soil moisture (cm^3 cm^{-3}) is (a) 0.027, (b) 0.092, (c) 0.195, (d) 0.258, (e) 0.368, and (f) 0.435.

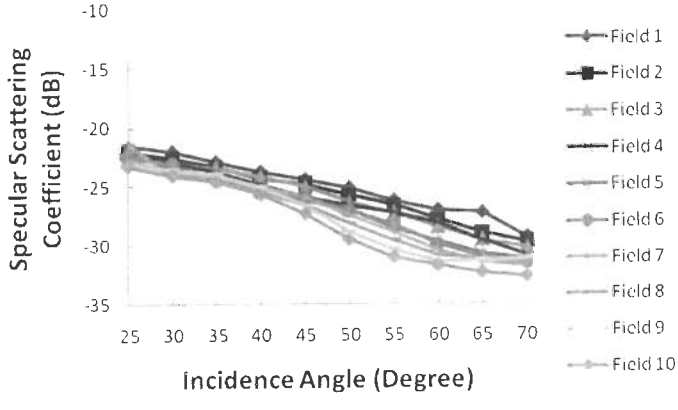

(a)

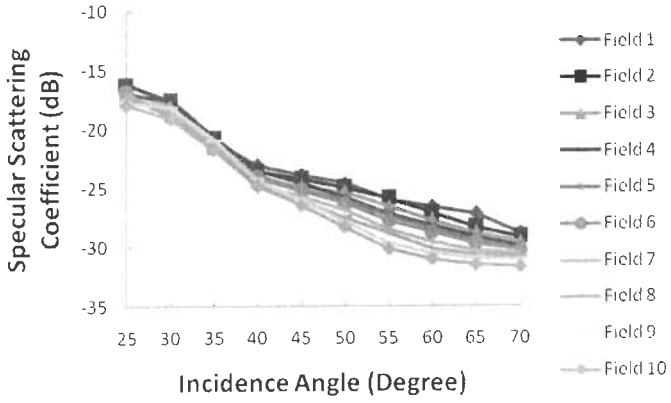
Specular Scattering Coefficient (dB)
-10
-15
-20
-25
-30
-35
25 30 35 40 45 50 55 60 65 70
Incidence Angle (Degree)
Field 1
Field 2
Field 3
Field 4
Field 5
Field 6
Field 7
Field 8
Field 9
Field 10

(b)

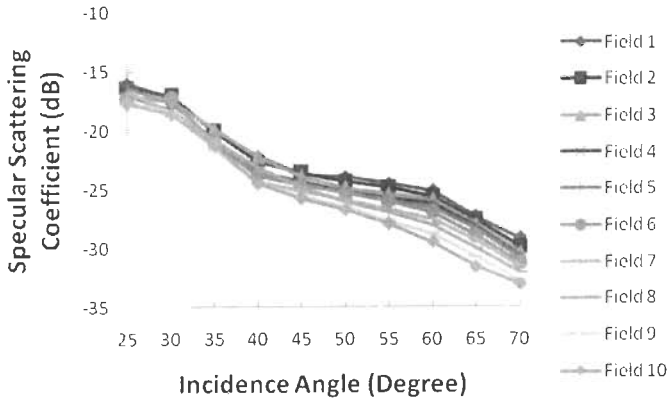
Specular Scattering Coefficient (dB)
-10
-15
-20
-25
-30
-35
25 30 35 40 45 50 55 60 65 70
Incidence Angle (Degree)
Field 1
Field 2
Field 3
Field 4
Field 5
Field 6
Field 7
Field 8
Field 9
Field 10

(c)

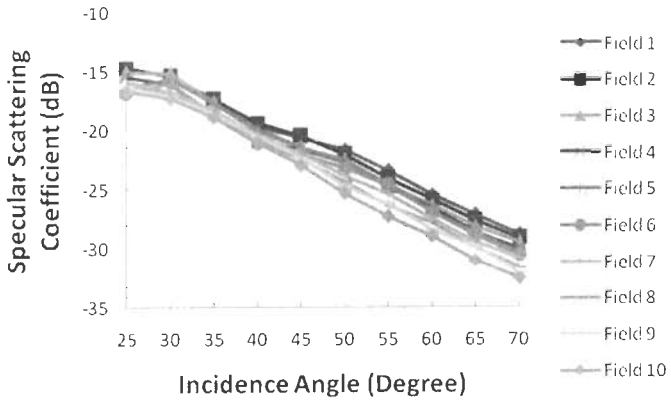
Specular Scattering Coefficient (dB)
-10
-15
-20
-25
-30
-35
25 30 35 40 45 50 55 60 65 70
Incidence Angle (Degree)
Field 1
Field 2
Field 3
Field 4
Field 5
Field 6
Field 7
Field 8
Field 9
Field 10

(d)

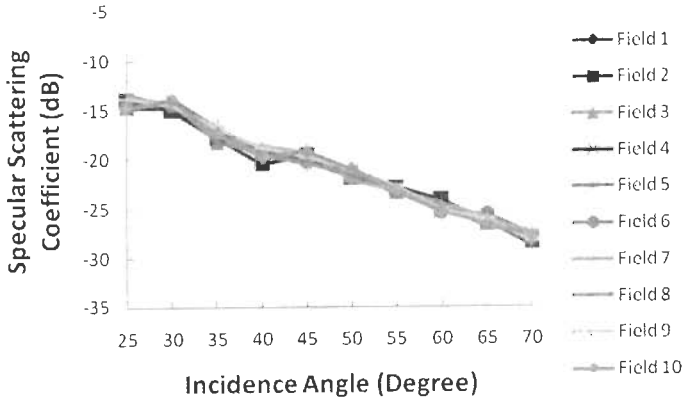

(e)

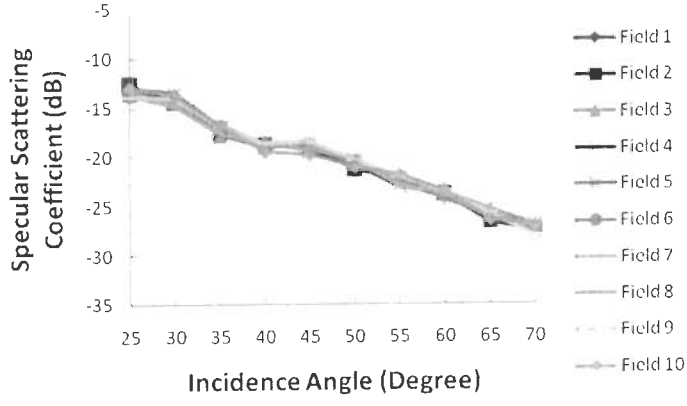

(f)

Figure 4.6. Represents the change in specular scattering coefficient with incidence angel for five different soil textue fields in HH–polarization at rms surfcace height 2.11 and correlation length 4.47 when volumetric soil moisture (cm^3 cm^{-3}) is (a) 0.027, (b) 0.092, (c) 0.195, (d) 0.258, (e) 0.368, and (f) 0.435.

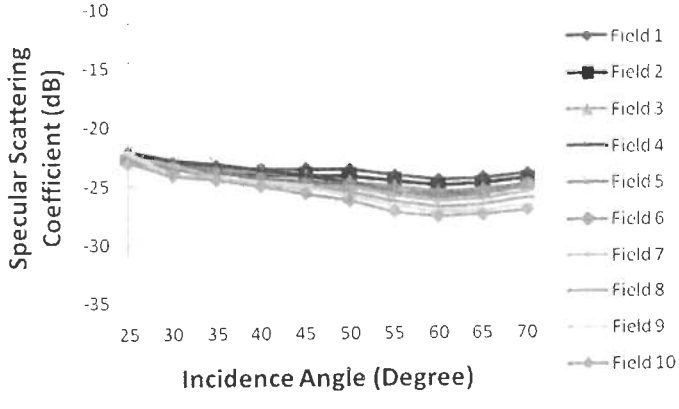

(a)

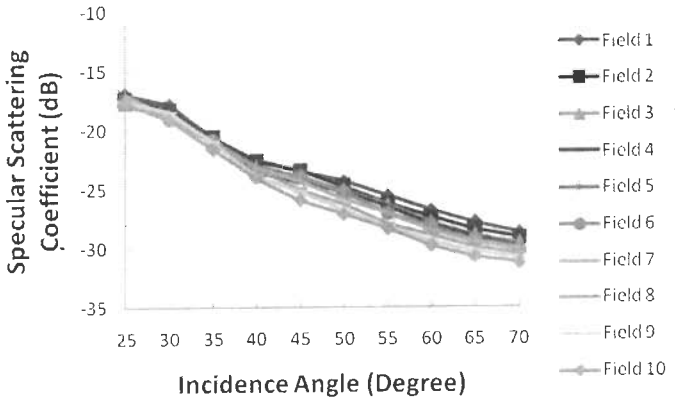
Specular Scattering Coefficient (dB)
-10
-15
-20
-25
-30
-35
25 30 35 40 45 50 55 60 65 70
Incidence Angle (Degree)
Field 1
Field 2
Field 3
Field 4
Field 5
Field 6
Field 7
Field 8
Field 9
Field 10

(b)

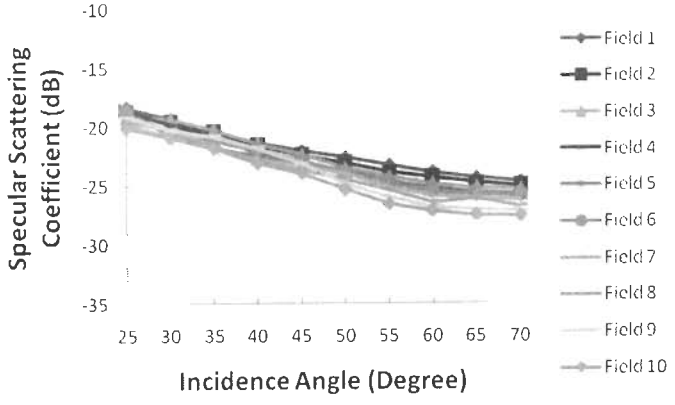
Specular Scattering Coefficient (dB)
-10
-15
-20
-25
-30
-35
25 30 35 40 45 50 55 60 65 70
Incidence Angle (Degree)
Field 1
Field 2
Field 3
Field 4
Field 5
Field 6
Field 7
Field 8
Field 9
Field 10

(c)

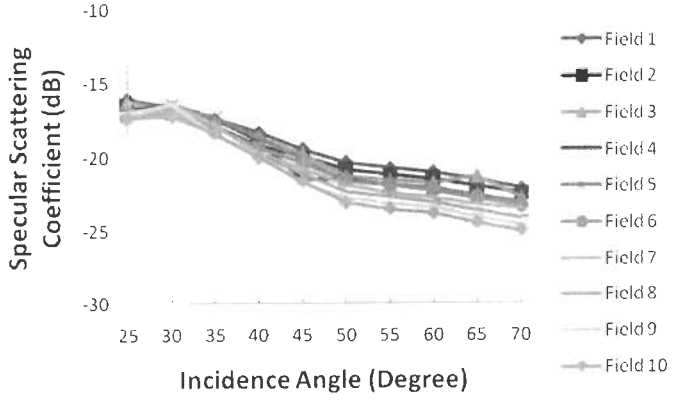
Specular Scattering Coefficient (dB)
-10
-15
-20
-25
-30
25 30 35 40 45 50 55 60 65 70
Incidence Angle (Degree)
Field 1
Field 2
Field 3
Field 4
Field 5
Field 6
Field 7
Field 8
Field 9
Field 10

(d)

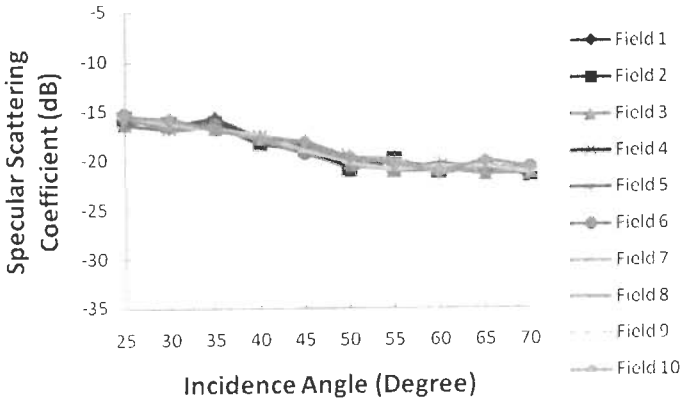

(e)

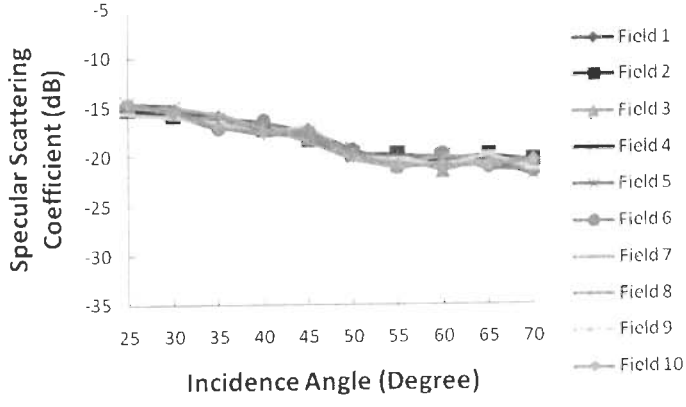

(f)

Figure 4.7. Represents the change in specular scattering coefficient with incidence angel for five different soil textue fields in HH–polarization at rms surfcace height 2.46 and correlation length 4.55 when volumetric soil moisture (cm^3 cm^{-3}) is (a) 0.027, (b) 0.092, (c) 0.195, (d) 0.258, (e) 0.368, and (f) 0.435.

(c) Specular Scattering Response with Change in Soil Moisture Content in VV–Polarization for Constant Roughness

Figures 4.8–4.12 explain the angular behavior of the specular scattering coefficient for five different soil texture fields at various moisture contents and periodic surface roughness conditions at 6 GHz in VV–polarization. The ADSSC with incidence angel when s = 0.43 cm and l = 4.68 cm and volumetric soil moisture content 0.027 cm^3 cm^{-3}, for higher sand constituent in soil i.e., Field 1 and Field 2 are 20.62 dB, 21.16 dB (Figure 4.8(a)), respectively, whereas for high clay content in soil, i.e., for Field 9 and Field 10 are 23.65 dB and 24.37 dB (Figure 4.8(a)), respectively. The change in specular scattering coefficient is less for higher silt constituent in soil.

Therefore, it can be concluded with these observations that the specular scattering coefficient at 6 GHz is capable of discriminating different soil texture fields in VV–polarization. The observations suggest that the discrimination among different soil texture fields is more prominent at higher incidence angel (i.e., $\theta \geq 45°$) than at lower incidence angles (i.e., $\theta < 45°$). Therefore, it may be inferred that higher incidence angles are more suitable than lower incidence angles for observing soil parameters. It is noticed that specular scattering coefficient for the different soil texture fields are approximately same in case of VV–polarization at higher soil moisture content (i.e., 0.368 cm^3 cm^{-3} and 0.435 cm^3 cm^{-3}) (Figures 4.8(e)–(f)).

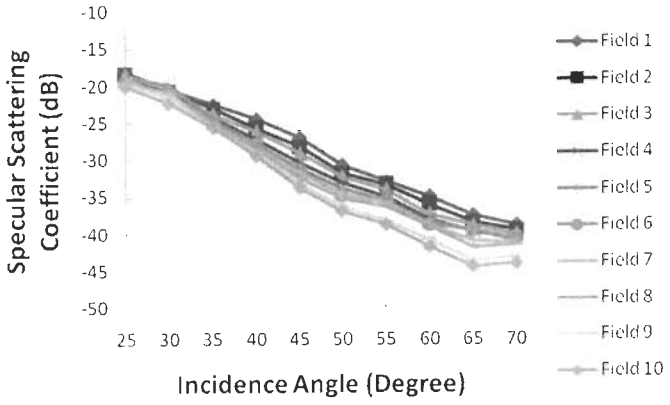

(a)

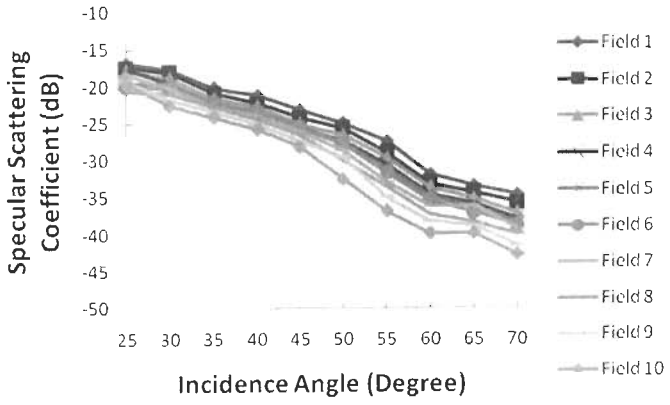

(b)

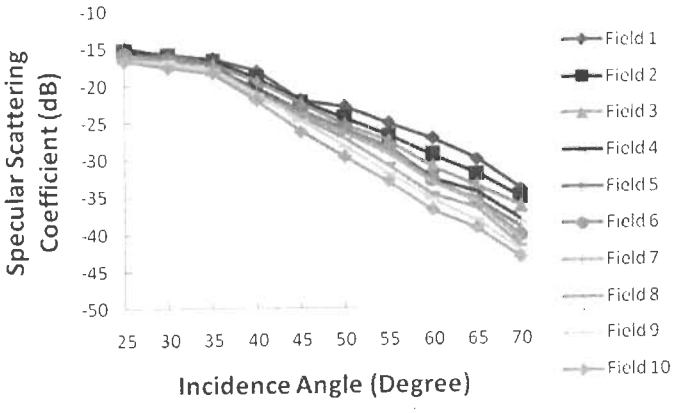
Specular Scattering Coefficient (dB)
-10
-15
-20
-25
-30
-35
-40
-45
-50
25 30 35 40 45 50 55 60 65 70
Incidence Angle (Degree)
Field 1
Field 2
Field 3
Field 4
Field 5
Field 6
Field 7
Field 8
Field 9
Field 10

(c)

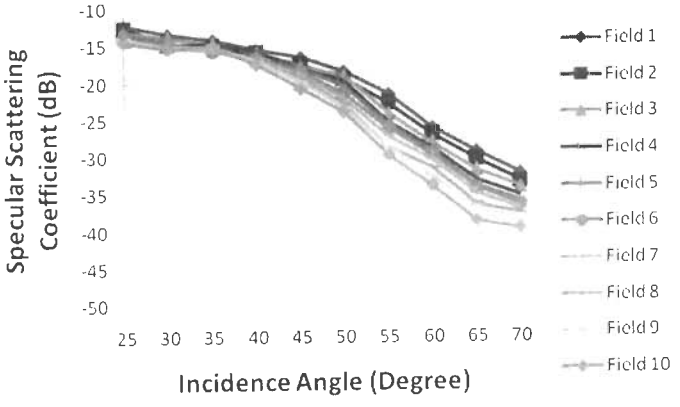
Specular Scattering Coefficient (dB)
-10
-15
-20
-25
-30
-35
-40
-45
-50
25 30 35 40 45 50 55 60 65 70
Incidence Angle (Degree)
Field 1
Field 2
Field 3
Field 4
Field 5
Field 6
Field 7
Field 8
Field 9
Field 10

(d)

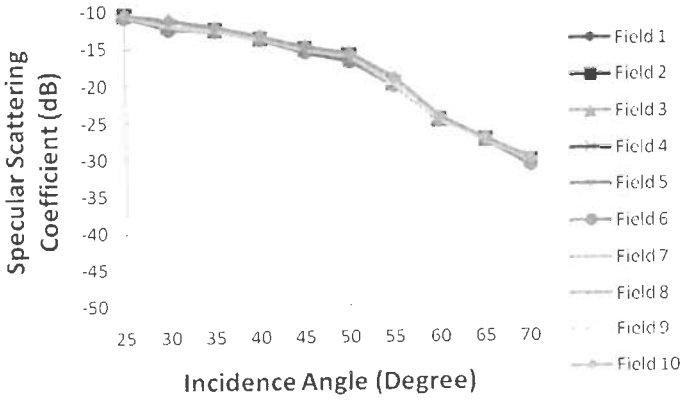
Specular Scattering Coefficient (dB)
-10
-15
-20
-25
-30
-35
-40
-45
-50
25 30 35 40 45 50 55 60 65 70
Incidence Angle (Degree)
Field 1
Field 2
Field 3
Field 4
Field 5
Field 6
Field 7
Field 8
Field 9
Field 10

(e)

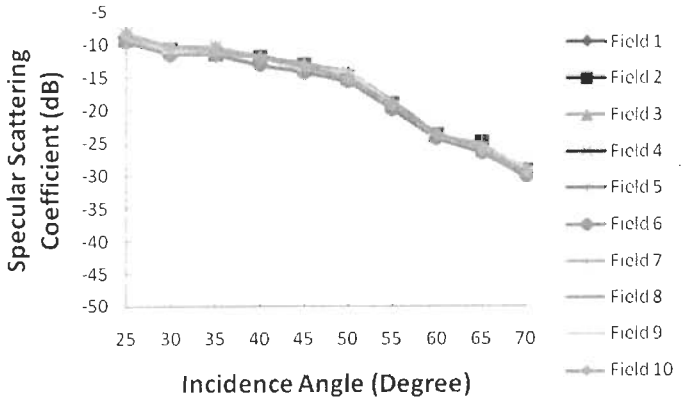

(f)

Figure 4.8. Represents the change in specular scattering coefficient with incidence angel for five different soil textue fields in VV–polarization at rms surfcace height 0.43 and correlation length 4.68 when volumetric soil moisture (cm^3 cm^{-3}) is (a) 0.027, (b) 0.092, (c) 0.195, (d) 0.258, (e) 0.368, and (f) 0.435.

(d) Specular Scattering Response in VV–Polarization for Change in Periodic Surface Roughness and Moisture Content

Figures 4.8–4.12 explain the behaviour of specular scattering coefficient for periodic roughness (s_2, l_2), (s_3, l_3), (s_4, l_4), (s_5, l_5), and (s_6, l_6), respectively for various soil moisture contents in VV–polarization at 6 GHz. The change in specular scattering coefficient was observed for the change in soil texture at all periodic roughness condition for fixed soil moisture, i.e., the ADSSC for Field 1 and Field 10 for periodic roughness (s_2, l_2) are 20.62 dB and 24.37 dB, respectively, whereas for periodic roughness (s_6, l_6) the ADSSC for Field 1 and Field 10 are 18.75 dB and 21.79 dB, respectively, at volumetric soil moisture content 0.027 cm^3 cm^{-3}. Further, the change in specular scattering coefficient with the change in soil texture for a range of periodic roughness values are observed up to particular soil moisture content (i.e., $m_v \leq 0.258$ cm^3 cm^3). Whereas, negligible changes in specular scattering coefficient with change in soil texture for a range of periodic surface roughness were observed for the higher soil moisture content (i.e., 0.368 cm^3 cm^{-3} and 0.435 cm^3 cm^{-3}).

The observations made at HH– and VV–polarization suggest the use of higher incidence angle to characterize the soil parameters with specular scattering response at 6 GHz. It was noticed from the 'e' and 'f' part of the Figures 4.3–4.12 that there is no clear cut distinction in specular scattering coefficient with change in soil texture at all incidence angles in both like polarizations when volumetric soil moisture, m_v, is ≥

0.368. In addition, it was observed in HH–polarization as well as in VV–polarization that soil periodic surface roughness has very less affect on the response of the specular scattering coefficient for different soil texture fields, i.e., the differentiation in different soil texture fields based on specular scattering coefficient can be noticed for a wide range of periodic surface roughness, i.e., s = 0.43 to 2.46 cm and l = 4.47 to 5.66 cm (Figures 4.3–4.12). In case of HH–polarization, it was noticed that the ADSSC decreases with increases in the rms surface height whereas, such effect was not observed in the case of VV–polarization.

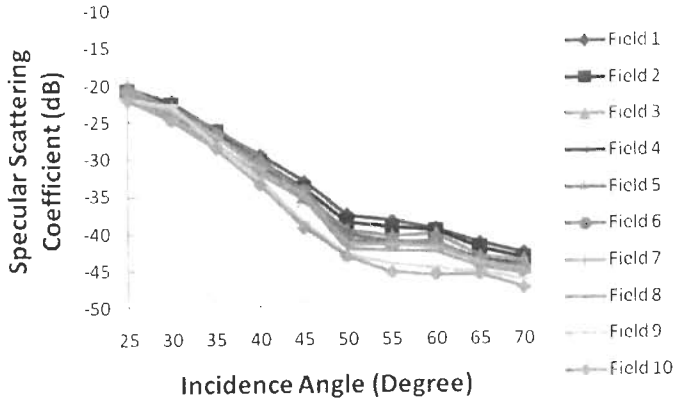

(a)

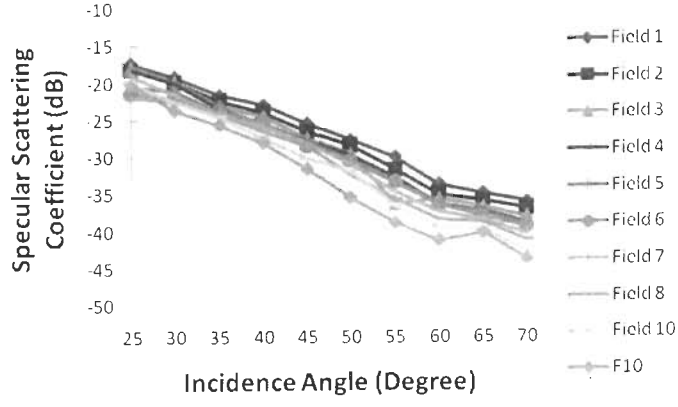

(b)

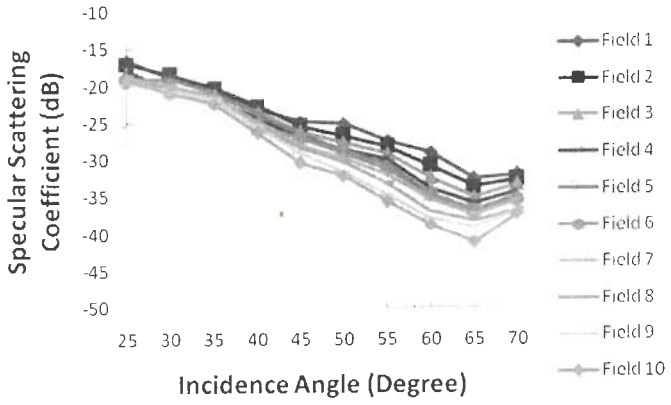
Specular Scattering Coefficient (dB)
-10
-15
-20
-25
-30
-35
-40
-45
-50
25 30 35 40 45 50 55 60 65 70
Incidence Angle (Degree)
Field 1
Field 2
Field 3
Field 4
Field 5
Field 6
Field 7
Field 8
Field 9
Field 10

(c)

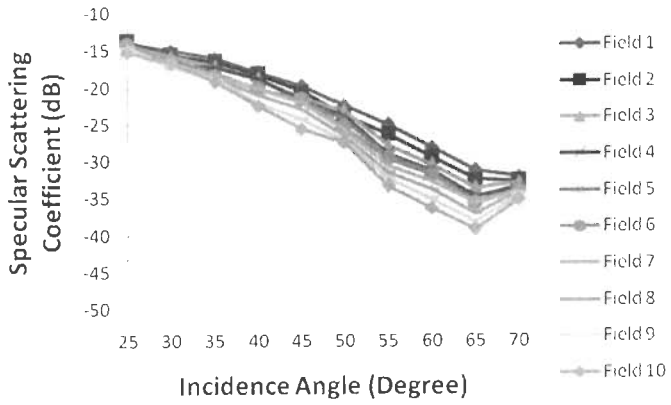
Specular Scattering Coefficient (dB)
-10
-15
-20
-25
-30
-35
-40
-45
-50
25 30 35 40 45 50 55 60 65 70
Incidence Angle (Degree)
Field 1
Field 2
Field 3
Field 4
Field 5
Field 6
Field 7
Field 8
Field 9
Field 10

(d)

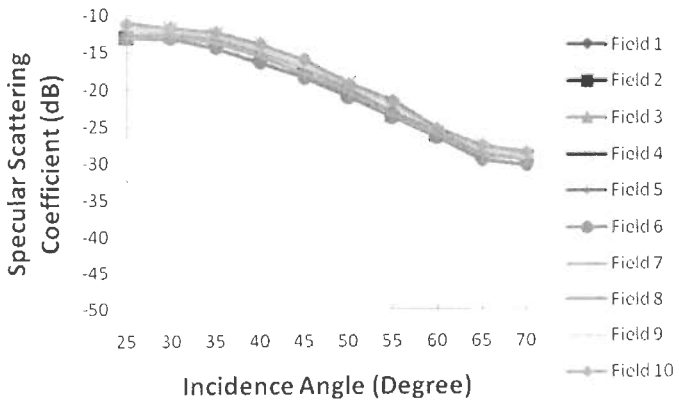
Specular Scattering Coefficient (dB)
-10
-15
-20
-25
-30
-35
-40
-45
-50
25 30 35 40 45 50 55 60 65 70
Incidence Angle (Degree)
Field 1
Field 2
Field 3
Field 4
Field 5
Field 6
Field 7
Field 8
Field 9
Field 10

(e)

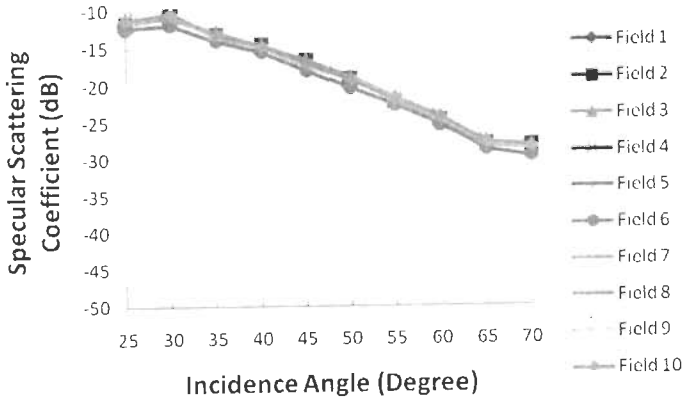

(f)

Figure 4.9. Represents the change in specular scattering coefficient with incidence angel for five different soil textue fields in VV–polarization at rms surfcace height 0.94 and correlation length 5.66 when volumetric soil moisture (cm^3 cm^{-3}) is (a) 0.027, (b) 0.092, (c) 0.195, (d) 0.258, (e) 0.368, and (f) 0.435.

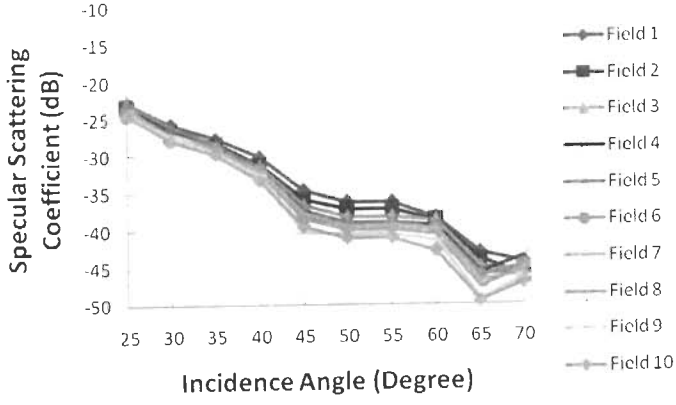

(a)

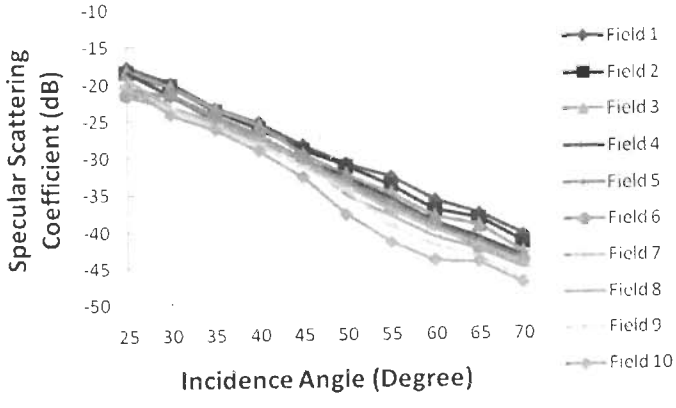

(b)

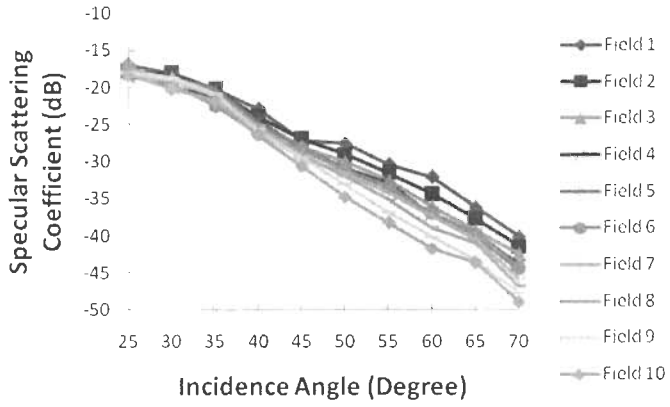
Specular Scattering Coefficient (dB)
-10
-15
-20
-25
-30
-35
-40
-45
-50
25 30 35 40 45 50 55 60 65 70
Incidence Angle (Degree)
Field 1
Field 2
Field 3
Field 4
Field 5
Field 6
Field 7
Field 8
Field 9
Field 10

(c)

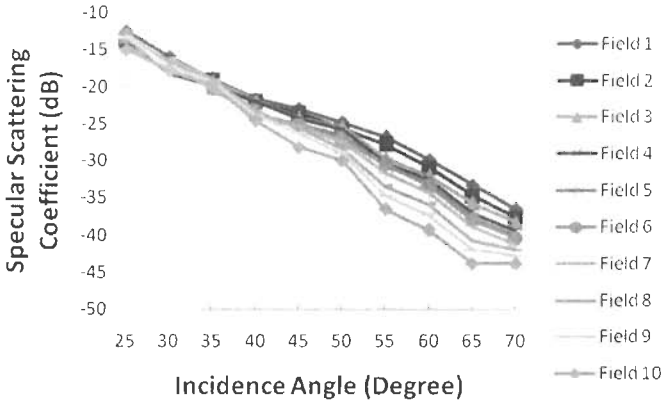
Specular Scattering Coefficient (dB)
-10
-15
-20
-25
-30
-35
-40
-45
-50
25 30 35 40 45 50 55 60 65 70
Incidence Angle (Degree)
Field 1
Field 2
Field 3
Field 4
Field 5
Field 6
Field 7
Field 8
Field 9
Field 10

(d)

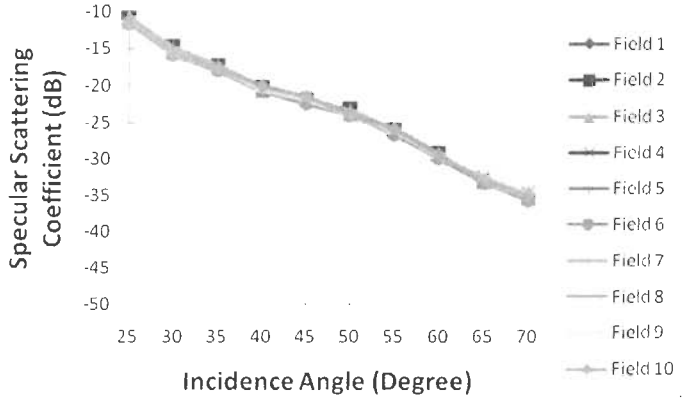
Specular Scattering Coefficient (dB)
-10
-15
-20
-25
-30
-35
-40
-45
-50
25 30 35 40 45 50 55 60 65 70
Incidence Angle (Degree)
Field 1
Field 2
Field 3
Field 4
Field 5
Field 6
Field 7
Field 8
Field 9
Field 10

(e)

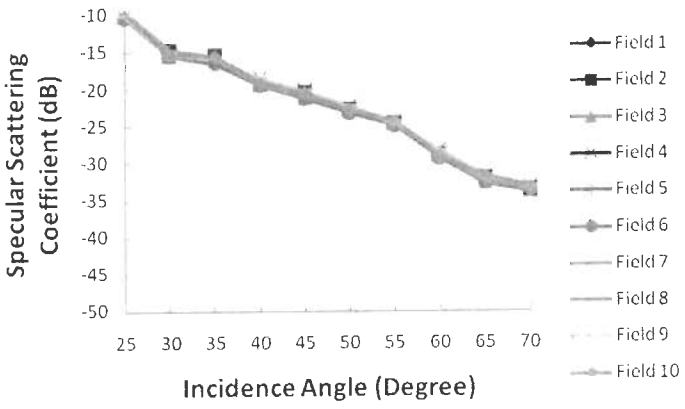

(f)

Figure 4.10. Represents the change in specular scattering coefficient with incidence angel for five different soil textue fields in VV–polarization at rms surfcace height 1.51 and correlation length 5.39 when volumetric soil moisture (cm^3 cm^{-3}) is (a) 0.027, (b) 0.092, (c) 0.195, (d) 0.258, (e) 0.368, and (f) 0.435.

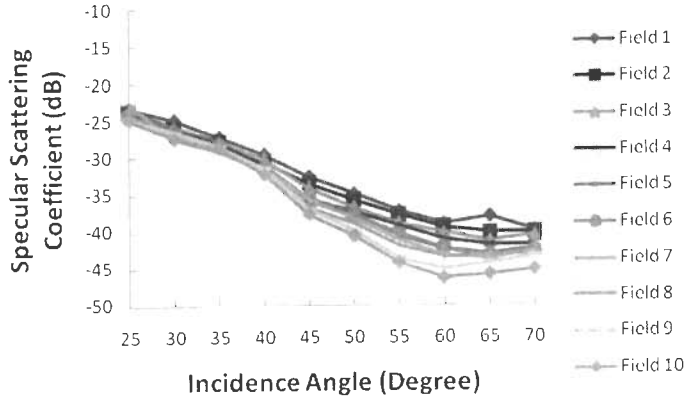

(a)

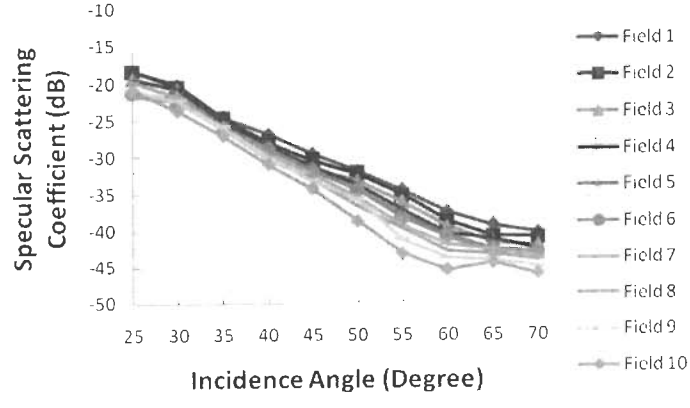

(b)

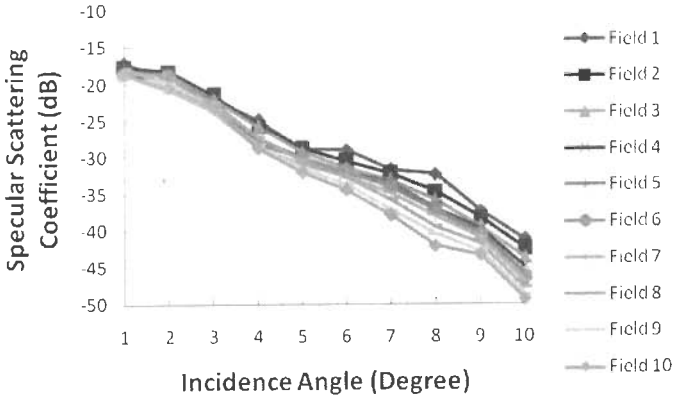
Specular Scattering Coefficient (dB)
-10
-15
-20
-25
-30
-35
-40
-45
-50
1 2 3 4 5 6 7 8 9 10
Incidence Angle (Degree)
Field 1
Field 2
Field 3
Field 4
Field 5
Field 6
Field 7
Field 8
Field 9
Field 10

(c)

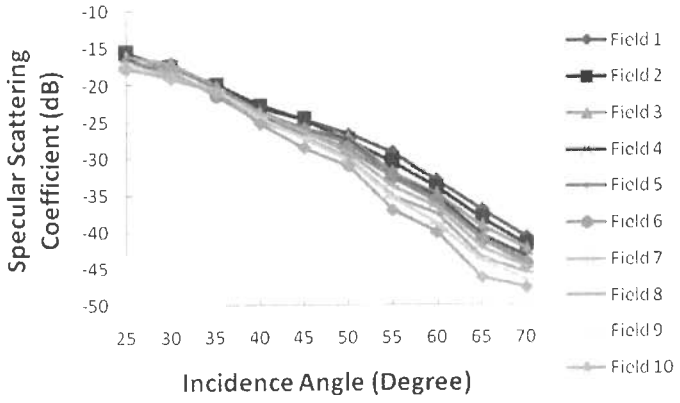
Specular Scattering Coefficient (dB)
-10
-15
-20
-25
-30
-35
-40
-45
-50
25 30 35 40 45 50 55 60 65 70
Incidence Angle (Degree)
Field 1
Field 2
Field 3
Field 4
Field 5
Field 6
Field 7
Field 8
Field 9
Field 10

(d)

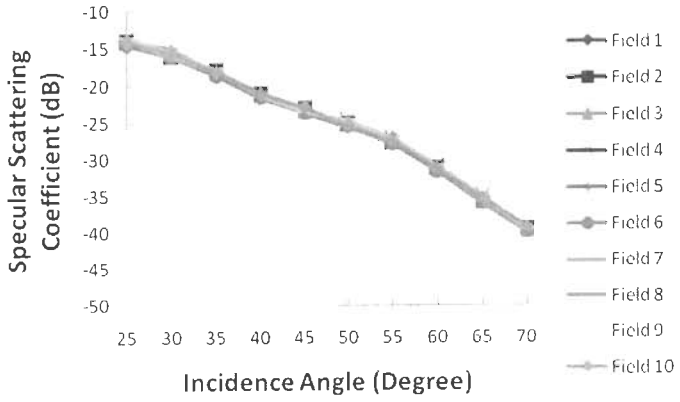
Specular Scattering Coefficient (dB)
-10
-15
-20
-25
-30
-35
-40
-45
-50
25 30 35 40 45 50 55 60 65 70
Incidence Angle (Degree)
Field 1
Field 2
Field 3
Field 4
Field 5
Field 6
Field 7
Field 8
Field 9
Field 10

(e)

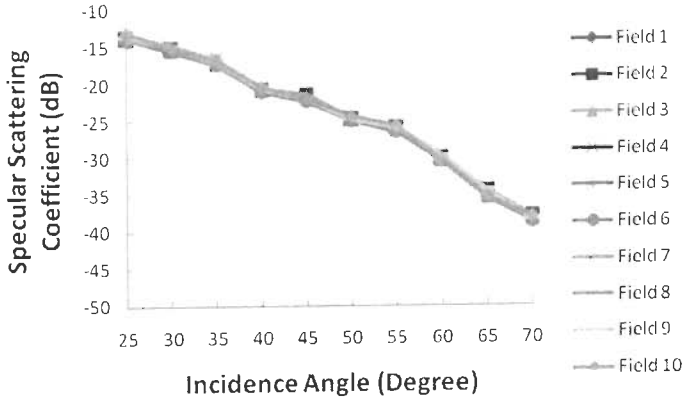

(f)

Figure 4.11. Represents the change in specular scattering coefficient with incidence angel for five different soil textue fields in VV–polarization at rms surfcace height 2.11 and correlation length 4.47 when volumetric soil moisture (cm^3 cm^{-3}) is (a) 0.027, (b) 0.092, (c) 0.195, (d) 0.258, (e) 0.368, and (f) 0.435.

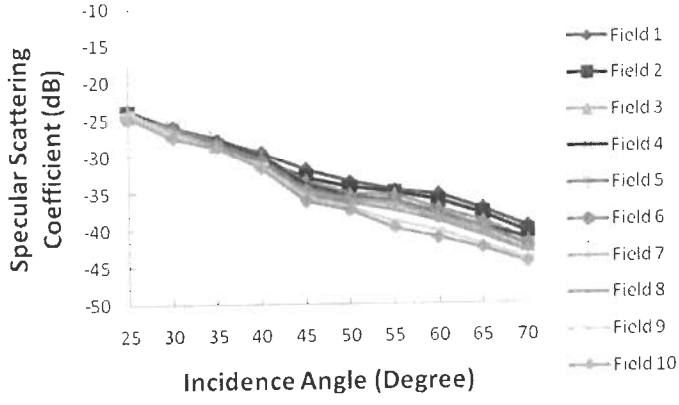

(a)

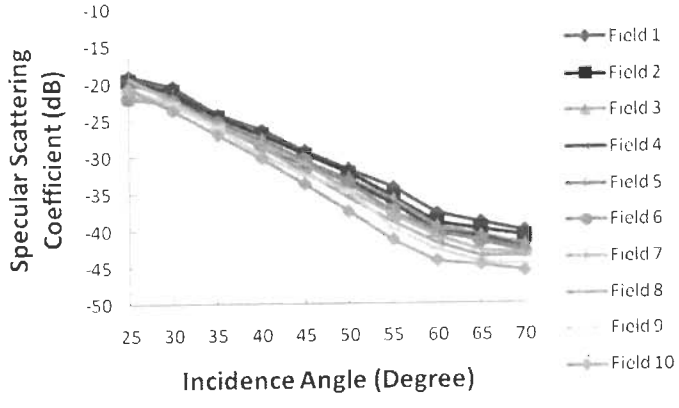

(b)

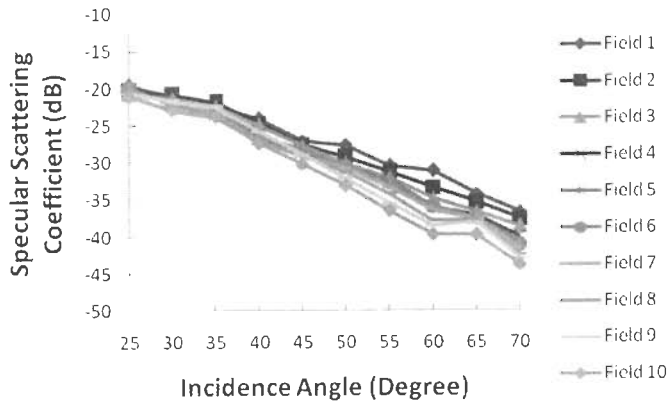
Specular Scattering Coefficient (dB)
-10
-15
-20
-25
-30
-35
-40
-45
-50
25 30 35 40 45 50 55 60 65 70
Incidence Angle (Degree)
Field 1
Field 2
Field 3
Field 4
Field 5
Field 6
Field 7
Field 8
Field 9
Field 10

(c)

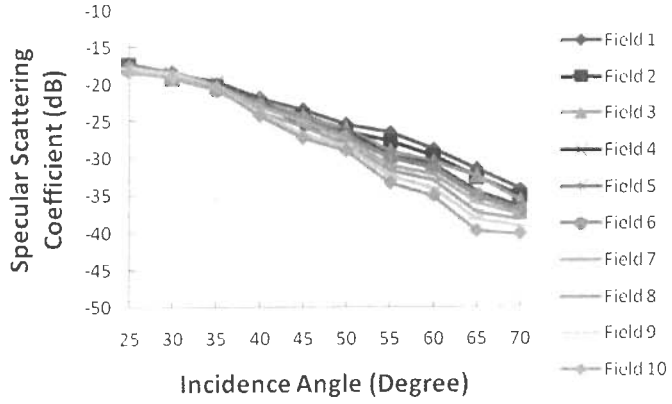
Specular Scattering Coefficient (dB)
-10
-15
-20
-25
-30
-35
-40
-45
-50
25 30 35 40 45 50 55 60 65 70
Incidence Angle (Degree)
Field 1
Field 2
Field 3
Field 4
Field 5
Field 6
Field 7
Field 8
Field 9
Field 10

(d)

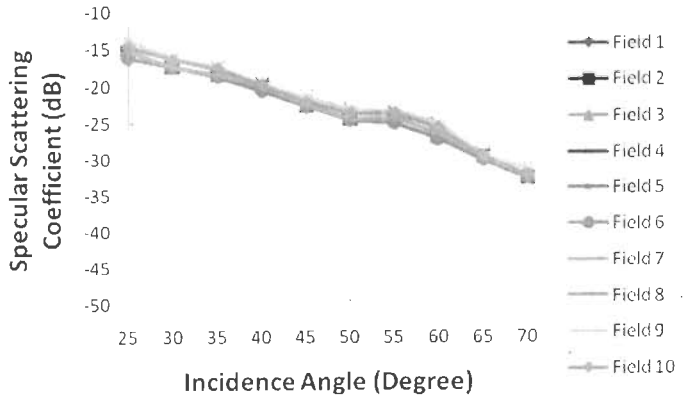
Specular Scattering Coefficient (dB)
-10
-15
-20
-25
-30
-35
-40
-45
-50
25 30 35 40 45 50 55 60 65 70
Incidence Angle (Degree)
Field 1
Field 2
Field 3
Field 4
Field 5
Field 6
Field 7
Field 8
Field 9
Field 10

(e)

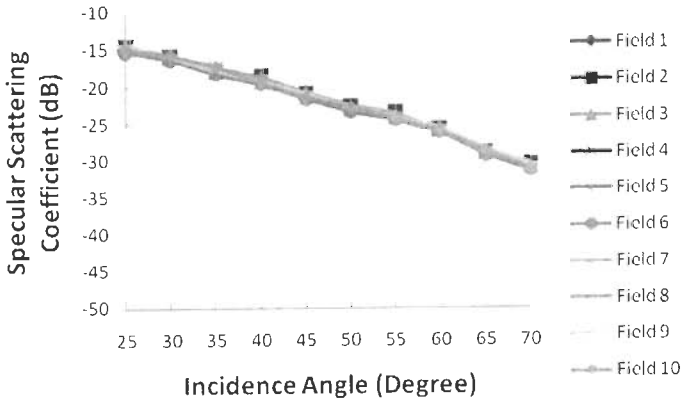

(f)

Figure 4.12. Represents the change in specular scattering coefficient with incidence angel for five different soil textue fields in VV–polarization at rms surfcace height 2.46 and correlation length 4.55 when volumetric soil moisture (cm^3 cm^{-3}) is (a) 0.027, (b) 0.092, (c) 0.195, (d) 0.258, (e) 0.368, and (f) 0.435.

4.5. Conclusion

This chapter has analyzed the effect of soil texture on specular scattering coefficient in the presence of various soil moisture and periodic roughness conditions at 6 GHz frequency of C-band. Experiments with scatterometer were carried out to compute the specular scattering coefficient in both like polarizations at different incidence angles. The analysis of specular scattering coefficient have been made for ten different soil texture fields by varying its moisture content from 0.027 cm^3 cm^{-3} to 0.425 cm^3 cm^{-3} and periodic surface roughness from smooth surface to 2.46 cm rms height. The change in specular scattering coefficient was observed with change in soil texture. Sand and clay constituents of soil have major effect on specular scattering coefficient whereas, very less effect on specular scattering coefficient was observed for change in silt constituent. The aforementioned observations were made for dry and smooth soil. It has been an important point to note that the differentiation among different soil texture fields based on specular scattering coefficient may be prominent at higher incidence angles (i.e., $\geq 45°$) than lower incidence angles (i.e., $< 45°$). Presence of soil moisture and periodic surface roughness is quite normal in natural conditions therefore effect of these parameters has also been studied. Firstly, moisture contents of the fields have been changed while retaining the surface smoothness. The observations led to conclude that the differentiation in specular scattering coefficient

for change in soil texture can be made up to soil moisture content 0.261 cm^3 cm^{-3} whereas, it is difficult to observe the change in specular scattering coefficient for different soil texture fields for higher moisture content, i.e., $m_v \geq 0.374$. Further, it was noticed that the change in periodic surface roughness have very less effect on the specular scattering coefficient when the interest is in the observation of soil texture, i.e., the change in specular scattering coefficient can be observed for the change in soil texture at different surface roughness conditions (i.e., s_1 to s_6). All these observations are equally noticeable in both like polarizations (i.e., HH– and VV–polarization) except for smooth soil in VV–polarization, where at lower soil moisture (i.e., 0.027 cm^3 cm^{-3}, 0.096 cm^3 cm^{-3} and 0.188 cm^3 cm^{-3}); Brewster angle effect can be observed. In a nutshell, it can be inferred that the soil texture has prominent effect on specular scattering coefficient and different soil texture fields can be distinguished based on specular scattering coefficient in both like polarizations at higher incidence angles (i.e., $\geq 45°$) for periodic roughness conditions (i.e., $s \leq 2.46$ cm) and moisture content, $m_v \leq 0.261$ cm^3 cm^{-3} at 6 GHz. Sand and clay constituents have major impact whereas silt constituent has very less effect on specular scattering coefficient. It was observed that the specular scattering coefficient decreases with the decrease in percentage of sand in soil whereas an opposite behavior was observed for clay constituent, i.e., specular scattering coefficient decreases with the increase in percentage of clay in soil. This effect has been observed at higher incidence angles (i.e., $\geq 45°$).

Chapter 5

Retrieval of Soil Parameters for Bistatic Data over Bare Field

The experimental analysis carried out explains the dependency of the specular scattering coefficient on soil parameters, i.e., soil texture, soil moisture and periodic surface roughness. Such observations led to the development of relationship between the specular scattering coefficient and soil parameters. This will be known as forward relationship which discusses the change in specular scattering coefficient with the change in soil texture, soil moisture and surface roughness and can be modeled based on the empirical developments or theoretical formulations. But, it is always a challenging task to develop algorithms to retrieve these soil parameters with the knowledge of scattering coefficient. Because several soil parameters depend on single scattering coefficient value. The algorithm should be developed in such a way which should be efficient to provide the promising solution for retrieval of soil parameters and at the same time should be simple enough to be applied on the data and it should require less *apriori* information. Therefore, after a rigorous study of various algorithms which are available for retrieval of soil parameters over bare fields, this

chapter discusses two approaches based on the copolarization ratio and multi–incidence angle to retrieve the soil parameters with requirement of less *apriori* information.

5.1. Introduction

Different soil parameters, i.e., soil moisture, surface roughness and soil texture play different roles in various applications. The information about the distribution of soil moisture plays key role in prediction of erosion, irrigation scheduling, improving crop yield prediction, climatology, meteorology as well as works as the indicator of general plant health [132, 135, 153, 169, 174]. Soil surface roughness is a significant factor in predicting infiltration, soil runoff, and flooding. It traps the water, due to which infiltration increases which in turn prevents soil runoff [80,115, 150, 182]. Further, texture is one of the most important soil characteristics because it influences many other properties of great significance to land use and management, such as porosity, infiltration, water holding capacity, and erodibility [32, 55, 119, 156]. These diversities in applications prompt to have the knowledge of spatial distribution of soil parameters. It has been discussed in Chapter 1 and Chapter 2. Quantitative analysis of these parameters can be obtained by the conventional methods which include the field visits and the measurements made during the field visits are type of point measurement. Conventional methods have two major limitations. Firstly, these are the point measurements and difficult to extend for a wide area due to the spatial variability in soil parameters and secondly, soil parameters especially soil moisture and surface roughness show temporal behavior and it is very cumbersome task to make field visits in frequent intervals of time to monitor these changes. The solution to these limitations lie with the radar remote sensing that has the capability to measure these soil parameters and it is much versatile to give the spatial distribution of soil parameters with the satellite based sensors as well as its temporal revisit can provide the estimation of soil parameters in frequent intervals. Most of the active microwave sensors on board satellite are in monostatic domain. Though, significant research is going on to retrieve the soil parameters in monostatic domain still the desired accuracy have to be obtained. It is discussed in Chapter 2 that the bistatic domain may prove itself worthy for retrieval of soil parameters because of its several advantage

over monostatic domain. Therefore, this chapter discusses the methodology based on the experiment carried out in bistatic domain. Details regarding the experiment and the methodology to retrieve the specular scattering coefficient have been discussed in Chapter 1. In Chapters 3 and 4 the analysis of specular scattering coefficient for change in soil texture with the variation in soil moisture and periodic surface roughness conditions at 10 GHz and 6 GHz has been discussed, respectively. Change in specular scattering coefficient was observed for change in soil texture for smooth and dry soil at 10 GHz frequency as well as at 6 GHz frequency for both like polarizations, i.e., HH– and VV–polarization. But, 10 GHz (X–band) possesses the limitation of periodic surface roughness. Even at lower periodic surface roughness (i.e., rms height = 0.9 cm) it is difficult to observe the change in specular scattering coefficient for change in soil texture at 10 GHz whereas this is not the case when the observation is carried out at 6 GHz. Therefore, this chapter utilizes the experimentally obtained specular scattering coefficient data at 6 GHz for the retrieval of soil parameters. Chapter 4 has analyzed in detail the response of specular scattering coefficient for soil texture with different field conditions (i.e., periodic roughness and moisture).

The specular scattering coefficient is a function of physical and dielectric property of the target, along with the frequency, polarization and incidence angle of the radar. In case of soil as the target, the parameters will be soil texture, soil moisture and surface roughness. Now, to interpret the characteristic of soil texture, soil moisture and surface roughness from the specular scattering coefficient is difficult and generally refereed as ill posed problem. Soil parameters, i.e., soil texture, soil moisture and surface roughness are earth's surface parameter and cannot be controlled. Therefore, the radar parameters, i.e., frequency, polarization and incidence angle can be optimized to provide good estimate of soil parameters. In this regard after a thorough study of various available algorithms as discussed in Chapter 2 (Section 2.5), this chapter discusses two approaches that involve the multi–polarization and multi–incidence angle data to retrieve the soil parameters by which requirement of *apriori* information may be minimized. The first approach that considers the copolarization ratio data minimizes the soil texture effect on specular scattering coefficient in retrieval of soil moisture. The second approach utilizes the multi–incidence angle data to retrieve the periodic surface roughness by minimizing

the soil texture and soil moisture effect. These retrieved periodic surface roughness values are subsequently used to estimate soil texture and soil moisture.

The use of scattering coefficient in different polarization and at different incidence angles has been widely used by several researchers to minimize the use of at least one soil parameter in retrieval of other soil parameters [30, 56, 115, 156, 159, 192, 232, 233,]. The copolarization approach has been used by the researchers to minimize the surface roughness when the objective is to retrieve the soil moisture [56, 30, 115]. The multi–incidence angle approach has been widely used to retrieve the rms surface height by minimizing the soil moisture effect [159, 192, 232, 233]. Both of these techniques have been frequently used for monostatic data whereas, the applicability of these approaches in bistatic domain has to be tested. Further, the copolarization ratio approach has been applied for rough surface to minimize the roughness however; the behaviour of copolarized data for smooth surface has to be tested. Therefore, in this chapter the copolarization ratio approach has been considered for retrieval of soil moisture for smooth surface with specular scattering data as well as the multi–incidence angle data has been utilized to retrieve the soil texture, soil moisture and periodic surface roughness.

The organization of the chapter is as following:

Section 5.2 presents theoretical background along with the formulation of Kirchhoff Scalar Approximation to compute the specular scattering coefficient in HH– and VV–polarization. Section 5.3 discusses the copolarization ratio approach for soil moisture retrieval as well as presents multi–incidence angle approach for retrieval of soil parameters, i.e., soil texture, soil moisture and periodic surface roughness. Finally, concluding remarks are made in section 5.4.

5.2 Theoretical Background

It is observed after the thorough literature review as discussed in chapter 2 that application of polarization and multi incidence angle approach may help to minimize the need of *apriori* information for retrieval of soil parameters from bistatic data. Therefore, two approaches have been considered in this chapter. Firstly, it was the aim to retrieve soil moisture of different fields with minimization of soil texture effect. Because, it is known from Equation 5.14 that radar wave interacts with

dielectric and dielectric is a function of moisture and soil texture. It is challenging to retrieve both parameters with single scattering coefficient. So, it is considered to minimize the soil texture effect for retrieving soil moisture directly from specular scattering data. For this purpose, we have considered the copolarization ratio approach after reviewing the literature as discussed in Chapter 2 and the behavior of the copolarized data for specular scattering case has been analyzed for the smooth field. It was observed that the copolarized data minimizes the soil texture effect and varies with the moisture content of soil (details are in Section 5.3.1(b)). The analysis shows the potentiality to use copolarized ratio for soil moisture retrieval. An empirical approach has been developed between the copolarized data and soil moisture which is further used for the retrieval of soil moisture. In addition to this, soil moisture is retrieved with commonly used theoretical model for bistatic, i.e., Kirchhoff scalar approximation and results have been compared.

But, the main aim was to retrieve the soil parameters (i.e., soil texture, soil moisture and surface roughness) with specular scattering coefficient. Therefore, the second approach involves the multi–incidence angle approach for retrieval of soil parameters with the need of minimum *apriori* information. This approach has been used because the applicability of first approach, i.e., copolarization ratio approach, is only for the smooth field and capable of retrieving the soil moisture only. However, the multi–incidence angle approach can been utilized to retrieve the periodic surface roughness parameters, i.e., rms height (s) and correlation length (l), and subsequently these retrieved values have been used in the Kirchhoff scalar approximation to retrieve the soil dielectric constant. Section 5.2.1 describes the equation for the computation of specular scattering coefficient with Kirchhoff scalar approximation. A simulation study based on Kirchhoff scalar approximation has been demonstrated in Section 5.3.2(a) which shows that the normalization of specular scattering data at one incidence angle to the other incidence angle provides the normalized specular scattering coefficient that is a function of periodic surface roughness and shows negligible change with soil moisture and soil texture. It has been discussed in Chapter 4 and 5 that specular scattering coefficient shows angular behavior for different fields (i.e., Field 1 to Field 10). Therefore, proper analysis of this behavior can be used to minimize the effect of some soil parameter while retrieving the others. It has been observed that normalization of specular scattering coefficient with reference incidence

angle (reference incidence angel the best incidence angle where maximum texture effect in observed, i.e., 60° as discussed in Section 5.3.2(c)) minimizes the soil texture and soil moisture effect and varies with surface roughness only. It gives strength to use such normalized specular scattering coefficient for observing surface roughness only. Some researchers have carried out the normalization of scattering coefficient data at one incidence angle to the other incidence angle in monostatic domain and observed that the normalized scattering coefficient is a function of roughness only whereas it shows very less dependency on soil moisture [159, 192, 232, 233].

5.2.1. Kirchhoff Scalar Approximation (SA) for Computation of Theoretical Specular Scattering Coefficient

The Kirchhoff Scalar Approximation provides a reasonable good fit to the experimental data in specular direction [43, 139, 140, 155, 156]. The formulation has been used to retrieve the soil moisture with *apriori* information of rms surface height and correlation length and the results were compared with the proposed approach.

Figure 1.2 (Chapter 1) shows the coordinate system for scattering geometry. Scattering coefficient under the scalar approximation is given by Equation 5.1 [202].

$$\sigma_{pq} = \sigma_{pqc} + \sigma_{pqn} + \sigma_{pqs} \tag{5.1}$$

where σ_{pqc}, σ_{pqn} and σ_{pqs} represent scattering coefficient due to coherent scattering , non–coherent scattering and scattering from surface slope, respectively.

$$\sigma_{pqc} = \pi k^2 |a_o|^2 \delta(q_x)\delta(q_y) e^{-q_z^2 s^2} \tag{5.2}$$

$$\sigma_{pqn} = (|a_o| k l/2)^2 \exp(-q_z^2 s^2) \sum_n^{\infty} \left(\frac{(q_z^2 s^2)^n}{n!\, n} \right) \exp\left(-\frac{(q_x^2 + q_y^2) l^2}{4n} \right) \tag{5.3}$$

$$\begin{aligned} \sigma_{pqs} &= -(ksl)^2 (q_z/2) \exp(q_z^2 s^2) \mathrm{Re}\{a_o (q_x a_1^* + q_y a_2^*)\} \\ &\quad \times \sum_{n=1}^{\infty} \left(\frac{(q_z^2 s^2)^{n-1}}{n!\, n} \right) \exp\left[-\frac{(q_x^2 + q_y^2) l^2}{4n} \right] \end{aligned} \tag{5.4}$$

Detailed expression regarding symbols in Equations 5.2, 5.3 and 5.4 can be found from the reference Ulaby *et al.* [202]. Here $k = 2\pi/\lambda$ where λ is wavelength. s

and l are the rms surface height and correlation length respectively. $\delta(q_x)$ and $\delta(q_y)$ are Dirac delta functions. In case of specular scattering $\theta = \theta_s$, $\varphi = 0$ and $\varphi_s = 0$.

$$q_x = k(\sin\theta_s \cos\varphi_s - \sin\theta\cos\varphi) = 0 \tag{5.5}$$

$$q_y = k(\sin\theta_s \sin\varphi_s - \sin\theta\sin\varphi) = 0 \tag{5.6}$$

$$q_z = k(\cos\theta_s - \cos\theta) = 2k\cos\theta \tag{5.7}$$

Final expression of specular scattering coefficient for the Kirchhoff Scalar Approximation is given by Equation 5.8.

$$\sigma_{pqc} = \pi k^2 |a_o|^2 \delta(0)\delta(0) e^{-q_z^2 s^2} + \left(|a_o| k l/2\right)^2 \exp\left(-(2k\cos\theta)^2 s^2\right) \sum_n^\infty \left(\frac{\left((2k\cos\theta)^2 s^2\right)^n}{n!\,n} \right) \tag{5.8}$$

Expression for a_0 is polarization dependent. In case of HH–polarization a_0 is given by Equation 5.9.

$$\begin{aligned} a_o &= -R_{\perp o}(\cos\theta + \cos\theta_s)\cos(\varphi_s - \varphi) \\ &= -R_{\perp o}(2\cos\theta) = -2R_{\perp o}\cos\theta \end{aligned} \tag{5.9}$$

where $R\perp_0$ is the Fresnel reflection coefficient for horizontal polarization and is given by Equation 5.10.

$$R_{\perp o} = \frac{\cos\theta - \sqrt{\varepsilon - \sin^2\theta}}{\cos\theta + \sqrt{\varepsilon - \sin^2\theta}} \tag{5.10}$$

In case of VV–polarization a_0 is give by Equation 5.11.

$$\begin{aligned} a_o &= R_{\parallel o}(\cos\theta + \cos\theta_s)\cos(\varphi_s - \varphi) \\ &= R_{\parallel o}(2\cos\theta) = 2R_{\parallel o}\cos\theta \end{aligned} \tag{5.11}$$

where $R_{\|0}$ is the Fresnel reflection coefficient for vertical polarization and is given by Equation 5.12.

$$R_{\|0} = \frac{\varepsilon \cos\theta - \sqrt{\varepsilon - \sin^2\theta}}{\varepsilon \cos\theta + \sqrt{\varepsilon - \sin^2\theta}} \tag{5.12}$$

5.3. Soil Parameters Retrieval Approaches

5.3.1. Approach 1: Copolarization Ratio Approach for Soil Moisture Retrieval

The approach has been developed considering the soil periodic surface roughness constant while varying the soil moisture and soil texture. In Chapter 4 the dependency of specular scattering coefficient on soil parameters, i.e., soil texture, soil moisture and periodic surface roughness has been discussed in detail. If the consideration is made to keep the soil periodic roughness constant while the observation is made by changing the moisture and soil texture, the specular scattering coefficient will be a function of soil moisture and soil texture only. It is quite difficult to retrieve the moisture and texture both with only one specular scattering coefficient. Therefore, if one parameter's effect on specular scattering coefficient is minimized then it will be easy to retrieve one parameter from one specular scattering coefficient. The minimization of soil texture effect can be obtained by utilizing the different sensor parameters, i.e., polarization, frequency and incidence angle. Therefore, to develop the retrieval algorithm for soil moisture, copolarization ratio approach has been utilized to minimize the soil texture effect.

The methodology has been developed based on ten different soil texture fields (Table 4.1) and six moisture conditions (Table 4.2) while the periodic surface roughness was kept constant (s = 0.43 and l = 4.68). Details regarding the different soil texture fields and soil moisture contents are provided in Chapter 4 (Table 4.1 and 4.2).

(a) Modeling Approach for Copolarization

Figure 5.1 illustrates the flow chart of the modeling approach to carry out the soil moisture retrieval by minimizing the soil texture effect. Following points discuss

in detail the approach that has been followed in the development of the proposed algorithm.

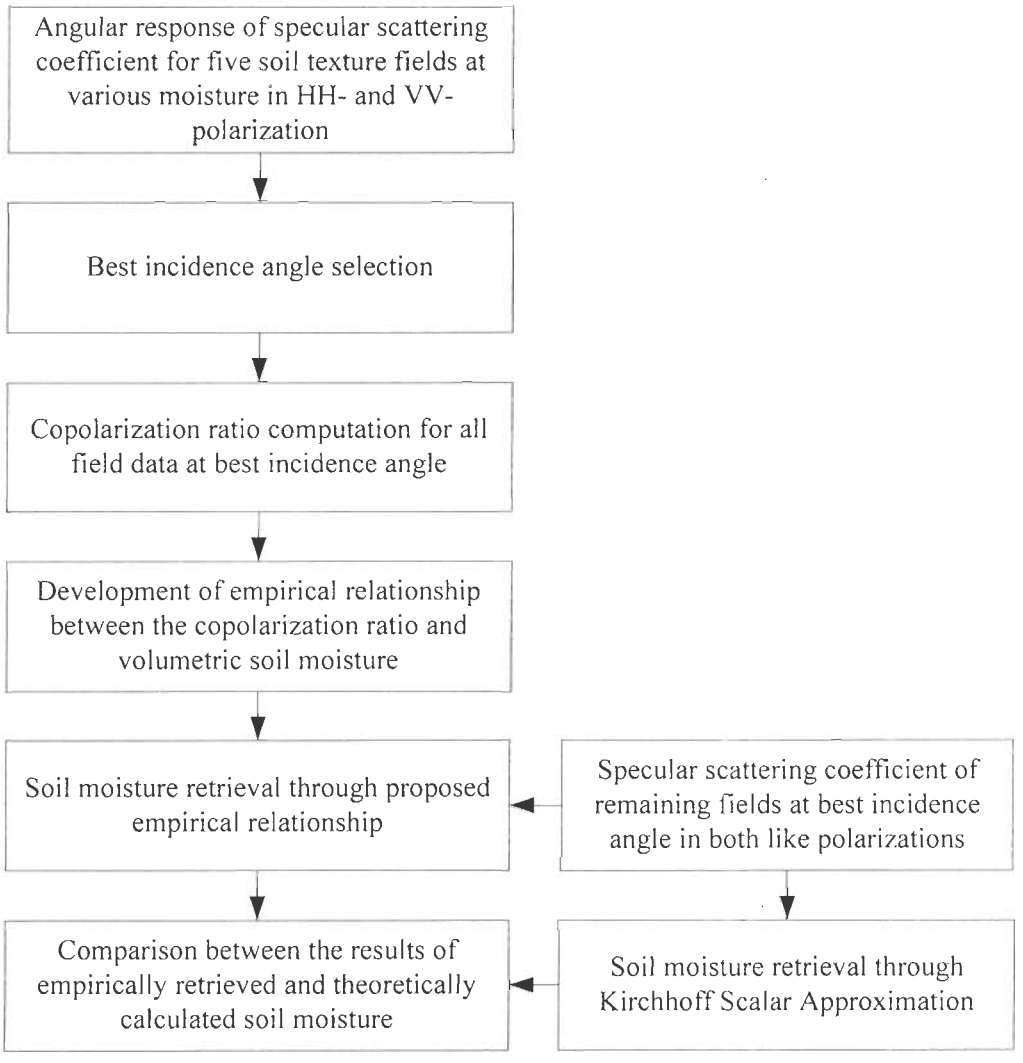

Figure 5.1. Flow chart for the proposed algorithm.

(i) Angular Response of Specular Scattering Coefficient: Change in specular scattering coefficient with incidence angle has been observed for all fields at 6 GHz in both like polarization as discussed in Chapter 4. The angular scattering response has been observed for different soil texture fields at various periodic surface roughness and moisture content.

(ii) Regression Analysis for Selection of Best Incidence Angle: Angle of incidence is an important dependent parameter for deciding the sensor parameters and retrieval algorithm. It has been shown in Chapter 4 that specular scattering coefficient shows the angular behavior for different soil texture and moisture conditions. It is difficult to segregate the individual effects like incidence angle effect on texture and moisture on specular scattering coefficient therefore there is a need to carry out statistical analysis by which the effect of the surface parameters on specular scattering coefficient on different incidence angles may be observed. One of the methods is regression analysis where coefficient of determination (R^2) tells about the percentage of dependence variable on independent variables. In our case, dependent variable is specular scattering coefficient and independent variables are soil texture and soil moisture. Therefore, multiple regression analysis was performed to realize the best incidence angle at which the specular scattering coefficient is more dependent on soil parameters.

(iii) Analysis of Copolarization Ratio Response: The effect of soil texture on specular scattering coefficient prompts one to minimize its effect for soil moisture retrieval. Therefore, it is important to carry out the copolarization ratio ($\sigma^{\circ}_{hh}/\sigma^{\circ}_{vv}$) study and check how it may be helpful to minimize the soil texture effect on the specular scattering. A detailed analysis of copolarization was performed for various soil texture fields with different moisture content. The obtained results are quite encouraging and imply that soil texture has negligible effect on copolarization ratio and the change in the copolarization ratio is obtained only with the soil moisture.

(iv) Development of Empirical Relation and Retrieval of Soil Moisture: The best incidence angle selection (step 1) and the minimization of the soil texture effect on copolarization ratio as well as its dependence on soil moisture content only (step 2), suggest a relationship between the copolarization ratio and volumetric soil moisture content. An empirical relationship has been developed between the copolarization ratio and soil moisture with good coefficient of determination. The soil moisture content can be retrieved by the inversion of this empirical relationship.

(b) Copolarization Ratio Response for Soil Texture with Different Soil Moisture Contents

Figures 5.2(a) and (b) represent the change in specular scattering coefficient with different soil texture at various soil moistures and constant periodic surface roughness in HH– and VV–polarization respectively at 60° incidence angle which is obtained through the regression analysis and detail regarding the regression analysis is discussed in Section 5.3.1(c). The change in specular scattering coefficient for different field is clearly evident for the both like polarizations. This signifies the effect of soil texture on the specular scattering coefficient. The copolarization ratio study was carried out to check the effect of soil texture on copolarization ratio. Figure 5.3 explains the behavior of the copolarization ratio for the change in soil texture field. It is evident from the figure that the value of copolarization ratio is approximately constant or there is very less variation with variation of soil texture at constant soil moisture is observed which indicates that copolarization ratio may be used to minimize the soil texture effect. The change in copolarization ratio is observed with the change in soil moisture content. The higher value of copolarization ratio is found for the lower value of soil moisture content and vice versa.

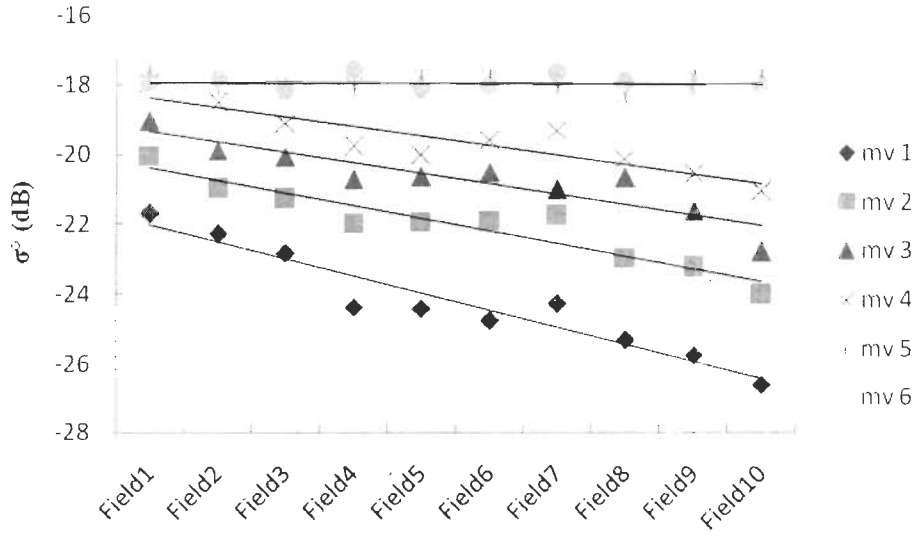

(a)

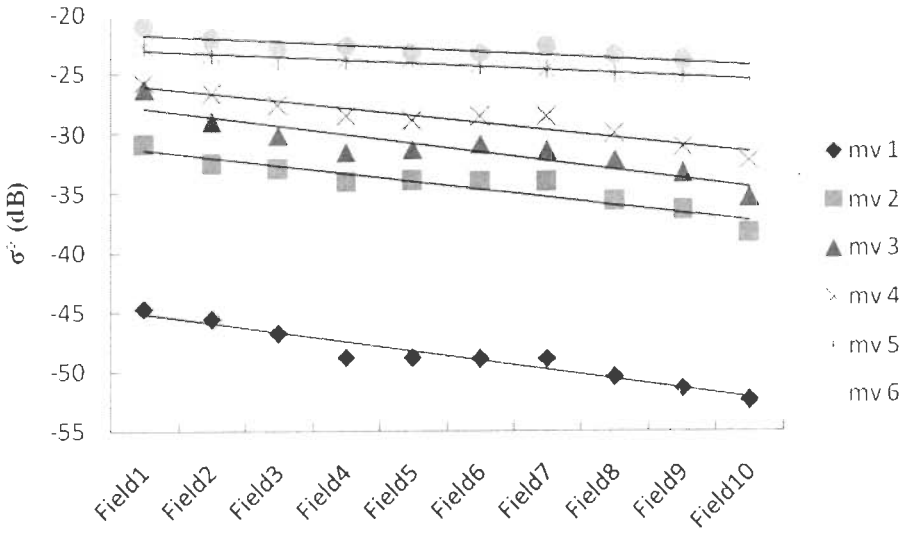

(b)

Figure 5.2. Specular scattering coefficient variation with change in soil texture field at different moisture condition for (a) HH–polarization (b) VV–polarization.

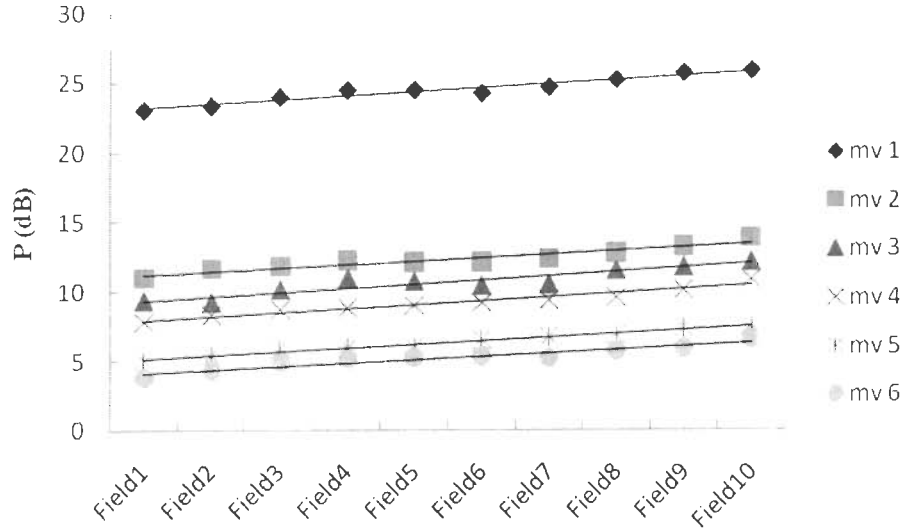

Figure 5.3. Copolarization ratio variation with change in soil texture field at different moisture condition.

(c) Implementation of Developed Soil Moisture Retrieval Approach based on Copolarization

Step1: The angular response of fields (Field 1 to Field 10) is discussed in Chapter 4 Figures 4.1–4.12. This shows quit good angular variation of specular

scattering coefficient for different fields at constant roughness is observed. So, as per our approach there is a need to select best incidence angel for observing the soil texture at 6 GHz.

Step2: It was discussed in Chapter 4 that specular scattering coefficient is highly dependent on angular variation for all soil texture fields in both like polarizations. Now in accordance with step 2 of modeling approach (Section 5.3.1(a)), multiple regression analysis was carried out keeping the soil texture (i.e., percentage of sand, silt, and clay) and soil moisture as independent variable and specular scattering coefficient as dependent variable. Results of regression analysis are shown in Table 5.1. Adjusted R^2 which shows the percentage of dependence of both soil parameters, i.e., soil moisture and soil texture on specular scattering coefficient along with the SE values are given in Table 5.1 for different incidence angle. Incidence angle greater than 45° provides the R^2 values that are always greater than 0.85 and 0.80 and SE is less than 1.01 and 1.50 in HH– and VV–polarization respectively, from which we may infer that higher incidence angle has better dependence on the specular scattering coefficient with soil texture and soil moisture as was observed experimentally also (Section 4.4.1 and Figures 4.2 and 4.3). The lower value of R^2 and higher value of SE (Standard error of Estimate) for VV–polarization in comparison to HH–polarization at higher incidence angle may be due to the Brewster angle effect observed in VV–polarization. The observation at lower incidence angle provides low R^2 and high SE, which led to the conclusion that lower incidence angles may not be quite suitable for characterizing the soil parameters when observations are made in specular direction at 6 GHz. Use of higher incidence angle for soil parameter characterization has also been recommended by Singh and Dubey [180], Cereldi *et al.* [30], Nashashibi and Ulaby [139, 140], Prakash *et al.* [156] for scattering in specular direction. The maximum value of R^2 is obtained at 60° incidence angle for both like polarizations. Hence, 60° incidence angle has been considered as the best suitable incidence angle for observing soil texture and soil moisture at 6 GHz in specular direction for the considered type of fields.

Table 5.1. Regression analysis results

HH–Polarization			VV–Polarization		
Incidence angle (degree)	R^2	SE	Incidence angle (degree)	R^2	SE
25	0.80	1.46	25	0.75	1.43
30	0.78	1.48	30	0.76	1.50
35	0.76	1.00	35	0.70	1.55
40	0.80	1.07	40	0.80	1.74
45	0.86	0.90	45	0.80	1.48
50	0.85	0.96	50	0.81	1.42
55	0.89	0.98	55	0.84	1.37
60	0.92	0.78	60	0.89	1.05
65	0.86	0.91	65	0.80	1.44
70	0.85	1.01	70	0.83	1.49

Step 3: Once the best incidence angle is obtained in step 2 then copolarization ratio at best incidence is computed for all considered fields. In our case best incidence angle is 60° for both like polarizations. The computed copolarization ratio for different fields is plotted in Figure 5.3. As it is discussed in Section 5.3.1(b) that copolarization ratio minimizes the effect soil texture and it can also be observed form Figure 5.4. Five different soil texture fields (Field 1, Field 3, Field 6, Field 8 and Field 10) with various soil moisture values were chosen for the development of the empirical relationship and the remaining five fields (Field 2, Field 4, Field 5, Field 7 and Field 9) were kept for the validation purposes (Table 4.2). Figure 5.4 shows the graph that has been plotted between the copolarization ratio and volumetric soil moisture content for five different soil texture fields. The empirical relation has been

developed between copolarization ratio (P) and volumetric soil moisture (m_v) based on these five soil texture fields with six moisture variation (i.e., total 30 different fields conditions were analyzed). The developed empirical relationship is given in Equation 5.13 where R^2 values are always greater than 0.95 and SE is less than 0.51.

$$P = a \times \ln(m_v) + b \tag{5.13}$$

The values of constants a and b are respectively -6.562 and -0.4658. These values are average of all the fields with the standard deviation of 0.081 and 0.1477 respectively for a and b.

(d) Validation and Comparison with KA Model

The developed empirical relationship is tested for retrieval of soil moisture content with the same set of fields and RMSE was 0.015 for retrieved soil moisture content. Furthermore, validation of this model has been carried out for different fields (Field 2, Field 4, Field 5, Field 7 and Field 9). The retrieved results for the volumetric soil moisture provide the good agreement with the observed soil moisture with RMSE of 0.021 between retrieved and observed soil moisture Figure 5.5.

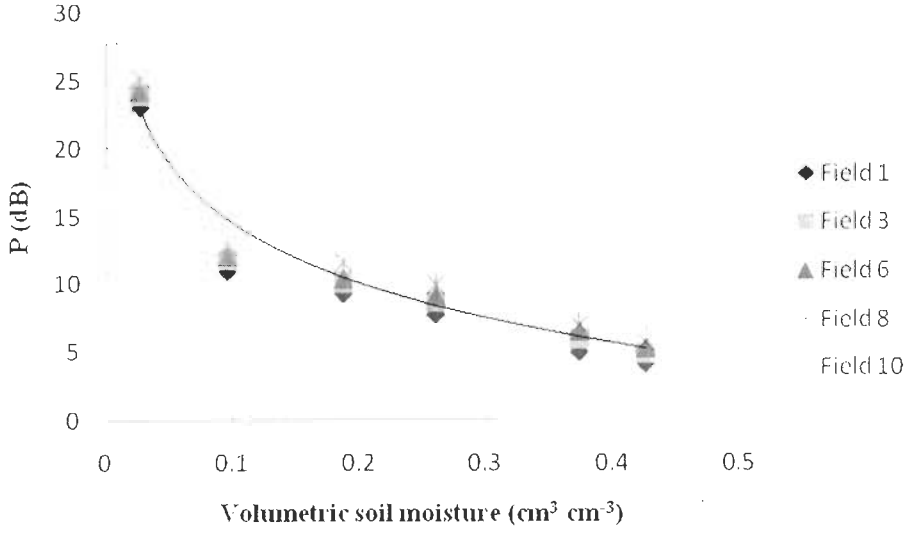

Figure 5.4. Change in copolarization ratio with volumetric soil moisture for different soil texture field.

In addition, F-test has been carried out to check the validity of retrieved results through empirical relationship. F-test determines how unlikely the result would have been if the two values compared really weren't different. The level of statistical significance was kept 0.05. The critical F value for the measurement was 1.86 and the F value for retrieved result of m_v in case of testing data is 1.33 and for validation data was 1.23. The F values are smaller than the critical F value which approves the significance of the developed empirical relationship.

A comparison has been drawn between soil moisture values retrieved through empirical relationship and Kirchhoff Scalar Approximation (SA). Equations 5.8 to 5.12 have been solved to retrieve the soil moisture content for both like polarization. The input parameters which are used to solve KA are observed specular scattering coefficient at 60° incidence angle for Fields Field 2, Field 4, Field 5, Field 7 and Field 9 with constant rms surface height (s = 0.43) and correlation length (l = 4.68). Figure 5.5 shows the comparison for observed values and the retrieved values of m_v through developed empirical relationship and SA in HH–polarization and VV–polarization. The RMSE are 0.021, 0.079 and 0.095 for empirical relationship, SA in HH–polarization and SA in VV–polarization respectively. The results clearly show that developed relationship performed better than the SA in both like polarizations.

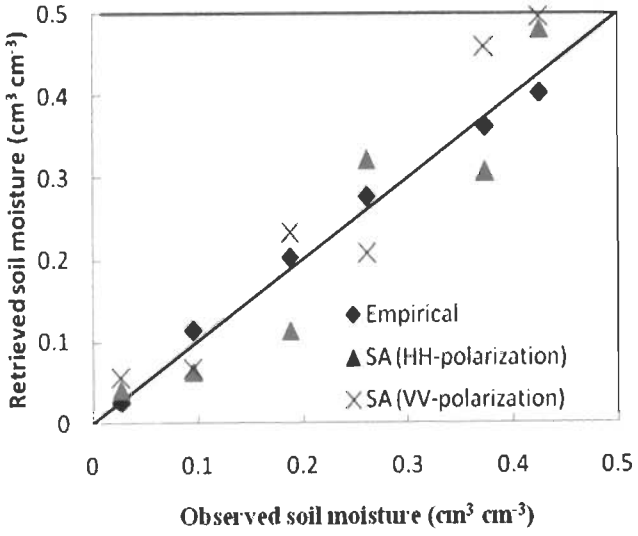

Figure 5.5. Comprasion between observed value of soil mooisture and soil moisture retrieved through developed emprical relationship, Kirchhoff Scalar Aproximation in HH–polarization and Kirchhoff Scalar Aproximation in VV–polarization.

5.3.2. Approach 2: Multi–Incidence Angle Approach for Retrieval of Soil Parameters, i.e., Soil Texture, Soil moisture and Surface Roughness

The proposed copolarization ratio approach in Section 5.3.1 poses the limitation of constant periodic surface roughness during the observation and is capable of retrieving the soil moisture content only. Therefore, there is a need to overcome the limitation applied on the periodic surface roughness condition and devise such a methodology that is capable of retrieving all the soil parameters, i.e., soil texture, soil moisture and periodic surface roughness. Multi–incidence angle approach serves the purpose very well. To develop the methodology based on the multi–incidence angle approach, ten different soil texture fields (Table 4.1) with six moisture (Table 4.2) and five periodic roughness conditions (Table 4.3) were chosen.

(a) Theoretical Approach

Scattering from the soil parameter is basically dependent on the soil dielectric constant and surface roughness. Therefore, the specular scattering coefficient can be represented with the product of the two functions defining the soil dielectric constant (ε) and the soil periodic surface roughness. The dielectric constant of the soil is dependent on the soil moisture (m_v) and the soil texture (i.e., sand, *s*, silt, *si*, and clay, *c*). The soil surface roughness is defined based on the rms surface height (s) and correlation length (l). Therefore, the specular scattering coefficient can be defined as the function soil dielectric constant and roughness as given in Equation 5.14.

$$\sigma^{\circ} = f(m_v, s, si, c)\, g(s, l) \tag{5.14}$$

It means that for retrieval of soil parameters, we have one dependent variable and 6 independent variables which is again a complex problem and is difficult to solve. Researchers have tried the various sensors parameters, i.e., multi–polarization, multi–incidence and multi–frequency to retrieve the soil parameters. So, it will be a good approach if it is possible to minimize the one or two dependent parameters and retrieve other parameters. The minimization of dependent parameters only is possible to use of sensor parameters i.e., different polarization, different frequency or multi-incidence angle. Because multi frequency again includes a lot of complexity [202], so

we have considered the multi–incidence angle approach. For this purpose, first we have carried out the simulation studies which are discussed as following:

Kirchhoff Scalar Approximation (Equation 5.8) was used to perform the simulation to check the multi–incidence effect for change in soil moisture, soil periodic surface roughness and soil texture. Earlier studies have shown that the SA works well in case of specular scattering for a range of soil surface parameters [43, 140]. In addition to this, the studies have shown that the scattering behavior described by the SA for periodic surface roughness is in good agreement to the scattering behavour described by the random rough surface [43]. Final expression of specular scattering coefficient for the Kirchhoff Scalar Approximation is given in Equation 5.8 [157, 202].

Soil texture and soil moisture explains the dielectric constant of the soil–water medium. Therefore in the simulation the effect of rms surface height, s, correlation length, l, and dielectric constant, ε, was analyzed. As we have observed from Table 5.1 that 60° is the best incidence angle, so we have considered 60° as reference angle. Now it important to check the individual effect, i.e., soil moisture, soil texture and surface roughness on normalized specular scattering coefficient as discussed in Section 5.2. We have considered 60° incidence angle as reference incidence angle and normalization has been carried out for other higher incidence angle (i.e., ≥ 45°) as it is observed that soil parameters effect is more prominent at higher incidence angle. HH–polarization has been considered based on regression analysis because better R^2 values were obtained than VV–polarization (Table 5.2). We have carried out the simulation for different $\Delta\sigma°$ values (i.e., $\Delta\sigma^{\circ}_{\theta\text{-}60}(dB) = \sigma^{\circ}_{\theta}(dB) - \sigma^{\circ}_{60}(dB)$, where $\theta = 45°$, 50°, 55°, 65°, 70°) but here we are showing only one result (i.e., $\Delta\sigma^{\circ}_{45\text{-}60}(dB) = \sigma^{\circ}_{45}(dB) - \sigma^{\circ}_{60}(dB)$). The simulation was made for five different rms surface height (s = 0.5 cm to 2.5 cm in step of 0.5 cm), six different dielectric constant (ε = 5 to 30 in step of 5) and four correlation length values (l = 3 cm to 6 cm in step of 1 cm). The selection of the field condition for the simulation study is based on the field conditions noticed during the experimental observations. Figure 5.6(a) depict the behaviour of the ratio of specular scattering coefficient (difference was taken for dB values) at 45° incidence angle to 60° incidence angle and referred as the normalized

specular scattering coefficient. It shows the negligible changes in normalized specular scattering coefficient values for the change in soil moisture content whereas, the significant changes can be noticed in normalized scattering coefficient values with rms surface height, s. Figure 5.6(b) represents the normalized scattering coefficient with the change in correlation length at various soil moisture content for constant rms surface height (s = 0.5 cm). The observation implies that a small change in normalized specular scattering coefficient values occurs with the change in correlation length, l. The dynamic range of normalized specular scattering coefficient with s is more prominent than l (Figures 5.6(a) and (b)). The dynamic range of normalized specular scattering coefficient with rms surface height is approximately 5.27 dB whereas the dynamic range of normalized scattering coefficient with correlation length is approximately 1.0 dB. Observations from Figures 5.6(a) and (b) suggest that the normalized scattering coefficient values are quite dependent on the soil periodic surface roughness, i.e., s and l whereas, negligible changes were observed with the change in dielectric constant of soil–water medium. Similar study was carried out by normalizing the specular scattering coefficient at some other incidence angle (i.e., 50°, 55°, 65° and 70°) while the specular scattering coefficient used to normalize was the specular scattering coefficient at 60° incidence angle. Conclusions made with these results were in good agreement with previously discussed results, i.e., the normalized specular scattering coefficient changes with the periodic roughness parameters (s and l) whereas, negligible changes were observed with soil moisture and soil texture. Studies carried out by the other researchers in monostatic domain have reported that the normalized scattering coefficient values varies with the soil periodic surface roughness and negligible changes were observed with the change in dielectric constant [159, 230, 232]. From these results we can infer that a empirical relationship can be developed among normalized specular scattering coefficient, s and l which can be further utilized to retrieve the periodic roughness parameters (s and l) and subsequently utilized with SA to provide the soil dielectric constant.

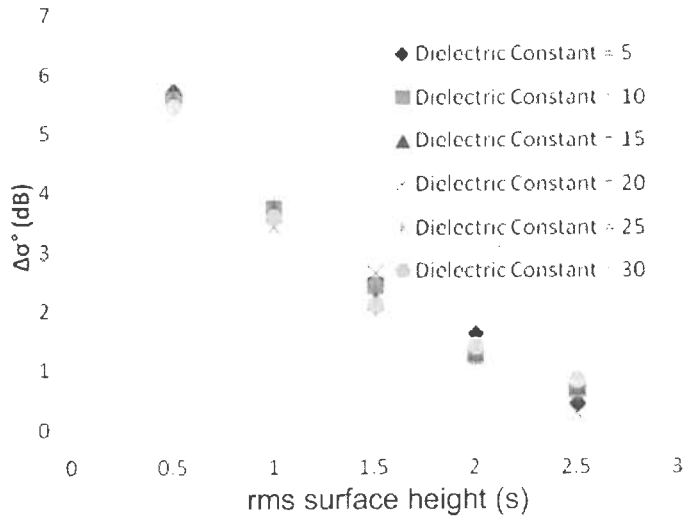

(a)

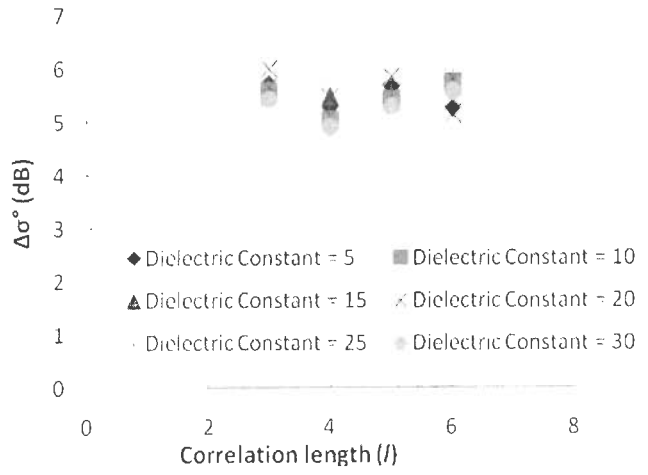

(b)

Figure 5.6. Simulation result for normalized specular scattering coefficient (a) with rms surface height for constant correlation length ($l = 3$) and different dielectric constant and (b) with correlation length, l. for constant rms surface height ($s = 0.5$) and different dielectric constant.

(b) Modeling Approach with Multi-Incidence Angle Approach

Figure 5.7 depicts the flow chart for the retrieval of soil parameters, i.e., soil texture, soil moisture, and periodic surface roughness. Approach involved in the retrieval of soil parameters is explained in the following steps:

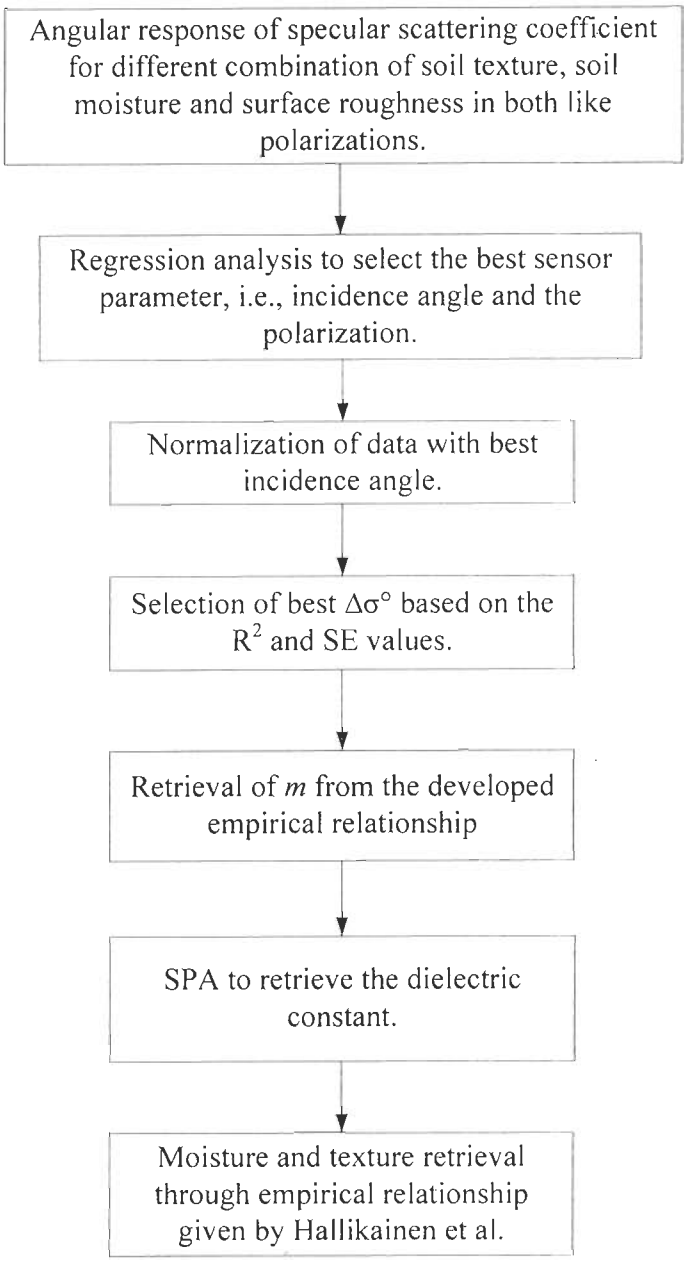

Figure 5.7. Flow chart for the retrieval algorthim of soil parameters.

Step 1. Response of specular scattering coefficient was analyzed for change in soil parameters (i.e., soil texture, soil moisture, and periodic surface roughness) and sensor parameters (i.e., incidence angle and polarization).

Step 2. It is important to choose the sensor parameters that best represent the change in specular scattering coefficient with soil parameters. The angular behavior of specular scattering coefficient along with the dependency of specular scattering coefficient on soil texture, soil moisture and periodic surface roughness has been discussed in Chapter 4 (Section 4.4). For this purpose a multiple regression analysis has been carried out where σ^0 is considered as dependent and rms surface height, correlation length and moisture are considered as independent. The adjusted R^2 value and SE have been computed and based on maximum R^2 and minimum SE the best incidence angle can be selected.

Step 3. The specular scattering coefficient values at higher incidence angle (θ = 45°, 50°, 55°, 65°, 70°) were normalized with the specular scattering coefficient values at reference incidence angle (i.e., 60°), i.e., $\Delta\sigma^{\circ}_{\theta-60}(dB) = \sigma^{\circ}_{\theta}(dB) - \sigma^{\circ}_{60}(dB)$, where θ = 45°, 50°, 55°, 65°, 70°. Because, higher incidence angles are showing more dependence of specular scattering coefficient on soil parameters as discussed in Chapter 4. The analysis of the $\Delta\sigma^{\circ}$ reviled that the change in soil texture and soil moisture has negligible effect on the $\Delta\sigma^{\circ}$ values, where as $\Delta\sigma^{\circ}$ changes with the change in soil periodic surface roughness, described by its rms surface height, s, and correlation length, l (Detailed description is made in Section 5.3.2(c)). A quadratic relationship was observed among $\Delta\sigma^{\circ}$(dB), s and l and the selection of best combination of incidence angle was based on the maximum R^2 and minimum SE value.

Step 4. The developed empirical relationship provides s and l values based on the $\Delta\sigma^{\circ}$ values. These s and l values are used as the input to Kirchhoff Scalar Approximation, SA to retrieve the dielectric constant of the soil.

Step 5. The empirical relationship developed by the Hallikainen *et al.* [78] was used to retrieve the soil moisture and soil texture values.

(c) Implementation for Retrieval of Soil Parameters with Proposed Approach of Multi–Incidence

In accordance with step 1 of the modeling approach, Chapter 4 describes the specular scattering coefficient response for soil texture, soil moisture and periodic surface roughness in both like polarizations and explain the angular variation as well.

Step 2: Regression analysis to choose the best sensor parameters, i.e., incidence angle and the polarization. Therefore, regression analysis was performed and the results of regression analysis are given in Table 5.2. Regression analysis was performed by taking the soil parameters as independent parameter and specular scattering coefficient as dependent parameter. It can be noticed from Table 5.2 that the value of R^2 is greater than 0.85 and SE is less than 0.11 for the higher incidence angles ($\theta \geq 45°$) in HH–polarization. Similar is the case for VV–polarization, where R^2 values are always greater than the 0.78 and SE is lesser than 1.52 for higher incidence angles ($\theta \geq 45°$).

Table 5.2. Multiple regression analysis results

HH–polarization			VV–polarization		
Incidence angle (degree)	R^2	SE	Incidence angle (degree)	R^2	SE
25	0.70	1.66	25	0.70	1.71
30	0.74	1.52	30	0.74	1.63
35	0.71	1.41	35	0.69	1.58
40	0.78	1.28	40	0.74	1.59
45	0.87	1.08	45	0.79	1.38
50	0.86	0.99	50	0.81	1.52
55	0.88	0.91	55	0.80	1.35
60	0.91	0.81	60	0.89	1.11
65	0.85	0.96	65	0.81	1.34
70	0.86	1.11	70	0.81	1.41

It can be infered that higher incidence angle may be more suitable for observing soil parameters (i.e., soil texture, soil moisture and periodic surface roughness) with specular scattering at 6 GHz. The maximum value of R^2 is 0.91 and minimum value of SE is 0.81 at 60° incidence angle in HH–polarization (in comparison to both like polarization). Therefore, scattering coefficient at 60° in HH–polarization has been considered as reference for further steps.

Step 3: Normalization of the specular scattering coefficient at higher incidence angles, i.e., 45°, 50°, 55°, 65°, and 70° (as these incidence angles are more suitable than the lower incidence angle to observe the soil parameters) with the specular scattering coefficient at reference incidence angle (60°) in HH–polarization is carried out which gives the $\Delta\sigma^{\circ}$(i.e., $\sigma^{\circ}_{\theta 1} - \sigma^{\circ}_{\theta 2}$, where θ_1 is 45°, 50°, 55°, 65°, or 70° and θ_2 is 60°). The behavour of specular scattering coefficient at different incidence angles was analyzed for 10 different soil texture fields, 6 moisture contents and 5 periodic roughness conditions. The total number of field conditions studied was 300. Out of these 300 field conditions, 75 field conditions have been chosen for the development of empirical relationship while remaining field conditions were kept for the validation process.

Figures 5.8(a)–(e) represent variation of normalized specular scattering coefficient (i.e., $\Delta\sigma^{\circ}_{45-60}(dB)$, $\Delta\sigma^{\circ}_{50-60}(dB)$, $\Delta\sigma^{\circ}_{55-60}(dB)$, $\Delta\sigma^{\circ}_{65-60}(dB)$, and $\Delta\sigma^{\circ}_{70-60}(dB)$) with soil periodic surface roughness. It can be observed from these figures that the normalized specular scattering coefficient varies with the soil periodic surface roughness while there is negligible change in the normalized specular scattering coefficient with the change in soil moisture and soil texture. The maximum change noticed in normalized specular scattering coefficient value for the change in soil texture and soil moisture is 0.59 dB, 0.63 dB, 0.54 dB, 0.52 dB, and 0.58 dB for $\Delta\sigma^{\circ}_{45-60}$, $\Delta\sigma^{\circ}_{50-60}$, $\Delta\sigma^{\circ}_{55-60}$, $\Delta\sigma^{\circ}_{65-60}$, and $\Delta\sigma^{\circ}_{70-60}$, respectively whereas the dynamic range of normalized specular scattering coefficient for the change in rms surface height is 5.95 dB, 4.37 dB, 1.79 dB, 1.02 dB, and 1.21 dB for $\Delta\sigma^{\circ}_{45-60}$, $\Delta\sigma^{\circ}_{50-60}$, $\Delta\sigma^{\circ}_{55-60}$, $\Delta\sigma^{\circ}_{65-60}$, and $\Delta\sigma^{\circ}_{70-60}$, respectively. These observations suggest the strong dependence of normalized scattering coefficient on the rms surface height and a weak dependence on soil texture and soil moisture content.

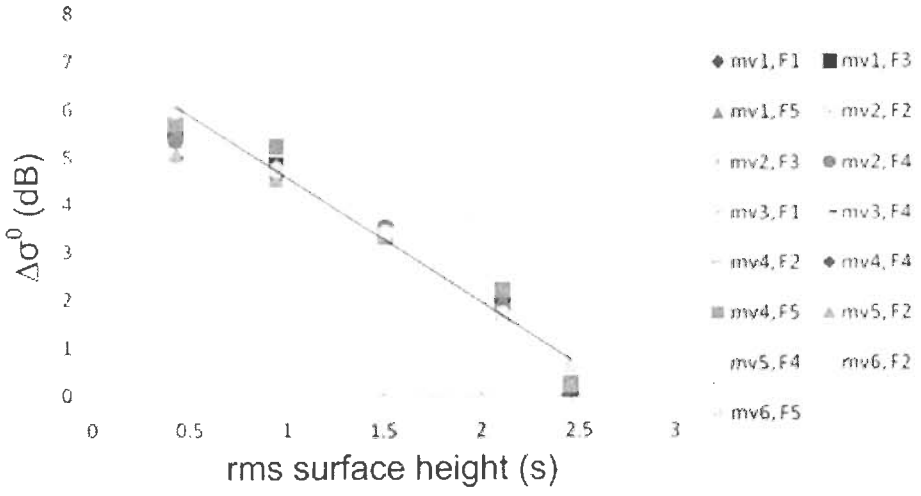
8
7
6
5
4
3
2
1
0
0
0.5
1
1.5
2
2.5
3
$\Delta\sigma^0$ (dB)
rms surface height (s)
mv1, F1
mv1, F3
mv1, F5
mv2, F2
mv2, F3
mv2, F4
mv3, F1
mv3, F4
mv4, F2
mv4, F4
mv4, F5
mv5, F2
mv5, F4
mv6, F2
mv6, F5

(a)

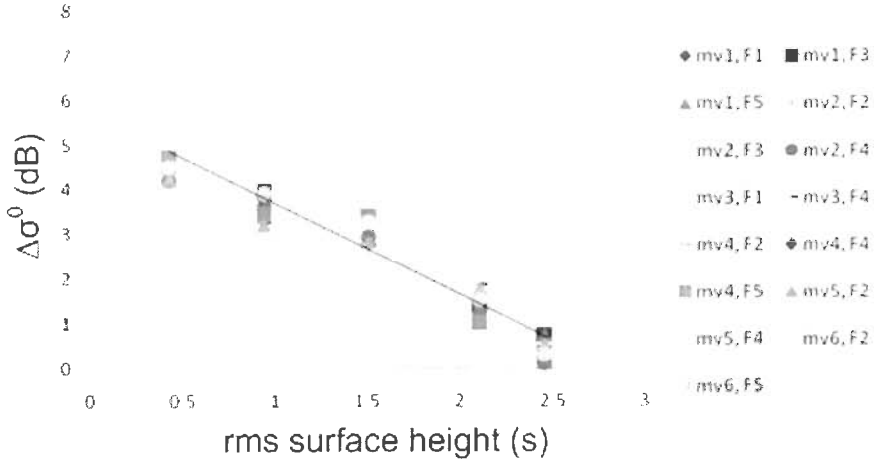
8
7
6
5
4
3
2
1
0
0
0.5
1
1.5
2
2.5
3
$\Delta\sigma^0$ (dB)
rms surface height (s)
mv1, F1
mv1, F3
mv1, F5
mv2, F2
mv2, F3
mv2, F4
mv3, F1
mv3, F4
mv4, F2
mv4, F4
mv4, F5
mv5, F2
mv5, F4
mv6, F2
mv6, F5

(b)

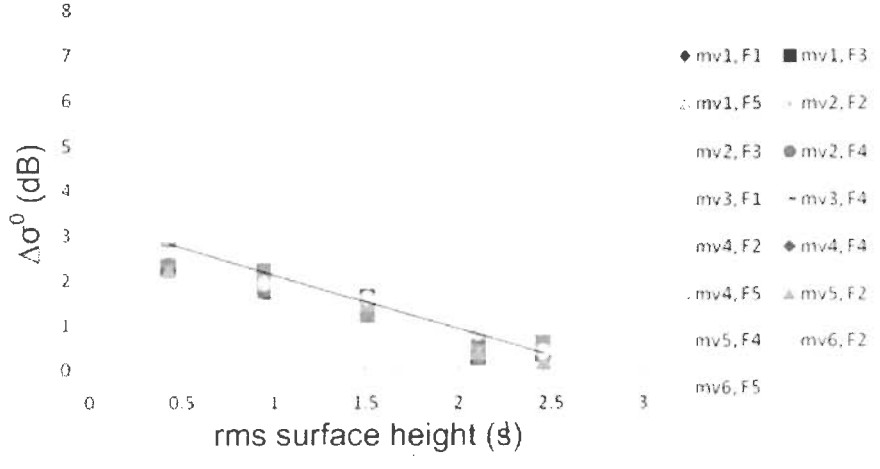
8
7
6
5
4
3
2
1
0
0
0.5
1
1.5
2
2.5
3
$\Delta\sigma^0$ (dB)
rms surface height (s)
mv1, F1
mv1, F3
mv1, F5
mv2, F2
mv2, F3
mv2, F4
mv3, F1
mv3, F4
mv4, F2
mv4, F4
mv4, F5
mv5, F2
mv5, F4
mv6, F2
mv6, F5

(c)

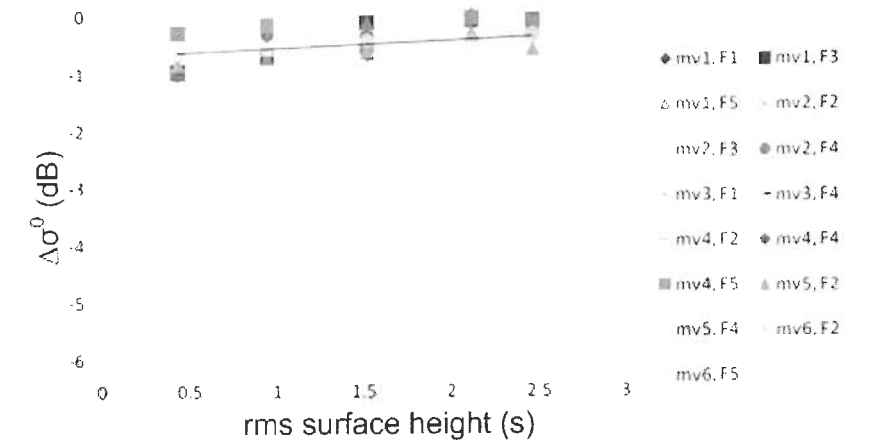

(d)

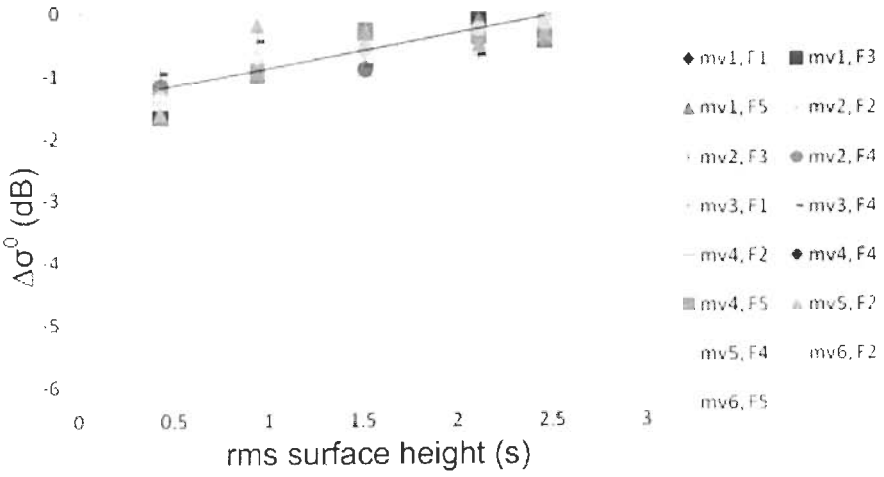

(e)

Figure 5.8. Response of $\Delta\sigma°$ (dB) for rms surface height when the normalization was performed with (a) 45°, (b) 50° (c) 55°, (d) 65°, and (e) 70°.

The simulation study discussed in Section 5.3.2(a) emphasizes the dependence of $\Delta\sigma^{\circ}(dB)$ on rms surface height and correlation length which confirms the experimental findings (Figure 5.8). Therefore, on the basis of curve fitting method, various relations have been analyzed to develop an empirical formula for s, l and $\Delta\sigma^{\circ}(dB)$ and a quadratic relationship was observed among $\Delta\sigma^{\circ}(dB)$, s and l. R^2 and SE values for normalized specular scattering coefficient at different incidence angles are provided in Table 5.3. It can be noticed from Table 5.3 that $\Delta\sigma^{\circ}_{45-60}(dB)$ have the highest value of R^2 (0.97) and lowest value of SE (0.43). Therefore, the quadratic relationship between $\Delta\sigma^{\circ}_{45-60}(dB)$, s and l was used as an empirical relationship for the

Table 5.3. R^2 and SE values for normalized data

	R^2	SE
$\Delta\sigma^{\circ}_{45-60}(dB)$	0.97	0.43
$\Delta\sigma^{\circ}_{50-60}(dB)$	0.93	0.76
$\Delta\sigma^{\circ}_{55-60}(dB)$	0.90	0.81
$\Delta\sigma^{\circ}_{65-60}(dB)$	0.87	1.83
$\Delta\sigma^{\circ}_{70-60}(dB)$	0.82	1.44

retrieval of soil periodic surface roughness (i.e., *s* and *l*). The empirical relationship is give by Equation 5.15.

$$\Delta\sigma^{\circ}_{45-60}(dB) = \alpha \times s + \beta \times l^{2} + \gamma \tag{5.15}$$

where α, β and γ are the empirical constant and the value of α, β and γ are -2.4545, 0.0447 and 5.7387 respectively.

Step 4 of the modeling approach discusses the retrieval of the periodic roughness parameters, i.e., *s* and *l* with the help of developed empirical relationship (Equation 5.15). The developed empirical equation provides a relationship between the normalized specular scattering coefficient (specular scattering coefficient at 45° incidence angle normalized with the specular scattering coefficient at 60° incidence angle) and periodic roughness parameters (i.e., *s* and *l*) in HH–polarization. To retrieve the *s* and *l* value from Equation 5.15, Nelder–Mead simplex algorithm is used. For the purpose *fminsearch* function of Matlab 7 was utilized. The Nelder–Mead simplex algorithm is a popular search method for multidimensional unconstrained minimization. It attempts to minimize a scalar-valued nonlinear function of *n* real variables using only function values, without any derivative information. The Nelder–Mead method thus falls in the general class of direct search methods and commonly used in nonlinear regression problems [146]. The developed empirical relationship was tested for the retrieval of the *s* and *l* with the same set of fields that were used to develop the empirical relationship. The Root mean square error (RMSE) was 0.019 and 0.042 for the retrieval of *s* and *l*, respectively. The

validation of the empirical relationship was made with the remaining 225 field conditions. Figure 5.9(a) and (b) show the plot between the retrieved and observed value of the rms surface height (s) and correlation length (l), respectively. The RMSE for the retrieval of s and l is 0.027 and 0.051, respectively. The retrieved results give the strength that the periodic roughness condition of the field can be retrieved with multi–incidence angle data (i.e., normalized specular scattering coefficient) thus minimizing the *apriori* information (i.e., periodic roughness conditions of the field) required for the retrieval of the soil moisture and soil texture.

The retrieved periodic surface roughness values are subsequently used as an input to the Kirchhoff Scalar Approximation for the retrieval of dielectric constant of soil. The retrieved s and l values were used in Equation 5.16 to compute the Fresnel reflection coefficient in HH–polarization.

$$R_{\perp 0} = \frac{1}{2\cos\theta} \times \sqrt{\frac{\sigma_{pq}}{\pi k^2 \delta(0)\delta(0) e^{-q_z^2 s^2} + (kl/2)^2 \exp\left(-(2k\cos\theta)^2 s^2\right) \sum_n^{\infty} \left(\frac{\left((2k\cos\theta)^2 s^2\right)^n}{n!n} \right)}} \tag{5.16}$$

Equation 5.10 (Fresnel reflection coefficient in HH–polarization) was utilized to retrieve the dielectric constant of the soil by substituting the value of $R_{\perp 0}$ retrieved through Equation 5.16. To solve the equation 7, *fsolve* function of Matlab 7 was employed.

Step 5: The retrieved dielectric constant value in step 4 is used in step 5 for the retrieval of soil moisture and soil texture. The empirical relationship developed by the Hallikainen *et al.* [78] and given in Equation 5.17 describes the dielectric constant of soil as the function of soil moisture and soil texture. Therefore, this relationship was used to retrieve the soil moisture and soil texture.

$$\varepsilon = (a_0 + a_1 S + a_2 C) + (b_0 + b_1 S + b_2 C) m_v + (c_0 + c_1 S + c_2 C) m_v^2 \tag{5.17}$$

where a_i, b_i, and c_i (i=0 to 2) are empirical constants. S and C respectively are sand and clay texture components of soil in percent by weight and m_v is volumetric soil

moisture content. The Nelder–Mead simplex algorithm was used for the retrieval of sand percentage, clay percentage and volumetric soil moisture content. The rest part of the soil constituents may include silt and gravel.

(d) Validation

Figures 5.9(a)–(e) represent the graph between the observed versus retrieved results for rms surface height, correlation length, volumetric soil moisture, percentage of sand, percentage of silt and percentage of clay. The retrieved results are in good agreement with the ground truth data. Root mean square error (RMSE) for the retrieval of rms surface height, correlation length, volumetric soil moisture, percentage of sand, and percentage of clay are 0.027, 0.051, 0.036, 5.94, and 8.15 respectively.

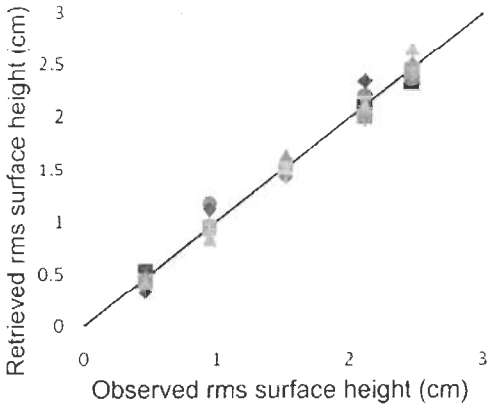

(a)

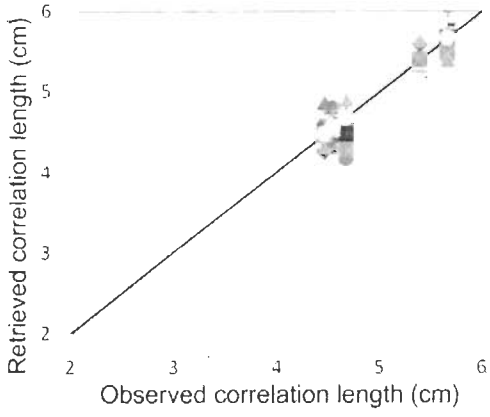

(b)

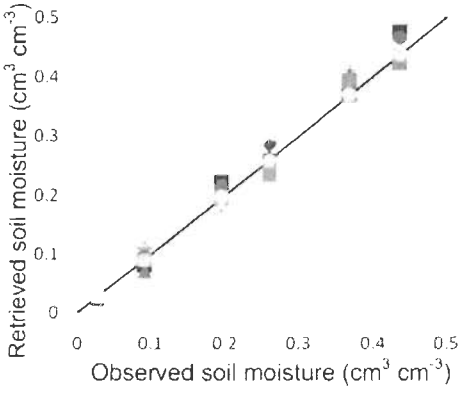

(c)

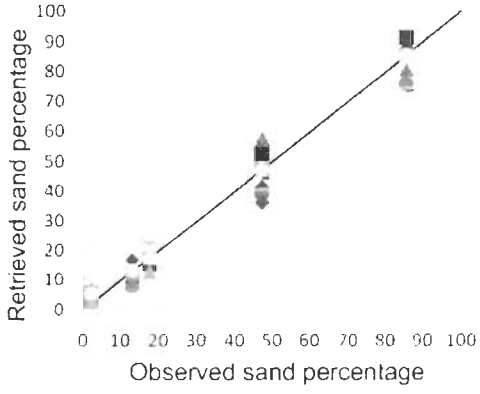

(d)

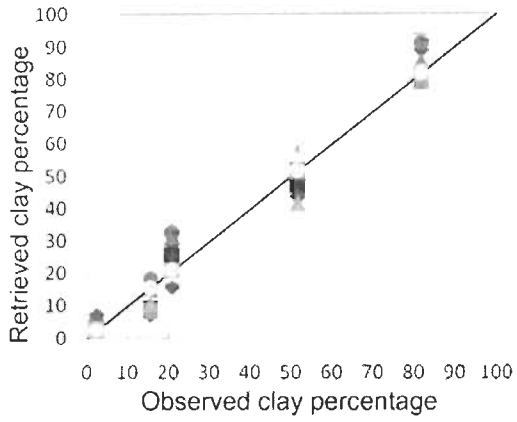

(e)

Figure 5.9. Represent the graph between the observed verses retrieved result for (a) rms surface height, (b) correlation length, (c) volumetric soil moisture, (d) percentage of sand, and (e) percentage of clay.

5.4. Conclusion

This chapter analyzes the role of various sensor parameters (multi–polarization and multi–incidence) in retrieval of soil parameters, i.e., soil texture, soil moisture and periodic surface roughness by which the need of *apriori* information can be minimized. It was noticed that generally in the models soil texture effect is not considered for retrieving the soil moisture which may affect the accuracy of the retrieved soil moisture because texture is quit dependent on specular scattering coefficient. Therefore copolarization ratio study was performed to minimize the soil texture effect at constant roughness. Copolarization ratio study revealed that the change in soil constituent has the least effect on the copolarization ratio and approximately same copolarization ratio was observed for all soil texture fields at constant soil moisture. It was also observed that the change in copolarization ratio is obtained with the change in soil moisture content. It indicates that the use of copolarization ratio may help in retrieval of the soil moisture quit accurately because it is less dependent to soil texture. Therefore, an empirical relationship has been developed between copolarization ratio and volumetric soil moisture. The retrieved results of soil moisture are in good agreement with ground truth data. Further a comparison of retrieved soil moisture with proposed copolarization ratio approach and

Kirchhoff Scalar Approximation approach has been carried out and it was found that the proposed copolarization approach performed better than the Kirchhoff Scalar Approximation.

The developed copolarization ratio technique was capable of retrieving the soil moisture content only as it considers constant periodic surface roughness throughout the observation. Therefore, multi–incidence angle approach was developed to retrieve soil parameters, i.e., soil texture, soil moisture and periodic surface roughness. For the applicability of the multi–incidence angle approach, 60° incidence angle and HH–polarization was found to be the most appropriate sensor parameter at 6 GHz to observe the considered fields. A normalization process was carried out and it was observed that $\Delta\sigma^{\circ}$ has negligible effect for the variation of soil texture and soil moisture where as it varies with the periodic surface roughness. A quadric relationship was observed between $\Delta\sigma^{\circ}$ and periodic roughness parameters (i.e., s and l). The retrieval of soil parameters was made using developed empirical relationship, Kirchhoff Scalar Approximation, and empirical relationship developed by Hallikainen *et al.* [78]. The obtained results are quite encouraging and the study may be explored for future bistatic airborne/spaceborne missions.

Chapter 6

Fusion of Information Approach to Retrieve Soil Moisture with Two Different Satellite Data: SAR and Optical

Chapter 3 and 4 discussed about the specular scattering response of soil texture in presence of soil moisture and surface roughness at X– and C–band, respectively. However, Chapter 5 has utilized the copolarization ratio and multi–incidence angle approach to retrieve soil parameters, i.e., soil texture, soil moisture and surface roughness in bistatic domain. The study in bistatic domain has been carried out due to its several advantages as discussed in Chapter 1 and 2. But in present scenario, most of the existing airborne and spaceborne sensors are in monostatic domain and soil moisture retrieval is still a challenging task in vegetation covered areas. Therefore, in this chapter, efforts have been made to retrieve the soil moisture in vegetated area with data available from satellite based sensors.

Soil moisture retrieval in the vegetated area is a cumbersome process due to the involved scattering phenomenon that inherits the volume scattering from the vegetation and surface scattering from the underlying soil. This chapter deals with this problem by fusing the information available from synthetic aperture radar data and optical data in order to circumvent the vegetation characterization that is needed to explain the scattering phenomenon from the vegetation.

6.1. Introduction

Estimation of spatial distribution of soil moisture is important in many applications such as hydrology, meteorology, agronomy, climatology and many other earth sciences [153]. Active microwave remote sensing provides us avenue to estimate the spatial distribution of soil moisture over a large area [132, 146, 154, 193, 211]. Alternatively, soil moisture can be measured by various methods. The most direct methods are in situ measurements. They are usually reasonably accurate and can provide the good estimates of soil moisture, but they are point measurements. Therefore, it is very difficult to generalize the estimate of soil moisture for a large area of study from such point estimates because of the immense spatial variability of soil moisture at small scales. Also, because of logistic constraints, the spatial coverage of in situ measurements is usually rather limited.

Synthetic aperture radar (SAR) images are capable of providing the estimate of soil moisture because the measured data in SAR is scattering coefficient which is highly dielectric dependent parameter and the studies have shown that the dielectric constant of soil changes with soil moisture condition [15, 202]. SAR technique provides the images with high spatial resolution therefore, the moisture estimation with SAR images can be mapped with local variations which is not possible in case of measurement with scatterometer. The retrieval of soil moisture is an ill–posed problem because scattering coefficient depends on several other parameters, e.g., in case of vegetated area, the scattering coefficient is affected not only by the vegetation parameters but also by the underlying surface roughness. The SAR images available before 2002 were in single configuration (i.e., single frequency, polarization and incidence angle) but from the launch of ENVISAT ASAR after that PALSAR sensor multi–configuration (i.e., multi–incidence, multi–polarization) data in now available.

Presently the SAR satellites are available with high spatial resolution with short revisit time which offers the estimation of soil moisture at local scale in regular interval, e.g., RADARSAT–2, ENVISAT, TerraSAR–X, PALSAR.

The most prevalent techniques for soil moisture retrieval in vegetated areas are the techniques based on the water cloud model and change detection [2, 17, 131, 137, 145, 220]. Some researchers have utilized the optical data to characterize the vegetation and subsequently applied this information with SAR data to retrieve soil moisture [141, 214]. Major points of all these techniques along with their limitation have been discussed in Chapter 2. Besides the vegetation, soil surface roughness is another factor of concern in soil moisture retrieval studies. The minimization of surface roughness in most of the cases has been dealt with the copolarization approach and this has been discussed in Chapter 2.

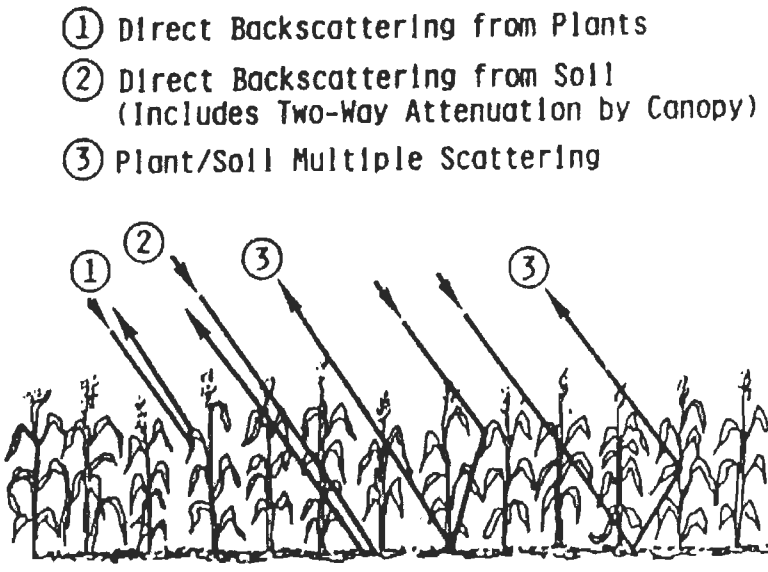

Figure 6.1. Backscattering behavior of microwave form vegetated area [203].

The dependency of scattering coefficient on soil moisture proves its usefulness in retrieval studies of soil moisture but, the presence of vegetation hampers the accuracy drastically. Microwave has the capability to penetrate the vegetation, therefore providing the estimate of soil moisture, but the complex behavior of scattering coefficient in presence of vegetation makes the task difficult. Figure 6.1 shows backscattering of microwave in vegetated area. Therefore, the backscattered signal is total sum of the volume scattering from the canopy, surface scattering by the

underlying soil surface and multiple interaction involving both the canopy and the soil surface [203]. Still it is challenging to minimize the vegetation effect for retrieval of vegetation covered soil moisture with SAR images. In this regard, optical data which provides the information of vegetation cover may be used as complementary information for retrieval of vegetation covered soil moisture. Therefore, the information available from SAR and optical data can be fused to provide the estimation of vegetation covered soil moisture. The objective of this chapter is therefore to analyze the feasibility of relating the information available from SAR data and optical data to envisage such an approach that mostly rely on the information content of satellite images and require minimum *apriori* information. The concept of such an approach arises as the vegetation can be modeled through the SAR data as well as the optical data. In case of SAR data the backscattering is affected by the vegetation cover and contains the information regarding vegetation whereas, the normalized difference vegetation index (NDVI) provides a good estimate of the crop cover [214]. The utilization of the information content from the optical data reduces the requirement of the *apriori* information which is required in the vegetation parameters characterization. Therefore, this chapter focuses these problems of vegetation for retrieving the vegetation covered soil moisture and emphasizes on two approaches by developing empirical relationship between the normalized scattering coefficient and NDVI to incorporate the vegetation effect in soil moisture retrieval.

Chapter has been organized as following:

Section 6.2 provides the brief discussion about the data used along with the study area. The preprocessing of the data acquired is presented in Section 6.3. Section 6.4 describes the model development for soil moisture retrieval in vegetated areas. Section 6.5 deals with the first approach of soil moisture retrieval whereas, Section 6.6 presents second approach of soil moisture retrieval in vegetated areas. A comparison has been made between the first and second approach in Section 6.7 and finally Section 6.8 draws the conclusion of the study performed.

6.2. Study Area and Data Used

Two sets of satellite images comprising Roorkee city, Manglaur town (Uttarakhand, India) and its surrounding areas were chosen for the study. The satellite

images used for the development of algorithm and the validation are ALOS–PALSAR (Advanced Land Observing Satellite – Phased Array type L–band Synthetic Aperture Radar), a SAR data and MODIS (Moderate–resolution Imaging Spectroradiometer), an optical data. The detailed description of the study area and data used are provided in Chapter 1. Summary of data used is provided in Table 6.1.

Extensive ground truth survey was carried out to measure the soil moisture and surface roughness. Total 60 areas were selected to measure the volumetric soil moisture and rms surface height. In these 60 areas, 30 areas belongs to the PAL–1 image that has been used to develop and test the algorithm whereas, remaining 30 area belongs to the PAL–2 image and has been used to validate the developed algorithm. The study area is mostly flat and consist of water, urban, vegetation and bare soil classes. Wheat, sugarcane and mustard are the crop of the April month.

6.3. Preprocessing of PALSAR and MODIS Data

6.3.1. PALSAR Data

ALOS–PALSAR data acquired was of level 1.1 VEXCEL format data. Figure 6.2 illustrate the flow chart of the preprocessing the PALSAR level 1.1 VEXCEL format data. SARSCAPE 4.1, dedicated SAR data processing software developed by SARMAP and works with the integration with ENVI (Environment for Visualizing Images) used for data preprocessing. The data provided by the ERSDAC (Earth Remote Sensing Data Analysis Center) is single look complex slant range full polarimetric focused data. The data is imported through SARSCAPE. The imported SLC files were calibrated using defined polarimetric calibration matrices using SARSCAP. Polarimetric calibration minimizes the impact of non ideal behavior of a full–polarimetric SAR acquisition system in order to obtain an estimate of the scattering matrix of the imaged objects as accurate as possible from their available measurement. Polarization synthesis function of SARSCAPE allow the synthesizing a new set of SLC data in desired orthogonal basis. In the present case, it has been used for synthesizing SLC data in circular basis (Left Left–, Left Right–, Right Left– and Right Right–polarization) from the linear basis (Horizontal Horizontal–, Horizontal Vertical–, Vertical Horizontal– and Vertical Vertical–polarization).

Table 6.1. Description of data used

Data	Data ID	Acquisition ID	Date	Pixel spacing	Image size (pixels)	Area covered (Km)	Upper left		Lower right	
							Latitude	Longitude	Latitude	Longitude
PALSAR	PAL–1 (Test image)	PASL110090 40617112609 08110063	April 06, 2009	25 m	850 × 850	21.25 × 21.25	30.000° N	77.803° E	29.823° N	77.980° E
	PAL–2 (Validate image)	PASL110090 40617111809 08110062	April 06, 2009	25 m	850 × 850	21.25 × 21.25	29.859° N	77.847° E	29.682° N	78.024° E
MODIS	MOD–1 (Band–1 and Band–2) (Test image)	MOD09Q1.A 2009093.h24 v06.005.2009 099200537	April 03, 2009	250 m	85 × 85	21.25 × 21.25	30.000° N	77.803° E	29.823° N	77.980° E
	MOD–2 (Band–1 and Band–2) (Validate image)	MOD09Q1.A 2009093.h24 v06.005.2009 099200537	April 03, 2009	250 m	85 × 85	21.25 × 21.25	29.859° N	77.847° E	29.682° N	78.024° E

Speckle, which looks like the "salt and pepper" noise, is a result of interference among the coherent echoes of the individual scatterers within a resolution cell and it is an inherent problem in SAR images [69, 103, 217]; therefore to reduce the speckle Wishart Gamma map filter was used. 5 × 5 window size was chosen due to its suitability of preserving the texture information [128]. Target reciprocity (i.e., HV = VH and LR = RL) is assumed in filter operation. Further the multilooking is performed to improve the radiometric resolution. For ALOS PALSAR data multilooked factor was selected as 7, in order to avoid oversampling effect in geocoding. The digital elevation model was extracted using technique GTOPO 30 for terrain correction prior to geocoding. Then nearest neighbor resampling method was applied to data for radiometric calibration [128].

6.3.2. MODIS Data

MODIS data was acquired from sensor Terra for 8 days composite reflectance product (MOD09) at 250 m spatial resolution. This contains the red (645 nm) and near–infrared (858 nm) surface reflectance product. Both the bands were calibrated and geometrically rectified to UTM coordinates [81, 85] with ENVI 4.6 software.

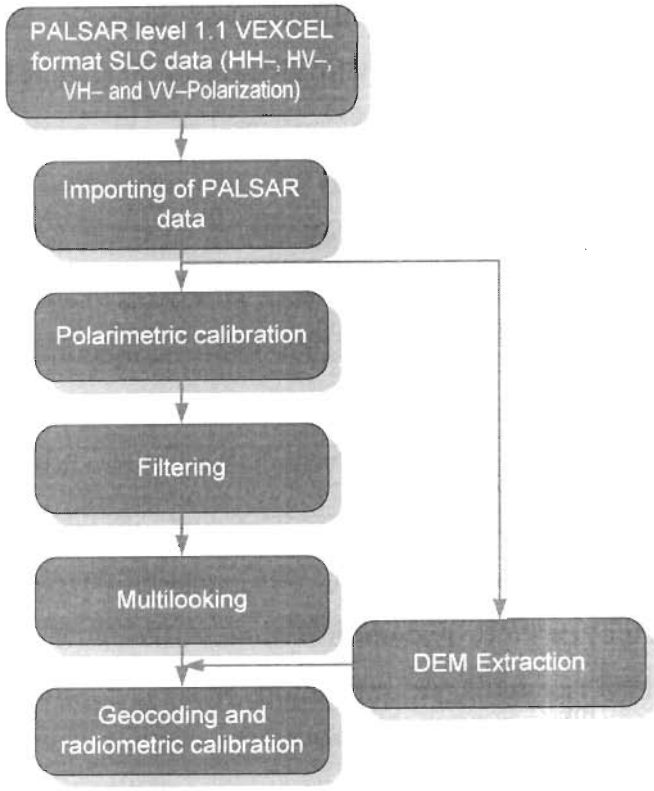

Figure 6.2. Flow chart for preprocessing the PALSAR data.

6.4. Model Development

As discussed in above section that exiting approaches like water cloud model or change detection need a lot of *apriori* information or complex to solve it for soil moisture retrieval under vegetation cover. Therefore, attempt has been made to minimize these problems. A theoretical background behind the proposed model is discussed here and after that its implementation with satellite data. Two different approaches have been formulized for soil moisture retrieval over vegetated areas with satellite data.

6.5. Approach 1

6.5.1. Theoretical Background for Soil Moisture Retrieval Algorithm

It has been discussed in Section 6.1 that scattering from vegetated area is affected by the vegetation cover and underlying soil characteristics (Figure 6.1). Soil characteristics are generally defined by soil moisture and surface roughness. Therefore, the retrieval of soil moisture can be made with proper knowledge of surface roughness and vegetation cover. It has also been briefly discussed in Section 6.1 and in detail in Chapter 2 that optical data has been utilized to describe the various vegetation parameters and NDVI which describe the vegetation abundance can be efficiently included in algorithm development to model vegetation in association with scattering coefficient value to retrieve soil moisture. Therefore, Approach 1 makes use of NDVI in conjunction with scattering coefficient to retrieve soil moisture.

Theoretical, empirical and semi–empirical models have been developed by several researchers that describe the dependence of scattering coefficient of bare soil on moisture and roughness condition of soil [5, 48, 80, 144, 193, 202]. The advantage and their limitations have been discussed with fairer detail in Chapter 2. The model developed by Dubois *et al.* [48] has been used due to its simplicity and wide range of applicability. Details regarding it have been provided in Chapter 2. Further, the Dubois model can be solved to provide the dielectric constant of soil without enquiring about the surface roughness conditions.

Therefore, Approach 1 utilizes the NDVI to include the vegetation effect in algorithm development and Dubois equation has been used to compute the bare soil scattering coefficient to normalize the scattering coefficient of vegetated area. A flow

chart is given in Figure 6.3 for the retrieval of soil moisture in the vegetated area. Following sections will discuss the detailed procedure.

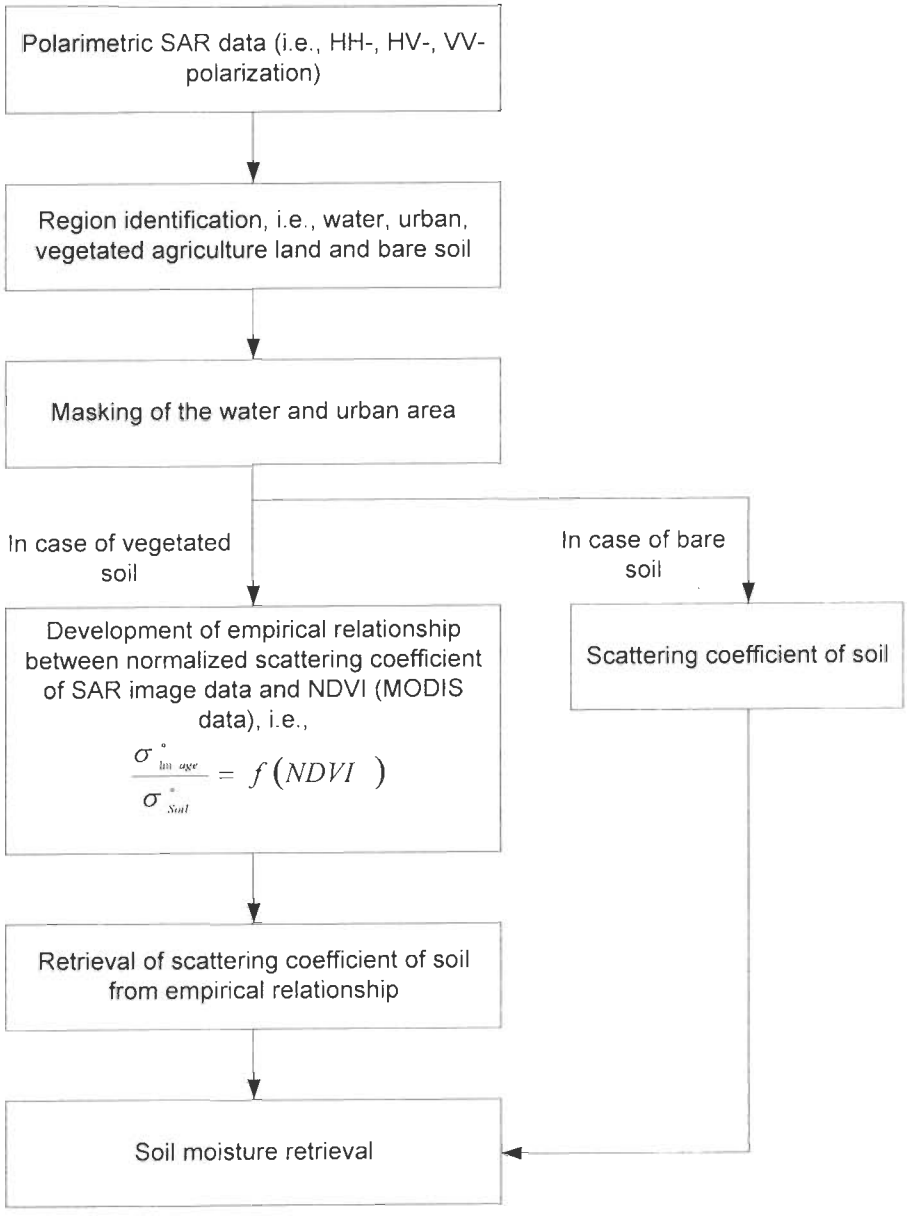

Figure 6.3. Flow chart for the retrieval of soil moisture: Approach 1.

6.5.2 Development of Vegetation Covered Soil Moisture Algorithm

Different steps involved in development and implementation are discussed as following.

(a) Step 1

As it is shown in the flow chart 6.3, SAR data is preprocessed as given in Section 6.3.1.

(b) Step 2

It is important to mask the water bodies and urban areas in the image to avoid the uncertainties. So, decision tree classifier [128] is used which is discussed below.

(i) Classification of PALSAR Image with Decision Tree Classifier: In study areas, there is no clear cut demarcation between the various land cover classes, i.e., it is very difficult to find out the agriculture or urban area for a large stretch (tens of kilometers) therefore, it is always the possibility to find the mixed land cover classes. In general one may obtain the urban areas (e.g., villages) along with the water bodies (e.g., canals, ponds) within the stretch of agriculture land and such type of other mixed classes. Due to this the satellite image of any area of interest will contain all these land cover classes mixed. This arise the need as a prerequisite to classify the image in various land cover classes so that the region of interest in the image can be clearly marked. In present case, a knowledge based approach has been applied to classify the PALSAR image and find out the vegetated and bare land remarkably. The PALSAR image classification has been carried out based on decision tree classifier [128]. It is an efficient tool for land cover classification and based on data mining technique [54, 128, 133, 134, 188]. The decision tree classifier uses knowledge based approach that is developed through knowledge of data obtained by empirical evidence and their experimental validation. Figure 6.4 illustrates the flow chart of the classification scheme. Backscattering coefficient that involves the various polarization characteristic (linear, circular, linear 45°, co– and cross–polarized ratios for both linear and circular polarization) have been utilized to classify the image in urban, water, vegetated land (tall vegetation and short vegetation) and bare soil. The decision limits in the knowledge based approach were based on the empirical evidence and the

experimental validation. First of all, the water bodies were distinguished from other classes by the condition $\sigma^{\circ}_{HV} < -30$ dB and $\sigma^{\circ}_{45x} < -25$ dB. The case when $\sigma^{\circ}_{HV} \leq -18$ dB and $\sigma^{\circ}_{HV}/\sigma^{\circ}_{VV} \geq -11$ dB [48, 54], the classified area can be characterized as tall vegetation or urban. Therefore, urban and tall vegetation were separated on the basis of cross polarization ratio of circular polarization which is negative for urban and positive for forest [188]. The bare soil which exhibit the surface scattering can be distinguished with the condition $\sigma^{\circ}_{HH}/\sigma^{\circ}_{VV} < 0$ dB, $\sigma^{\circ}_{HV} < -27$ dB and $\sigma^{\circ}_{RR} < -10$ dB [14, 54]. Further, the short vegetation can be classified based on the criterion $\sigma^{\circ}_{HV}/\sigma^{\circ}_{VV}$ greater than or equal to −11 dB and σ°_{HH} is less than or equal to −18 dB [48]. Pixels that do not satisfy any of the said conditions have been termed as unclassified. The developed classification algorithm was tested on pixel–by–pixel basis [128]. The overall accuracy was estimated 92.52% and 90.14% for PAL–1 and PAL–2 image, respectively. Classification of urban and water areas will help to mask these areas in SAR images while retrieving the vegetation covered soil moisture.

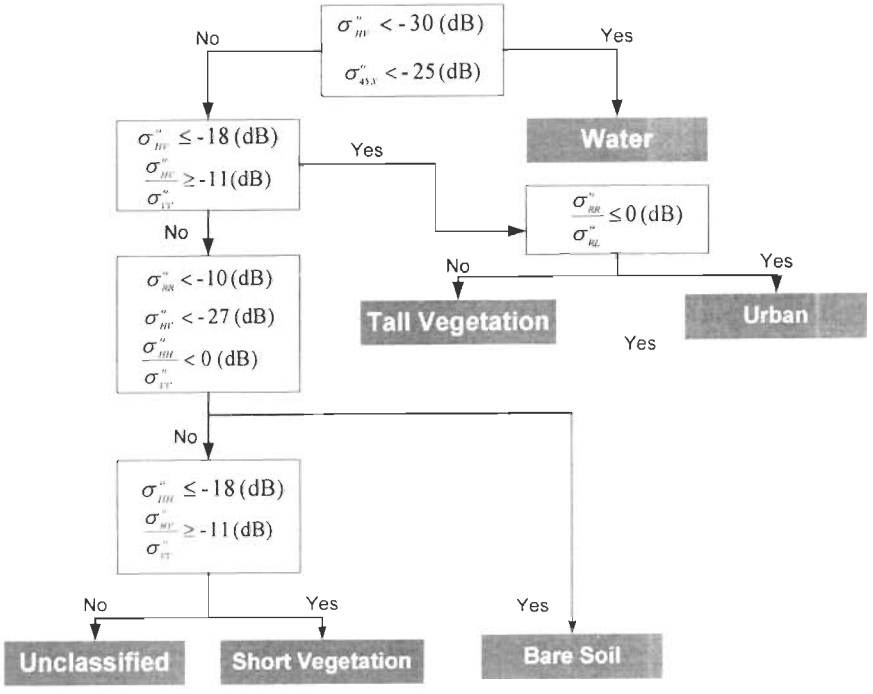

Figure 6.4. Flow chart for the decision tree classifier.

(c) Step 3

As discussed in previous sections and Figure 6.1 that vegetation over the soil has an important role for retrieving the vegetation covered soil moisture. So, vegetation effect is minimized by using optical (MODIS) data and it is modeled as following.

(i) Vegetation Modeling in SAR Data: As a first step to the algorithm development, there is emphasis to model vegetation with scattering coefficient of the obtained image. The semi–imperial approach, proposed by Attema and Ulaby [8], which is based on water cloud to determine the backscattering coefficient of vegetation covered area has been utilized by several researchers [2, 17, 178, 220]. This approach requires the parameterization of vegetation and the parameterization may include vegetation height, vegetation water content, leaf area index, biomass and other vegetation parameters. The change detection techniques are the other SAR based techniques to retrieve soil moisture in vegetated area and consider the scattering from vegetated area as time invariant process, which restrict its applicability [131, 137, 145]. In this regard, problem of vegetation should be solved for the retrieval of vegetation covered soil moisture. Therefore, as an alternative to the vegetation parameterization and change detection techniques, a more simplified approach in the form of normalizing the backscattering coefficient of the image has been utilized [88].This approach mostly rely on the information content of the image and the vegetation characterization is fulfilled with the utilization of the optical data. Joseph *et al.* [88] has modeled the vegetation effect by considering the Vegetation Water Content (VWC) and developed an empirical relation between normalized scattering coefficient and VWC. Nevertheless, the Approach 1 considered in this chapter utilizes the NDVI as the vegetation modeling for retrieval of vegetation covered soil moisture with PALSAR data.

In general, the scattering coefficient depends on sensor parameters and target parameters. Now in particular, if the sensor parameters are fixed, the scattering coefficient will depend on the target parameters, e.g., in case of vegetated area, scattering coefficient will depend on vegetation characteristic as well as underlying soil parameters, i.e., soil moisture and surface roughness. The soil moisture is generally computed based on the dielectric constant of the moist soil. Therefore,

scattering coefficient obtained from SAR data ($\sigma^0_{PP\,Image}$) from the vegetated area can be represented by Equation 6.1.

$$\sigma^0_{PP\,Image} = f(\text{Vegetation, dielectric constant of moist soil, surface roughness}) \tag{6.1}$$

Dielectric constant of moist soil and surface roughness may be represented by soil parameters and Equation 6.1 can be rewritten as Equation 6.2.

$$\sigma^0_{PP\,Image} = f(\text{Vegetation, Soil parameters}) \tag{6.2}$$

It is known that the scattering coefficient of the bare soil (i.e., $\sigma^0_{PP\,Soil}$) depends only on the soil parameters, i.e., dielectric constant and surface roughness and may be represented as Equation 6.3.

$$\sigma^0_{PP\,Soil} = f(\text{Soil parameters}) \tag{6.3}$$

Equation 6.2 and 6.3 suggest that the normalization of scattering coefficient of the vegetated area to the scattering coefficient of the bare soil will provide the normalized value that will be the function of the vegetation characteristic [87, 88]. In the case of PALSAR image, the observation frequency is fixed throughout the image acquisition whereas, incidence angle depends on the local topography. The study area considered for the present study is fairly flat therefore, the incidence angle is considered constant throughout the study area. The different images available for the same area of interest are with the different polarization (HH–, HV–, VH– and VV–polarization). So that, in the case of PALSAR image, with the availability of different polarization images, the normalized scattering coefficient ($\Delta\sigma^0_{PP}$) can be written as Equation 6.4, where PP represent for HH–, VV– or HV–polarization.

$$\Delta\sigma^0_{PP} = \frac{\sigma^0_{PP\,Image}(\text{Vegetation , Soil parameters})}{\sigma^0_{PP\,Soil}(\text{Soil parameters})} = f(\text{Vegetation}) \tag{6.4}$$

$\Delta\sigma^0_{PP}$ represents only the function of vegetation that gives an impact that this vegetation function $\Delta\sigma^0_{PP}$ can be correlated with other vegetation parameter like NDVI, which represent the vegetation function only. So, there is a need to develop relationship between $\Delta\sigma^0_{PP}$ and NDVI for characterization of $\Delta\sigma^0_{PP}$. In the present case for the development of the soil moisture retrieval in vegetation covered area, HH– and VV–polarization have been taken into account. Therefore, PP will represent either HH– or VV–polarization only.

Computation of Bare Soil Backscattering Coefficient

The approach developed in the Section 6.5.2(c) (Equation 6.4) to characterize the vegetation with the normalized scattering coefficient will require the *apriori* knowledge of scattering coefficient of bare soil at the time of model development. Therefore, 30 test areas were chosen for in situ measurement of soil moisture and surface roughness under the vegetation cover at the time of image acquisition. The field survey was carried out with GPS and the measurement methodology of soil moisture and surface roughness has been discussed in Section 1.3.3 and Section 1.3.4 respectively. The backscattering coefficient of the bare soil was computed with the help of Dubois model [48] in HH–polarization ($\sigma^0_{HH\,Soil}$) and VV–polarization ($\sigma^0_{VV\,Soil}$). Dubois *et al.* [48] model has been utilized as it provides the direct relationship between the scattering coefficient in HH– and VV–polarization and soil parameters (i.e., soil moisture and surface). Further, Dubois *et al.* [48] model can be solved to provide the dielectric constant of soil as function of scattering coefficient in HH– and VV–polarization and does not require the characterization of soil surface roughness (This has been discussed in Section 6.5.2(d)). Equations 6.5 and 6.6 provide the expression for $\sigma^0_{HH\,Soil}$ and $\sigma^0_{VV\,Soil}$, respectively as described by Dubois *et al.* [48].

$$\sigma^0_{HH\,Soil} = 10^{-2.75}\frac{\cos^{1.5}\theta}{\sin\theta^5}10^{0.028\varepsilon\tan\theta}(ks\sin^{1.4}\theta)\lambda^{0.7} \tag{6.5}$$

$$\sigma^0_{VV\,Soil} = 10^{-2.35}\frac{\cos^{3}\theta}{\sin\theta}10^{0.046\varepsilon\tan\theta}(ks\sin^{3}\theta)^{1.1}\lambda^{0.7} \tag{6.6}$$

The required input parameters in Dubois equations are rms surface height (s) and dielectric constant (ε) as soil parameters and incidence angle (θ) and wavelength (λ) as sensor parameters. Incidence angle and wavelength are 24° and 23.6 cm, respectively for PALSAR image of the study area. The dielectric constant (ε) of soil can be measured with the empirical relationship provided by Equation 6.7 [75].

$$\varepsilon = 3.03 + 9.3m_v + 146m_v^2 - 76.7m_v^3 \tag{6.7}$$

where m_v is the volumetric soil moisture content and to estimate volumetric soil moisture content, field survey was carried out. Eight to ten samples were collected from each test area (total 30 test areas were chosen) to measure the volumetric soil moisture at a field scale.

Equations 6.5 and 6.6 require the characterization of surface roughness in form of rms surface height (s). Therefore, during the field visit, the soil surface roughness was estimated with the help of pin profilometer as given by Rahman *et al.* [158]. The roughness of the field during the observation was found to be approximately constant and the average rms surface height was observed 0.53 cm with standard deviation 0.06 cm.

(ii) Use of NDVI as the Vegetation Parameter: The Normalized Difference Vegetation Index (NDVI) is almost linearly related to the vegetation abundance and therefore, can represent the vegetation effect in the soil moisture retrieval studies [214]. NDVI is defined as the ratio of the difference and sum of the spectral response at the infrared wavelength (band 2 for MODIS) and red wavelength (band 1 for MODIS) which is written as Equation 6.8.

$$\text{NDVI} = \frac{\rho_{\text{NIR}} - \rho_{\text{RED}}}{\rho_{\text{NIR}} + \rho_{\text{RED}}} = \frac{\text{Band 2} - \text{Band 1}}{\text{Band 2} + \text{Band 1}} \tag{6.8}$$

where ρ_{NIR} and ρ_{RED} are the reflectance at NIR band and RED band respectively.

The possible ranges of the NDVI values are -1 to +1. In the case of vegetation the NDVI values typically ranges from 0.1 to 0.6, where the lower values indicate the lower density of vegetation and the higher values represent the higher density of

vegetation i.e., more greenness of the vegetation. The negative values of the NDVI represent the water bodies whereas the values approximate to zero indicate the presence of the soil and rock [106].

(iii) Development of Relationship Between $\Delta\sigma^0_{PP}$ *and NDVI as Equation 6.4*: It is discussed in Section 6.5.2(c) that normalized scattering coefficient ($\Delta\sigma^0_{PP}$) is a function of vegetation parameter and can be retrieved with PALSAR image whereas NDVI which characterizes the vegetation in optical data can be retrieved with MODIS data. Therefore, this section investigates the relationship between the $\Delta\sigma^0_{PP}$ (Equation 6.4) and NDVI (Equation 6.8). Following steps explain the detailed procedure.

- Test images (PAL–1 and MOD–1) were utilized to monitor the change in normalized scattering coefficient with NDVI and for the purpose 30 test areas were taken into account to develop the empirical relationships.
- The spatial resolution of PALSAR and MODIS image is 25 m and 250 m, respectively. Therefore, the averaging of 10 × 10 pixel of PALSAR image has been performed to match the resolution of PALSAR image with MODIS image.
- The rescaled PALSAR image was co–registered with MODIS image.
- Changes in $\Delta\sigma^0_{PP}$ with the NDVI have been checked as NDVI is the descriptor of the vegetation and normalized scattering coefficient explains the vegetation effect in SAR (as discussed in Section 6.5.2(c)).
- The NDVI values have been obtained through the MODIS data and $\Delta\sigma^0_{PP}$ have been retrieved through the PALSAR data.
- In the development of the empirical relationship between $\Delta\sigma^0_{PP}$ and NDVI, the considered value of $\Delta\sigma^0_{PP}$ is in decibel (dB). The developed empirical relationship $\Delta\sigma^0_{PP}$ (dB) is a function of NDVI and is given as Equation 6.9.

$$\Delta\sigma^0_{PP}\ (\text{dB}) = P_1 \times (NDVI)^2 + P_2 \times (NDVI) + P_3 \tag{6.9}$$

The detailed description of empirical relationship along with empirical coefficients (P_1, P_2 and P_3) and its values have been made in Section 6.5.3(a)).

(d) Step 4

(i) Retrieval of Soil Moisture: The retrieval of soil moisture with PALSAR and NDVI (retrieved by MODIS image) data has been discussed in the following steps.

- The relationship between $\Delta\sigma^0_{PP}$ and NDVI developed in Equation 6.9 will provide the value of $\Delta\sigma^0_{PP}$ (dB) with the known values of NDVI.
- The bare soil scattering coefficient in HH– and VV–polarization can be retrieved with the relationship $\Delta\sigma^0_{PP} = \sigma^0_{PP\ Image} / \sigma^0_{PP\ Soil}$ (Equation 6.4). Therefore, bare soil scattering coefficient can be written as Equation 6.10.

$$\sigma^0_{PP\ Soil}\ (\text{dB}) = \sigma^0_{PP\ Image}\ (\text{dB}) - (P_1 \times (NDVI)^2 + P_2 \times (NDVI) + P_3) \qquad (6.10)$$

- Equation 6.10 will provide the scattering coefficient of bare soil in HH– and VV–polarization with the normalized scattering coefficient obtained through the PALSAR image and NDVI values obtained through the MODIS data.
- The retrieved scattering coefficient values of the bare soil will contain the information of the soil moisture as well as surface roughness. Therefore, to minimize the roughness effect in the retrieval of soil moisture, copolarization approach has been utilized [30, 56, 115, 156] and Dubois equations in HH– and VV–polarization have been solved to provide an equation that is the function of dielectric constant only and independent to surface roughness.
- This solution of equation provides the flexibility to apply the retrieval algorithm over a wide range of roughness conditions without requirement of characterizing the surface roughness. The solution is given by Equation 6.11.

$$\varepsilon = \frac{10 \times \sigma^0_{VVSoil}(dB) - 11 \times \sigma^0_{HHSoil}(dB) + 110 \times \log(C_1) - 100 \times \log(C_2)}{1.52 \times \tan(\theta)} \qquad (6.11)$$

where

$$C_1 = 10^{-2.75} \frac{\cos^{1.5}\theta}{\sin\theta^5} (k \sin^{1.4}\theta) \lambda^{0.7}$$

and

$$C_2 = 10^{-2.35} \frac{\cos^3\theta}{\sin\theta} (k \sin^3\theta)^{1.1} \lambda^{0.7}$$

- The Dubois equations have been solved to provide the dielectric constant of the soil (Equation 6.11) and volumetric soil moisture is retrieved by Equation 6.12 [75].

$$m_v = -5.3\times10^{-2} + 2.92\times10^{-2}\varepsilon - 5.5\times10^{-4}\varepsilon^2 + 4.3\times10^{-6}\varepsilon^3 \qquad (6.12)$$

where ε is the dielectric constant of soil. It is assumed that soil texture has negligible effect on backscattering coefficient from crop covered soil because many researchers are using directly this from for retrieving soil moisture [75–77].

6.5.3. Implementation of Approach 1 on SAR Image

(a) Implementation on the Test Image (PAL–1 and MOD–1)

The developed algorithm is tested on the images PAL–1 and MOD–1 and various steps involved in this are given as following.

- PALSAR image of the test region (PAL–1) is classified into various land cover features, according to the procedure discussed in Section 6.5.2(b).
- Figure 6.5(a)–(c) show the color composite PALSAR image (HH = red, HV = green, VV = blue), corresponding classified PALSAR image and location of different classes on the classified image, respectively. The image has been classified into urban (red), water (blue), short vegetation (green), long vegetation (sea green) and bare soil (sienna). The overall classification accuracy was estimated as 92.52%.
- The regions which are considered has crops like wheat, sugarcane and mustered at that time.
- The urban and water region of the classified image is masked. The masking is performed with the intent to demarcate the vegetation and bare soil region, as the algorithm have been developed for the vegetated areas and bare soil for soil moisture retrieval.
- Figure 6.6 shows the classified masked image. The size of the PAL–1 image considered was 850 × 850, i.e., the total number of pixel was 722500. After

masking the image, 515313 pixels correspond to the vegetated area and 11084 pixels correspond to the bare soil.

- Figure 6.7 (a) and 6.7 (b) show the MODIS band–1 and band–2 image of the test area respectively and Figure 6.7 (c) shows the corresponding NDVI image. The NDVI values of the test region ranges from 0.25 to 0.43.
- Due to the difference in the spatial resolution of the PALSAR image (25 m) and MODIS (250 m) data, PALSAR image pixel values corresponding to the MODIS pixel value were averaged as explained in Section 6.5.2(c)(iii).

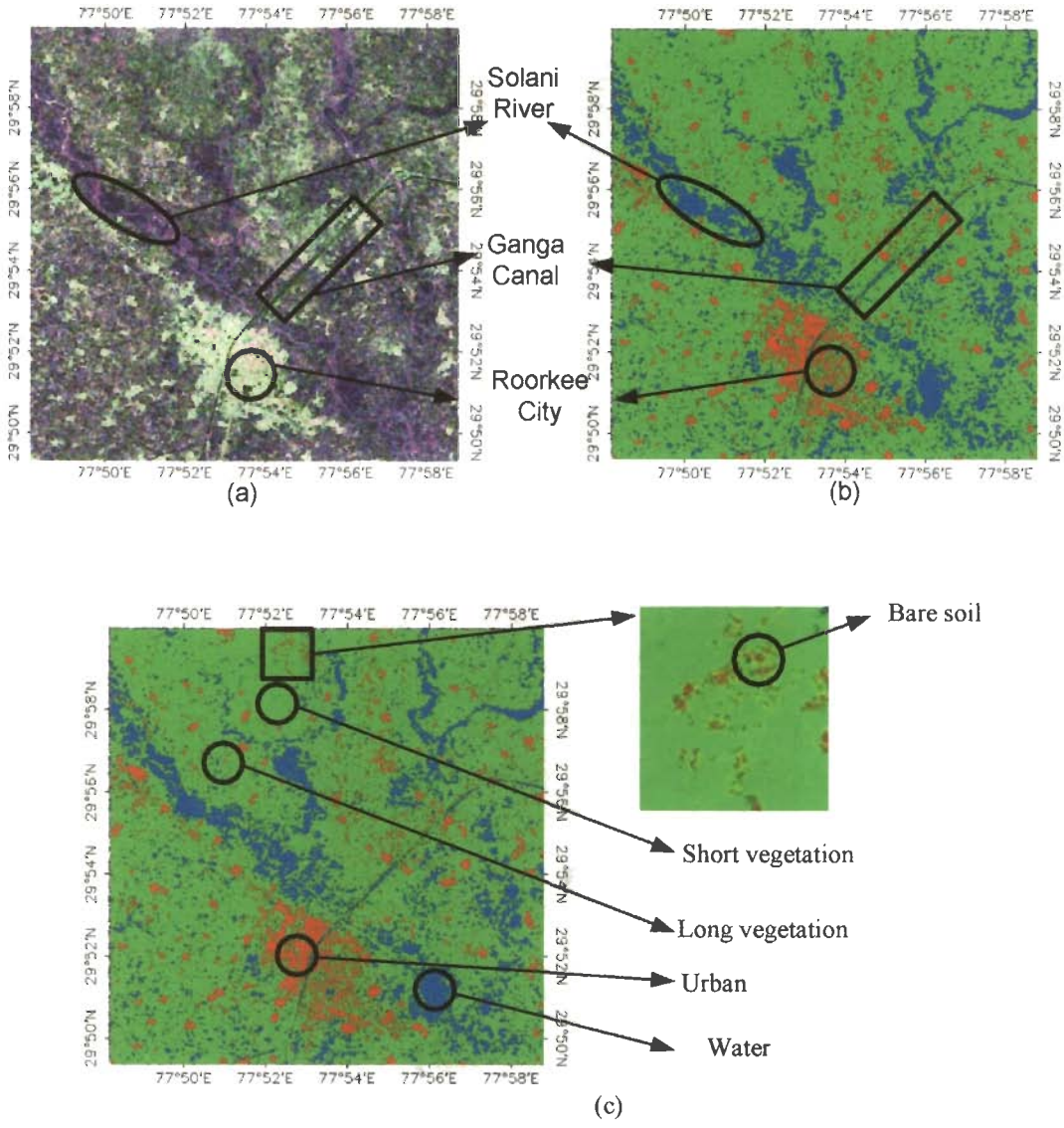

Figure 6.5. PALSAR test image (PAL–1, pixel spacing = 25 m) (a) color composite image (HH = red, HV = green, VV = blue) (b) classified image (red = urban, blue = water, green = short vegetation, sea green = long vegetation and sienna bare soil) (c) Location of different classes on the classified image.

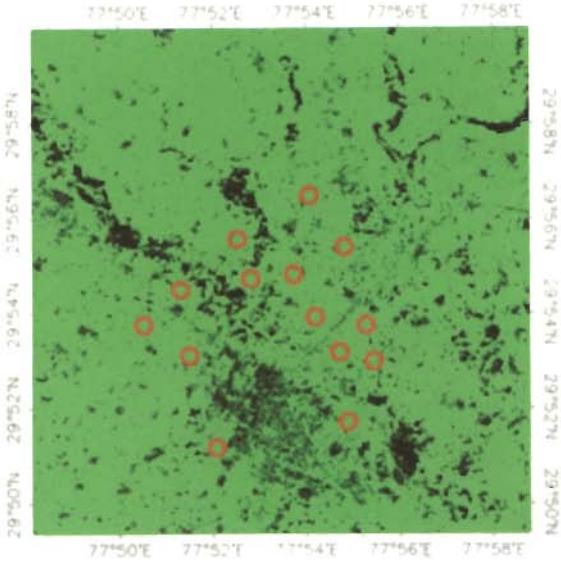

Figure 6.6. Classified masked image of the PALSAR test data (PAL–1) showing some of the test areas (in circle) used for in situ measurement of the soil moisture and surface roughness for development of algorithm.

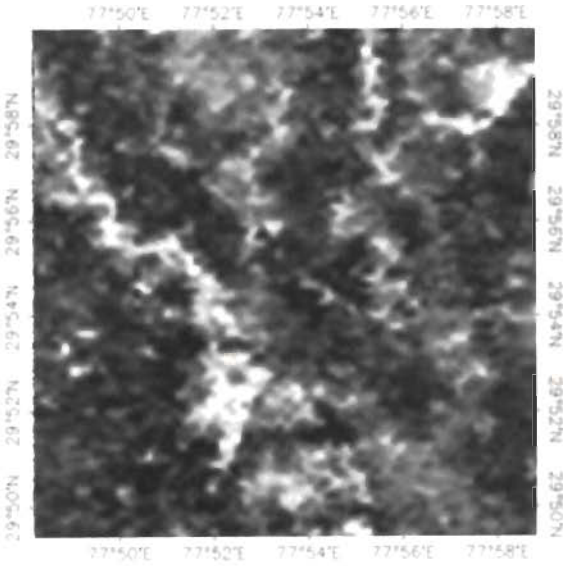

(a)

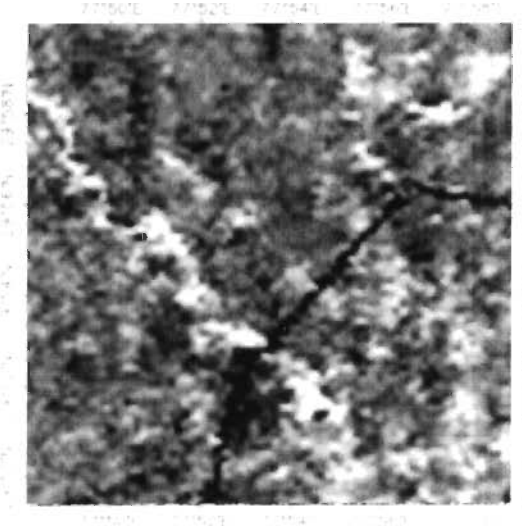

(b)

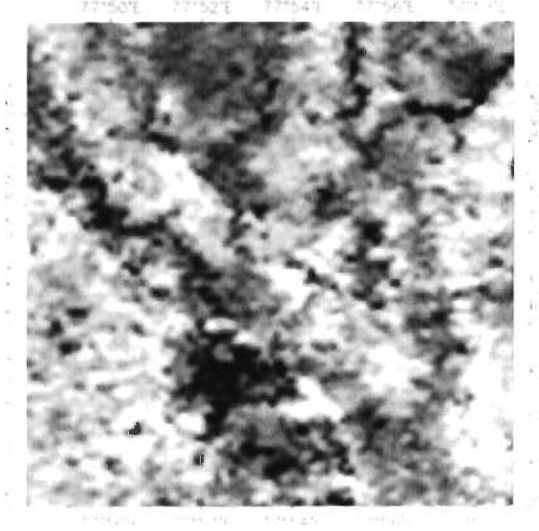

(c)

Figure 6.7. Test image of MODIS (MOD–1) of (a) band–1 image (b) band–2 image (c) NDVI image.

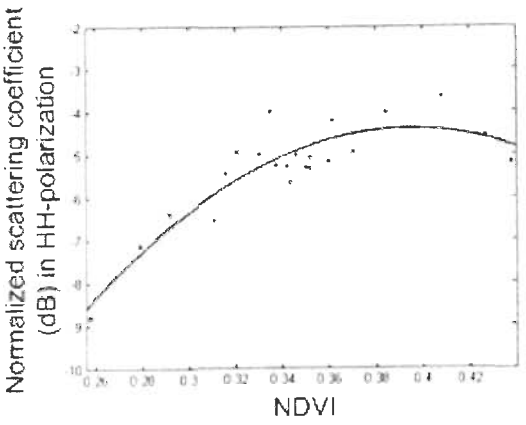

(a)

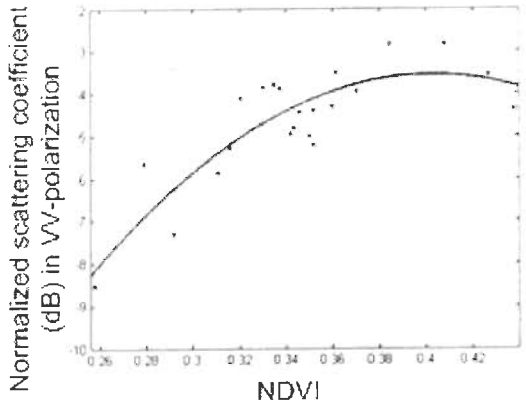

(b)

Figure 6.8. Response of normalized scattering coefficient (a) in HH–polarization (b) in VV–polarization.

- The variation of the normalized scattering coefficient in the HH–polarization ($\Delta\sigma^0_{HH}$ varies –3.64 dB to –8.82 dB) and VV–polarization ($\Delta\sigma^0_{VV}$ varies –2.82 dB to –8.53 dB) with NDVI (varies 0.25 to 0.43) is shown in Figures 6.8(a) and (b), respectively. The change in the normalized scattering coefficient with the NDVI led to the development of the empirical relation provided by Equation 6.9.
- The developed empirical relationship is quadric in HH–polarization as well as in VV–polarization, except the difference in the empirical coefficients. The empirical coefficients P_1, P_2 and P_3 in case of the HH–polarization were –218.1, 172.2 and –38.41, respectively with coefficient of determination (R^2) 0.83 and

root mean square error (RMSE) 0.5313. Further, in case of the VV–polarization P_1, P_2 and P_3 were –241.7, 201.3 and –41.8, respectively with R^2 = 0.81 and RMSE = 0.7241.

- The developed empirical relationship (Equation 6.9) facilitates to retrieve $\Delta\sigma^0_{HH}$ (dB) and $\Delta\sigma^0_{VV}$ (dB) with the NDVI values of MODIS image (MOD–1).
- These normalized scattering coefficients in conjunction with the scattering coefficients of PALSAR image ($\sigma^0_{HH\ Image}$ (dB) and $\sigma^0_{VV\ Image}$ (dB)) provides the scattering coefficient of the soil ($\sigma^0_{HH\ Soil}$ (dB) and $\sigma^0_{VV\ Soil}$ (dB)) with help of Equation 6.10.
- The dielectric constant of the soil is retrieved by Equation 6.11 by substituting $\sigma^0_{HH\ Soil}$ (dB) and $\sigma^0_{VV\ Soil}$ (dB) and the corresponding volumetric soil moisture constant is obtained from Equation 6.12.
- The retrieved soil moisture map is shown in Figure 6.9 where black areas of image are the masked pixels. Figure 6.10 shows the volumetric soil moisture values retrieved through the developed algorithm and the observed volumetric soil moisture values. The root mean square error (RMSE) for the retrieval of the soil moisture is 0.036.

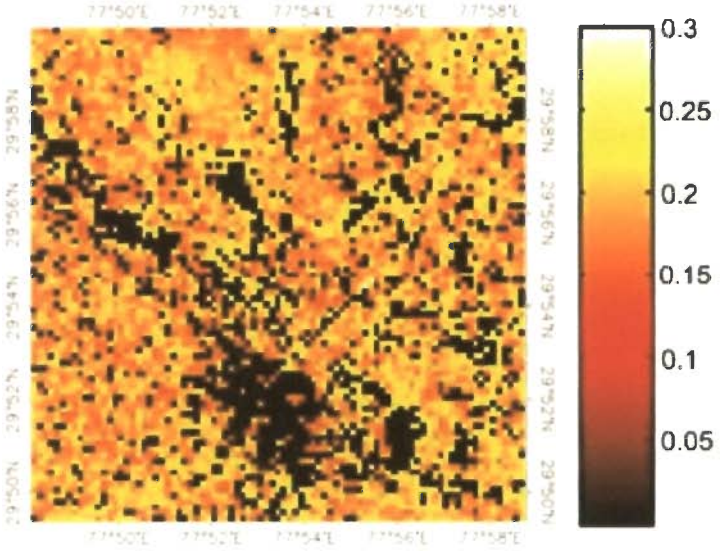

Figure 6.9. Soil moisture map of the test area. Pixels with black colour represent masked area.

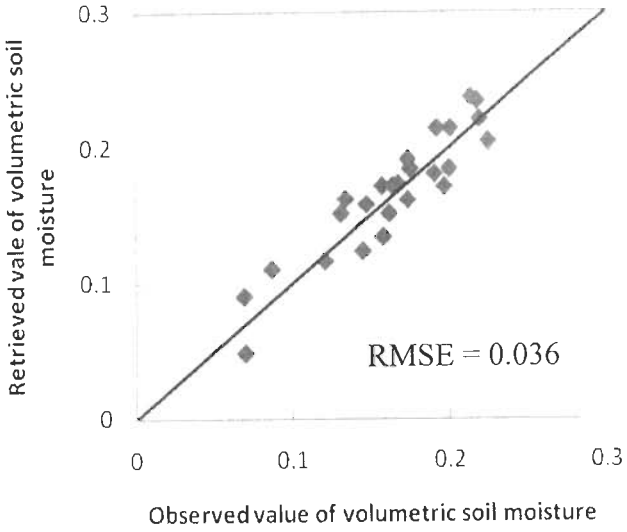

Figure 6.10. Graph between the observed and retrieved value of volumetric soil moisture for the test area.

(b) Validation of Approach 1

The developed algorithm has been validated on PAL–2 and MOD–2 images. In this region also the similar type of crops were found. A detailed analysis is as following.

- The land cover was approximately similar to the land cover of test area. The classification of the PALSAR image of the validating region (PAL–2) was carried out with the procedure laid down in Section 6.5.2(c) and image was classified into urban (red), water (blue), short vegetation (green), long vegetation (sea green) and bare soil (sienna). The overall accuracy was estimated 90.14%.
- Figures 6.11(a)–(c) show the color composite PALSAR image (HH = red, HV = green, VV = blue), corresponding classified PALSAR image and the masked image (urban and water region masked), respectively, respectively. The PAL–2 image was also of size 850 × 850, i.e. contains the 722500 pixel. After masking the image the number of pixel for vegetation area and bare soil are 595653 and 12091 respectively.
- Figure 6.12 shows the corresponding NDVI image retrieved through the MODIS data (MOD–2), which varies from 0.25 to 0.44.

- The PALSAR pixels corresponding to the MODIS pixel were averaged as the procedure was performed in the case of test PALSAR image and explained in Section 6.5.2(c)(iii).
- The empirical relationship developed for the test region was used in case of validating region also (i.e., the retrieved empirical coefficient P_1, P_2, and P_3 were same as for the test image) and similar procedure was carried out to retrieve the soil moisture values.
- The retrieved soil moisture image is shown in Figure 6.13 whereas Figure 6.14 shows the volumetric soil moisture retrieved through the developed algorithm and the observed volumetric soil moisture values. The root mean square error (RMSE) for the retrieval of the soil moisture was 0.041.

The retrieved soil moisture values in the case of test area as well as the validating area show quite good agreement with the observed ground truth values.

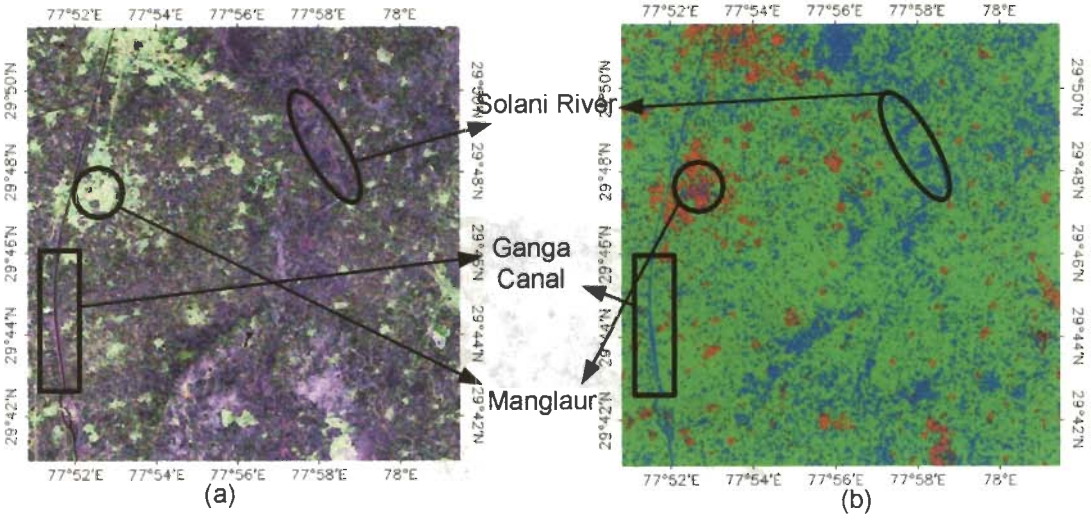

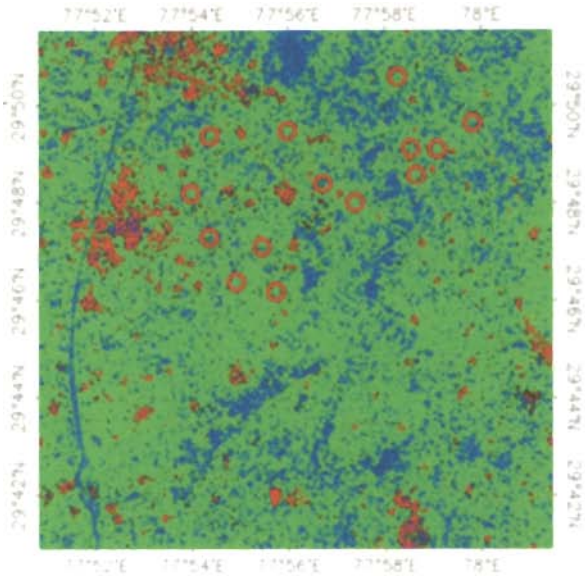

(c)

Figure 6.11. PALSAR validating image (PAL–2, pixel spacing = 25 m) (a) color composite image (HH = red, HV = green, VV = blue) (b) classified image (red = urban, blue = water, green = short vegetation, sea green = long vegetation and sienna bare soil) (c) classified masked image with some of the area marked with circle that was used for in situ measurmet of moisture and roughness to validate the results.

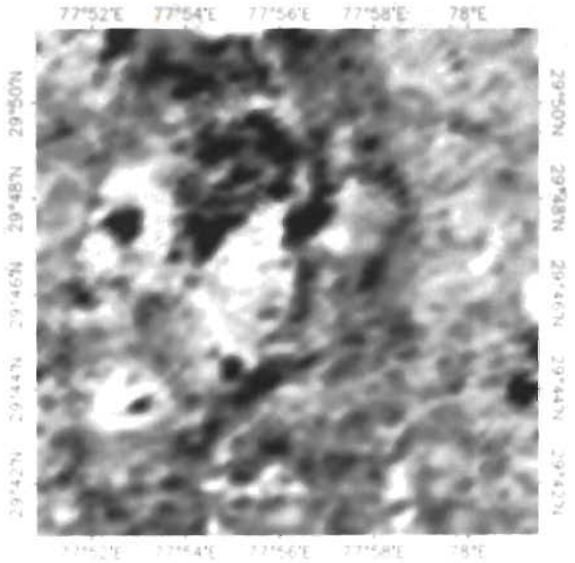

Figure 6.12. NDVI image of validating region.

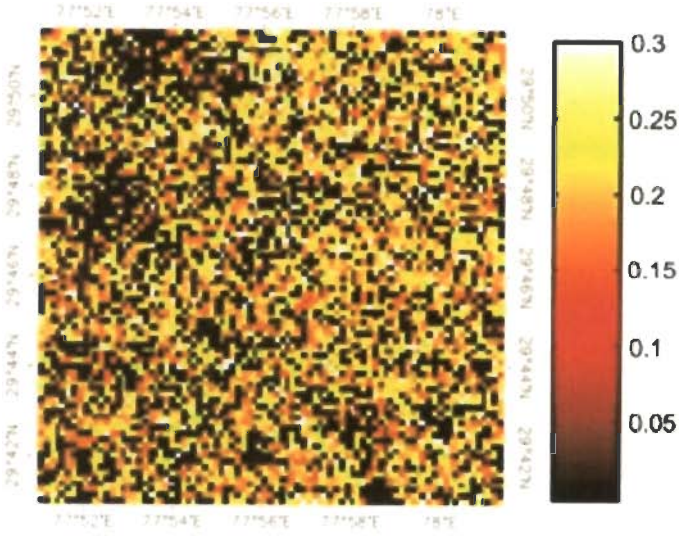

Figure 6.13. Soil moisture map of the validating image. Pixels with black colour represent masked area.

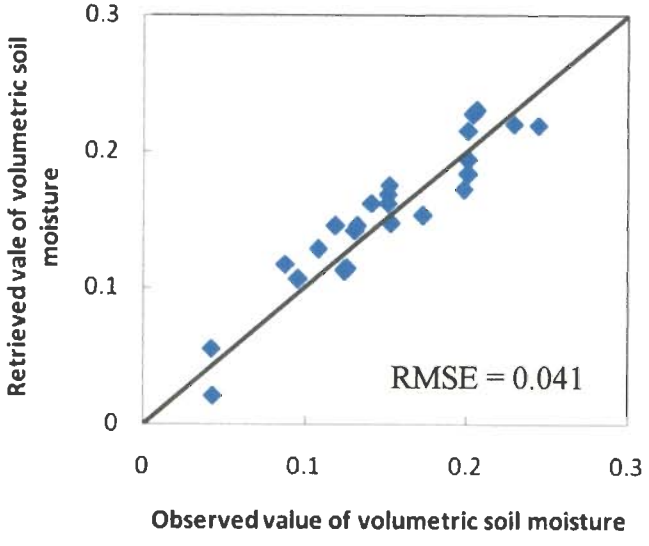

Figure 6.14. Observed and retrieved value of volumetric soil moisture for the validating area.

6.6. Model Development: Approach 2

Soil moisture retrieval methodology discussed in Approach 1 provides quite satisfactory results and proves the use of share of information from SAR and MODIS data for soil moisture retrieval over vegetated areas. The approach adopted in this method was to normalize the scattering coefficient of vegetated area obtained from

PALSAR data with scattering coefficient of bare soil computed with Dubois equations in HH– and VV–polarization. The in situ measurements of soil moisture and surface roughness have been used for the computation of scattering coefficient of bare soil of the corresponding area. Thus, the adopted approach provided the normalized scattering coefficient as function of NDVI (detailed discussion has been presented in Section 6.5).

To minimize the dependency of field knowledge a second approach based on dry soil is considered and tested for soil moisture retrieval in vegetated areas. It means that the normalization of scattering coefficient of vegetated area can also be performed with the scattering coefficient of dry soil [214]. This normalization scheme will provide the normalized scattering coefficient as a function of soil moisture and vegetation characteristic defined by NDVI. This approach has been developed in the following sections. Figure 6.15 depict the flowchart of the soil moisture retrieval in vegetated areas. The classified masked image obtained for Approach 1 has been used to develop the model for soil moisture retrieval.

6.6.1. Theoretical Background

(a) Vegetation Modeling in SAR Image

As discussed in Section 6.5.2(c)(i) the scattering coefficient from vegetated area depends on the scattering from the vegetation and the underlying soil. The scattering from the soil is basically a function of the soil dielectric constant defined by dielectric constant of the soil and its moisture content and surface roughness. Therefore the scattering coefficient form a vegetated area can be written as a function of vegetation, dielectric constant of moist soil and surface roughness (Equation 6.13).

$$\sigma^{0}_{\text{PP Image}} = f(\text{Vegetation, dielectric constant of moist soil, surface roughness}) \tag{6.13}$$

The scattering coefficient of bare dry soil ($\sigma^{0}_{\text{PP Dry Soil}}$) is dependent on the dielectric constant of dry soil and surface roughness and can be written as Equation 6.14.

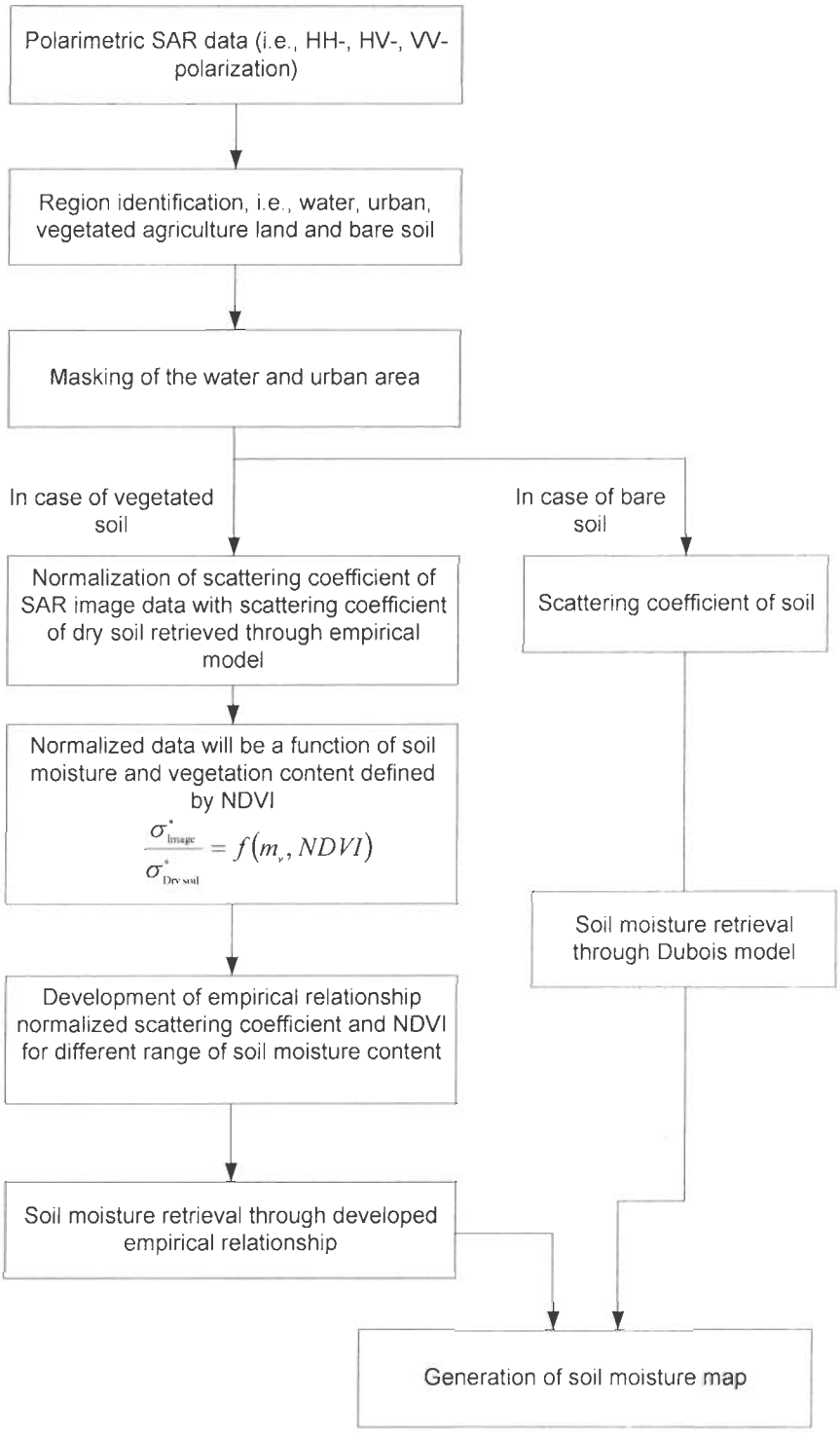

Figure 6.15. Flow chart for the retrieval of soil moisture: Approach 2.

$$\sigma^{0}_{PP\ Dry\ soil} = f(\text{dielectric constant of dry soil, surface roughness}) \quad (6.14)$$

It can be inferred from Equations 6.13 and 6.14 that the normalization of the scattering coefficient from the vegetation area to the scattering coefficient of the dry soil would let to the development of a function which will depend on soil moisture and vegetation [214]. Therefore the normalized scattering coefficient can be written as Equation 6.15.

$$\Delta\sigma^{0}_{PP\ Image\ -\ Dry\ soil} = \frac{\sigma^{0}_{PP\ Image}(\text{Vegetation, dielectric constant of moist soil, surface roughness})}{\sigma^{0}_{PP\ Soil}(\text{dielectric constant of dry soil, surface roughness})}$$

therefore

$$\Delta\sigma^{0}_{PP\ Image\ -\ Dry\ soil} = f(\text{Vegetation, soil moisture}) \quad (6.15)$$

where PP represents the polarization of the SAR image. The algorithm development in the present case has been dealt with the HH–polarization.

(b) Computation of the Bare Soil Scattering Coefficient

The development of the algorithm is based on the normalization of the scattering coefficient of the vegetated area that is available through the PALSAR image to the scattering coefficient of the dry soil which can be calculated by Dubois *et al.* model (Equation 6.5) directly as it is known that the dielectric constant of dry soil is 3.03 (Equation 6.7). The sensor parameter used for the computation of scattering coefficient were the PALSAR sensor parameters, i.e., the incidence angle and wavelength with values 24° and 23.6 cm, respectively. The rms surface height observed was 0.53 cm, as discussed in Section 6.5.2(c)(i), as well as, the dielectric constant of dry soil was considered to be 3.03.

(c) Vegetation Modeling with Optical Image

NDVI is used to describe the vegetation with optical image. MODIS band–1 and band–2 image have been acquired for the computation of NDVI. The description of vegetation with NDVI has been provided in Equation 6.8.

6.6.2. Development of Relationship between $\Delta\sigma^0_{PP}$ and NDVI

It is discussed in Section 6.6.1(a) by Equation 6.15 that $\Delta\sigma^0_{\text{PP Image - Dry soil}}$ is a function of soil moisture and vegetation and vegetation can be described by the NDVI as discussed in Section 6.6.1(c). Therefore the relationship between $\Delta\sigma^0_{\text{PP Image - Dry soil}}$ and NDVI has been explored. The development of relationship is based on the in situ measurements of soil moisture made during the field visit in the test region (PAL–1 image). The moisture values obtained during the field visit were grouped in range, i.e., $m_{v1} \leq 0.10$, $0.10 < m_{v2} \leq 0.15$, $0.15 < m_{v3} \leq 0.20$, $0.20 < m_{v4} \leq 0.25$ and $m_{v5} > 0.25$. Based on these values a set of isometric lines were observe between $\Delta\sigma^0_{\text{PP Image - Dry soil}}$ and NDVI as shown in Figure 6.16. The $\Delta\sigma^0_{\text{PP Image - Dry soil}}$ values changed from 4.28 dB to 1.48 dB, from 3.11 dB to –0.42 dB, from 3.03 dB to –0.20 dB, from 0.81 dB to –1.07 dB and from –0.51 dB to –1.49 dB for m_{v1} to m_{v5}, respectively. The NDVI values changed from 0.29 to 0.40, from 0.29 to –0.50, from 0.24 to 0.38, from 0.27 to 0.48 and from 0.34 to 0.43 for m_{v1} to m_{v5}, respectively. It can be observed from the Figure 6.16 that for each NDVI the variation in $\Delta\sigma^0_{\text{Image - Dry soil}}$ in vertical direction is due to soil moisture. The vertical variation decreases as the NDVI increases, signifying that the sensitivity of $\Delta\sigma^0_{\text{Image - Dry soil}}$ decrease for soil moisture with the increase in NDVI [214]. The set of isometric line were regressed and a series of soil moisture equations (6.16A–6.16E) were obtained. The coefficient of determination (R^2) for all regressed isometric lines was greater than 0.81.

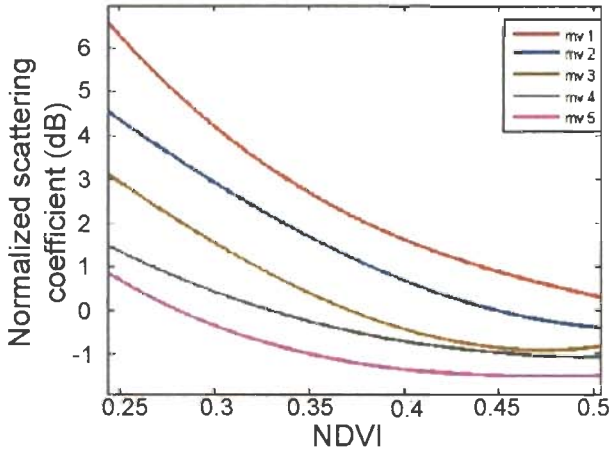

Figure 6.16. Response of normalized scattering coefficient for NDVI at different soil moisture contents.

$$m_{v1} \leq 0.10; \quad \Delta\sigma^{\circ} \leq -165.5\,(\mathrm{NDVI})^3 + 263.7\,(\mathrm{NDVI})^2 - 149.2\,(\mathrm{NDVI}) + 29.72 \tag{6.16A}$$

$$0.10 < m_{v2} \leq 0.15; \quad \Delta\sigma^{\circ} \leq 60.8\,(\mathrm{NDVI})^3 - 14.83\,(\mathrm{NDVI})^2 - 34.49\,(\mathrm{NDVI}) + 12.97 \tag{6.16B}$$

$$0.15 < m_{v3} \leq 0.20; \quad \Delta\sigma^{\circ} \leq 96.22\,(\mathrm{NDVI})^3 - 38.16\,(\mathrm{NDVI})^2 - 28.7\,(\mathrm{NDVI}) + 11 \tag{6.16C}$$

$$0.20 < m_{v4} \leq 0.25; \quad \Delta\sigma^{\circ} \leq -28.52\,(\mathrm{NDVI})^3 + 73.32\,(\mathrm{NDVI})^2 - 52.32\,(\mathrm{NDVI}) + 10.3 \tag{6.16D}$$

$$m_{v5} > 0.25; \quad \Delta\sigma^{\circ} \leq -107\,(\mathrm{NDVI})^3 + 172.4\,(\mathrm{NDVI})^2 - 91.4\,(\mathrm{NDVI}) + 14.46 \tag{6.16E}$$

Similar result were obtained by Wang *et al.* [214]. Wang *et al.* [214] have carried out the study by normalizaing the scattering coefficient of the wet season image to the dry season image and they have developed the emprical relationship between the normalized scattering coefficient and the NDVI. Howerve, for the Approach 2, the normalization of the scattering coefficent have been carried out by computing the scattering coefficnent of dry soil with Dubois *et al.* [48] Model by this the data of dry season may be not required.

6.6.3. Retrieval of Soil Moisture with Approach 2

Equations 6.18A–6.18E provides a set of equation relating normalized scattering coefficient with NDVI for different range of soil moisture. The volumetric soil moisture can be retrieved utilizing these equations provided the normalized scattering coefficient and NDVI of the area of interest. The normalized scattering coefficient has been obtained from the PALSAR image by normalizing the scattering coefficient of PALSAR data with scattering coefficient of dry soil whereas, the NDVI values has been obtained from the MODIS band–1 and band–2 images. Following scheme has been adopted in the retrieval of soil moisture.

First of all, the NDVI value obtained from the MODIS has been substituted in Equation 6.16E and checked the condition of validity. If the condition is satisfied the moisture lie for m_{v5} range otherwise the validity condition of Equation 6.17D is checked and the procedure is followed up to the condition of Equation 6.16A.

6.6.4. Implementation of Approach 2 on SAR Image

(a) Implementation on the Test Area

Classified masked image of PALSAR data (PAL–1) along with NDVI values retrieved from MODIS image (MOD–1) of test region has been utilized to retrieve the volumetric soil moisture content (Figure 6.6 and 6.7(c), respectively).

- Scattering coefficient of PAL–1 image was normalized with scattering coefficient of the dry soil computed with the Dubois *et al.* [48] model (Equation 6.15).
- NDVI values were computed with the band–1 and band–2 of the MOD–1 image.
- The empirical relationship developed in Section 6.6.2 (Equation 6.16) was utilized to retrieve the soil moisture as described in Section 6.6.3.
- Figure 6.17 shows the retrieved soil moisture map of the test region. The RMSE for the estimation of volumetric soil moisture was 0.039. Figure 6.18 shows the observed and retrieved values of volumetric soil moisture.

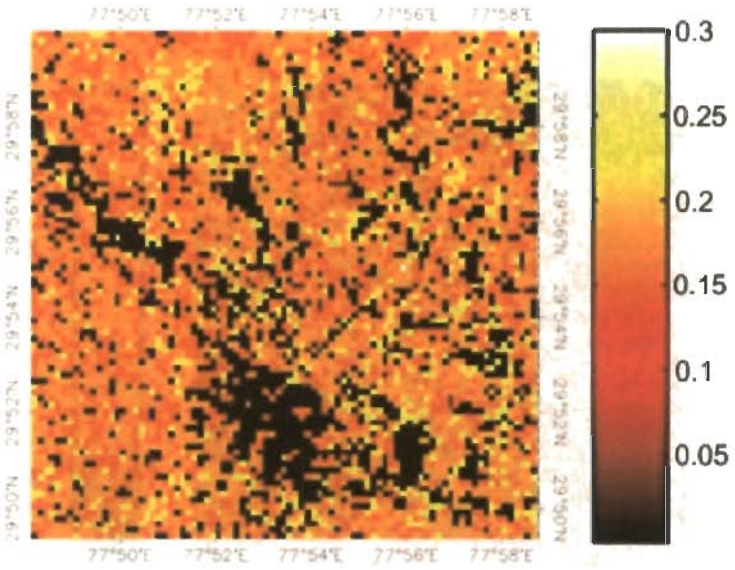

Figure 6.17. Moisture image of test region retrieved by Approach –2. Pixels with black colour represent masked area.

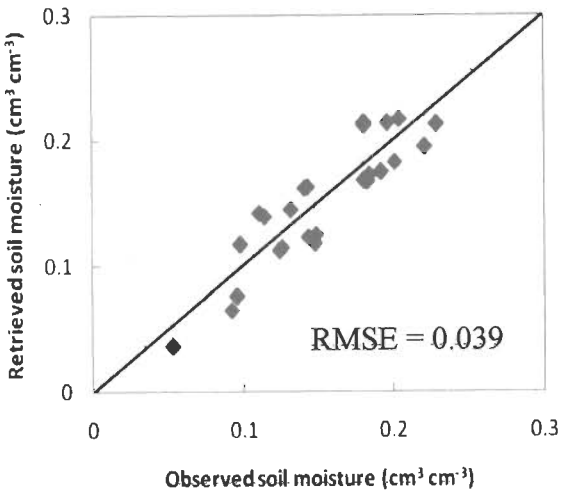

Figure 6.18. Observed and retrieved values of volumetric soil moisture of test area.

(b) Validation of Algorithm

Classified masked image of PALSAR data (PAL–2) along with NDVI values retrieved from the MODIS image (MOD–2) of validating region has been utilized to retrieve the volumetric soil moisture content. Figure 6.19 shows the retrieved soil moisture map of the test region. The RMSE for the estimation of volumetric soil moisture was 0.052. Figure 6.20 shows the observed and retrieved values of volumetric soil moisture.

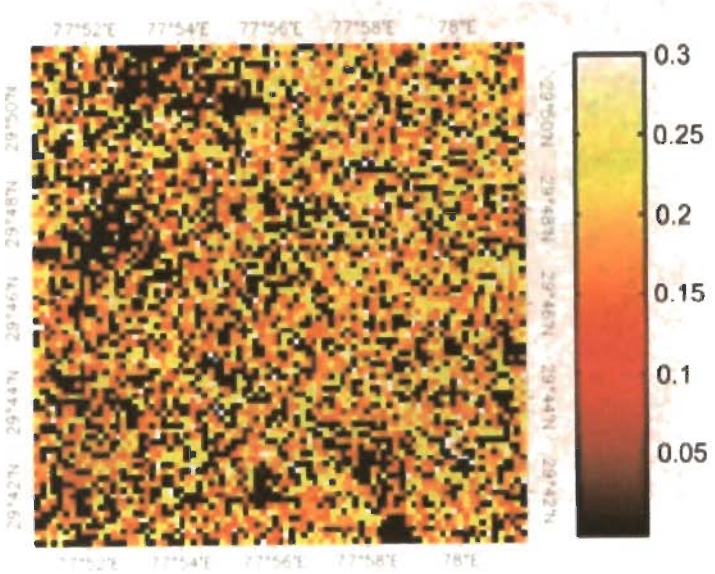

Figure 6.19. Moisture image of test region retrieved by Approach –2. Pixels with black colour represent masked area.

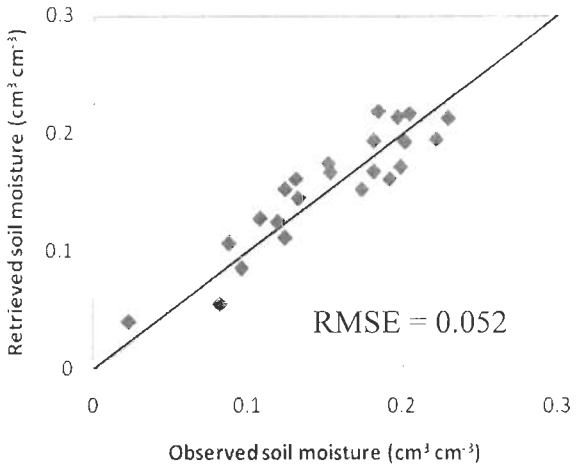

Figure 6.20. Observed and retrieved values of volumetric soil moisture of validating area.

6.7. Comparison of Approach 1 and Approach 2

Approach 1 and Approach 2 of soil moisture retrieval in vegetation area presents two different normalizing schemes that have been devised to normalize the scattering coefficient of PALSAR image of vegetated area by which MODIS data can be used. The first approach employs in situ measurement of soil moisture as well as surface roughness for computation of bare soil scattering coefficient and subsequently utilized this value to normalize the scattering coefficient of vegetated area. It is difficult to measure the surface roughness in the fields. The second approach does not require the in situ measurement of soil moisture and normalizes the scattering coefficient of the vegetated area with scattering coefficient of dry bare soil however the in situ measurements are required at the later stage of algorithm development. The scattering coefficient of the bare soil has been computed with Dubois equation. In both the approaches, empirical relationship between normalized scattering coefficient and NDVI was developed. First approach utilizes both like polarization, i.e., HH– and VV–polarization whereas; the second approach utilizes only the HH–polarization. The *apriori* knowledge of surface roughness is required in the phase of the algorithm development in both the approaches. But, the first approach which utilizes HH– as well as VV–polarization minimizes the roughness effect in retrieval of soil moisture by solving the Dubois equation in HH– and VV– polarization utilizing the

copolarization ratio approach. The second approach does not apply such an approach and considers the surface roughness of the development phase. The Approach 1 provides a simple relationship between the normalized scattering coefficient and NDVI whereas; Approach 2 provides a set of equations which are tested for their validity range to provide the moisture value. Though, both the approaches require the *apriori* information of soil moisture and surface roughness at the time of algorithm development, the Approach 1 provide an upper hand in implementation as it does not require the surface roughness as an input parameter for moisture retrieval in vegetated area and rely only on the information content of satellite images, i.e., SAR and NDVI data.

The empirical coefficients in the both the approaches have been computed for the vegetation cover of the test area. Though, the validation of the developed approaches has been made for different area and provides good results, the area of validation contains approximately similar land cover and vegetation type. Therefore, there may be the possibility of the site dependency when the approach is applied in different land cover with different vegetation type, but being a conceptual approach their empirical coefficient can be computed for respective test region and their applicability can be ensured.

6.8. Conclusion

The study carried out in this chapter acknowledges the problem of soil moisture retrieval in vegetated region and develop algorithms based on the information fusion approach of PALSAR, a SAR data and MODIS, an optical data. The emphasis of the fusion approach is due to the complementary information available by the SAR and optical data. SAR data contains the information of vegetation characteristic as well as the underlying soil characteristic that includes the soil moisture. But due to the complex scattering behavior of microwave data it is very much difficult to segregate the vegetation effect from the scattering value when the aim is to retrieve vegetation covered soil moisture. Now, at this point, the optical data, especially NDVI values that are computed from optical data and explain the abundance of vegetation, can be efficiently utilized to incorporate the vegetation effect in SAR modeling. In this manner, the fusion approach provides good alternative

to retrieve vegetation covered soil moisture which is very complex task when dealt with SAR data only. Therefore, in this chapter fusion approach has been utilized with PALSAR, a SAR data and MODIS, an optical data. The PALSAR data was efficiently utilized with polarimetric capability to classify the land cover in urban, water, vegetation and bare soil and subsequently to mask the urban and water region. The problem of vegetation characterization in retrieval of soil moisture from SAR images has been dealt with optical image by appropriately utilizing the NDVI, a vegetation index. Two different approaches have been developed that discusses the relationship between normalized scattering coefficient and NDVI. Both the approaches provide different set of relationship between normalized scattering coefficient and NDVI due to different normalization process adopted. The developed algorithms for both the approaches were tested on the first set of images (PAL–1 and MOD–1) on which the algorithm was developed and thereafter validated on the second set of images (PAL–2 and MOD–2). The obtained results are in good agreement with the ground truth data and approaches have potential to retrieve soil moisture under vegetation cover to with minimum need of *apriori*.

Chapter 7

Conclusion and Future Scope

This chapter aims to provide the key conclusion of the research carried out in this thesis and the future scope has been given in later part of this chapter.

7.1. Contribution of the Thesis

Present thesis has emphasized to study and critically analyze the soil texture effect in bistatic domain at 10 GHz and 6 GHz and develop the retrieval algorithm for minimum need of *apriori* information. It also emphasized to retrieve soil moisture over vegetated area with satellite data. To fullfil these studies a ground based bistatic scatterometer is ingeniously designed at 10 GHz and 6 GHz which had the capability to change the polarization and incidence angle. By this soil parameters effect is critically analyzed and retrieval algorithm is developed. Also, two different kinds of satellite data, i.e., PALSAR based on active microwave remote sensing concept and MODIS data on optical domain have been used to develop fusion approach for soil moisture retrieval over vegetated area. The main conclusions and contributions of the thesis are as following:

- The research in characterization of soil parameters, i.e., soil texture, soil moisture and surface roughness has been devoted to monostatic domain but still the uncertainty exists. Further, soil moisture and surface roughness have been prominently used as soil parameters in active microwave remote sensing studies whereas the role of soil texture has been neglected. But, studies have demonstrated a significant effect of soil texture on microwave scattering. Therefore, the study was carried out to observe the soil texture effect (changing the percentage of sand from 38.7% to78.4%, percentage of silt from 9.1% to 35.8% and percentage of sand from 4.3% to 18.7%) on specular scattering while varying soil moisture (i.e., 0.10 cm^3 cm^{-3} to 0.21 cm^3 cm^{-3}) and periodic surface roughness (i.e., 0.9 and 1.4 cm) at 10 GHz. It was observed that specular scattering coefficient changes with the change in soil texture and the effect was clearly observable for smooth soil at different moisture conditions for higher incidence angles (i.e., $\geq 50°$). The surface roughness has major effect on specular scattering coefficient when objective is to observe the soil texture effect on specular scattering. It was difficult to observe the change in specular scattering coefficient with change in soil texture for different surface roughness values at 10 GHz. Therefore, it may be inferred that effect of soil texture with specular scattering coefficient at 10 GHz can be observed for smooth surface at different soil moisture content but it is difficult to observe the soil texture effect on specular scattering coefficient at different surface roughness conditions.
- The difficulty in observing the effect of soil texture on specular scattering coefficient at 10 GHz for rough surface led to carry out experiments at 6 GHz. It was observed that change in specular scattering coefficient occurs with change in soil texture at different roughness conditions (i.e., smooth surface to s = 2.46 cm) at 6 GHz. Sand and clay constituents of soil have more effect than silt constituent of soil on the specular scattering coefficient. It was observed that due to decrease in sand percentage, specular scattering coefficient decreases, but on the contrary, decrease in percentage of clay in soil increases the specular scattering coefficient. The change in percentage of silt has negligible effect on the specular scattering coefficient. All these observations were noticed for higher incidence angles (i.e., $\geq 45°$) whereas at

lower incidence angles (i.e., < 45°) it was difficult to observe the change in specular scattering coefficient with change in soil texture, i.e., with percentage change in sand, silt and clay constituents. The change in specular scattering coefficient with change in soil texture was observed for lower soil moisture contents ($m_v \leq 0.261$ cm^3 cm^{-3}) whereas for higher soil moisture contents ($m_v <$ 0.261 cm^3 cm^{-3}) it was difficult to observe change in specular scattering coefficient with change in soil texture.

- Retrieval of soil parameters form the observed scattering coefficient is another important task. In general, theoretical, empirical and semi–empirical equations provide the direct relationship, i.e., scattering coefficient as the function of soil parameters. The retrieval of soil parameters, i.e., soil texture, soil moisture and surface roughness is complex processes due to the dependency of several soil parameters on single scattering coefficient. Therefore, various sensor parameters (i.e., incidence angle, polarization and frequency) can be utilized to minimizes the effect of one or more soil parameters to retrieve the other soil parameter. In this regard, copolarization ratio study was explored and it was observed that the copolarization ratio minimize the soil texture effect and varies only with soil moisture content when the surface roughness was kept constant. This approach was utilized to retrieve the soil moisture content by minimizing the soil texture effect. The copolarization ratio posses the limitation of constant surface roughness. Therefore, multi–incidence angle approach have been studied and it was observed that the normalized specular scattering coefficient (i.e., specular scattering coefficient at one incidence divided by scattering coefficient at other incidence angles) changes with the change in surface roughness, whereas negligible changes were observed with the change in soil moisture and soil texture. This approach was firstly exploited to retrieve surface roughness (i.e., s and l) and subsequently these roughness values were used to retrieve soil texture and soil moisture.
- Till now the satellite data is available in monostatic domain and in future the availability of data will be in bistatic domain. So, by seeing the availability of satellite data, another task to retrieve the soil moisture over vegetated area with satellite data has been considered which is still a challenging task. Timely estimation of soil moisture at local and global scale is required in many

applications such as environmental modeling, weather forecasting, agriculture and many more. Most of the soil moisture retrieval algorithms, applicable on existing satellite data, have been developed for bare soil. Bare soil is a special case because for most of time in a year soil is covered with vegetation. Therefore, the accuracy of these approaches suffers severely when applied in vegetated area. In this regard, Fusion based approaches, utilizing the SAR and optical data, have been developed to retrieve the vegetation covered soil moisture. The potential of fusion approach is from the ability of SAR and optical data to characterize the vegetation. SAR data has capability to characterize the vegetation as well as underlying soil parameters, i.e., soil moisture and surface roughness. But, the scattering coefficient that is the measured parameter becomes the function of vegetation and soil parameters. Therefore, it becomes complex task to retrieve the vegetation covered soil moisture with SAR data only. Further, the optical remote sensing, especially the NDVI, explains the abundance of vegetation and therefore can be utilized to model vegetation parameter in soil moisture retrieval scheme with SAR data. The PALSAR, a SAR data and MODIS, an optical data have been efficiently utilized to retrieve vegetation covered soil moisture. The MODIS data has been used to compute the NDVI map of the respective area. Two fusion approaches have developed with PALSAR and NDVI data. The first approach normalizes the scattering coefficient of vegetated area with the scattering coefficient of bare soil retrieved through the Dubois et al. model and for the purpose in situ measurement of soil moisture and surface roughness were carried out. The second approach normalizes the scattering coefficient of the vegetated area with scattering coefficient of dry soil which has been computed with Dubois *et al.* model. Different empirical relationships have been developed for both the approaches that involve normalized scattering coefficient and NDVI. These empirical relationships have been used to retrieve the vegetation covered soil moisture. The obtained results were in good agreement with the observed data and the approach can be utilized with minimum *apriori* information with data available from satellite based sensors only.

7.2. Future Scope

Based on the research work carried out and its applicability in various domains, following are the points that may be carried out in future:

- The experimental work which was conducted to characterize the soil parameters in specular direction, that is specific case of bistatic domain, may be useful for future bistatic mission such as TandEM–X and cartwheel satellite system.
- The other major objective of the study was to check the response of soil texture on specular scattering and this study may be helpful in near future to generate soil texture map with the availability of data in specular direction.
- The applicability of multi–incidence angle approach for retrieval of soil parameters with specular scattering data has been tested and validated. This approach can be explored for future bistatic missions to retrieve soil parameters, i.e., soil texture, soil moisture and surface roughness.
- The problem of soil moisture retrieval in vegetated area has been dealt with fusion approach. The PALSAR and MODIS data have been efficiently utilized to retrieve vegetation covered soil moisture. This approach can be explored to develop soil moisture monitoring system with satellite data only.

Bibliography

[1] Altese, E., Bolognani, O., Mancini, M. and Troch, P.A., 1996, Retrieving soil moisture over bare soils from ERS–1 synthetic aperture radar data: Sensitivity analysis based on a theoretical surface scattering model and field data. *Water Resources Research*, **32**, 653–662.

[2] Alvarez–Mozos, J., Casali, J., Gonzalez-Audicana, M. and Verhoest, N.E.C., 2006, Assessment of the operational applicability of RADARSAT–1 data for surface soil moisture estimation. *IEEE Transactions on Geoscience and Remote Sensing*, **44**, pp. 913–924.

[3] Aly, Z., Bonn, F.J. and Magagi, R., 2007, Analysis of the backscattering coefficient of salt–affected soils using modeling and RADARSAT–1 SAR data. *IEEE Transactions on Geoscience and Remote Sensing*, **45**, pp. 332–341.

[4] Anderson, M.C., Neale, C.M.U., Li, F., Norman, J.M., Kustas, W.P., Jayanthi, H. and Chavez, J., 2004, Upscaling ground observations of vegetation water content, canopy height, and leaf area index during SMEX02 using aircraft and Landsat imagery. *Remote Sensing of Environment*, **92**, pp. 447–464.

[5] Anguela, T.P., Zribi, M., Baghdadi N. and Loumagne, C., 2010, Analysis of local variation of soil surface parameters with TerraSAR–X radar data over bare agriculture fields. *IEEE Transactions on Geoscience and Remote Sensing*, **48**, pp. 874–881.

[6] Apparao, K.V.S. and Rao, V.C.S., 1995, *Soil testing-laboratory manual and question bank*, pp. 18–28 (New Delhi: Laxmi Publication).

[7] Arvor, D., Jonathan, M., Meirelles, M.S.P., Dubreuil, V. and Lecerf, R., 2008, Comparison of multitemporal MODIS–EVI smoothing algorithms and its

contribution to crop monitoring. In *IEEE International Geoscience and Remote Sensing Symposium*, **2**, pp. II958–II961.

[8] Attema, E.P.W. and Ulaby, F.T., 1978, Vegetation modeled as a water cloud. *Radio Science*, **13**, pp. 357–364.

[9] Aubert, M., Baghdadi, N., Zribi, M., Douaoui, A., Loumagne, C., Baup, F., El Hajj, M. and Garrigues, S., 2001, Analysis of TerraSAR-X data sensitivity to bare soil moisture, roughness, composition and soil crust. *Remote Sensing of Environment*, **115**, 1801–1810.

[10] Baghdadi, N., Cerdan, O., Zribi, M., Auzet, V., Darboux, F., El Hajj, M. and Kheir, B.R., 2008, Operational performance of current synthetic aperture radar sensors in mapping soil surface characteristic in agricultural environments: application to hydrological and erosion modeling. *Hydrological Processes*, **22**, pp. 9–20.

[11] Baghdadi, N., Holah, N. and Zribi, M., 2006, Soil moisture estimation using multi–incidence and multi–polarization ASAR data. *International Journal of Remote Sensing*, **27**, pp. 1907–1920.

[12] Baghdadi, N., King, C., Chanzy, A. and Wigneron, J.P., 2002, An empirical calibration of the integral equation model based on SAR data, soil moisture and surface roughness measurement over bare soils. *International Journal of Remote Sensing*, **23**, pp. 4325–4340.

[13] Baghddadi, N. and Zribi, M., 2006, Evaluation of radar backscatter models IEM, Oh, and Dubious using experimental observation. *International Journal of Remote Sensing*, **27**, pp. 3831–3852.

[14] Baronti, S., Del Frate, F., Ferrazzoli, P., Paloscia, S., Pampaloni, P. and Schiavon, G., 1995, SAR polarimetric features of agricultural areas. *International Journal of Remote Sensing*, **16**, 2639–2656.

[15] Barrett, B.W., Dwyer, E. and Whelan, P. 2009, Soil moisture retrieval from active spaceborne microwave observations: an evaluation of current techniques. *Remote Sensing*, **1**, pp. 210–242.

[16] Beaudoin, A., Toan, T.L. and Gwyn, Q.H.J., 1990, SAR observations and modeling of the C–band backscatter variability due to multiscale geometry and soil moisture. *IEEE Transactions on Geoscience and Remote Sensing*, **28**, pp. 886–895.

[17] Bindlish, R. and Barros, A.P., 2001, Parameterization of vegetation backscatter in radar–based soil moisture estimation. *Remote Sensing of Environment*, **76**, pp. 130–137.

[18] Bindlish, R., Jackson, T., Sun, R., Cosh, M., Yueh, S. and Dinardo, S., 2009, Combined passive and active microwave observations of soil moisture during CLASIC. *IEEE Geoscience and Remote Sensing Letters*, **6**, pp. 644–648.

[19] Biswas, S. and Lohani B., 2008, Development of high resolution 3d sound propagation model using lidar data and air photo. *The International Archives of the Photogrammetry, Remote Sensing and Spatial Information Sciences*, **37**, pp. 1735–1740.

[20] Blumberg, D.G., Ronen, G., Ben–Asher, J., Freilikher, V., Vulfson, L.D. and Kotlyard, A.L., 2006, Utilizing a P–band scatterometer to assess soil water saturation percent of a bare sandy soil. *Journal of Hydrology*, **318**, pp. 374–378.

[21] Bolognani, O., Mancini, M. and Rosso, R., 1996, Soil moisture profiles from multi frequency radar data at basin scale. *Meccanica*, **31**, pp. 59–72.

[22] Bonn, F. and Dixon, R., 2005, Monitoring flood extent and forecasting excess runoff risk with RADARSAT–1 data. *Natural Hazards*, **35**, pp. 377–393.

[23] Brogioni, M., Macellono, G., Paloscia, S., Pampaloni, P., Pettinato, S. and Ticconi, F., 2007, Bistatic scattering from bare soils: sensitivity to soil moisture and surface roughness. In *IEEE International Geoscience and Remote Sensing Symposium*, pp. 77–80.

[24] Brown, R.B., 2003, Soil Texture. Available online at: http://edis.ifas.ufl.edu/ss169.

[25] Bryant, R., Moran, M.S., Thoma, D.P., Collins, C.D.H., Skirvin, S., Rahman, M., Slocum, K., Starks, P., Bosch, D. and González–Dugo, M. P., 2007, Measuring surface roughness height to parameterize radar backscatter models for retrieval of surface soil moisture. *IEEE Transactions on Geoscience and Remote Sensing*, **4**, pp. 137–141.

[26] Callens, M., Verhoest, N.E.C. and Davidson, M.W., 2006, Parameterization of tillage–induced single–scale soil roughness from 4–m profiles. *IEEE Transactions on Geoscience and Remote Sensing*, **44**, pp. 878–888.

[27] Canada Centre for Remote Sensing/Natural Resources Canada, 2008, Fundamentals of Remote Sensing. Ottawa, Ontario, Canada.

[28] Casanova, J.J., Judge, J. and Jang M., 2007, Modeling transmission of microwaves through dynamic vegetation. *IEEE Transactions on Geoscience and Remote Sensing*, **45**, pp. 3145–3149.

[29] Cassola, M.R., Baumgartner, S., Krieger G. and Moreira A., 2010, Bistatic TerraSAR-X/F-SAR spaceborne–airborne SAR experiment: description, data processing and results. *IEEE Transactions on Geoscience and Remote Sensing*, **48**, pp. 781–794.

[30] Ceraldi, E., Franceschetti, G., Iodice, A. and Riccio, D., 2005, Estimating the soil dielectric constant via scattering measurements along the specular direction. *IEEE Transactions on Geoscience and Remote Sensing*, **43**, pp. 295–305.

[31] Champion, I., 1996, Simple modeling of radar backscattering coefficient over a bare soil: variation with incidence angle, frequency and polarization. *International Journal of Remote Sensing*, **17**, pp. 783–800.

[32] Chang, D., Kothari, R. and Islam, S., 2003, Classification of soil texture using remotely sensed brightness temperature over the Southern Great Plains. *IEEE Transactions on Geoscience and Remote Sensing*, **41**, pp. 664–674.

[33] Chen, Y., Gu, Y., Gu, J. and Yang, J., 2005, Particle filter based road detection in SAR image. In *IEEE International Symposium on Microwave, Antenna, Propagation and EMC Technologies for Wireless Communications*, pp. 301–305.

[34] Chrysoulakis, N., Herlin, I., Prastacos, P., Yahia, H., Grazzini, J. and Cartalis, C., 2007, An improved algorithm for the detection of plumes caused by natural or technological hazards using AVHRR imagery. *Remote Sensing of Environment*, **108**, pp. 393–406.

[35] Collaro, A., Franceschetti, G., Migliaccio, M. and Riccio, D., 1999, Gaussian rough surfaces and Kirchhoff approximation. *IEEE Transactions on Geoscience and Remote Sensing*, **2**, pp. 392–398.

[36] Comblet, F., Khenchaf, A., Baussard, A. and Pellen, F., 2006, Bistatic synthetic aperture radar imaging: theory, simulations, and validations. *IEEE Transactions on Geoscience and Remote Sensing*, **54**, 3529–3540.

[37] Crow, W.T., Wagner, W. and V. Naeimi, 2010, The impact of radar incidence angle on soil–moisture–retrieval skill. *IEEE Transactions on Geoscience and Remote Sensing Letters*, **7**, pp. 501–505.

[38] Curie, N.C. and Well, G.W., 1989, Radar cross section measurement concepts. In: *Radar reflectivity measurement: Technique and Applications*, Curie, N.C. (Ed.), pp. 61–91 (Norwood, MA: Artech House).

[39] Curtis, J.O., 2001, Moisture effects on the dielectric properties of soils. *IEEE Transactions on Geoscience and Remote Sensing*, **39**, pp. 125–128.

[40] Dabrowska-Zielinska, K., Inoue, Y., Kowalik, W. and Gruszczynska, M., 2007, Inferring the effect of plant and soil variables on C– and L–band SAR backscatter over agricultural fields, based on model analysis. *Advances in Space Research*, **39**, pp. 139–148.

[41] Davidson, M.W.J., Le Toan, T., Mattia, F., Satalino, G., Manninen, T. and Borgeaud, M., 2000, On the characterization of agricultural soil roughness for radar remote sensing studies. *IEEE Transactions on Geoscience and Remote Sensing*, **38**, pp. 630–640.

[42] Davidson, M.W.J., Mattia, F., Satalino, G., Verhoest, N.E.C., Le Toan, T., Borgeaud, M., Louis, J.M.B. and Attema, E., 2003, Joint statistical properties of RMS height and correlation length derived from multisite 1–m roughness measurements. *IEEE Transactions on Geoscience and Remote Sensing*, **41**, pp.1651–1658.

[43] De Roo, R.D. and Ulaby, F.T., 1994, Bistatic specular scattering from rough dielectric surfaces. *IEEE Transactions on Antennas and Propagation*, **42**, pp. 220–231.

[44] Dekker, P.L., Mallorqui, J.J., Morales, P.S. and Marcos, J.S., 2008, Phase synchronization and doppler centroid estimation in fixed receiver bistatic SAR systems. *IEEE Transactions on Geoscience and Remote Sensing*, **46**, pp. 3459-3471.

[45] Dong, Y., Milne, A.K. and Forster, B.C., 2001, Segmentation and classification of vegetated areas using polarimetric SAR image data. *IEEE Transactions on Geoscience and Remote Sensing*, **39**, pp. 321–329.

[46] Du, Y., Qi, Y., Chen, H. and Kong, J. A., 2006, Bistatic scattering model for rough surfaces. In *IEEE International Geoscience and Remote Sensing Symposium*, pp. 2949–2952.

[47] Du, Y., Ulaby, F.T. and Dobson, M.C., 2000, Sensitivity to soil moisture by active and passive microwave sensors. *IEEE Transactions on Geoscience and Remote Sensing*, **38**, pp. 105–114.

[48] Dubois, P.C., Zyl, J.V. and Engam, T., 1995, Measuring soil moisture with imaging radars. *IEEE Transactions on Geoscience and Remote Sensing*, **33**, pp. 915–926.

[49] Duque, S., Dekker, P.L. and Mallorqui, J.J., 2010, Single–pass bistatic SAR interferometry using fixed–receiver configurations: theory and experimental validation. *IEEE Transactions on Geoscience and Remote Sensing*, **48**, pp. 2740-2749.

[50] Eangman, E.T. and Chauhan, N., 1995, Status of microwave soil moisture measurements with remote sensing. *Remote Sensing of Environment*, **51**, pp. 189–198.

[51] Elfouhaily, T.M. and Guerin, C.A., 2004, A critical survey of approximate scattering wave theories from random rough surfaces. *Waves Random Media* **14**, pp. R1–R40.

[52] Fang C., Wen H., Yirong W. and Pottier, E., 2007, An unsupervised segmentation with an adaptive number of clusters using the SPAN/H/α/A space and the complex Wishart clustering for fully polarimetric SAR data analysis. *IEEE Transactions on Geoscience and Remote Sensing*, **45**, pp. 3454–3467.

[53] Fernandez, P.D., Cantalloube, H., Vaizan, B., Krieger, G. and Moreira, A., 2008, Airborne bistatic synthetic aperture radar. In Bistatic Radar: Emerging technology, M. Cherniakov (Ed.), pp. 159–210 (West Sussex: John Wiley & Sons Ltd.).

[54] Ferrazzoli, P., Paloscia, S., Pampaloni, P., Schiavon, G., Sigismondi, S. and Solimini, D., 1997, The potential of multifrequency polarimetric SAR in assessing agricultural and arboreous biomass. *IEEE Transactions on Geoscience and Remote Sensing*, **35**, pp. 5–17.

[55] Fooladmand, H.R. and Sepaskhah, A.R., 2006, Improved estimation of the soil particle–size distribution from textural data, *Biosystem Engineering*, **94**, pp. 133–138.

[56] Franceschetti, G., Iodice, A., Maddaluno, S. and Riccio, D., 2000, A fractal–based theoretical framework for retrieval of surface parameters from electromagnetic backscattering data. *IEEE Transactions on Geoscience and Remote Sensing*, **38**, pp. 641–650.

[57] Fung, A.K. and Chen, K.S., 2004, An update of the IEM surface backscattering model. *IEEE Transactions on Geoscience and Remote Sensing Letters*, **1**, pp. 75–77.

[58] Fung, A.K., Dawson, M.S., Chen, K.S., Hsu, A.Y., Engman, E.T., O'Neill, P.O. and Wang, J., 1996, A modified IEM model for scattering from soil surfaces with application to soil moisture sensing. In *IEEE International Geoscience and Remote Sensing Symposium*, pp. 1297–1299.

[59] Fung, A.K., Lee, Z. and Chen, K.S., 1992, Backscattering from randomly rough dielectric surface. *IEEE Transactions on Geoscience and Remote Sensing*, **30**, pp. 356–369.

[60] Fung, K.F., Zuffada, C and Hsieh, 2001, Incoherent bistatic scattering from the sea surface at L–band. *IEEE Transactions on Geoscience and Remote Sensing*, **39**, pp. 1006–1012.

[61] Gairola, R.M., Pokhrel, S., Varma, A.K. and Agarwal, V.K., 2006, Multiparameter microwave retrieval algorithms: performance of neural networks. *Current Science*, **91**, pp. 1382–1387.

[62] Ghosh, S. and Chakrabarty A., 2008, Estimation of capacitance of different conducting bodies by the method of rectangular subareas. *Journal of Electrostatics*, **66**, pp. 142 –146.

[63] Ghosh, S. and Lohani, B., 2007, Near-realistic and 3D visualisation of LiDAR data. In *ISPRS Joint Workshop on Visualisation and exploration of Geospatial data*, pp. 1–6.

[64] Ghosh, S., Chakrabarty, A. and Sanyal, S., 2005, Loaded wire antenna as EMI sensor. *Progress In Electromagnetics Research*, **54**, pp. 19–36.

[65] Gohil, B.S., Mathur, A.K. and Pandey, P.C., 1994, An algorithm for sea surface temperature estimation from ERS–1 ATSR using moisture dependent coefficients: a simulation study. *International Journal of Remote Sensing*, **15**, pp. 1161–1167.

[66] Grazzini, J., Turiel, A. and Yahia, H., 2005, Presegmentation of high–resolution satellite images with a multifractal reconstruction scheme based on an entropy criterium. In *IEEE International Conference on Image Processing*, pp. I649–I 652.

[67] Grazzini, J., Yahia, H., Herlin, I. and Turiel, A., 2003, Analysis and comparison of functional dependencies of multiscale textural features on

monospectral infrared images. In *IEEE International Geoscience and Remote Sensing Symposium*, **3**, pp. 2045–2047.

[68] Grippa, M. and Woodhouse, I.H., 2002, Validation of surface scattering models across large footprints for global scatterometer applications. *IEEE Transactions on Geoscience and Remote Sensing*, **40**, pp. 2229–2233.

[69] Gu, J., Yang, J., Zhang, H., Peng, Y., Wang, C. and Zhang, H., 2004, Speckle filtering in polarimetric SAR data based on the subspace decomposition. *IEEE Transactions on Geoscience and Remote Sensing*, **42**, pp. 1635–1641.

[70] Guha, D and Siddiqui, J Y, 2004, Effect of a cavity enclosure on the resonant frequency of inverted microstrip circular patch antenna. *IEEE Transactions on Antennas and Propagation*, **52**, pp. 2177–2180.

[71] Guha, D and Siddiqui, J Y., 2003, Resonant frequency of circular microstrip antenna covered with dielectric superstrate. *IEEE Transactions on Antennas and Propagation*, **51**, pp. 1649–1652.

[72] Guha, D and Siddiqui, J Y., 2004, Resonant frequency of equilateral triangular microstrip. *IEEE Transactions on Antennas and Propagation*, **52**, pp. 2174–2177.

[73] Guha, D and Siddiqui, J.Y., 2002, New CAD model to calculate the resonant frequency of inverted microstrip circular patch antennas. *Microwave and Optical Technology Letters*, **35**, pp. 434–437.

[74] Guha, D., 2001, Resonant frequency of circular microstrip antennas with and without air gaps. *IEEE Transactions on Antennas and Propagation*, **49**, pp. 55–59.

[75] Hajnsek, I., 2001, Inversion of surface parameters using polarimetric SAR. In Department of Geoinformatik, Institute of Geography Jena, Germany: Friedrich-Schiller University.

[76] Hajnsek, I., Jagdhuber, T., Schon, H. and Papathanassiou, K.P., 2009, Potential of estimation soil moisture under vegetation cover by means of PolSAR. *IEEE Transactions on Geoscience and Remote Sensing*, **47**, pp. 442–454.

[77] Hajnsek, I., Pottier, E. and Cloude, S.R., 2003, Inversion of surface parameters from polarimetric SAR. *IEEE Transactions on Geoscience and Remote Sensing*, **41**, pp. 727–744.

[78] Hallikainen, M.T., Ulaby, F.T., Dobson, M.C., El–Rayes, M.A. and Wu, L., 1985, Microwave dielectric behavior of wet soil–Part I: empirical models and experimental observations. *IEEE Transactions on Geoscience and Remote Sensing*, **23**, pp. 25–34.

[79] Hoffmann, J., 2005, The future of satellite remote sensing in hydrogeology. *Hydrogeology Journal*, **13**, pp. 247–250.

[80] Holah, N., Baghdadi, N., Zribi, M., Bruand, A. and King, C., 2005, Potential of ASAR/ENVISAT for the characterization of soil surface parameters over bare agricultural fields. *Remote Sensing of Environment*, **96**, pp. 78–86.

[81] Houborg, R., Soegaard, H. and Boegh, E., 2007, Combining vegetation index and model inversion method for the extraction of key vegetation biophysical parameters using Terra and Aqua MODIS reflectance data. *Remote Sensing of Environment*, **106**, pp. 39–58.

[82] Hsieh, C., Fung, A.K., Nesti, G., Sieber, A.J. and Coppo, P., 1997, A further study of the IEM surface scattering model. *IEEE Transactions on Geoscience and Remote Sensing*, **35**, 901–909.

[83] Jackson, T.J., 2002, Remote sensing of soil moisture: implications for groundwater recharge. *Hydrogeology Journal*, **10**, pp. 40–51.

[84] Jackson, T.J., Schmugge, J. and Engman, E.T., 1996, Remote sensing applications to hydrology: soil moisture. *Hydrological Sciences Journal*, **41**, pp. 517–520.

[85] Jonathan, M., Meirelles, M.S.P., Berroir, J.P., Herlin, I., 2006, Regional scale land use/ land cover classification using temporal series of MODIS data. In *ISPRS Mid-Term Symposium, Remote Sensing: from Pixel to Process*, pp. 1–3.

[86] Jordan, E.C. and Balmain, K.G., 2003, *Electromagnetic waves and radiating systems*. (New Delhi: Prentice Hall of India Private Limited).

[87] Joseph, A.T., Van der Velde, R., O'Neill, P.E., Lang, R. and Gish, T., 2010, Effects of corn on C– and L–band radar backscatter: A correction method for soil moisture retrieval. *Remote Sensing of Environment*, **114**, 2417–2430.

[88] Joseph, A.T., Velde, R., O'Neill, P.E., Lang, R. H. and Gish, T., 2008, Soil moisture retrieval during a corn growth cycle using L–band (1.6 GHz) radar observation. *IEEE Transactions on Geoscience and Remote Sensing*, **46**, pp. 2365–2374.

[89] Judge, J., Galantowicz, J.F. and Anthony, W., 2001, A comparison of ground-

based and satellite–borne microwave radiometric observations in the Great Plains. *IEEE Transactions on Geoscience and Remote Sensing*, **39**, pp. 1686–1696.

[90] Khadhra, K.B., Borner, T., Chandra, M., Zink, M. and Hounam, D., 2007, Soil parameter estimation and analysis of bistatic scattering X–band controlled measurement. In *IEEE International Geoscience and Remote Sensing Symposium*, pp. 3706–3709.

[91] Khairnar, D.G., Merchant, S.N. and Desai, U.B., 2007, Radial basis function neural network for pulse radar detection. In *IEE Proceedings of Radar, Sonar and Navigation*, **1**, pp. 8–17.

[92] Khairnar, D.G., Merchant, S.N. and Desai, U.B., 2008, Radar signal detection in non–Gaussian noise using RBF neural network. *International Journal on Computers*, **3**, pp 32–39.

[93] Khenchaf, A., 2001, Bistatic scattering and depolarization by randomly rough surfaces: application to the natural rough surfaces in X–band. *Waves Random Media*, **11**, pp. 61–89.

[94] Krieger, G and Moreira, A., 2004, Spaceborne Bi– and Multistatic SAR: potential and challenges. *IEE Proceedings–Radar, Sonar and Navigation*, **153**, pp. 184–198.

[95] Krieger, G. and Moreira, A., 2005, Multistatic SAR satellite formations: potentials and challenges. In *IEEE International Geoscience and Remote Sensing Symposium*, **4**, pp. 2680– 2684.

[96] Krieger, G., Fiedler, H., Hounam, D. and Moreira, A., 2003, Analysis of system concepts for bi– and multi–static SAR missions. In *IEEE International Geoscience and Remote Sensing Symposium*, pp. 770–772.

[97] Krieger, G., Moreira, A., Fiedler, H., Hajnsek, I., Werner, M., Younis, M. and Zink, M., 2007, TanDEM–X: A satellite formation for high-resolution SAR interferometry. *IEEE Transactions on Geoscience and Remote Sensing*, **45**, pp. 3317–3341.

[98] Kseneman, M., Gleich, D. and Cucej, Z., 2011, Soil Moisture estimation using high–resolution spotlight TerraSAR–X data, *IEEE Geoscience and Remote Sensing Letters*, **8**, pp. 686–690.

[99] Kumar, R., Sarkar, A. and Pandey, P.C., 1999, Estimation of ocean depths off Goa coast using ERS–1 Synthetic Aperture Radar. *Continental Shelf*

Research, **19**, pp. 171–181.

[100] Kuria, D., Hui, L., Koike, T., Tsutsui, H. and Graf, T., 2006, Multi–frequency response to periodic roughness. In *IEEE International Geoscience and Remote Sensing Symposium*, pp. 1744–1747.

[101] Leconte, R., Brissette, F., Galarneau, M. and Rousselle, J., 2004, Mapping near–surface soil moisture with RADARSAT–1 synthetic aperture radar data. *Water Resources Research*, **40**, pp. 1–13.

[102] Lee, J.S., Grunes, M.R., Ainsworth, T.L., Pottier, E., Krogager, E. and Boerner, W.M., 2000, Quantitative comparison of classification capability: fully-polarimetric versus partially polarimetric SAR. In *IEEE International Geoscience and Remote Sensing Symposium*, **3**, pp. 1101–1103.

[103] Lee, J.S., Grunes, M.R., Schuler, D.L., Pottier, E. and Ferro–Famil, L., 2006, Scattering–model–based speckle filtering of polarimetric SAR data. *IEEE Transactions on Geoscience and Remote Sensing*, **44**, pp. 176–187.

[104] Li, Z. and Jin, Y.Q., 2000, Bistatic scattering from fractal rough surface in numerical finite element method. In *International Symposium on Antennas, Propagation and EM Theory*, pp. 382–385.

[105] Lievens, H. and Verhoest, N.E.C., 2011, On the retrieval of soil moisture in wheat fields from L–band SAR based on water cloud modeling, the IEM, and effective roughness parameters. *IEEE Geoscience and Remote Sensing Letters*, **8**, pp. 740–744.

[106] Lillesand, T., Kiefer, R.W. and Chipman, J., 2007, *Remote Sensing and Image Interpretation* (Wiley India Pvt. Ltd).

[107] Lin, H., Chen, J., Pei, Z., Zhang, S. and Hu, X., 2009, Monitoring sugarcane growth using ENVISAT ASAR data. *IEEE Transactions on Geoscience and Remote Sensing*, **47**, pp. 2365–2374.

[108] Loew, A. and Mauser, W., 2006, A semiempirical surface backscattering model for bare soil surfaces based on a generalized power law spectrum approach. *IEEE Transactions on Geoscience and Remote Sensing*, **44**, pp. 1022–1035.

[109] Lohani, B. and Singh, R., 2007, Effect of data density, scan angle, and flying height on the accuracy of building extraction using LiDAR data. *Geocarto International*, **23**, pp. 81-94.

[110] Lohani, B., Mason, D.C., Scott, T.R. and Sreenivas, B., 2006, Extraction of

tidal channel networks from aerial photographs alone and combined with laser altimetry. *International Journal of Remote Sensing*, **27**, pp.5–25.

[111] Lucas, N.S., Sanjeevi, S. and Barnsley, M., 2002, Sub–pixel habitat mapping of a coastal dune ecosystem. *Applied Geography*, **22**, pp. 253–270.

[112] Luis, A.J. and Pandey, P.C., 2005, Characteristics of atmospheric divergence and convergence in the Indian Ocean inferred from scatterometer winds. *Remote Sensing of Environment*, **97**, pp. 231–237.

[113] Macelloni, G., Nesti, G., Pampaloni, P., Sigismondi, S., Tarchi, D. and Lolli, S., 2000, Experimental validation of surface scattering and emission models. *IEEE Transactions on Geoscience and Remote Sensing*, **38**, 459–469.

[114] Macelloni, G., Paloscia, S., Pampaloni, P. and Santi, E., 2003, Global scale monitoring of soil and vegetation using SSM/I and ERS wind scatterometer. *International Journal of Remote Sensing*, **24**, pp. 2409–2425.

[115] Magagi, R.D. and Kerr, Y.H., 2001, Estimating surface soil moisture and soil roughness over semiarid areas from the use of the copolarization ratio. *Remote Sensing of Environment*, **75**, pp. 432–445.

[116] Mancini, M., Hoeben, R. and Troch, P.A., 1999, Multifrequency radar observations of bare surface soil moisture content: A laboratory experiment. *Water Resources Research*, **35**, 1827–1838.

[117] Marcos, J.S., Dekker, P.L., Mallorqui, J.J., Aguasca, A. and Prats, P., 2007, SABRINA: A SAR bistatic receiver for interferometric applications. *IEEE Transactions on Geoscience and Remote Sensing*, **4**, pp. 307-311.

[118] Margarit, G., Mallorqui, J.J. and Pipia, L., 2010, Polarimetric characterization and temporal stability analysis of urban target scattering. *IEEE Transactions on Geoscience and Remote Sensing*, **48**, pp. 2038-2048.

[119] Maselli, F., Gardin, L. and Botta, L., 2008, Automatic mapping of soil texture through the integration of ground, satellite and ancillary data. *International Journal of Remote Sensing*, **29**, pp. 5555–5569.

[120] Massonnet, D., 2001, The interferometric cartwheel: a constellation of passive satellites to produce radar images to be coherently combined. *International Journal of Remote Sensing*, **22**, pp. 2413–2430.

[121] Matkin, B.L., Mullins, J.H. and Ferster, T.J., 2002, Bistatic reflectivity measurement on various terrains at X, Ku, Ka, and W–band frequencies. In *IEEE Radar Conference*, pp. 266–271.

[122] Mattia, F., Toan, T.L., Souyris, J.C., Carolis, G.D., Floury, N., Posa, F. and Pasquariello, G., 1997, The effect of surface roughness on multifrequency polarimetric SAR data. *IEEE Transactions on Geoscience and Remote Sensing*, **35**, pp. 954–966.

[123] Mattikalli, N.M., Engman, E.T., Ahuja, L.R. and Jackson, T.J., 1998, Microwave remote sensing of soil moisture for estimation of profile soil property. *International Journal of Remote Sensing*, **19**, pp. 1751–2439.

[124] Matzler, C., 1998, Microwave permittivity of dry sand. *IEEE Transactions on Geoscience and Remote Sensing*, **36**, pp. 317–319.

[125] McNairn, H., Champagne, C., Shang, J., Holmstrom, D. and Reichert, G., 2009, Integration of optical and synthetic aperture radar (SAR) imagery for delivering operational annual crop inventories. *ISPRS Journal of Photogrammetry and Remote Sensing*, **64**, pp. 434–449.

[126] Michelson, D.B., Liljeberg, B.M. and Pilesjo, P., 2000, Comparison of algorithms for classifying Swedish landcover using Landsat TM and ERS–1 SAR data. *Remote Sensing of Environment*, **71**, pp. 1–15.

[127] Mironov, V.L., Dobson, M.C., Kaupp, V.H., Komarov, S.A. and Kleshchenko, V.N., 2004, Generalized refractive mixing dielectric model for moist soils. *IEEE Transactions on Geoscience and Remote Sensing*, **42**, pp. 773–785.

[128] Mishra, P., 2010. Study of Polarimetric analysis of PALSAR images for terrain classification, M.Tech. Dissertation, Indian Institute of Technology Roorkee, Roorkee, India.

[129] Mittal, G. and Singh, D., 2010, Critical analysis of microwave scattering response on roughness parameter and moisture content for periodic rough surfaces and its retrieval. *Progress In Electromagnetics Research*, **100**, pp. 129–152.

[130] Moccia, A., Vetrella, S. and Bertoni, R., 2000, Mission analysis and design of a bistatic synthetic aperture radar on board a small satellite. *Acta Astronautica*, **47**, pp. 819–829.

[131] Moran, S.M., Hymer, D.C., Qi, J. and Kerr, Y., 2002, Comparison of ERS-2 SAR and Landsat TM imagery for monitoring agricultural crop and soil conditions. *Remote Sensing of Environment*, **79**, pp. 243–252.

[132] Moran, S.M., Peters–Lidard, C.D., Watts, J.M. and McElroy, S., 2004, Estimating soil moisture at the watershed scale with satellite–based radar and land surface models. *Canadian Journal of Remote Sensing*, **30**, pp. 805–826.

[133] Mota, G., Muller, S., Feitosa, R., Meirelles, M.S.P. and Vieira, H., 2003, An evaluation of knowledge-based interpretation applied to low–resolution satellite images. In *IEEE International Geoscience and Remote Sensing Symposium*, **6**, pp. 3896–3898.

[134] Mota, G.L.A, Feitosa, R.Q., Coutinho, H.L.C., Liedtke, C.E., Muller, S., Pakzad, K. and Meirelles, M.S.P., 2007, Multitemporal fuzzy classification model based on class transition possibilities. *ISPRS Journal of Photogrammetry and Remote Sensing*, **62**, pp. 182–200.

[135] Mozos, J.A., Casali, J., Audicana, M.G. and Verhoest, N.E.C., 2006, Assessment of the operational applicability of RADARSAT–1 data for surface soil moisture estimation. *IEEE Transactions on Geoscience and Remote Sensing*, **44**, pp. 913–924.

[136] Mukhopadhyay, M., Kundu, A. and Chakrabarty, A., 2007, Augmentation of noise free speech recognizer using adaptive microphone array. *IETE Technical Review*, **24**, pp 385–393.

[137] Narayan, U., Lakshmi, V. and Jackson, T.J., 2006, High resolution change estimation of soil moisture using L–band radiometer and radar observations made during the SMEX02 experiments. *IEEE Transactions on Geoscience and Remote Sensing*, **44**, pp. 1545–1554.

[138] Narayanan, R.M., Pardipuram, R. and Rundquist, D.C., 1994, Statistical characteristics of simulated radar imagery from bare soil surfaces: effects of surface roughness and soil moisture variability. *IEEE Transactions on Geoscience and Remote Sensing*, **32**, pp. 159–168.

[139] Nashashibi, A.Y. and Ulaby, F.T., 2003, Millimeter–wave polarimetric bistatic radar scattering from rough soil surfaces. In *IEEE International Geoscience and Remote Sensing Symposium*, pp. 788–790.

[140] Nashashibi, A.Y. and Ulaby, F.T., 2007, MMW polarimetric radar bistatic scattering from a random surface. *IEEE Transactions on Geoscience and Remote Sensing*, **45**, pp. 1743–1755.

[141] Notarnicola, C., Angiulli, M. and Posa, F., 2006, Use of radar and optical remotely sensed data for soil moisture retrieval over vegetated areas. *IEEE Transactions on Geoscience and Remote Sensing*, **44**, pp. 925–935.

[142] Oh, Y., 2004, Quantitative retrieval of soil moisture content and roughness from multipolarized radar observation of bare soil surface. *IEEE Transactions on Geoscience and Remote Sensing*, **42**, pp. 596–601.

[143] Oh, Y., 2007, Effect of surface profile length on the backscattering coefficients of bare surfaces. *IEEE Transactions on Geoscience and Remote Sensing*, **45**, pp. 632–638.

[144] Oh, Y., Sarabandi, K. and Ulaby, F.T., 1992, An empirical modal and an inversion technique for radar scattering from bare soil surfaces. *IEEE Transactions on Geoscience and Remote Sensing*, **30**, pp. 370–381.

[145] Oldak, A., Jackson, T.J., Starks, P. and Elliot, R., 2003, Mapping near–surface soil moisture on regional scale using ERS–2 SAR data. *International Journal of Remote Sensing*, **24**, pp. 4579–4598.

[146] Paloscia, S., Pampaloni, P., Pettinato, S. and Santi, E., 2008, A comparison of algorithms for retrieving soil moisture from ENVISAT/ASAR images. *IEEE Transactions on Geoscience and Remote Sensing*, **46**, pp. 3274–3284.

[147] Pandey, P.C. and Hariharan, T.A., 1984, Advances in microwave remote sensing of the ocean and atmosphere, *Proceedings of the Indian National Science Academy (Earth and Planetary Science)*, **93**, pp. 257–282.

[148] Pandey, P.C. and Kakar, R., 1982, An empirical microwave emissivity model for a foam–covered sea. *IEEE Journal of Oceanic Engineering*, **OE-7**, pp.135–140.

[149] Pandey, P.C., Gairola, R.M. and Gohil, B.S., 1986, Wind–wave relationship from SEASAT radar altimeter data. *Boundary–Layer Meteorology*, **37**, pp.263–269.

[150] Pant, T., Singh, D. and Srivastava, T., 2010, The potential application of fractal approach for surface roughness retrieval: A study for simulated surfaces. *Geomatics, Natural Hazards and Risk*, **1**, pp. 243–257.

[151] Paramesha and Chakrabarty, A., 2008, Waveguide as a near–field measuring probe of the two–element array radiator. *Progress in Electromagnetics Research*, **7**, pp. 245–255.

[152] Park, S., Moon, W.M. and Kim, D., 2009, Estimation of surface roughness parameter in intertidal mudflat using airborne polarimetric SAR data. *IEEE Transactions on Geoscience and Remote Sensing*, **47**, pp. 1022–1031.

[153] Pathe, C., Wagner, W., Sabel, D., Doubkova, M. and Basara, J.B., 2009, Using ENVISAT ASAR global mode data for surface soil moisture retrieval over Oklahoma, USA. *IEEE Transactions on Geoscience and Remote Sensing*, **47**, pp. 468–480.

[154] Pierdicca, N., Pulvirenti, L., Bignami, C., 2010, Soil moisture estimation over vegetated terrains using multitemporal remote sensing data. *Remote Sensing of Environment*, **114**, pp. 440–448.

[155] Pierdicca, N., Pulvirenti, L., Ticconi, F. and Brogioni, M., 2008, Radar bistatic configuration for soil moisture retrieval: A simulation study. *IEEE Transactions on Geoscience and Remote Sensing*, **46**, pp. 3252–3264.

[156] Prakash, R., Singh, D. and Pathak, N.P., 2009, Microwave specular scattering response of soil texture at X–band. *Advances in Space Research*, **44**, pp. 801–814.

[157] Prakash, R., Singh, D. and Pathak, N.P., 2010, The effect of soil texture on soil moisture retrieval for specular scattering at C–band. *Progress in Electromagnetic Research*, **108**, pp. 177–204.

[158] Rahman M.M., Moran M.S., Thoma D.P., Bryant R., Sano E.E., Collins C.D.H., Skirvin S., Kershner C., and Orr B.J., 2007, A derivation of roughness correlation length for parameterizing radar backscatter models. *International Journal of Remote Sensing*, **18**, pp. 3995–4012.

[159] Rahman, M.M., Moran, M.S., Thoma, D.P., Bryant, R., Collins, C.D.H., Jackson,T., Orr, B.J. and Tischler, M., 2008, Mapping surface roughness and soil moisture and moisture using multi–angle radar imagery without ancillary data. *Remote Sensing of Environment*, **112**, pp. 391–402.

[160] Rahman, M.M., Moran, M.S., Thoma, D.P., Bryant, R., Sano, E.E., Collins, C.D.H., Skirvin, S., Kershner, C. and Orr, B.J., 2007, A derivation of roughness correlation length for parameterizing radar backscatter models. *International Journal of Remote Sensing*, **28**, pp. 3995–4012.

[161] Rakotoarivony, L., Taconet, O., Vidal–Madjar, D., Bellemain, P. and Benallegue, M., 1996, Radar backscattering over agricultural bare soils. *Journal of Electromagnetic Waves and Applications*, **10**, pp. 187–209.

[162] Rao, P.V.N., Raju, C.S. and Rao, K.S., 1990, Microwave remote sensing of soil moisture elimination of texture effect. *IEEE Transactions on Geoscience and Remote Sensing*, **28**, pp. 148–151.

[163] Reddy, M.A., 2008, *Remote Sensing and Geographical Information Systems*. (India: BS Publications).

[164] Ruello, G., Sanchez, P.B., Iodice, A., Mallorqui, J.J., Riccio, D., Broquetas, A. and Franceschetti, G., 2006, Synthesis, construction, and validation of a fractal surface. *IEEE Transactions on Geoscience and Remote Sensing*, **44**, pp. 1403–1412.

[165] Sabburg, J., Ball, J.A.R. and Hancock, N.H., 1997, Dielectric behavior of moist swelling soils at microwave frequencies. *IEEE Transactions on Geoscience and Remote Sensing*, **35**, pp. 784–787.

[166] Saha, K., Shah, P., Merchant, S.N. and Desai, U.B., 2009, A novel multi–focus image fusion algorithm using edge information and K–mean segmentation. In *IEEE International Conference on Information, Communications and Signal Processing*, pp. 1–5.

[167] Sahebi, M.R., Bonn, F. and Gwyn, Q.H.J., 2003, Estimation of the moisture content of bare soil from RADARSAT–1 SAR using simple empirical models. *International Journal of Remote Sensing*, **24**, pp. 2575–2582.

[168] Saillard, M. and Sentenac, A., 2001, Rigorous solutions for electromagnetic scattering from rough surfaces. *Waves Random Media*, **11**, pp. R103–R137.

[169] Saleh, K., Kerr, Y.H., Richaume, P., Escorihuela, M.J., Panciera, R., Delwart, S., Boulet, G., Maisongrande, P., Walker, J.P., Wursteisen, P. and Wigneron, J.P., 2009, Soil moisture retrievals at L–band using a two–step inversion approach (COSMOS/NAFE'05 Experiment). *Remote Sensing of Environment*, **113**, pp.1304–1312.

[170] Sang–Eun, P., Ferro–Famil, L., Allain, S. and Pottier, E., 2008, Analysis of polarimetric surface scattering in high resolution SAR. In *IEEE International Geoscience and Remote Sensing Symposium*, **3**, pp. III394–III397.

[171] Sanjeevi, S., 1996, Morphology of dunes of the Coromandel coast of Tamil Nadu, A satellite data based approach for coastal landuse planning. *Landscape and Urban Planning*, **34**, pp. 189–195.

[172] Sanjeevi, S., Vani, K. and Lakshmi, K., 2001, Comparison of conventional and wavelet transform techniques for fusion of IRS-1C, LISS-III and PAN

images. In, *22nd Asian Conference on Remote Sensing*, pp. 1–6.

[173] Santi, E., Paloscia, S., Pampaloni, P. and Pettinato, S., 2009, Ground–based microwave investigations of forest plots in Italy. *IEEE Transactions on Geoscience and Remote Sensing*, **47**, pp. 3016–3025.

[174] Satalino, G., Mattia, F., Davidson, M.W.J., Toan, T.L., Pasquariello, G. and Borgeaud, M., 2002, On current limits of soil moisture retrieval from ERS–SAR data. *IEEE Transactions on Geoscience and Remote Sensing*, **40**, pp. 2438–2447.

[175] Schneider, R.Z., Papathanassiou, K., Hajnsek, I. and Moreira, A., 2006, Polarimetric and interferometric characterization of coherent scatterers in urban areas. *IEEE Transactions on Geoscience and Remote Sensing*, **44**, pp. 971–984.

[176] Shanmugam, P., Ahn, Y., H. and Sanjeevi, S., 2006, A comparison of the classification of wetland characteristics by linear spectral mixture modelling and traditional hard classifiers on multispectral remotely sensed imagery in southern India. *Ecological Modelling*, **194**, pp. 379–394.

[177] Shi, J., Wang, J., Hsu, A.Y., O'Neill, P.E. and Engman, E.T., 1997, Estimation of bare surface soil moisture and surface roughness parameter using L–Band SAR image data. *IEEE Transactions on Geoscience and Remote Sensing*, **35**, pp. 1254–1266.

[178] Sikdar, M. and Cumming, I., 2004, A modified empirical model for soil moisture estimation in vegetated areas using SAR data. In *IEEE International Geoscience and Remote Sensing Symposium*, **2**, pp. 803–806.

[179] Silver, W.L., Neff, J., McGroddy, M., Veldkamp, E., Keller, M. and Cosme, R., 2000, Effects of soil texture on belowground carbon and nutrient storage in a lowland Amazonian forest ecosystem. *Ecosystems*, **3**, pp. 193–209.

[180] Singh, D. and Dubey, V., 2007, Microwave bistatic polarization measurements for retrieval of soil moisture using an incidence angle approach. *Journal of Geophysical Engineering*, **4**, pp. 75–82.

[181] Singh, D. and Kathpalia, A., 2007, An efficient modeling with GA approach to retrieve soil texture, moisture and roughness from ERS–2 SAR data. *Progress in Electromagnetic Research*, **77**, pp. 121–136.

[182] Singh, D., 2005, A Simplistic incidence angle approach to retrieve the soil moisture and surface roughness at X–Band. *IEEE Transactions on Geoscience and Remote Sensing*, **43**, pp. 2606–2611.

[183] Singh, D., Singh, K.P., Herlin, I. and Sharma, S.K., 2003, Ground–based scatterometer measurements of periodic surface roughness and correlation length for remote sensing. Advances in Space Research, **11**, pp. 2281–2286.

[184] Singh, T.N. and Singh, V., 2005, An intelligent approach to prediction and control ground vibration in mines. *Geotechnical and Geological Engineering*, **23**, pp. 249–262.

[185] Singh, T.N. and Verma, A.K., 2010, Sensitivity of total charge and maximum charge per delay on ground vibration. *Geomatics, Natural Hazards and Risk*, **1**, pp. 259–272.

[186] Singh, V., Singh, T.N. and Singh, V., 2010, Image processing applications for customized mining and ore classification. *Arabian Journal of Geosciences*, DOI: 10.1007/s12517-010-0125-2.

[187] Sinha, S., Singh, T.N., Singh, V.K. and Verma, A.K., 2010, Epoch determination for neural network by self-organized map (SOM). *Computational Geosciences*, **14**, pp. 199–206.

[188] Skriver, H., Dall, J., Le Toan, T., Quegan, S., Ferro–Famil, L., Pottier, E., Lumsdon, P. and Moshammer, R., 2005. Agriculture classification using POLSARdata. In *Proceedings of the 2nd International Workshop on Applications of SAR Polarimetry and Polarimetric Interferometry*, pp. 1–6.

[189] Song, K., Zhou, X. and Fan, Y., 2009, Empirocally adopted IEM for retrieval of soil moisture from radar backscattering coefficients. *IEEE Transactions on Geoscience and Remote Sensing*, **47**, pp. 1662–1672.

[190] Sreenivas, K., Venkataratnam, L., and Rao, P.V.N., 1995, Dielectric property of salt–affected soil. *International Journal of Remote Sensing*, **16**, pp. 641–649.

[191] Srivastava, H.S., Patel, P. and Navalgund, R.R., 2006, Incorporating soil texture in soil moisture estimation from extended low–1 beam mode RADARSAT–1 SAR data. *International Journal of Remote Sensing*, **27**, pp. 2587–2598.

[192] Srivastava, H.S., Patel, P., Manchanda, M.L. and Adiga, S., 2003, Use of multi–incidence angle RADARSAT–1 SAR data to incorporate the effect of

surface roughness in soil moisture estimation. *IEEE Transactions on Geoscience and Remote Sensing*, **41**, pp. 1638–1640.

[193] Srivastava, H.S., Patel, P., Sharma, Y. and Navalgund, R.R., 2009, Large–area soil moisture estimation using multi–incidence–angle RADARSAT–1 SAR data. *IEEE Transactions on Geoscience and Remote Sensing*, **47**, pp. 2528–2535.

[194] Tabatabaeenejad, A. and Moghaddam, M., 2011, Radar retrieval of surface and deep soil moisture and effect of moisture profile on inversion accuracy, *IEEE Transactions on Geoscience and Remote Sensing*, **8**, pp. 478–482.

[195] TanDEM–X–a valuable partner for TerraSAR–X, Available online at: http://www.infoterra.de /terrasar–x/tandem–x–mission.html

[196] Thoma, D.P., Moran, M.S., Bryant, R., Rahman, M., Holifield–Collins, C.D. and Skirvin, S., 2006, Comparison of four models to determine surface soil moisture from C–band radar imagery in a sparsely vegetated semiarid landscape. *Water Resources Research*, **42**, pp.1–12.

[197] Tien, K.J.C., Judge, J. and Jacobs, J.M., 2004, Passive microwave remote sensing of soil moisture, evapotranspiration, and vegetation properties during a growing season of cotton. In *IEEE International Geoscience and Remote Sensing Symposium*, pp. 2795–2498.

[198] Tien, K.J.C., Roger, D.D.R., Judge, J. and Pham, H., 2007, Comparison of calibration techniques for ground–based C–band radiometers. *IEEE Transactions on Geoscience and Remote Sensing*, **4**, pp. 83–87.

[199] Trebits, R.N., 1989, Radar cross section. In *Radar reflectivity measurement: Technique and Applications*, N. C. Curie (Ed.), pp. 51–59 (Norwood, MA: Artech House).

[200] Turiel, A., Grazzini, J. and Yahia, H., 2005, Multiscale techniques for the detection of precipitation using thermal IR satellite images. In *IEEE Geoscience and Remote Sensing Letters*, **2**, pp. 447–450.

[201] Ulaby, F.T., Dubois, P.C. and Zyl, J.V., 1996, Radar mapping of surface soil moisture. *Journal of Hydrology*, **184**, pp. 57–84.

[202] Ulaby, F.T., Moore, R.K. and Fung, A.K., 1982, *Microwave remote sensing–active and passive–vol. 2* (Reading, MA: Addison Wesley).

[203] Ulaby, F.T., Moore, R.K. and Fung, A.K., 1986, *Microwave remote sensing–active and passive–vol. 3* (Reading, MA: Addison Wesley).

[204] Ulaby, F.T., Sarabandi, K., McDonald, K., Whitta, M. and Dobsona, M.C., 1990, Michigan microwave canopy scattering model. *International Journal of Remote Sensing*, **11**, pp. 1223–1253.

[205] Van Oevelen, P.J., 1998, Soil moisture variability: a comparison between detailed field measurements and remote sensing measurement techniques. *Hydrological Sciences Journal*, **43**, pp. 511–520.

[206] Varma, A.K., Gairola, R.M., Kishtawal, C.M., Pandey, P.C. and Singh, K.P., 1999, Rain rate estimation from nadir–looking TOPEX/POSEIDON microwave radiometer (TMR) for correction of radar altimetric measurements. *IEEE Transactions on Geoscience and Remote Sensing*, 37, pp. 2556–2568.

[207] Varma, A.K., Pokhrel, S., Gairola, R.M. and Agarwal, V.K., 2003, An empirical algorithm for cloud liquid water from MSMR and its utilization in rain identification. *IEEE Transactions on Geoscience and Remote Sensing*, **41**, pp. 1853–1858.

[208] Varma, A.K., Pokhrel, S., Gairola, R.M. and Agarwal, V.K., 2006, Study of geophysical parameters associated with the Orissa super cyclone using active and passive microwave remote sensing measurements. *International Journal of Remote Sensing*, **27**, pp. 3753–3765.

[209] Verhoest, N.E.C., Lievens, H., Wagner, W., Alvarez–Mozos, J., Moran, M.S. and F. Mattia, 2008, On the soil roughness parameterization problem in soil moisture retrieval of bare surfaces from synthetic aperture radar. *Sensors*, **8**, pp. 4213–4248.

[210] Verma, A.K. and Singh, T.N., 2010, Modeling of a jointed rock mass under triaxial conditions. *Arabian Journal of Geosciences*, **3**, pp. 91–103.

[211] Wagner, W., Bloschl, G., Panpaloni, P., Calvet, J.C., Bizzarri, B., Wigneron, J.P. and Kerr, Y., 2007, Operational readiness of microwave remote sensing of soil moisture for hydrology applications. Nordic Hydroliogy, **38**, pp. 1–20.

[212] Wal, D., Herman, P.M.J. and Dool, A.W., 2005, Characterization of surface roughness and sediment texture of intertidal flats using ERS SAR imagery. *Remote Sensing of Environment*, **98**, pp. 96–109.

[213] Walker, J.P., Houser, P.R. and Willgoose, G.R., 2004, Active microwave remote sensing for soil moisture measurement: a field evaluation using ERS–2. *Hydrological Processes*, **18**, pp. 1975–1997.

[214] Wang, C., Qi, J., Moran, S. and Marsett, R., 2004, Soil moisture estimation in a semiarid rangeland using ERS–2 and TM imagery. *Remote Sensing of Environment*, **90**, pp. 178–189.

[215] Wang, J.R. and Schmugge, T.J., 1980, An empirical model for the complex dielectric permittivity of soil as a function of water content. *IEEE Transactions on Geoscience and Remote Sensing*, **18**, pp. 288–295.

[216] Williams, K.K. and Greeley, R., 2004, Laboratory and field measurements of the modification of radar backscatter by sand. *Remote Sensing of Environment*, **89**, pp. 29–40.

[217] Woodhouse, I.H., 2006, *Introduction to microwave remote sensing* (CRC Press, Taylor & Francis Group).

[218] Wu, T. and Chen, K., 2004, A reappraisal of the validity of the IEM model for backscattering from rough surfaces. *IEEE Transactions on Geoscience and Remote Sensing*, **42**, pp. 743–753.

[219] Wu, T., Chen, K., Shi, J., Lee, H. and Fung, A.K., 2008, A study of an AIEM model for bistatic scattering from randomly rough surface. *IEEE Transactions on Geoscience and Remote Sensing*, **46**, pp. 2584–2598.

[220] Xu, L., Li, J. and Niu, R., 2010, Soil moisture estimation over Jianghan plain using ENNISAT ASAR data. In *International conference on Multimedia Technology*, pp. 1–4.

[221] Xu, P. and Tsang, L., 2007, Bistatic scattering and emissivities of lossy dielectric surfaces with exponential correlation functions. *IEEE Transactions on Geoscience and Remote Sensing*, **45**, pp. 62–72.

[222] Yahia, H., Herlin, I., Turiel, A., Chrysoulakis, N., Prastacos P. and Grazzini, J., 2007, Multifractal pre–processing of AVHRR images to improve the determination of smoke plumes from large fire. In *IEEE International Geoscience and Remote Sensing Symposium*, pp. 5335–5338.

[223] Yang, J., Peng, Y.N., and Lin, S.M., 2001, Similarity between two scattering Matrices. *Electronics Letters*, **37**, pp. 193–194.

[224] Yang, J., Xiong, T., Peng, Y.N., 2006, Polarimetric SAR image classification by using generalized optimization of polarimetric contrast enhancement. *International Journal of Remote Sensing*, **27**, pp. 3413–3424.

[225] Yang, J., Yamaguchi, Y., Boerner, W. and Lin, S., 2000, Numerical methods for solving the optimal problem of contrast enhancement. *IEEE Transactions*

on Geoscience and Remote Sensing, **38**, pp. 965–971.

[226] Yilmaz, M.T., Hunt Jr, E.R. and Jakson, T.J., 2008, Remote sensing of vegetation water content from equivalent water thickness using satellite imagery. *Remote Sensing of Environment*, **112**, pp. 2514–2522.

[227] Zaveri, M.A., Merchant, S.N. and Desai, U.B., 2006, Tracking of multiple point targets using multiple model based particle filtering in infrared image sequence. *Optical Engineering*, **45**, pp. 1–15.

[228] Zhai, Y., Thomasson, J.A., Boggess, J.E. and Sui, R., 2006, Soil texture classification with artificial neural networks operating on remote sensing data. *Computers and Electronics in Agriculture*, **54**, pp. 53–68.

[229] Zhang, X., Younan, N.H. and King, R.L., 2003, Soil texture classification using wavelet transform and maximum likelihood approach. In *IEEE International Geoscience and Remote Sensing Symposium*, pp. 2888–2890.

[230] Zribi, M. and Dechambre, M., 2002, A new model to retrieve soil moisture and roughness from C–band radar data. *Remote Sensing of Environment*, **84**, pp. 42–52.

[231] Zribi, M., Andre, C. and Decharme, D., 2008, A method for soil moisture estimation in Western Africa based on the ERS scatterometer. *IEEE Transactions on Geoscience and Remote Sensing*, **46**, pp. 438–448.

[232] Zribi, M., Baghdadi, N., Holah, N. and Fafin, O., 2005, New methodology for soil surface moisture estimation and its application to ENVISAT–ASAR multi–incident data inversion. *Remote Sensing of Environment*, **96**, pp. 485–496.

[233] Zribi, M., Le Hegarat–Mascle, S., Ottle, C., Kammoun, B. and Guerin, C., 2003, Surface soil moisture estimation from the synergistic use of the (multi–incidence and multi–resolution) active microwave ERS wind scatterometer and SAR data. *Remote Sensing of Environment*, **86**, pp. 30–41.

Author's Publications

International Journals

[1] Prakash, R., Singh, D. and Pathak, N.P., 2010, The effect of soil texture in soil moisture retrieval for specular scattering at C–band. *Progress in Electromagnetic Research*, **108**, pp. 177–204.

[2] Prakash, R., Singh, D. and Pathak, N.P., 2009, Microwave specular scattering response of soil texture at X–band," *Advances in Space Research, Elsevier Publication*, **44**, pp. 801–814.

[3] Prakash, R., Singh, D. and Pathak, N.P., Specular scattering response for soil texture, soil moisture, surface roughness and its retrieval through multi–incidence angle data. *IEEE Transactions on Geoscience and Remote Sensing*, under process after first review.

[4] Prakash, R., Singh, D. and Pathak, N.P., A fusion approach to retrieve soil moisture with SAR and optical data. IEEE Journal of Selected Topics in Applied Earth Observations and Remote Sensing, under process after first review.

International Conferences

[1] Singh, D., Prakash, R. and Pathak, N.P., SAR and optical data utilization for soil moisture retrieval in vegetated region. In *The Asia-Pacific Conference on Synthetic Aperture Radar, 26–30 September 2011*, Seoul, South Korea, Accepted.

[2] Singh, D., Prakash, R. and Pathak, N.P., Satellite image application for retrieving the crop covered soil moisture. In *International Conference on Geophysical Sciences- Energy, Climate Change and Evolution of Human Society, ICON GSECCES' 10*, Varanasi, India, 21–23 December 2010, Accepted.

[3] Prakash, R., Singh, D. and Pathak, N.P., Soil moisture retrieval in vegetated area with the utilization of Polarimetric SAR and MODIS data. In *International Conference on Microwaves, Antenna, Propagation and Remote Sensing, ICMARS '10*, Jodhpur, India, 14–17 December 2010, pp. 97–98.

[4] Singh, D. and Prakash, R, Multi-incidence angle approach for soil parameter retrieval at C-band with specular scattering. In *38th COSPAR Scientific Assembly,* Bremen, Germany, 18–25 July 2010, Accepted.

[5] Prakash, R., Singh, D. and Pathak, N.P., X–Band bistatic scatterometer performance for soil texture retrieval using statistical inversion approach. In *IEEE Geoscience and Remote Sensing Symposium, 2010. IGARSS '10*, Hawaii, USA, 25–30 July 2010, Accepted.

[6] Prakash R. and Singh D., Microwave sensitivity analysis of soil texture at C-band with bistatic scatterometer for remote sensing. In *International Conference on Recent Advances in Microwave Theory and Applications, Microwave-08,* Jaipur, India, 21–24 November 2008, pp. 211–213.

[7] Singh D. and Prakash R., Sensitivity of bistatic microwave scattering for soil texture at X-band for remote sensing. In *37th COSPAR Scientific Assembly*, Montreal, Canada, 13–20 July 2008, Accepted.

National Conferences

[1] Prakash, R., Singh, D. and Pathak, N.P., Critical analysis of specular scattering for soil texture and soil moisture retrieval at C-band. In *2nd Rashtriya Yuva Yaigynik Sammelan 2010*, Dehradun, India, 6–7 February 2010, pp. 106.

[2] Prakash, R., Singh, D. and Pathak, N.P., Specular scattering for soil texture retrieval at X-band. In *National Seminar on Radar Remote Sensing and Its Applications, 2009*, Roorkee, India, 25–56 September 2009, pp. 7.

[3] Prakash, R., Singh, D. and Pathak, N.P., Bistatic scatterometer performance for soil texture analysis and its retrieval at C-band. In *ISRS Symposium 2009*, Nagpur, India, 17–19 September 2009, pp. 1–11.